

**DEVELOPMENT OF MICROWAVE IMAGING SYSTEM USING
MULTISTATIC CONFIGURATION WITH PHASE SHIFTER FOR
SPATIAL OBJECT DETECTION**

AFZAN NAJIHA BINTI MOHD KHAIRI



UNIVERSITI TEKNIKAL MALAYSIA MELAKA

**DEVELOPMENT OF MICROWAVE IMAGING SYSTEM
USING MULTISTATIC CONFIGURATION WITH PHASE
SHIFTER FOR SPATIAL OBJECT DETECTION**

AFZAN NAJIHA BINTI MOHD KHAIRI

**THIS REPORT IS SUBMITTED IN PARTIAL FULFILMENT
OF THE REQUIREMENTS FOR THE DEGREE OF BACHELOR
OF ELECTRONIC ENGINEERING WITH HONOURS**

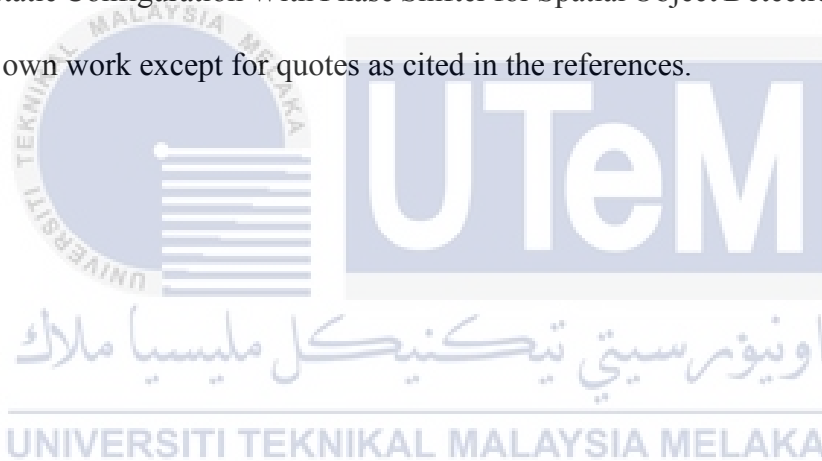


**FACULTY OF ELECTRONIC AND COMPUTER
ENGINEERING
UNIVERSITI TEKNIKAL MALAYSIA MELAKA**

JULY 2021

DECLARATION

I declare that this report entitled “Development Of Microwave Imaging System Using Multistatic Configuration With Phase Shifter for Spatial Object Detection” is the result of my own work except for quotes as cited in the references.



Signature:

Author : AFZAN NAJIHA BINTI MOHD KHAIRI

Date : 19 JUNE 2021

APPROVAL

I hereby declare that I have read this thesis and in my opinion this thesis is sufficient in terms of scope and quality for the award of Bachelor of Electronic Engineering with Honours.



اونيورسيتي تيكنيكل مليسيا ملاك

Signature _____

UNIVERSITI TEKNIKAL MALAYSIA MELAKA

Supervisor Name : PM DR MOHAMAD ZOINOL ABIDIN BIN ABD.

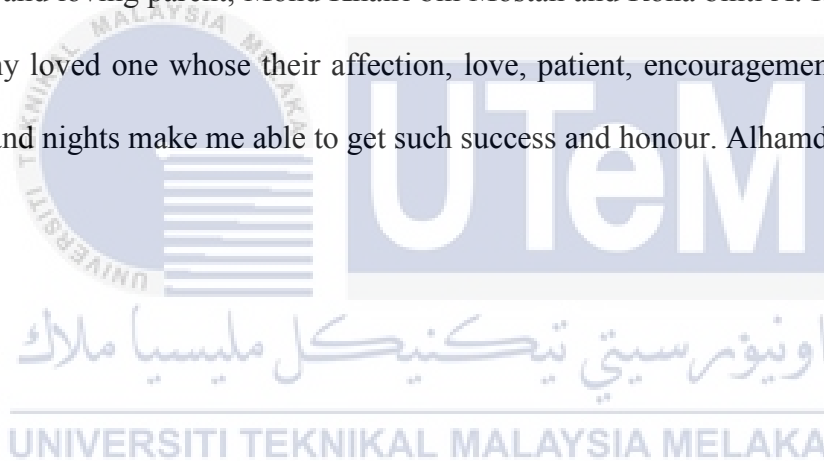
AZIZ

Date : **25 June 2021**
.....

Prof. Madya Dr. Mohamad Zoinol Abidin Bin Abd Aziz
Profesor Madya
Fakulti Kejuruteraan Elektronik dan Kejuruteraan Komputer
Universiti Teknikal Malaysia Melaka (UTeM)
Hang Tuah Jaya
76100 Durian Tunggal, Melaka

DEDICATION

My humble effort I dedicated to Allah the All Mighty for granting me my sweet and loving parent, Mohd Khairi bin Mostan and Roha binti A. Hamid, siblings and my loved one whose their affection, love, patient, encouragement and prays of days and nights make me able to get such success and honour. Alhamdulillah.



ABSTRACT

There are many imaging techniques nowadays such as X-Ray, CT scan, MRI and Microwave Imaging System (MWI). The MWI system seem to be the most safest and inexpensive compare to others systems. However, there are three configurations in microwave imaging which are Monostatic, Bistatic and Multistatic. Multistatic configuration system is able to scan 360° without mechanical and physical movement. However, the radiated signal in multistatic configuration can be cancelled or reduced due to the phase differential. Therefore, this project aims to be developed the MWI system using multistatic configuration with phase shifter for spatial detection. The MIMO (4x4) MWI system based on multistatic configuration system has been developed to detect the Defected Material (DM). The microwave sensors with 0° , 45° , and 90° phase have been designed and fabricated based on Vivaldi structure at frequency on 3.924GHz. All sensors meet the minimum reflection coefficient requirement of -10dB. Next, the 4x4 multistatic MWI system has also been setup for spatial detection testing. Meanwhile, water, soap, sand, soil, sugar, flour and plasticine were selected for material under test (MUT). The metal, lime, rubber and plastic were chosen as the defected material under test for spatial detection measurement. The measurement result shows that the average efficiency of the system is 26.95%. The

system can detect plastic and rubber better in water and sand with efficiency of 50%.

The highest efficiency of 62.5% achieved when system try to detect the plastic in soil.

Therefore, the developed system can be used in detection of plastic material.



ABSTRAK

Terdapat banyak teknik pengimejan pada masa kini seperti X-Ray, imbasan CT, MRI dan Sistem Pengimejan Gelombang Mikro (MWI). Sistem MWI dilihat sebagai sistem yang paling selamat dan murah berbanding dengan sistem lain. Walau bagaimanapun, terdapat tiga konfigurasi dalam pengimejan gelombang mikro iaitu Monostatik, Bistatik dan Multistatik. Sistem konfigurasi multistatik mampu mengimbas 360 darjah tanpa pergerakan mekanikal dan fizikal. Walau bagaimanapun, isyarat radiasi dalam konfigurasi multistatik boleh dibatalkan atau dikurangkan kerana pembuzaan fasa. Oleh itu, projek ini bertujuan untuk membina sistem MWI menggunakan konfigurasi multistatik dengan fasa peralihan untuk pengesanan kedudukan (spasial). Sistem MWI MIMO (4x4) berdasarkan sistem konfigurasi multistatik telah dibangunkan untuk mengesan Bendasing (DM). Sensor gelombang mikro dengan fasa peralihan sebanyak 0-darjah, 45-darjah, dan 90-darjah telah direka dan dihasilkan berdasarkan struktur Vivaldi pada kekerapan 3.924GHz. Semua sensor memenuhi keperluan pekali refleksi minimum -10dB. Seterusnya, sistem MWI multistatik 4x4 juga telah disediakan untuk ujian pengesanan spatial. Sementara itu, air, sabun, pasir, tanah, gula, tepung dan tanah liat dipilih untuk bahan uji kaji (MUT). Logam, limau, getah dan plastik dipilih sebagai bahan bendasing di bawah ujian untuk pengukuran pengesanan kedudukan (spasial). Hasil bacaan dan pembezaan nilai voltan menunjukkan bahawa kecekapan purata sistem adalah 26.95%. Sistem ini dapat mengesan plastik dan getah dengan lebih baik dalam

air dan pasir dengan kecekapan 50%. Kecekapan tertinggi sebanyak 62.5% dicapai apabila sistem cuba mengesan plastik di dalam tanah. Oleh itu, sistem yang dibangunkan boleh digunakan dalam pengesanan bahan plastik.



ACKNOWLEDGEMENTS

My deepest gratitude goes to Allah S.W.T who has provided all the strength that I need to complete this whole project. I would also like to thank to several persons who helped me directly or indirectly to conduct this project. I owe a deep thanks to my project supervisor and express my greatest appreciation to Prof. Madya Dr. Mohamad Zoinol Abidin bin Abdul Aziz for all his guidance, encouragement, assistance and support in completing this project. I cannot thank him enough for all the all favor he has done in order for me to get all the results needed.

I am also extremely thankful to the Lab Technicians, Mr. Sufian and Mr. Imran for assisting and guiding me to use all the laboratory equipment with the fabrication and measurement process. Not to forget, Mrs. Nuruliswa for guiding me to do every process of the project, from designing the antenna until setting up the whole system.

My greatest thank you also addressed to my mother and father who has always support my financial, siblings and my loved one who listened to all my problems and helped me get through it all. Last but not least, thank you to all my friends, Farah Liyana, Wan Nazira Edora, Ain Syafiqah and Azmin Sabrina as they have contributed such a big support throughout this project.

TABLE OF CONTENTS

Declaration	i
Approval	i
Dedication	i
Abstract	ii
Abstrak	iv
Acknowledgements	vi
TABLE OF CONTENTS	vii
List of Figures	xi
List of TABLES	xvi
List of Symbols and Abbreviations	xviii
List of Appendices	xx
CHAPTER 1: INTRODUCTION	1
1.1 Project Introduction	1
1.2 Project Objectives	3
1.3 Problem Statement	3
1.4 Project Scope	4

CHAPTER 2: BACKGROUND STUDY	6
2.1 Microwave Imaging System	7
2.2 Microwave Imaging System Configuration	9
2.3 Microwave Imaging Sensors	12
2.4 Phase Shifter	14
2.5 Table of Literature Review	17
2.5 Summary	25
CHAPTER 3: METHODOLOGY	26
3.1 Overview of the Project	27
3.2 Microwave System Development	30
3.3 Microwave Sensor Design	31
3.3.1 Microwave Sensor Design Process	31
3.3.2 Simulation Process	35
3.3.3 Fabrication Process	36
3.4 Signal Processing Unit	38
3.4.1 RF to DC Converter	38
3.4.2 Microcontroller.	39
3.4.3 TFT Display	42
3.5 Microwave Imaging System Testing	44
3.5.1 Calibration Process	44

3.5.2	Single Input Single Output (1x1)	45
3.5.3	Single Input Multiple Output (1 x 2)	46
3.5.4	Multiple Input Multiple Output.	47
3.5.5	Material Characterization	49
3.5.6	Spatial Detection Test	50
3.6	Summary	54
CHAPTER 4: RESULT ANALYSIS AND DISCUSSION		55
4.1	Microwave Sensor Parameter	56
4.2	RF to DC Converter	59
4.3	Single Input Single Output	61
4.4	Single Input Single Output, SIMO (1 x 2)	61
4.5	Multiple Input Multiple Output, MIMO	63
4.5.1	Multiple Input Multiple Output (2 x 2)	63
4.5.2	Multiple Input Multiple Output (4 x 4)	64
4.6	Material Characterization	66
4.7	Spatial Detection Measurement	70
4.8	Summary	75
CHAPTER 5: CONCLUSION AND FUTURE WORKS		76
5.1	Conclusion	77
5.2	Future Work and Recommendation	78

REFERENCES	80
APPENDICES	84
APPENDIX A	85
APPENDIX B	92
APPENDIX C	133
APPENDIX D	151
APPENDIX E	159



LIST OF FIGURES

Figure 1. 1: (a) X-ray. (b) Computed Tomography. (c) Magnetic Resonance Imaging.	2
Figure 2. 1: Conventional Microwave Imaging Sensing System [1]	7
Figure 2. 2: Microwave Imaging System [4]	8
Figure 2. 3: Basic MWI block diagram.	8
Figure 2. 4: Monostatic Configuration System	9
Figure 2. 5: First Bistatic Configuration System	10
Figure 2. 6: Second Bistatic Configuration System	10
Figure 2. 7: Multistatic Configuration System	11
Figure 2. 8: MISO multistatic. [13]	12
Figure 2. 9: MIMO multistatic. [14]	12
Figure 2. 10: (a) Structure of Vivaldi Antenna. (b) Structure of Antipodal Vivaldi Antenna (AVA) [11]	13
Figure 2. 11: (a) Top view of the Microstrip-fed Vivaldi antenna. (b) Bottom view of the Microstrip-fed Vivaldi Antenna[18]	14
Figure 2. 12: (a) Standard Schiffman phase shifter, (b) Double Schiffman phase shifter, (c) Double Parallel Schiffman phase.[19]	15
Figure 2. 13: Layout of the 45 degree double parallel Schiffman phase shifter using (a) CST & (b) ADS.[19]	15
Figure 2. 14: Prototype of proposed phase shifter for 8 elements antenna feeding network; top is the upper side; below is the bottom side [20]	16

Figure 2. 15: (a) A construction of the 8 element phase shifter. (b) Simulation result of coefficient phase for 4 different scenarios. [20]	16
Figure 3. 1: Flowchart for Antenna Design	27
Figure 3. 2: Flowchart for RF converter.	28
Figure 3. 3: Flowchart for Signal Processing Unit.	28
Figure 3. 4: Flowchart for whole full system.	29
Figure 3. 5: Overall block diagram system for MWI system with multistatic configuration.	30
Figure 3. 6: (a) Front view (b) Rear view	32
Figure 3. 7: (a) Setting for the designed antenna with 3 – 6GHz operating frequency and the E-field, H-field and Farfield monitor are tick for simulation process. (b) Frequency range setting for simulation. (c) front view of Vivaldi antenna. (d) rear view of the antenna. (e) perspective view of the antenna with port.	35
Figure 3. 8: Fabrication process	36
Figure 3. 9: (a) Printed antenna design on tracing paper. (b)UV exposure machine to print the antenna from tracing paper to FR4. (c) Etching station. (d) Resist layer strip station.	37
Figure 3. 10: (a) Drying Machine (b) Substrate Cutter.	37
Figure 3. 11: (a) Front view & (b) Rear view of fabricated Vivaldi antenna on the FR4. (c) The fabricated Phase shifter on Vivaldi Antenna.	38
Figure 3. 12: Jumper wire connection and Soldered DIP Pin on AD8318.	39
Figure 3. 13: RF detector AD8318 Module.	39
Figure 3. 14: Arduino MEGA 2560 Pinout	39
Figure 3. 15: 3.5 inch TFT display output pin.	40
Figure 3. 16: circuit connection between Arduino MEGA and TFT screen	40
Figure 3. 17: Library Call	41
Figure 3. 18: Analog input	41

Figure 3. 19: Voltage and power display	42
Figure 3. 20: TFT Screen display	42
Figure 3. 21: AD8313 connection with Arduino and TFT screen	43
Figure 3. 22: Identifying Power Input for system (wired)	45
Figure 3. 23: Dielectric measurement process.	45
Figure 3. 24: Measurement Setup in SISO configuration.	46
Figure 3. 25: Block diagram of SISO measurement	46
Figure 3. 26: Block diagram of MIMO of 2x2.	47
Figure 3. 27: Block diagram of MIMO (2x2)	47
Figure 3. 28: (a) & (b) MIMO (2x2) configuration.	48
Figure 3. 29: Block Diagram of MIMO (4x4) configuration.	48
Figure 3. 30: Eight antennas in MIMO (4x4) configuration.	48
Figure 3. 31: Material characterization testing on soap.	49
Figure 3. 32: List of Material 1, from left Soil, Sugar, Flour, Soap, Water, Soil and Plasticine.	50
Figure 3. 33: Spatial detection setup for Soap + Metal. Soap as Material 1 and Metal as Material 2.	50
Figure 3. 34: List of Material 2, from left, Metal, Plastic, Lime and Rubber.	51
Figure 3. 35: Arrangement of sensors for spatial detection for (a) 0^0 phase shifter, (b) 45^0 phase shifter, and (c) 90^0 phase shifter.	53
Figure 3. 36: Spatial Detection test.	53
Figure 4. 1: Return Loss for original (0^0) antenna	56
Figure 4. 2: Directivity for original (0^0) antenna at 3.924GHz.	56
Figure 4. 3: Gain for original (0^0) antenna at 3.924GHz.	57
Figure 4. 4: Simulation comparison return loss for all phase shifters.	57

Figure 4. 5: Simulation comparison of S2,1 for all phase shifters.	58
Figure 4. 6: Simulation comparison of phase for all phase shifters.	58
Figure 4. 7: Simulation comparison of gain at 3.924GHz for all phase shifters.	58
Figure 4. 8: Simulation comparison of directivity at 3.924GHz for all phase shifters.	59
Figure 4. 9: Graph input power versus output voltage at 3.924GHz for all receiver	60
Figure 4. 10: Graph input power versus output voltage at 3.6GHz from datasheet	60
Figure 4. 11: SISO configuration at 3.924GHz with 10cm diameter.	61
Figure 4. 12: Output voltage for all phase shifter, 0° , 45° , 90° , 135° , 180° and 270° at Receiver 1 and Receiver 2.	62
Figure 4. 13: Arrangement of antennas for MIMO (2x2)	63
Figure 4. 14: Output Voltage for MIMO (2x2) on Air (Free space) and Empty Bottle.	63
Figure 4. 15: (a) Arrangement of 45° phase shifter for free space and empty bottle detection on MIMO (4x4) configuration. (b) Signal transmitted from 45° phase shifter simultaneously.	64
Figure 4. 16: Output Voltage for MIMO (4x4) on Air (Free space) and Empty Bottle for 45° phase shifter.	64
Figure 4. 17: (a) Arrangement of 90° phase shifter for free space and empty bottle detection on MIMO (4x4) configuration. (b) Signal transmitted from 90-degree phase shifter simultaneously.	65
Figure 4. 18: Output Voltage for MIMO (4x4) on Air (Free space) and Empty Bottle for 90° phase shifter.	65
Figure 4. 19: Material 1 Characterization test on 0° phase shifter.	67
Figure 4. 20: Material 1 characterization on 45° phase shifter.	68
Figure 4. 21: Material 1 characterization on 90° phase shifter.	69
Figure 4. 22: Result for Soil+Plastic for 0° phase shifter	70
Figure 4. 23: Spatial Detection Result for Soil+Plastic for 45° phase shifter	72

Figure 4. 24: Spatial Detection Result for Soil+Plastic for 90⁰ phase shifter



LIST OF TABLES

Table 2. 1: Review Microwave Imaging System	17
Table 2. 2: Recent study on Monostatic and Bistatic configuration.	18
Table 2. 3: Recent study on Multistatic configurations.	20
Table 2. 4: Recent study on Antenna design used in MWI system.	23
Table 2. 5: Recent study on Phase Shifter.	24
Table 3. 1: System design specification	30
Table 3. 2: Microwave sensor specification	31
Table 3. 3: List of antenna's parameter	33
Table 3. 4: Mathematical Equations of Vivaldi Antenna	33
Table 3. 5: Equation for length of the transmission line.	34
Table 3. 6: Length of feeding line for every phase shifter at the 50Ω line impedance.	34
Table 3. 7: Connection summary	43
Table 3. 8: Configuration for system testing	44
Table 3. 9: Arrangement of SIMO tested on free space.	47
Table 3. 10: Variation of testing on MIMO (4x4)	49
Table 3. 11: Classification of Material 1 and Material 2.	51
Table 3. 12: List of combination Material 1+Material 2.	51

Table 4. 2: Average Voltage Output for SIMO configuration	62
Table 4. 3: Average value of dielectric constant for all material.	66
Table 4. 4: Output Voltage for Material 1 characterization on 0^0 phase shifter	67
Table 4. 5: Output Voltage for Material 1 characterization on 45^0 phase shifter.	68
Table 4. 6: Output Voltage for Material 1 characterization on 90^0 phase shifter.	69
Table 4. 7: Difference of Vout when Material 2 is inserted for 0^0 phase shifter.	71
Table 4. 8: Difference of Vout when Material 2 is inserted for 45^0 phase shifter	72
Table 4. 9: Difference of Vout when Material 2 is inserted for 90^0 phase shifter	73
Table 4. 10: Overall efficiency for all combinations on all phase shifter.	74



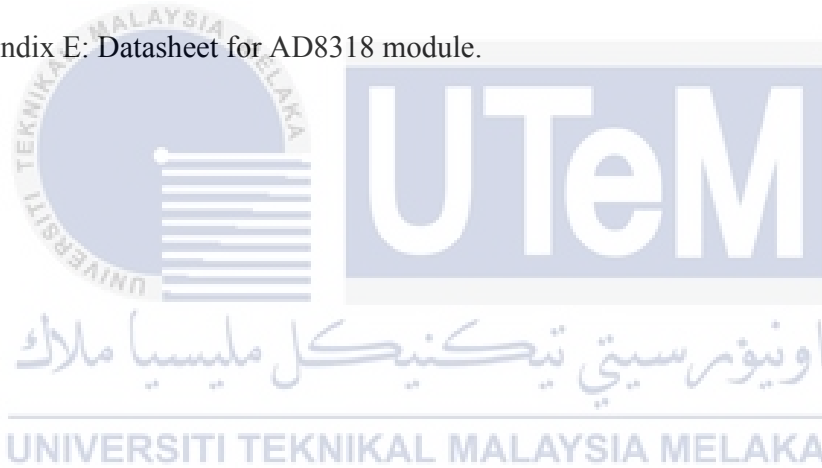
LIST OF SYMBOLS AND ABBREVIATIONS

MWI	:	Microwave Imaging
RF	:	Radio Frequency
MRI	:	Magnetic Resonance Imaging
CT	:	Computed Tomography
CST	:	Computer Simulation Technology
SUT	:	Subject Under Test
MUT	:	Material Under Test
SIMO	:	Single Output Multiple Output
MISO	:	Multiple Input Single Output
MIMO	:	Multiple Input Multiple Output
ADS	:	Advanced Design System
AVA	:	Antipodal Vivaldi Antenna
UV	:	Ultra Violet
TFT	:	Thin Film Transmitter
FR	:	Flame Retardant
UWB	:	Ultra Wideband
GHz	:	Gigahertz
dB	:	Decibel

BAVA	:	Balance Antipodal Vivaldi Antenna
MAVA	:	Modified Antipodal Vivaldi Antenna
mm	:	millimeter
VNA	:	Vector Network Analyzer
PC	:	Personal Computer
RMA	:	Random Multiple Access
FPGA	:	Field Programmable Gate Array
SNR	:	Signal-to-Noise Ratio
FDTD	:	Finite Difference Time Domain
FFT	:	Fast Fourier Transform
SAR	:	Synthetic Aperture Radar
TSAR	:	Tools for System Availability and Reliability
ADC	:	Analog-to-Digital Converter
SMA	:	Sub Miniature Version A
L	:	Length of the substrate
W	:	Width of the substrate
M	:	Opening mouth of the flare
FL	:	Flare length
SL	:	Slot line
di	:	Diameter
TL	:	Feeding Line gap
I1	:	Width of first feeding line
I2	:	Width of second feeding line
W1	:	Length of the first feeding line
W2	:	Length of the second feeding line

LIST OF APPENDICES

Appendix A: Arduino source code	83
Appendix B: Raw data from laboratory experiments	93
Appendix C: Antenna simulation results	139
Appendix D: Experiment and laboratory work images	157
Appendix E: Datasheet for AD8318 module.	165



CHAPTER 1:

INTRODUCTION



1.1 Project Introduction

Microwave Imaging (MWI) is an imaging technique that is used to detect or locate hidden or embedded objects in a structure by using electromagnetic waves. There are many other detection systems such as X-Ray, Computed Tomography (CT) Scan and Magnetic Resonance Imaging (MRI). However, for CT and X-Ray are using an ionized radiation for scanning that is very harmful for human body as it might result in tissues damage. Meanwhile for MRI, it uses a powerful magnetic wave which is very high in cost design and is very rarely found in most hospitals. As for MWI, it uses a non-ionized radiation that is clearly harmless and non-destructive to human body. Thus, the MWI system are mostly being used as detection system for medical applications and threat detection.

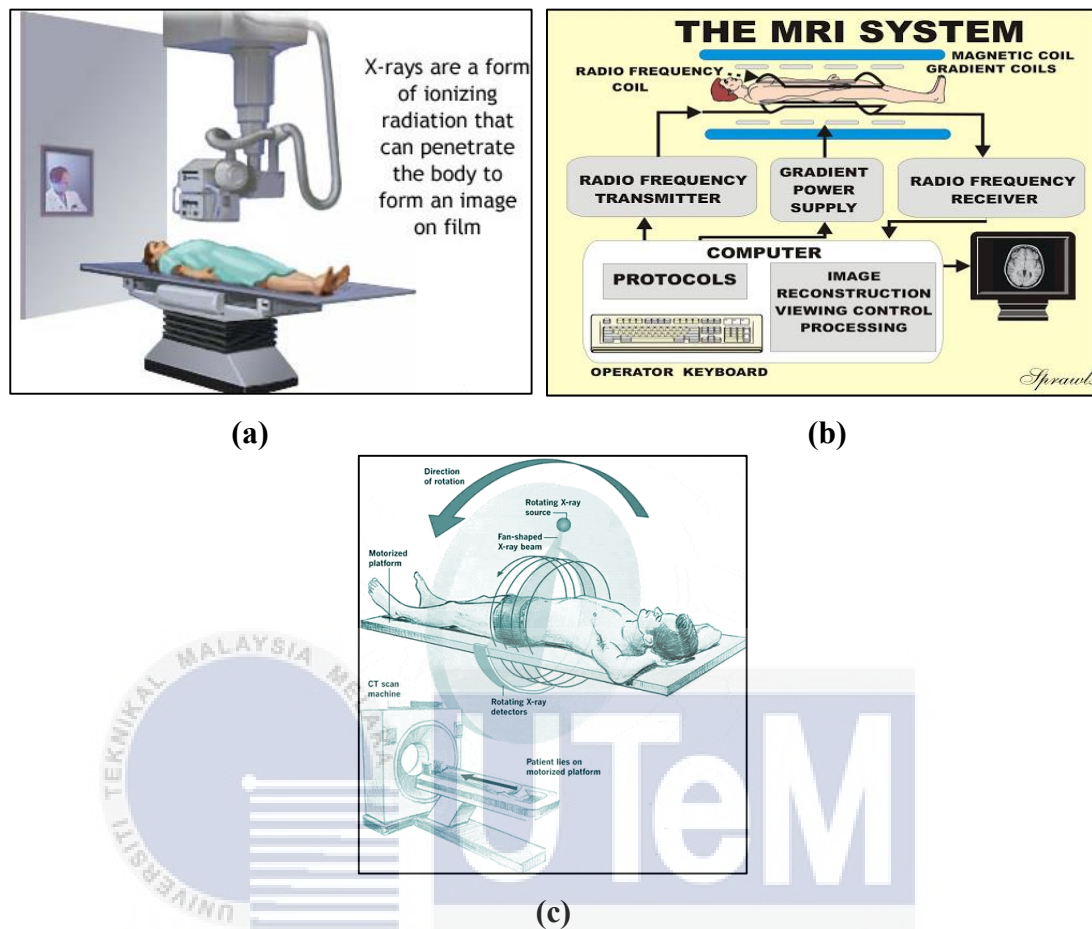


Figure 1. 1: (a) X-ray. (b) Computed Tomography. (c) Magnetic Resonance Imaging.

The MWI send signal which can be used to detect an unknown object by using the reflected or scattered signal. There are three (3) types of configurations available for MWI which are, Monostatic, Bistatic and Multistatic. Monostatic and Bistatic configuration requires complex system in order to perform the detection coverage on the whole 360-degree. Hence, for this project is focusing on the development of MWI system with Multistatic configuration. The new developed MWI system will be used to detect material 2 inside material 1. The system will consist of four (4) parts which are, sensors that is designed with phase shifter arranged in multistatic configuration, RF detector, microcontroller and signal display module. The system will operate within the frequency of 3 to 6 GHz. The process of developing the system will include

simulations, fabrication and testing. The result will then be displayed on the TFT screen in form of output voltage value. The proposed system will introduce a phase shifter configuration of 45° and 90° that is designed in the sensors for spatial detection system.

1.2 Project Objectives

The main objective of this project is to develop a multistatic microwave imaging system that is capable to detect the existence of different material by using a different phase shifter in frequency range of 3 to 6 GHz. The microwave sensors with different phase shifter of 45° , 90° , 135° , 180° , and 270° are designed based on the Vivaldi antenna structure.

1.3 Problem Statement

Nowadays, various methods to obtain patient information are used in medical diagnosis applications. The existing system for object characterization are ultrasound, X-Ray, Computed Tomography (CT), Magnetic Resonance Imaging (MRI) and Microwave Imaging (MWI). However, technology can be both helpful and harmful in many aspects, as X-ray and CT are using the ionized radiation which very harmful for human. MRI is made up from very powerful magnet that is expensive and hard to get. Meanwhile, MWI that uses non-ionized radiation in electromagnetic wave is safer for human and inexpensive.

However, the three types of configurations in MWI which are, Monostatic, Bistatic and Multistatic configuration have both advantages and disadvantages. Monostatic configuration is using only 1 sensor which act as transceiver and the signal only cover on the reflected spot of a surface of the subject under test (SUT). Meanwhile, as its

name Bistatic, it only uses 2 sensors to transmit and receive signal that move either in 1 transmission line or reflected signal and only cover on that particular area. However, both monostatic and bistatic may cover the whole object if it uses switching and rotating system. Thus, the system will be much complex and time-consuming as the transmitting signal will be captured and stored data gradually every time the system rotates

Those problems can be solve by using multistatic configuration as it uses multiple transmitters and receivers which has proven as a real-time imaging due to its ability to scan 360-degree angle of the SUT. It is also less time consuming and more efficient that monostatic and bistatic. Despite the fast imaging, this system still has its weakness when all of the components used in this system are identical, by mean all cables and sensors have the same length and parameters, the transmitted and received signal will all be exactly the same. So, when all signals are being transmitted simultaneously in the time domain with the same magnitude and time, there might be an increasing in wavelength or worse, the signal will collided to one another resulting of signal cancellation which the receiver will not receive any information. Therefore, in order to endure any weaknesses stated above, the development of microwave imaging system using multistatic configuration with phase shifter for spatial object detection is proposed.

1.4 Project Scope

The scope of this project focuses on the designing, fabrication, simulation and measurement. Below are the detailed scope of this project:-

1. Design, simulate and fabricate the 0° , 45° , 90° , 135° , 180° , and 270° phase shifter on the Microwave sensors based on Vivaldi antenna structure using CST software for operating frequency of 3 to 6 GHz. The sensor will be fabricated by using chemical etching technique on FR4 substrate board. While the measurement of the sensor parameters will be done by using Vector Network Analyzer and Antenna Anechoic Chamber Measurement system. The parameters to be tested are, return loss, directivity, gain, bandwidth and radiation pattern.
2. Development of signal processing unit will be done by using RF detector module AD8318, Arduino MEGA and TFT screen display. Then, testing and verify the signal processing unit using frequency of 3.924GHz with input power from -20dBm to 20dBm.
3. Development of SIMO (1x2), MIMO (2x2) and MIMO (4x4) multistatic MWI system by integrating signal generator, microwave sensors, cables and signal processing unit.
4. There are two types of system functional measurement process will be done. First, the Material 1 which include water, soap, sand, soil, sugar, flour and plasticine. Second, Material 2 which are metal, lime, plastic and rubber.

CHAPTER 2:

BACKGROUND STUDY



In this chapter, the review of previous works was done regarding the multistatic configuration for microwave imaging system, including the phase shifter. The first sections explain the definition of microwave imaging. For the second section will be discuss on the type of antennas in microwave imaging. Meanwhile for the third section discusses on the configuration type in microwave imaging system. Next, the discussion on phase shifter that is applied in the antenna and last but not least is about the display platform for this project.

2.1 Microwave Imaging System

There are many varieties of imaging techniques that is being employed for object detection and characterization. A number of them are, X-Ray, Computed Tomography (CT) scan, Magnetic Resonance Imaging (MRI) and so on. However, Microwave Imaging (MWI) technique is additional reliable and preferable. Study has proven that microwaves, with its wavelength much longer than X-Rays will have a great potential for imaging sensing [1]. Plus, the use of non-ionizing radiations and inexpensive also portable devices serve a great advantages offered by MWI especially to medical imaging system [2]. In other studies, microwave imaging method have the potential to discriminate between cancerous growths and healthy or benign tissues as it can safely be performed frequently. Meanwhile for the MRI or CT scan are expensive and not sufficiently accessible and they cannot being used often due to the ionizing radiation and associated the user's health risk [3].

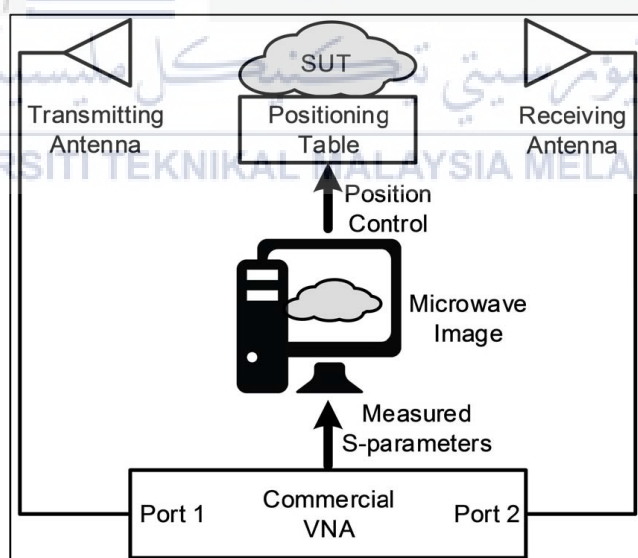


Figure 2. 1: Conventional Microwave Imaging Sensing System [1]

Microwave imaging involves the use of antenna arrays that operates at the microwave and millimetre-wave frequencies in order to capture images and characterize the object. Commonly, there will be one or more antennas in the array

illuminate the scene with a radio-frequency (RF) signal and some of the signal will reflect back to the other antennas, which record both amplitude and phase of the reflected signal [4].

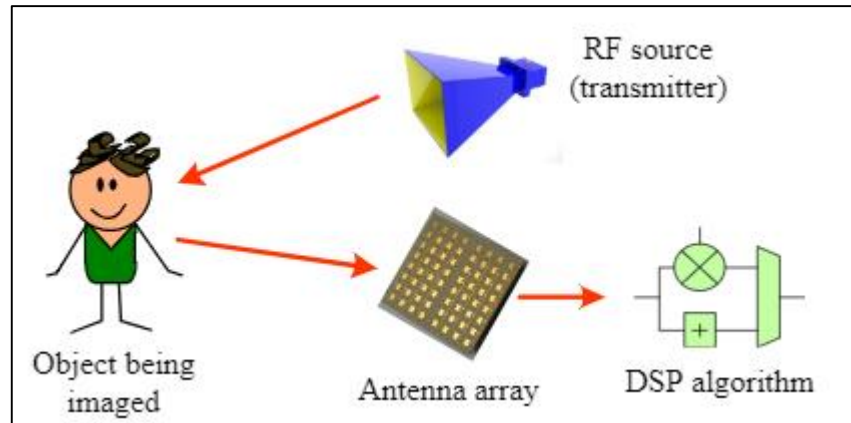


Figure 2. 2: Microwave Imaging System [4]

Microwave imaging in medical field is generally considered an emerging technique as it is still very challenging to obtain an accurate and effective dielectric reconstruction [5]. However, microwave imaging system is using the microwaves as a medium to interact with the target to obtain information and it may as well being used in the through-wall imaging and imaging of tissues under skin due to their ability to penetrate. A study also explains that the electromagnetic waves will scattered when they encounter with any dielectric change in path of their propagation or obstacle that comes in their path will scatter the waves [6]. This scattering event helps to gather information to provide the target shape and position of the investigation domain.

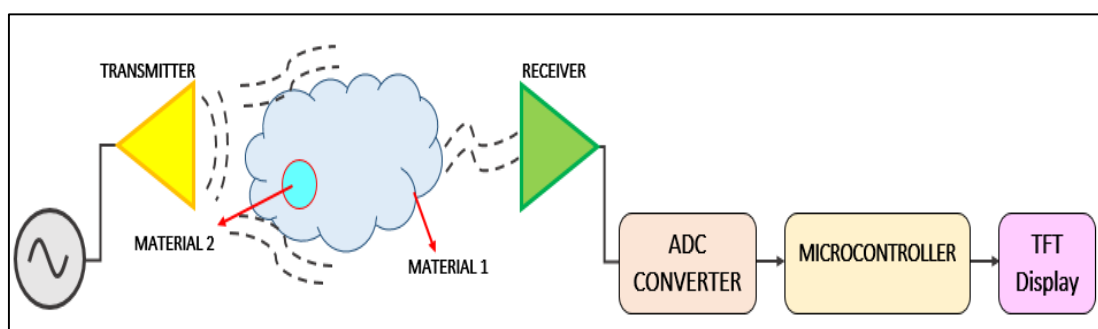


Figure 2. 3: Basic MWI block diagram.

2.2 Microwave Imaging System Configuration

This section will discuss on the types of configurations in microwave imaging system, which are Monostatic, Bistatic and Multistatic configurations. Including the number of antennas used in every configurations and the complexity of the systems.

Basically, a monostatic configuration in MWI uses only a single antenna which act as a transceiver. In some applications, monostatic imaging systems are used to inspect a structure-under-test only on one side using the transceiver antenna for irradiation and reception of the signal [7]. Monostatic also known as quantitative imaging technique that has the reflectivity function to represent the hidden object by using approximations to simplify the imaging problem and then they use-back the propagation to reconstruct the unknown image.

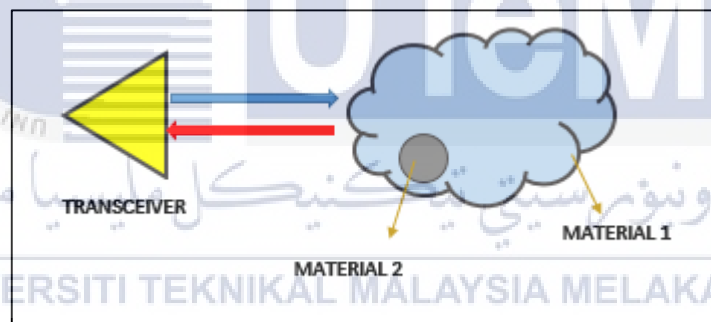


Figure 2. 4: Monostatic Configuration System

Since monostatic can only transmit and receive signal on one particular reflections of the object, so it need a more complex system to rotate the antenna so that each reflected signal might cover 360^0 area of the object.

Unlike monostatic, the bistatic system uses two antennas which each act as a transmitter and a receiver. The main difference between monostatic and bistatic configurations is that the separation of transmitter and receiver antenna. However, a co-located transmitter and receiver are not considered a bistatic system, even though they do not use a common antenna. To be taken into account, a bistatic system with

the separation of transmitter and receiver should be huge enough relative to the usual target size [8].

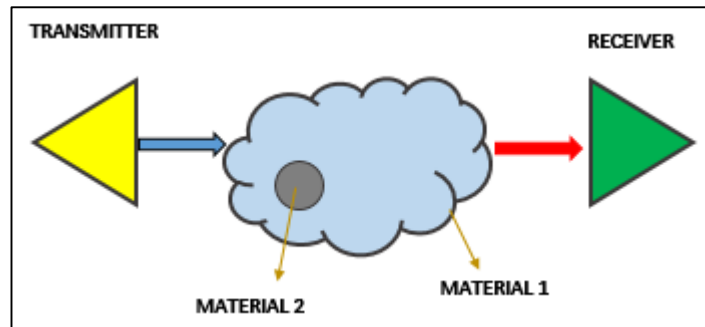


Figure 2. 5: First Bistatic Configuration System

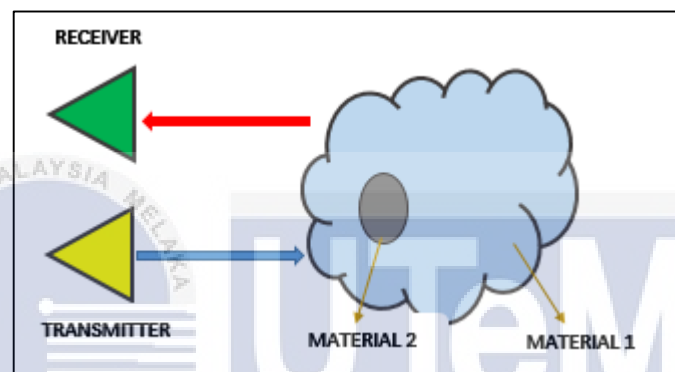


Figure 2. 6: Second Bistatic Configuration System

From Figure 2.5 and Figure 2.6 above, the movement of signal for bistatic configuration could be in either reflected signal or in one transmission line. The blue arrow referring to the transmitting signal, meanwhile the red arrow is the receiver signal movement. This means that, by using the bistatic configuration, the signal will only cover in that one transmission line or on the specific reflected spot on the object. Thus, monostatic and bistatic configurations needs the motor and switching system in order to cover the whole 360^0 object and storing the data for one scan at a time. Hence, it is not a real-time imaging system.

Multistatic consists of multiple transmitter and receiver antennas [8]. It can either be a Multiple Input Multiple Output (MIMO), Single Input Multiple Output (SIMO) or Multiple Input Single Output (MISO). A microwave imaging system that uses

multistatic configuration are extremely fast in term of measurement duration. Since the antenna number increase, the cost of the imaging system also increases. In such a ways, it will increase the sample for screening purposes and provide more information about the image domain as the dimensional and cross-sectional area increases [9].

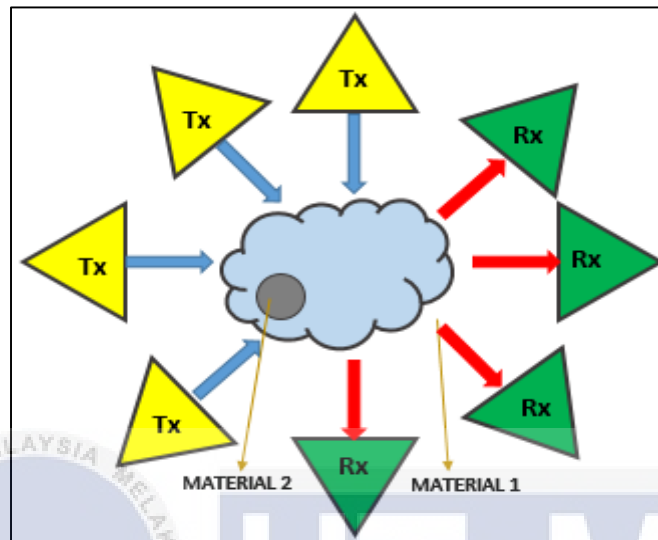


Figure 2. 7: Multistatic Configuration System

From Figure 2.7 above, it clearly be seen that the multiple transmitter and receiver antennas have covered the whole 360° of the object. As mentioned above, that the Multistatic configuration can consist of either multiple input multiple output (MIMO), Single Input Multiple Output (SIMO) or Multiple Input Single Output (MISO). Based on a research, the MIMO configuration used in the system consist of four transmitter and fourteen receiver which is used in the MWI system that is applied to detect the breast cancer [10]. The SIMO configuration consist of one transmitter and fourteen receiver for MWI system and is applied for breast cancer detection [11]. Meanwhile the MISO configuration is used in a research as there are three transmitter and one receiver in the MWI system for a non-destructive testing [12].

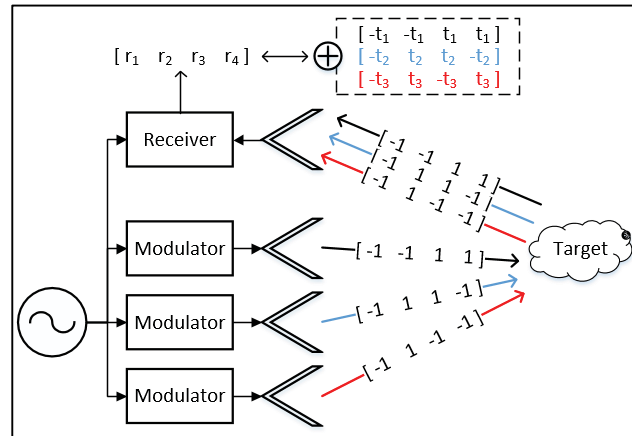


Figure 2. 8: MISO multistatic. [13]

This indicates that multistatic is a more simple system as it does not require a motor and switching system for rotating and storing data. Thus it is less time consuming and proved that multistatic configuration is a real-time imaging system. A research also said that by using a realistic radar-based environment that include 8-element antenna array, it could capture multistatic scattered signal around the image domain to detect brain injuries [14].



Figure 2. 9: MIMO multistatic. [14]

2.3 Microwave Imaging Sensors

The lightweight, smart, and universal sensor architecture is commonly used in radar, microwave imaging, and remote sensing applications. Due to its benefits, ultra-wideband antennas (UWB) have become a common antenna in order to satisfy the needs of the industry. Because of its high data rate and low power consumption, this antenna has piqued the interest of researchers in practical applications. [15]

The relative permittivity and conductivity of malignant tissue are significantly different in ultra-wideband antennas, allowing for adequate penetration depth and spatial resolution. The Vivaldi Antenna, according to analysis, has a radiation characteristic that is compatible with microwave imaging systems [10]. Based on different researcher, the range of frequency for UWB antenna is between 2 – 4GHz, 8.2 – 12.4GHz, and 3.1 – 10.6GHz [15-18]. Vivaldi antenna are vastly used in wireless and radar applications due to their broad bandwidth, low cross polarization and highly directive patterns after some modification by exponentially tapering both the inner and outer edges [16].

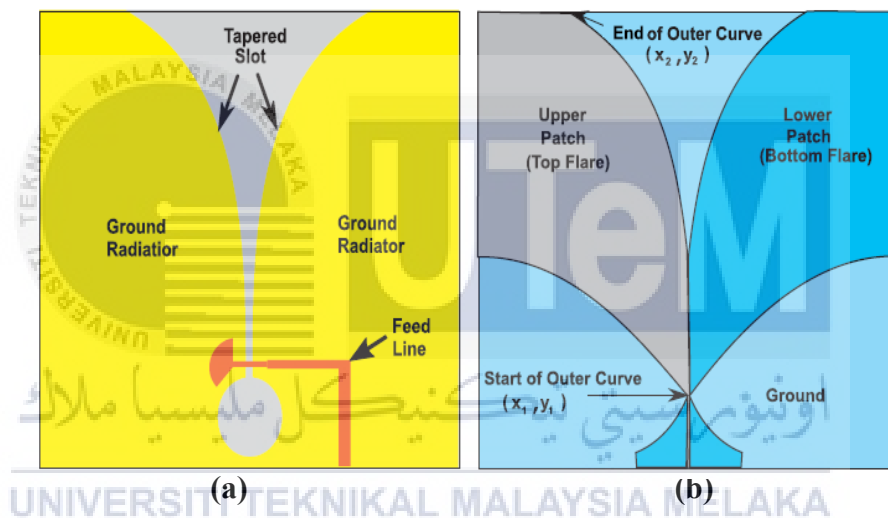


Figure 2. 10: (a) Structure of Vivaldi Antenna. (b) Structure of Antipodal Vivaldi Antenna (AVA) [11]

According to research in [11], Vivaldi antenna can be categorized in three type which is tapered slot Vivaldi antenna, Antipodal Vivaldi antenna (AVA) and Balance Antipodal Vivaldi antenna (BAVA). In their research, the AVA is said to have a high directivity with less signal distortion, good return loss and UWB band pulse shape interference is minimized. The conventional AVA is modified by adding a radiation flare and is specifically designed in the form of elliptical form. The Modified Antipodal Vivaldi antenna (MAVA) is design by using the FR4 substrate with dielectric constant $\epsilon_r = 4.4$,

thickness $h = 1.6$ mm, dielectric loss tangent $\delta = 0.02$ and the dimension of 100 mm x 90 mm [17].

A research by Samira Al'Habsi said that the Vivaldi type antenna is sort of “surfacetype” travelling-wave antenna which are not only efficient and lightweight, but also have the ability to function across a wide frequency range and create a symmetrical end-fire beam with good gain and low side lobes. The immobilized Microstrip-fed Vivaldi antenna with the frequency range of 8 to 23GHz with dimensions of 44.85 x 25.28mm, using the Taconic TLC-32 substrate, which has relative permittivity of 3.2 [18].

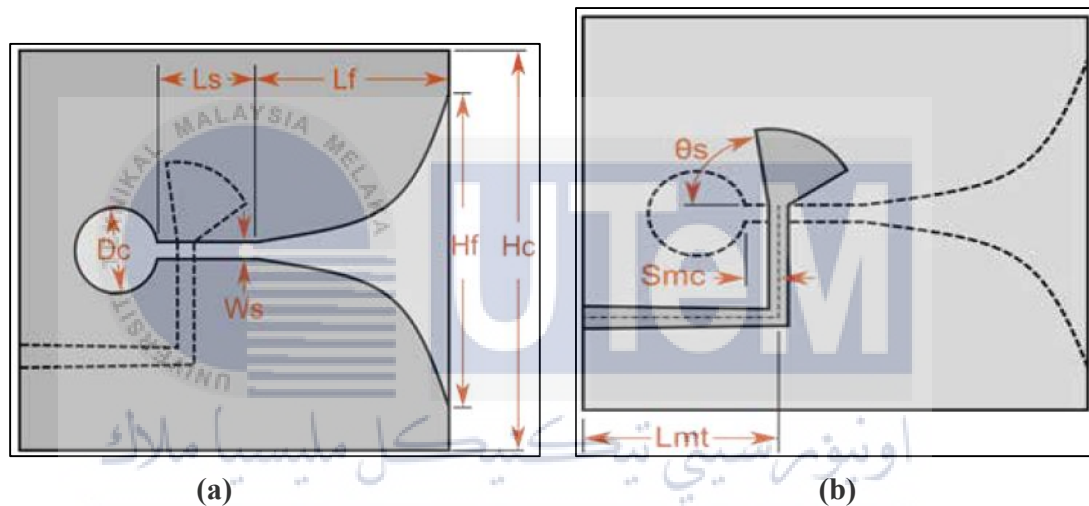


Figure 2. 11: (a) Top view of the Microstrip-fed Vivaldi antenna. (b) Bottom view of the Microstrip-fed Vivaldi Antenna[18]

2.4 Phase Shifter

A 45 degree and 90 degree differential phase shifter that operates in a certain frequency of 3.924GHz in this project. According to S. El Marini, a Ashiffman dual parallel phase shifter is used to develop the 45-degree microstrip phase shifter which is then simulated on the FR4 substrate $\epsilon_r = 4.4$, thickness 1.6 mm, dielectric loss tangent $\delta = 0.02$ using two electromagnetic simulation software, ADS from Agilent technologies and CST Microwave Studio. In term of return loss, insertion loss and phase shifter, the phase shift circuit performs admirably [19].

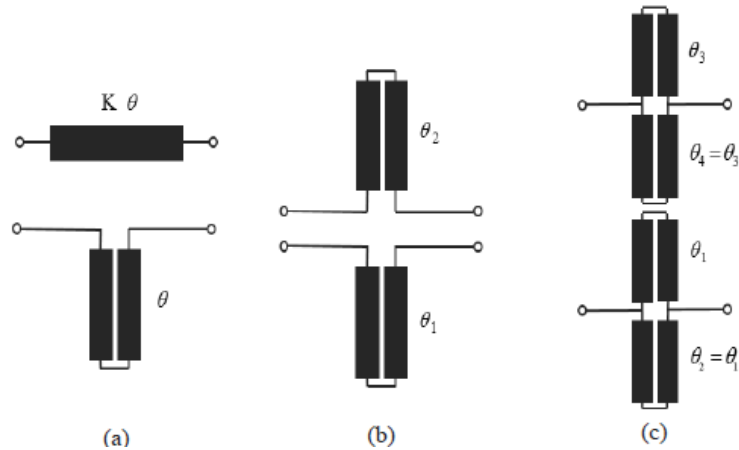


Figure 2.12: (a) Standard Schiffman phase shifter, (b) Double Schiffman phase shifter, (c) Double Parallel Schiffman phase shifter. [19]

The double parallel Schiffman phase shifter is expressed by:

$$\Delta\phi = \cos^{-1} \left(\frac{\rho_{\rho 2} - \tan^2 \theta_3}{\rho_{\rho 2} + \tan^2 \theta_3} \right) - \cos^{-1} \left(\frac{\rho_{\rho 1} - \tan^2 \theta_1}{\rho_{\rho 1} + \tan^2 \theta_1} \right)$$

$$\rho_{\rho 1} = \rho_1 \rho_2 \frac{Z_{001} + Z_{002}}{Z_{001} + Z_{002}}$$

$$\rho_{\rho 2} = \rho_3 \rho_4 \frac{Z_{003} + Z_{004}}{Z_{003} + Z_{004}}$$

Figure 2.13: Layout of the 45 degree double parallel Schiffman phase shifter using (a) CST & (b) ADS. [19]

Other than that, the development of capacitor-based phase shifter for antenna feeding network is also achieved by Diana Desiyanti [20] by using loaded-line phase

shifter technique by placing capacitor chips at the edge between 50Ω and 70.71Ω transmission lines. The feeding network is composed of microstrip transmission lines and impedance matching lines where these transmission belts and impedance matching lines are developed using a quarter-wavelength transformer process and mounted on an FR4 epoxy dielectric substrate with a relative permittivity of 4.3 and a thickness of 1.6mm and the size is 50mm x 300mm [20].

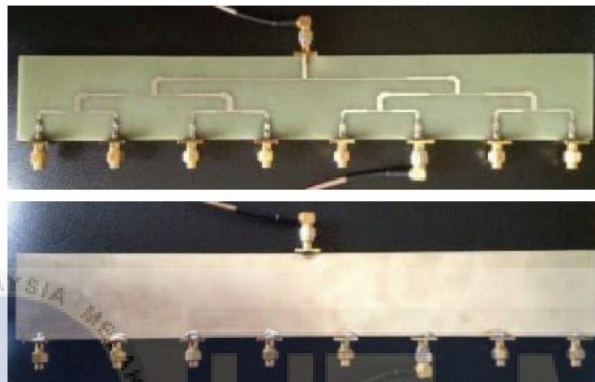


Figure 2.14: Prototype of proposed phase shifter for 8 elements antenna feeding network; top is the upper side; below is the bottom side [20]

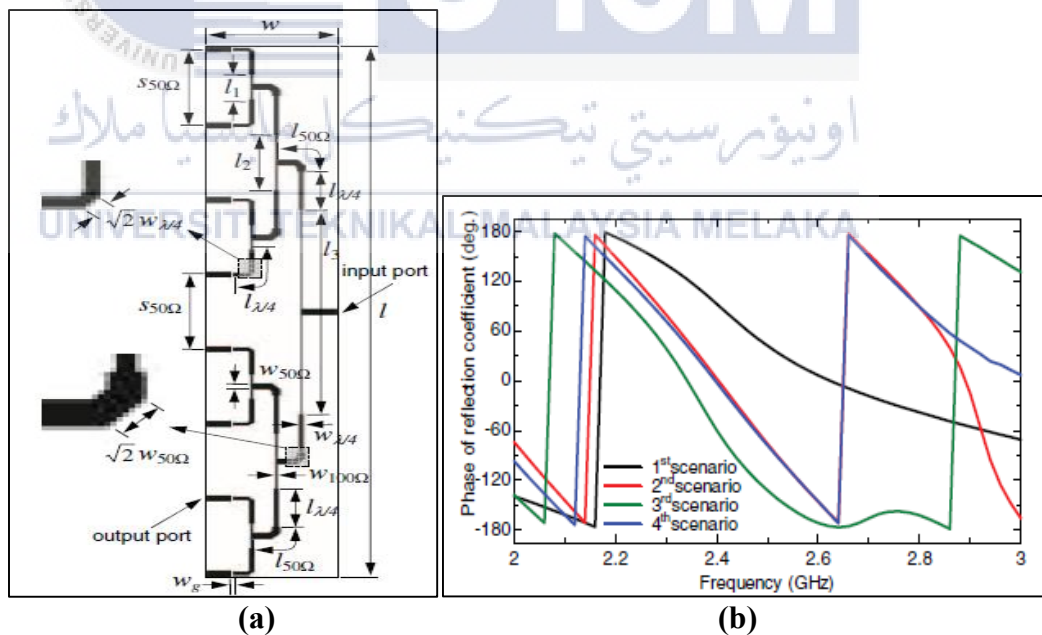
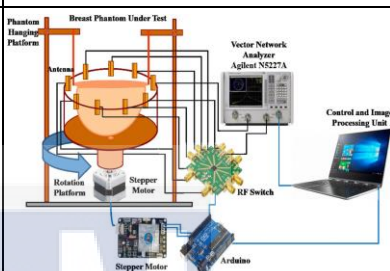

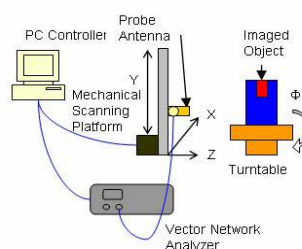


Figure 2.15: (a) A construction of the 8 element phase shifter. (b) Simulation result of coefficient phase for 4 different scenarios. [20]

2.5 Table of Literature Review

Tables below show comparisons of previous research studies about microwave imaging systems, configurations and antenna types. Table 2.1 shows some research on MWI system where most of the system uses frequency range of 1 – 10 GHz with Ultra Wideband antenna for image reconstruction.

Table 2. 1: Review Microwave Imaging System

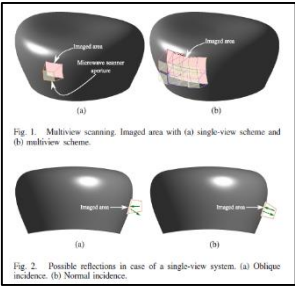
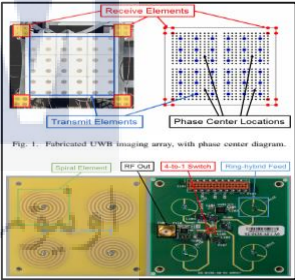
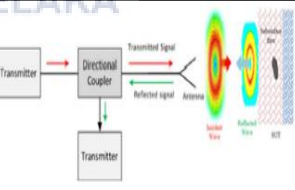
Reference	System	
2019 [1]	<ul style="list-style-type: none"> •Antipodal Vivaldi Antenna (9 array). Switching & rotating system, 1 transmit 8 receive. •Image constructed and display on PC. •Frequency : 3 – 7GHz 	
2018 [2]	<ul style="list-style-type: none"> •UWB antenna for tissue sensing using 31-element hemispherical array. Display on PC. •Frequency : 1 – 10GHz 	
2006 [3]	<ul style="list-style-type: none"> •Tapered slot UWB probe antenna as sensors connected to PC and VNA to control scanning process while scanning the rotated object •Frequency : 3 – 10GHz 	

<p>2016 [4]</p>	<ul style="list-style-type: none"> •Using sensor of planar cavity at K-band frequency. The image demonstrate the ability to perform imaging at diffraction limit. •Frequency : 18 – 26.5GHz 	
-----------------	---	--

Table 2.2 below are the Bistatic and Monostatic researches, where bistatic are using two (2) sensors in the system and signal move either on a transmission line or reflected. Meanwhile, monostatic are using only 1 sensor to transmit and receive the reflected signal.

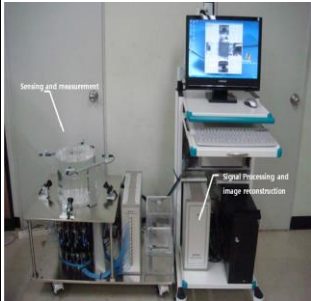
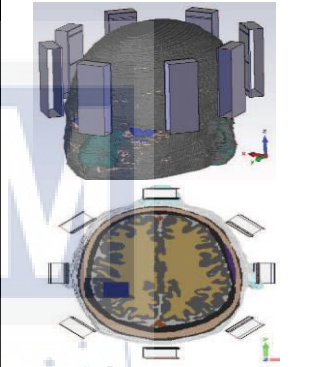
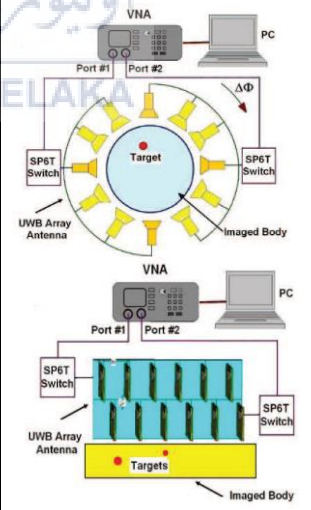
Table 2. 2: Recent study on Monostatic and Bistatic configuration.

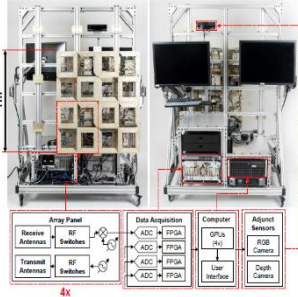
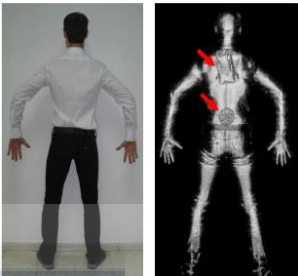
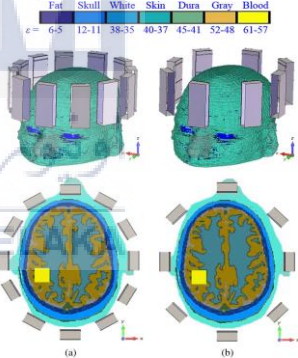
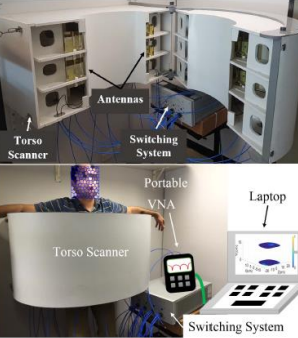
Reference	Sensors	Technique	
<p>Bistatic [5]</p>	<p>Using 2 antennas as receiver and transmitter. Frequency of 8.1 – 9.1GHz</p>	<ul style="list-style-type: none"> • Single conversion technique to display bone of chicken wing with hybrid phase detection algorithm. 	
<p>Bistatic [6]</p>	<p>Using 2 antennas. Frequency range of 17 – 20GHz.</p>	<ul style="list-style-type: none"> • RMA algorithm to create deblurred reflectivity image 	
<p>Bistatic [7]</p>	<ul style="list-style-type: none"> • 2 antennas as transmitter & receiver 	<ul style="list-style-type: none"> • Scan aperture synthesize using 	

	<ul style="list-style-type: none"> •Frequency : 6 – 10GHz 	<ul style="list-style-type: none"> linearized inverse in frequency domain • Using Born approximation for scattering signal 	
Monostatic [8]	<p>Synthetic Aperture Radar (Camera)</p> <ul style="list-style-type: none"> • Frequency : 20 – 30GHz 	<ul style="list-style-type: none"> • Application: real-time 3D microwave camera • Camera used for: multiview portable imager 	 <p>Fig. 1. Multiview scanning: Imaged area with (a) single-view scheme and (b) multiview scheme.</p> <p>Fig. 2. Possible reflections in case of a single-view system. (a) Oblique incidence. (b) Normal incidence.</p>
Monostatic [9]	<ul style="list-style-type: none"> •Circularly-Polarized Array •Frequency : 6 – 10Hz 	<ul style="list-style-type: none"> • Colored depth-coded to detect threat • Switching element using FPGA 	 <p>Fig. 1. Fabricated UWB Imaging array, with phase center diagram.</p> <p>Fig. 2. Possible reflections in case of a single-view system.</p>
Monostatic [10]	<p>Transceiver antenna</p> <ul style="list-style-type: none"> • Frequency : 24GHz 	<ul style="list-style-type: none"> • Illumination wave impinging the subject & deliver reflected wave to receiver antenna 	 <p>Block diagram of a transceiver antenna system showing Transmitter, Directional Coupler, Transmitted Signal, Reflected signal, Antenna, and Receiver.</p>

Next, Table 2.3 are some references on multistatic configurations where they are using multiple sensors with many techniques such as FDTD, reconstruction algorithm, and electronic switching techniques. Those technique are done for higher resolution, better SNR, image reconstruction and others.

Table 2. 3: Recent study on Multistatic configurations.

Reference	Antennas	Technique	
2011 [11]	16 antennas, (switching systems) Frequency : 500MHz – 3GHz	<ul style="list-style-type: none"> • Reconstruct actual dielectric property of tumor. • UWB radar technique for higher resolution and better SNR. 	
2015 [12]	8-element antenna array in CST simulations Frequency: 1 – 3GHz	<ul style="list-style-type: none"> • Using reflected wave to remove tissue layer. • FDTD technique for fast diagnose 	
2011 [13]	12 cylindrical and 12 planar array for scanning mixture to obtain dielectric properties. Frequency : 3 – 11GHz	<ul style="list-style-type: none"> • Microwave Image Reconstruction algorithm to construct image 	

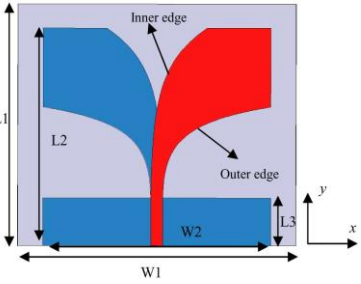
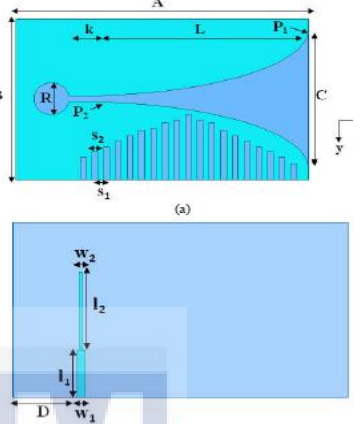
2018 [14]	<p>4 antenna array with 144 transmitter & 144 receiver</p> <p>Frequency : 24 – 29GHz</p>	<ul style="list-style-type: none"> • Send & receive reflected wave by switching • Uses FFT to construct image on PC 	
2013 [15]	<ul style="list-style-type: none"> • 3008 TX and 3008RX (reflected signal) • Frequency : 70 – 80GHz 	<ul style="list-style-type: none"> • Stepped frequency sweep to cover 64steps • Matched filtering method for SAR 	
2016 [16]	<ul style="list-style-type: none"> • 12-element & 8-element (simulation) • Frequency : 1.1 – 3.2GHz 	<ul style="list-style-type: none"> • Frequency-based image reconstruction algorithm to differ every layer of head. 	
2018 [17]	<ul style="list-style-type: none"> • 12-element antenna array (simulation) • Resonant frequency shifting (microwave switching) 	<ul style="list-style-type: none"> • Microwave imaging & radar-based multistatic algorithm to create 2D & 3D image • Frequency-based algorithm 	

	<ul style="list-style-type: none"> • Frequency : 0.75 – 1.75GHz 		
<p>2005 [18]</p>	<ul style="list-style-type: none"> • 4-element horn antenna receive signal in reflected wave • 7.5 – 12.5GHz 	<ul style="list-style-type: none"> • Using electronic switching in VNA. • High spec PC for stepping motor driver to rotate object 	
<p>2013 [19]</p>	<ul style="list-style-type: none"> • 16-element array (switching system) • 2 – 4GHz 	<ul style="list-style-type: none"> • Transmit short duration pulse & collect signal scatter within breast • Frequency-domain & time-domain measurement 	
<p>2015 [20]</p>	<ul style="list-style-type: none"> • Radio-frequency switch between antenna • Transmit short pulse at a time. Receive backscatter response. • 50MHz – 13GHz 	<ul style="list-style-type: none"> • Radar-based qualitative approach, TSAR algorithm. 	

For table 2.4 below are the researches on types of antennas used as sensors in MWI system. The Vivaldi antenna that operates on 1 – 10GHz are mostly used in this system.

Table 2. 4: Recent study on Antenna design used in MWI system.

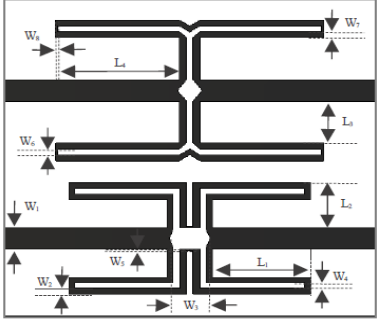
Reference	Antenna	Frequency	Config	
[1] 2019	Antipodal Vivaldi antenna	3 – 7GHz	Multistatic	
[2] 2018	UWB Vivaldi antenna	1 – 10GHz	Multistatic	
[12] 2015	Multistatic array antenna	1 – 3GHz	Multistatic	
[16] 2016	Multistatic antenna	1.1 – 3.2 GHz	Multistatic	
[18] 2016	Vivaldi Antenna	8 – 23GHz	Multistatic	
[19] 2019	Vivaldi antenna	8 – 13GHz	Multistatic	

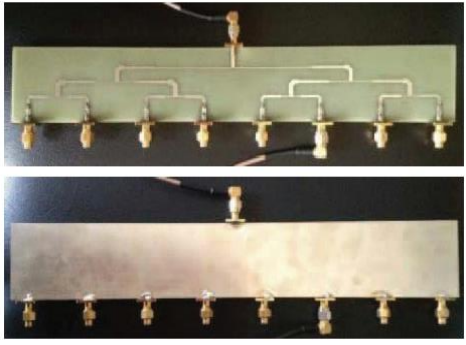
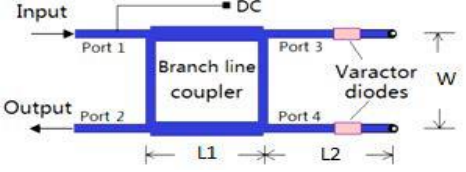
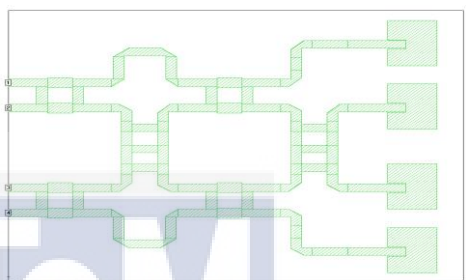
[21] 2008	Uwb antipodal 24ivaldi antenna	3.1- 10.6GHZ	Multistatic	
[22] 2016	Corrugated Tapered Slot antenna	7.5 – 12.5GHZ	Multistatic	

Lastly, on table 2.5 are the studies on phase shifter design. There are many type of phase shifters that uses frequency range of 1 to 5GHz. However, those phase shifter are way too complicated for this project.

UNIVERSITI TEKNIKAL MALAYSIA MELAKA

Table 2. 5: Recent study on Phase Shifter.

Reference	Type	Frequency	
[19] 2017	Double Parallel Schiffman coupled lines.	1.4 to 2.7GHz	

[20] 2015	Capacitor-based	2.4GHz	
[23] 2020	Tunable phase shifter	2GHz	
[24] 2010	Butler Matrix	5.2GHz	

2.5 Summary

Commonly, in MWI system, the uses of computer as a platform to show the analogue-to-digital conversion (ADC) and then display its end of result. According to [14] [21] the power density calculated inside the image domain is stored in a computer with 3.4GHz CPU and 16GB RAM. Other than that, a personal computer to measure a positioner rotation, instrument control, system calibration and data recording was used in [22]. The computer will also perform all sort of conversion, calculation and as a platform with the help of software such as MATLAB, ADS, CST and other related software. There have many studied about the microwave imaging system, MWI configurations, type of antenna used in MWI and phase shifter applied in MWI. These study aimed to characterize each of their subject-under-test with their very own specifications. Although there is a similarity among the past research studies in terms of their goals, they however differ in terms of performance achievement.

CHAPTER 3:

METHODOLOGY



The project approach is covered in this chapter, which includes a flowchart depicting the project methodology which includes design system specifications, design process, a parametric research on antenna parameter using CST software, signal processing unit and measurement process.

3.1 Overview of the Project

This project first examines MWI and its differences with other imaging methods such as MRI, X-Ray and CT. These techniques were compared to prove the important value of MWI for this project. Currently, three types of configurations are determined in MWI, namely, Monostatic, Bistatic and Multistatic configurations and the sensor selected for this system is Vivaldi antenna. From then, further research on phase delay was conducted to gain information and knowledge to come up with the required antenna's specifications. The CST Studio Suite Software is used to design and simulate the proposed phase shifter once it has met the required specifications. Upon satisfaction of the simulation result, the fabrication process will take place. The microcontroller is then configured to transfer the signal from RF detector to TFT screen display.

The system developed for the research project is shown in the form of a flow chart. The steps of the complete research endeavor are summarized in Figure 3.4. The flowchart include the full process for sensors, RF detector and signal processing units.

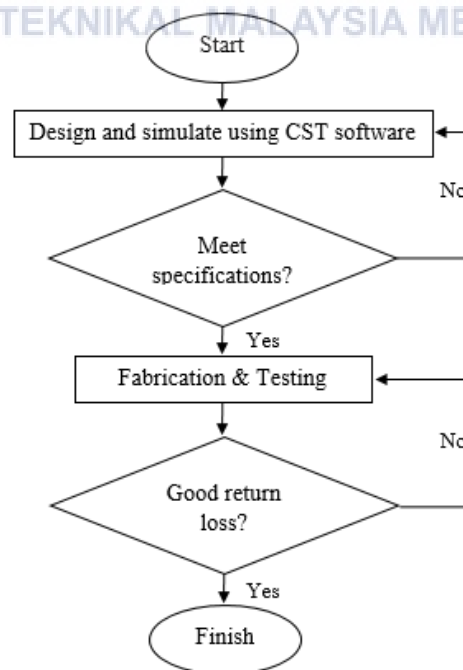


Figure 3. 1: Flowchart for Antenna Design

From Figure 3.1, the antenna is designed and simulated in CST software for all specification. There were 6 designs of antenna for different phase shifter which include the 0° , 45° , 90° , 135° , 180° , and 270° . When all results are in good condition, it will then go through fabrication and testing process.

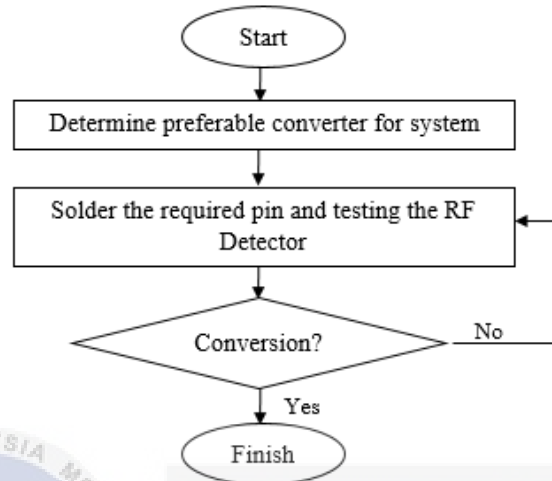


Figure 3. 2: Flowchart for RF converter.

Figure 3.2 shows the flowchart from choosing the suitable RF Detector module for the system specification to the conversion result of the tested RF detector module is compared to the module datasheet.

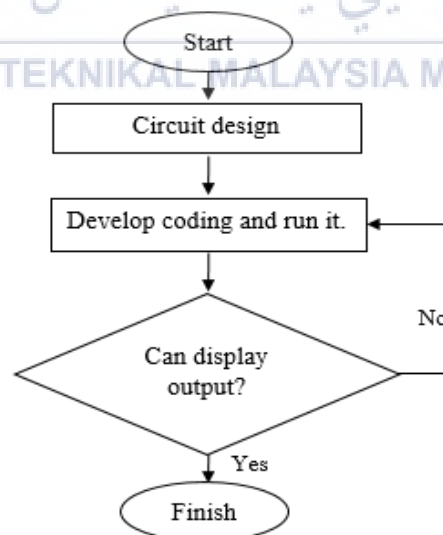


Figure 3. 3: Flowchart for Signal Processing Unit.

Figure 3.3 shows the coding process on signal processing unit which includes Arduino MEGA and TFT screen display. The circuit is designed before developing

the coding referring to its datasheet. When coding is develop according to the connection on circuit, run on the microcontroller to test its functionality and output display.

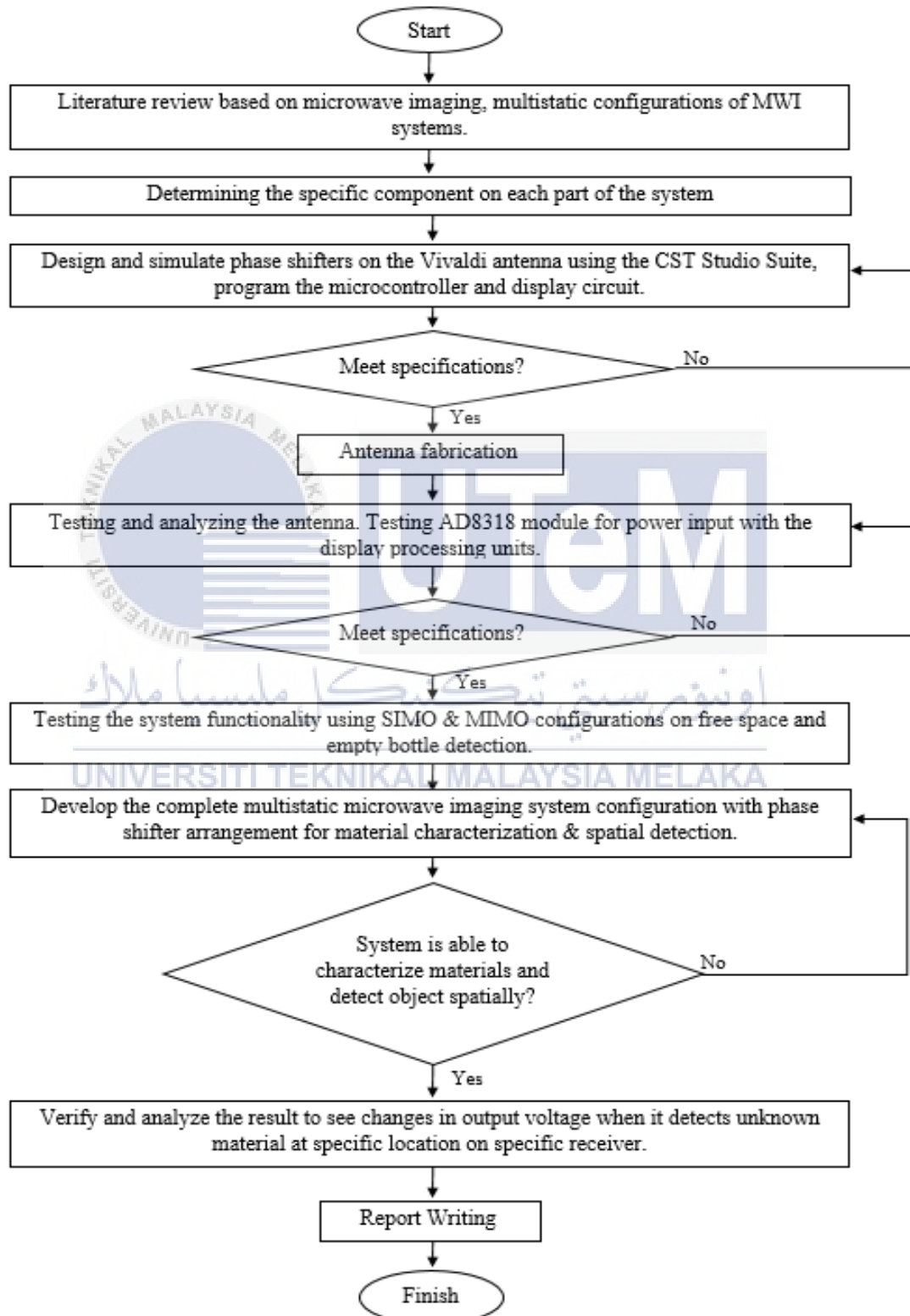


Figure 3. 4: Flowchart for whole full system.

3.2 Microwave System Development

The development of MWI system consist of four (4) major components which are sensor to transmits and receive signal, ADC converter to convert the signal from analog to DC voltage, signal processing units which uses microcontroller to process the signal to be displayed and the display units to show output. There are 3 types of system configuration to be tested in this project. First, single input multiple output (SIMO) that uses 1 transmitter and 2 receivers. The SIMO (1x2) will be tested for every phase shifter and observed its output voltage value on free space (air). Second configuration is multiple input multiple output (MIMO) (2x2) that uses 2 transmitter and 2 receivers to tests all the 0^0 phase shifter on free space and empty bottle. Lastly, multiple input multiple output (MIMO) (4x4) that is use for material characterization and spatial detection. Figure 3.5 below shows the overall block diagram of MIMO (4x4) for MWI system in this project and table 3.1 shows the design specification of the system.

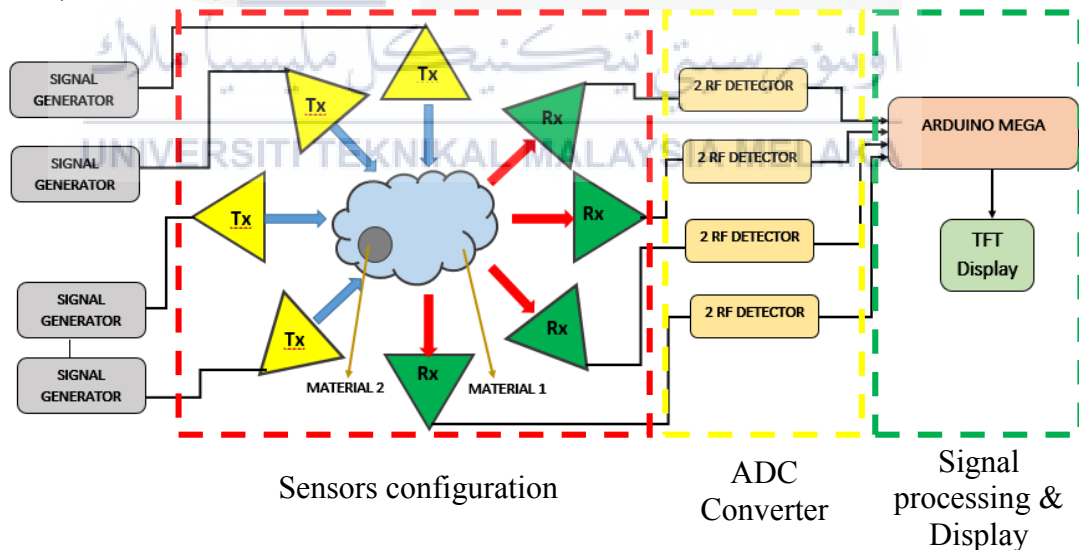


Figure 3. 5: Overall block diagram system for MWI system with multistatic configuration.

Table 3. 1: System design specification

Parameters	Value
------------	-------

Operating frequency , f	3 GHz – 6 GHz
Input power, P _{in}	15dBm
Supply voltage, V _{in}	9V
Distance, d (diameter of bottle)	10cm

3.3 Microwave Sensor Design

3.3.1 Microwave Sensor Design Process

A Wideband Tapered Slot Vivaldi Antenna is chosen for this project, based on [25], which is using the idea of sending microwave waves (between 1-4GHz) into the human brain and detecting the reflected signals created by the high dielectric constant between electrical characteristics of healthy and stroke-affected tissues. This antenna achieves unidirectional radiation pattern with a broadside gain of 2.9dB and front-to-back ratio of 14.6dB.

CST-Software is used to design and simulate the antenna which operates at a frequency range of 3GHz to 6GHz and return loss of below -10dB. The input impedance is 50Ω with the resonance frequency of 3.924GHz and gain of 6.43dBi. The efficiency of this antenna is more than 80% with the value of directivity of 8.33dBi. Table 3.1 below shows the list of design specification for the proposed antenna.

Table 3. 2: Microwave sensor specification

Specification	Value
Operating frequency	3 – 6 GHz
Lowest return loss	-43.19dB

Input impedance	50 Ω
Resonance frequency	3.924GHz
Radiation Pattern	Directional
Gain	6.43dBi
Efficiency	>80%
Directivity	8.33dBi

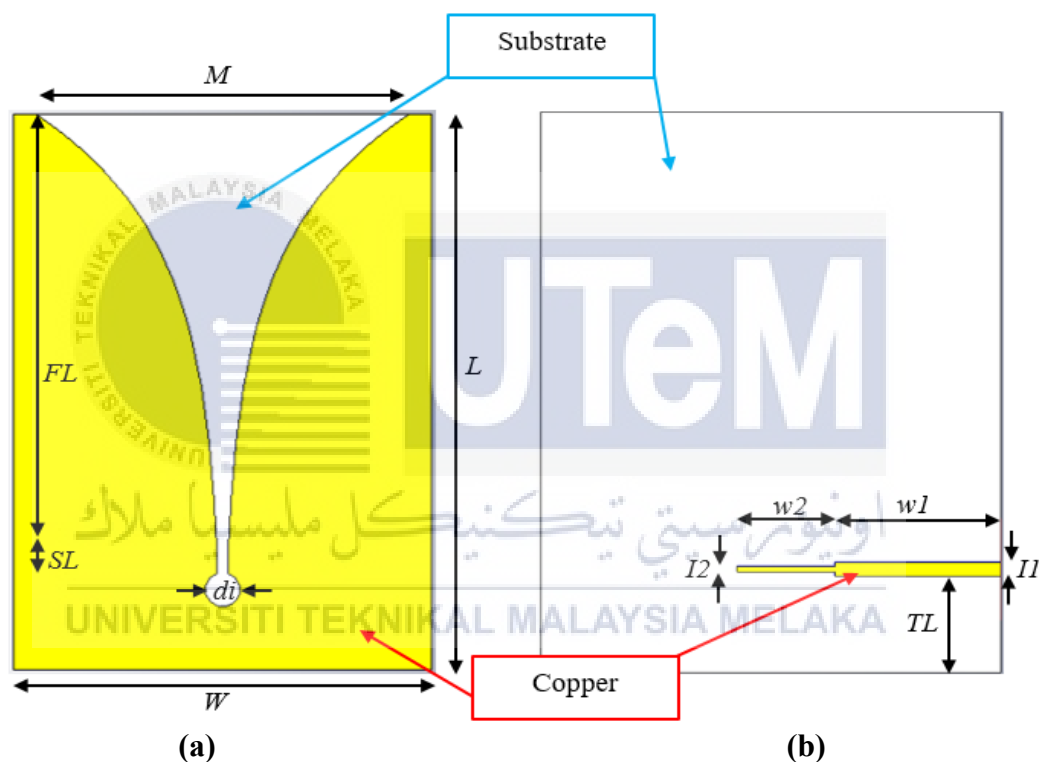


Figure 3. 6: (a) Front view (b) Rear view

Figure 3.6 is the Vivaldi antenna used in this project. The antenna is design on FR4 substrate board with thickness, h of 1.6mm and the dielectric constant, ϵ_r of 4.3. The dimension of the antenna is 104mm x 75mm. The design structure, parameter and its exponential taper which defined by the opening rate C is listed in table 3.2 and 3.3 below.

Table 3. 3: List of antenna's parameter

Parameter	Description	Value (mm)
W	Width of the substrate	67
L	Length of the substrate	104
M	Opening mouth of the flare	75
FL	Flare length	82
SL	Slot line	4
di	Diameter	6
TL	Feeding line gap	18
I1	Width of first feeding line	2.5
I2	Width of second feeding line	1
W1	Length of first feeding line (50Ω)	27
W2	Length of second feeding line	16

The design process for this antenna are using the formula in table 3.3 below.

Hence, the exact length and width can be determined for the range frequency used for this antenna. Meanwhile the exponential formula is to design the tapered slot and opening mouth of the Vivaldi antenna. Some of the parameters such as the flare length and diameter are using a parametric study process in order to achieve the good return loss and bandwidth.

Table 3. 4: Mathematical Equations of Vivaldi Antenna

Description	Equation
Length, L	$L \approx \frac{C}{f \sqrt{\epsilon r}}$

Width, W	$W \approx \frac{1}{2} \times \frac{C}{f \sqrt{\epsilon_r}}$
Exponential function	$y = Ae^{Bx} + B$
Opening mouth	$\pm \frac{MO}{2} = \pm \frac{A}{2} \times \exp^{r \cdot La}$

Next, the design of phase shifter of 45^0 and 90^0 which is determined by the length of feeding line at impedance of 50Ω . However, phase shifter only works in one specific frequency, which is 3.924GHz. This frequency is chosen based on the resonance frequency at original antenna. Table 3.4 below shows the equations for determining the length of every phase shifter and Table 3.5 shows the total calculated length for the phase shifter.

Table 3. 5: Equation for length of the transmission line.

Description	Equation
Effective dielectric constant	$\epsilon_e = \frac{\epsilon_r + 1}{2} - \frac{\epsilon_r - 1}{2} \cdot \frac{1}{\sqrt{1 + 12\left(\frac{d}{W}\right)}}$
Guided wavelength	$\lambda_g = \frac{c}{f \cdot \sqrt{\epsilon_e}}$

Table 3. 6: Length of feeding line for every phase shifter at the 50Ω line impedance.

Phase shifter at 50Ω	Length (mm)
Normal feeding line (0^0)	27
45^0	59.5
90^0	64.68
135^0	70

180 ⁰	33.16
270 ⁰	44.26

3.3.2 Simulation Process

CST Studio Suite 2019 is used for designing and simulate the antenna with its phase shifter. The antenna is designed according to the parameters on table 3.2 and 3.5. The simulation has been completed and all of the findings are available in Appendix C, which the discussion is presented in Chapter 4. The simulation are done in frequency range of 3 – 6 GHz. After the simulation step is finished, the antenna pattern is printed and fabrication process may begin.

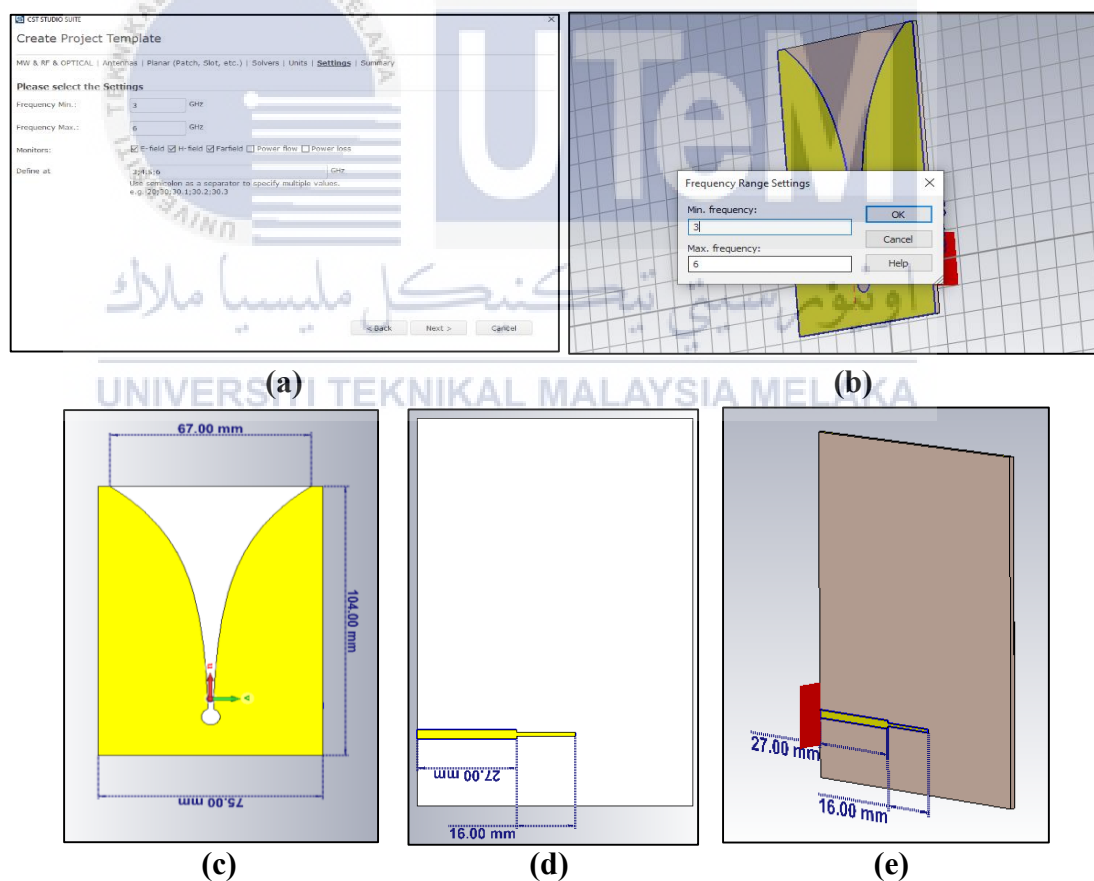


Figure 3. 7: (a) Setting for the designed antenna with 3 – 6GHz operating frequency and the E-field, H-field and Farfield monitor are tick for simulation process. (b) Frequency range setting for simulation. (c) front view of Vivaldi antenna. (d) rear view of the antenna. (e) perspective view of the antenna with port.

3.3.3 Fabrication Process

After the simulation result have been obtained, the fabrication process will then take place. The antenna is printed on the tracing paper using Corel software. As mentioned above, the antenna is constructed on the FR4 substrate. The fabrication process are as figure 3.8 below. Firstly, draw the antenna using CorelDRAW software and make sure all regions are being colored properly. Next, print the drawing on tracing paper and then by using UV ray exposure, the drawing is stamped on the FR4 substrate board. At the etching machine and resist layer strip station, the unwanted copper is being removed from the board.

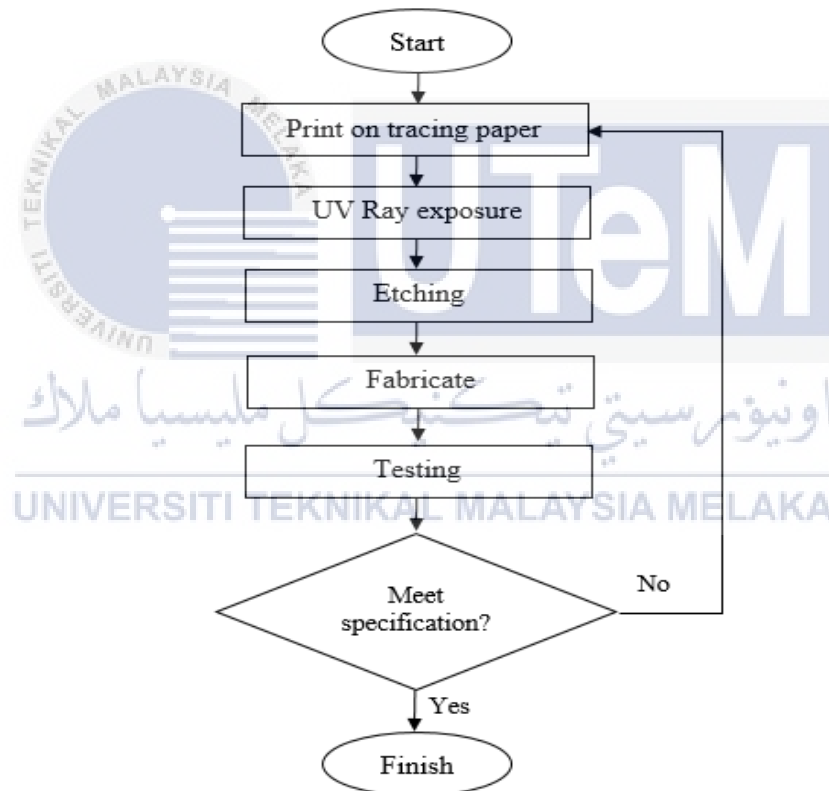


Figure 3. 8: Fabrication process

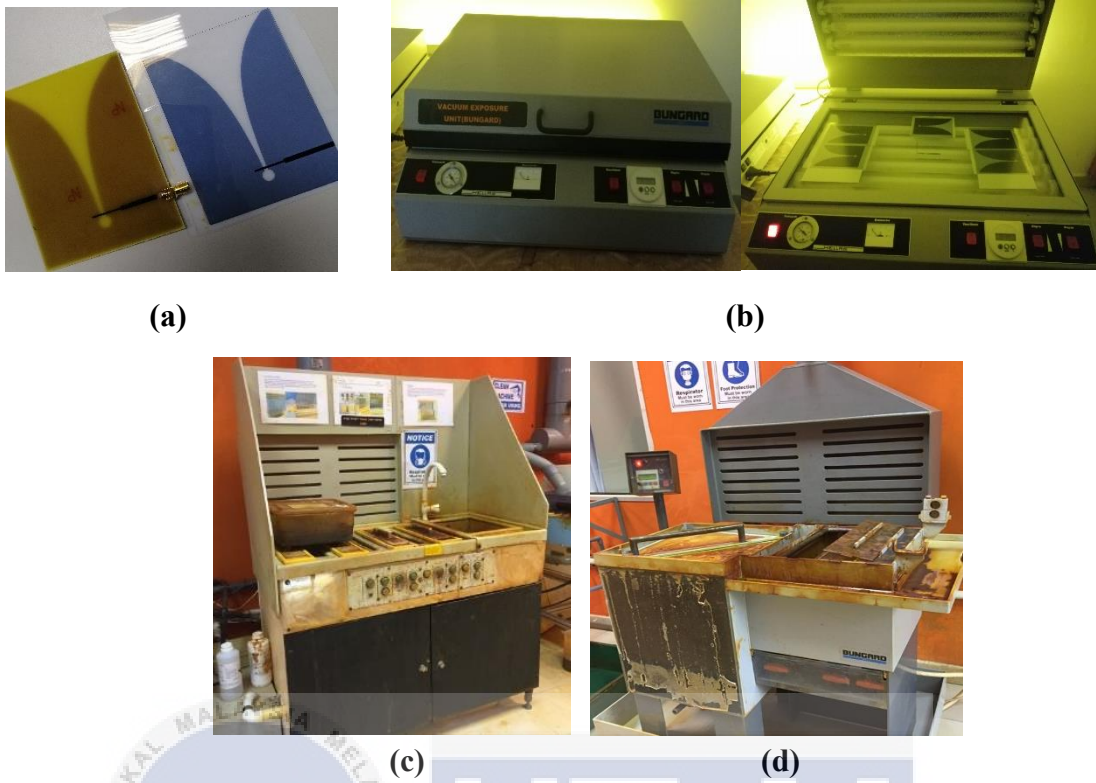


Figure 3. 9: (a) Printed antenna design on tracing paper. (b)UV exposure machine to print the antenna from tracing paper to FR4. (c) Etching station. (d) Resist layer strip station.

After finished the fabrication process, where it remove the copper on the substrate, clean the antenna using tap water and dries it out using drying machine before cutting the antenna on its specific shape. Lastly, solder the SMA (Sub Miniature Version A) connector to the feeding line of the antenna.

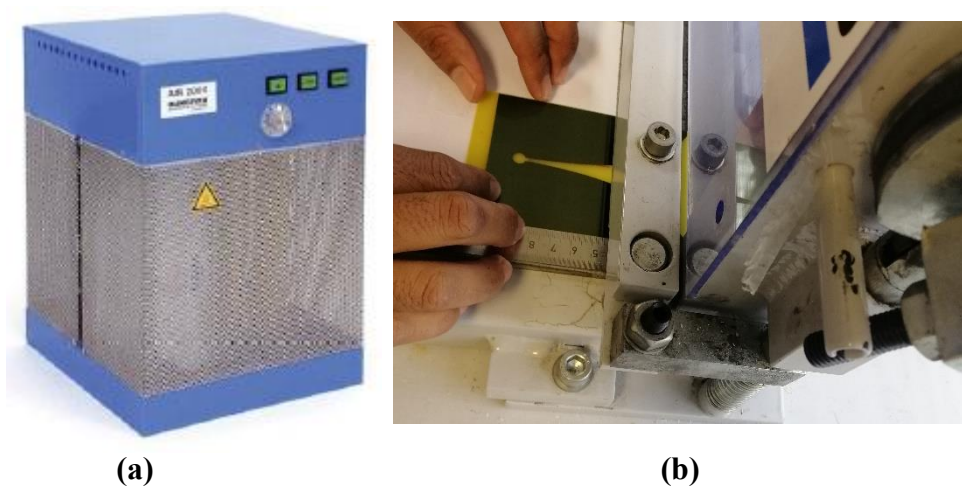


Figure 3. 10: (a) Drying Machine (b) Substrate Cutter.

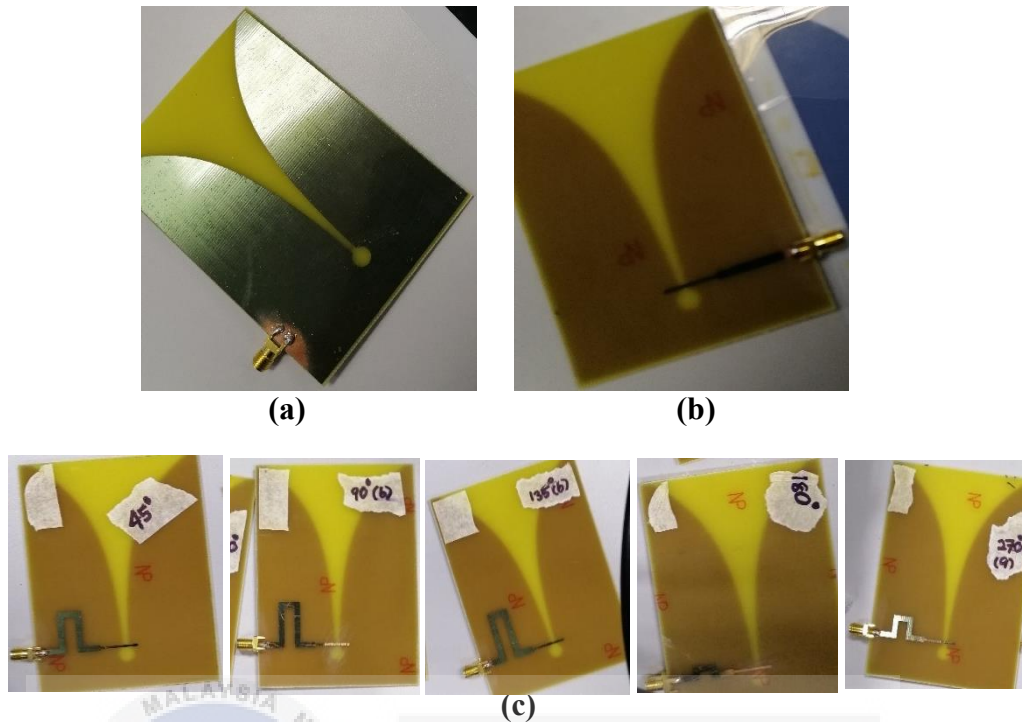


Figure 3. 11: (a) Front view & (b) Rear view of fabricated Vivaldi antenna on the FR4. (c) The fabricated Phase shifter on Vivaldi Antenna.

3.4 Signal Processing Unit

The signal processing unit includes 4 RF detectors AD8318 module, an Arduino MEGA 2560 and a 3.5 inch TFT display.

3.4.1 RF to DC Converter

The chosen RF Detector for this system is the AD8318 module which the operating frequency is 1 to 8GHz with input power between 5dBm to -65dBm, supply voltage of 7V to 15V and producing the output voltage in range of 0V to 2V. This module is also much affordable compared to other RF detector module. In order for this RF detector to work with the system, its DIP pin need to be soldered at the Vcc, Ground and Output Terminal so that it can connect to other component on the system. The Datasheet of this module is attached in Appendix E.

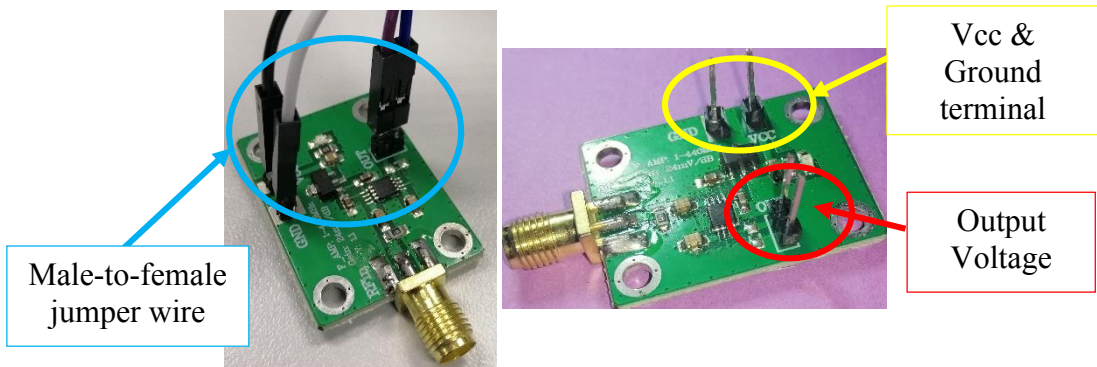


Figure 3. 12: Jumper wire connection and Soldered DIP Pin on AD8318.

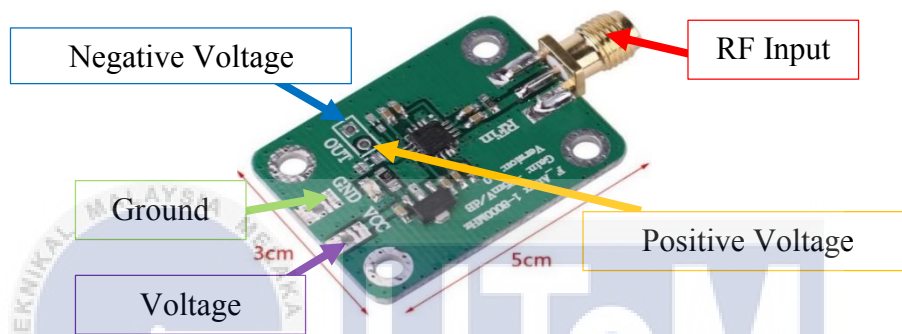


Figure 3. 13: RF detector AD8318 Module.

3.4.2 Microcontroller.

This project is using Arduino MEGA 2560 as the processing unit. Instead of using other Arduino modules, this module is the most suitable as it has many output pin and also large memory to store the coding. Arduino is also less complicated processing unit to be programmed as long as the library is installed in the Arduino IDE software.

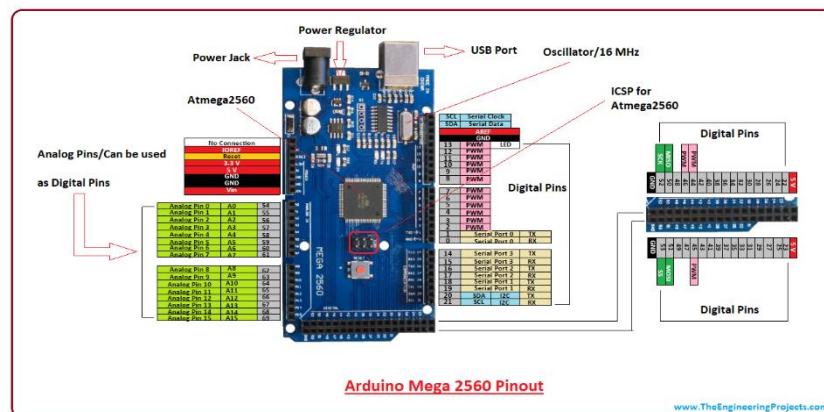


Figure 3. 14: Arduino MEGA 2560 Pinout

Next, for the display module, this system is using the 3.5" TFT screen display that is a portable touchscreen display module which is bigger than usual LCD display. This module is also chosen as it can display all 4 Receiver output at the same time. It can also display the output not just in number form but also in graph.



Figure 3. 15: 3.5 inch TFT display output pin.

Figure 3.16 below are the connection of Arduino MEGA and the TFT screen as a processing unit for this system. The analog input pin A7, A8, A9, and A10 of Arduino is connected to the output pin of RF detector AD8318 module.

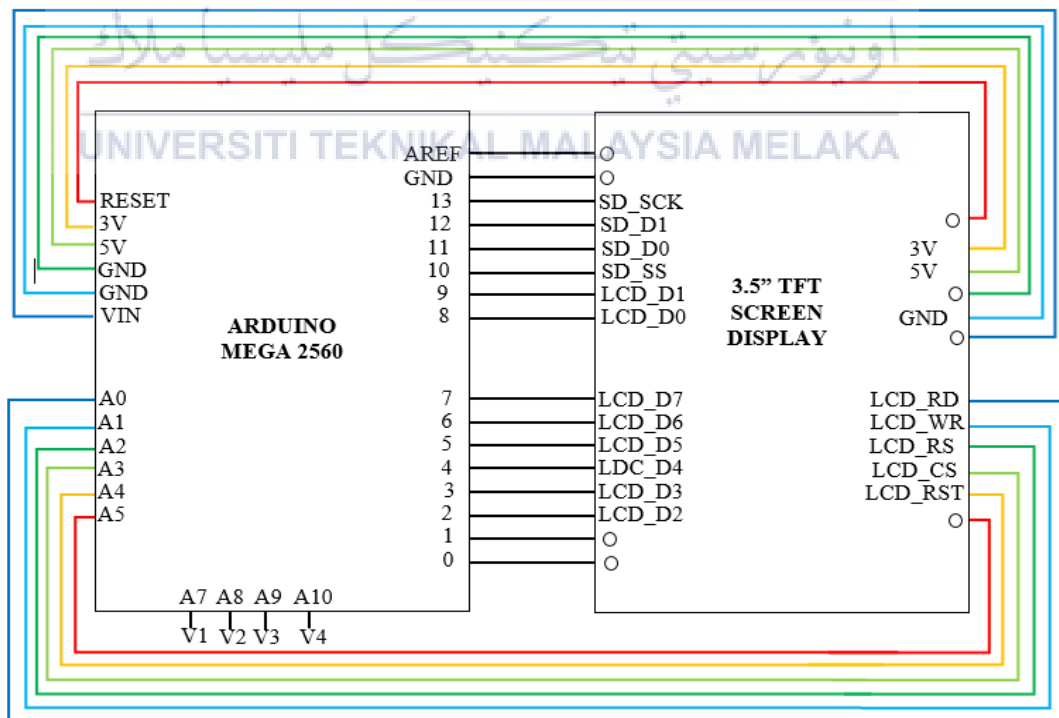


Figure 3. 16: circuit connection between Arduino MEGA and TFT screen

The coding for Arduino to display the value of output voltage from RF detector module on TFT screen is written on the Arduino IDE software. Below are some of the main function of the coding, meanwhile for the full coding can be found in Appendix A.

```
#include <UTFTGLUE.h>
UTFTGLUE myGLCD(0x9488, A2, A1, A3, A4, A0);

#include <Adafruit_GFX.h> // Core graphics library
#include <MCUFRIEND_kbv.h> // Hardware-specific library
MCUFRIEND_kbv tft;
```

Figure 3. 17: Library Call

From Figure 3.17, the *MCUFRIEND_kbv* is the library to run the TFT screen hardware as it is developed by the MCUFriend developer. Meanwhile the *Adafruit_GFX* is the core graphic library from Adafruit developer in order to run the TFT graphic visual output.

```
float voltage1 = analogRead(A7) * (5.0 / 1024.0);
float voltage2 = analogRead(A8) * (5.0 / 1024.0);
float voltage3 = analogRead(A9) * (5.0 / 1024.0);
float voltage4 = analogRead(A10) * (5.0 / 1024.0);
float x1 = voltage1 * -18.8016;
float x2 = voltage2 * -18.8016;
float x3 = voltage3 * -18.8016;
float x4 = voltage4 * -18.8016;

if ((voltage1 < 0.1) && (voltage2 < 0.1) && (voltage3 < 0.1) && (voltage4 < 0.1))
{
  voltage1 = 0.0;
  voltage2 = 0.0;
  voltage3 = 0.0;
  voltage4 = 0.0;
}
```

Figure 3. 18: Analog input

Figure 3.18 is the analog input setup. *Voltage1*, *voltage2*, *voltage3* and *voltage4* is connected to *analogRead* pin at *A7*, *A8*, *A9* and *A10* respectively. The conversion of the received power to the corresponding voltage is represent by the *x1*, *x2*, *x3* and *x4* values.

<pre>tft.fillScreen(BLACK); tft.setTextColor(WHITE); tft.setTextSize(1); tft.setCursor(30, 75); tft.print("Voltage 1:"); tft.setCursor(150, 75); tft.print(voltage1); tft.setCursor(30, 150); tft.print("power 1:"); tft.setCursor(120, 150); tft.print(x1); tft.setCursor(270, 75); tft.print("Voltage 2:"); tft.setCursor(390, 75); tft.print(voltage2); tft.setCursor(260, 150); tft.print("power 2:"); tft.setCursor(350, 150); tft.print(x2);</pre>	<pre>V"); dBm"); V"); dBm");</pre>	<pre>tft.setCursor(30, 225); tft.print("Voltage 3:"); tft.setCursor(150, 225); tft.print(voltage3); tft.setCursor(30, 300); tft.print("power 3:"); tft.setCursor(120, 300); tft.print(x3); tft.setCursor(270, 225); tft.print("Voltage 4:"); tft.setCursor(390, 225); tft.print(voltage4); tft.setCursor(260, 300); tft.print("power 4:"); tft.setCursor(350, 300); tft.print(x4); delay(10);</pre>
--	------------------------------------	---

Figure 3. 19: Voltage and power display

Figure 3.19 shows the received output voltage and power conversion are presented on the TFT screen. The *tft.setCursor(x,y)* command is used to set the coordinated of the position on the TFT screen where the *voltage1* is shown when *tft.print()* command is performed. *X* is the x-coordinate value and *y* is the y-coordinate value.

3.4.3 TFT Display

Figure 3.20 shows that the TFT's output is presented in the form of numbers. Due to the four inputs from the four AD8318 modules, the TFT displays four voltages ranging from voltage 1 to voltage 4.

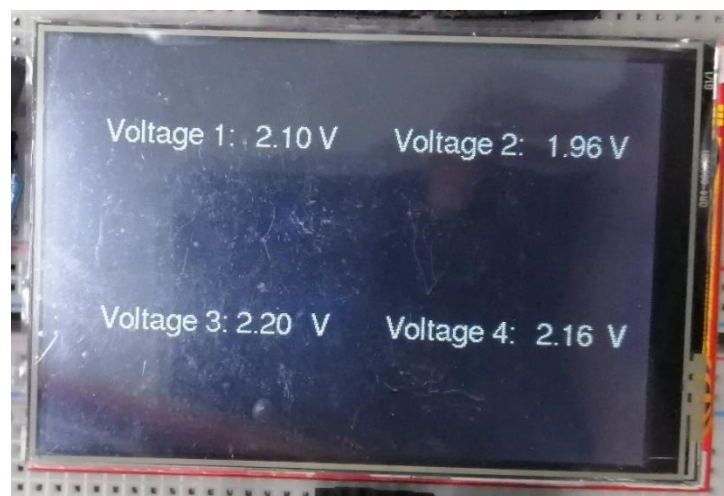


Figure 3. 20: TFT Screen display

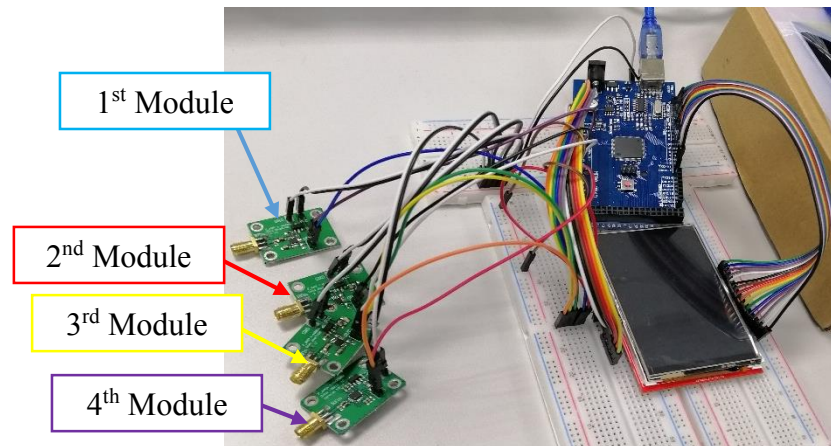


Figure 3. 21: AD8313 connection with Arduino and TFT screen

The voltage received from first module, which is linked to analogue pin A7, is Voltage 1, which is linked to analogue pin A7, is Voltage 1 is power 1. Voltage 2 is the voltage value received at analogue pin A8 from second module. Voltage 3 is the voltage value received from the third module connected to pin A9 and Voltage 4 is the voltage value received from the fourth module which connected to analogue pin A10. Table 3.6 below shows the output connection summary between AD8318 module, Arduino MEGA and TFT screen display.

Table 3. 7: Connection summary

Receiver	Module	Analog Pin	Voltage
1	1	A7	1
2	2	A8	2
3	3	A9	3
4	4	A10	4

3.5 Microwave Imaging System Testing

When all components are ready and being assembled as a full system, it is time to test the functionality of the developed system. Test with two different number of transmitter and receiver as in Table 3.7 below. At the beginning of the test, the air is going to be the material under test for this system.

Table 3. 8: Configuration for system testing

Configuration	Number of transmitter & receiver	Test subject
SIMO (Multistatic)	One transmitter, two receiver (1 x 2)	Air (free space)
MIMO (Multistatic)	Two transmitters, two receivers (2 x 2)	Air (Free space)
		Empty Bottle
	Four transmitters, four receivers (4 x 4)	Air
		Empty Bottle
		Material 1
	Material 1 + Material 2	

3.5.1 Calibration Process

Identifying the power input to be used for the whole system by using spectrum analyzer which connected to the laptop using the SynthHD software as the power supply under a specific frequency, 3.924GHz. The test was done to determine suitable value of power input is suitable for the AD8318 module.

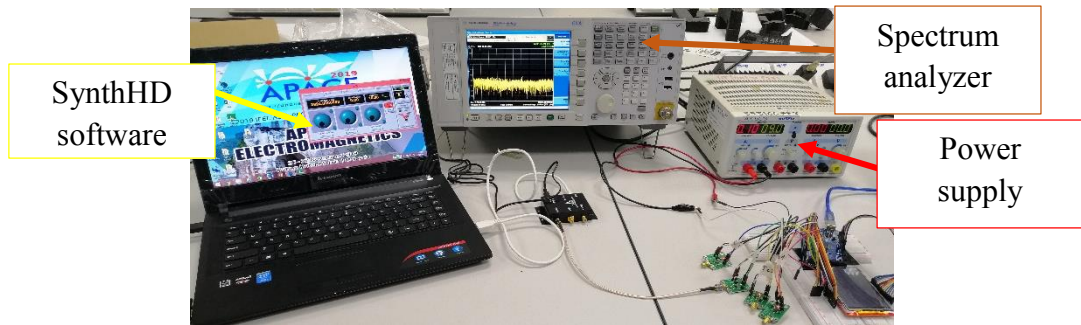


Figure 3. 22: Identifying Power Input for system (wired)

The value of power received is measured and the results are as in Appendix B. Besides determining the input power, all material to be used in this system such as water, soap, flour, sand, sugar, metal, plastic and so on need to test its dielectric properties before testing it in the system. This calibration is necessary in order to test the system accuracy for spatial object detection. Results for dielectric testing can be found in Appendix B.

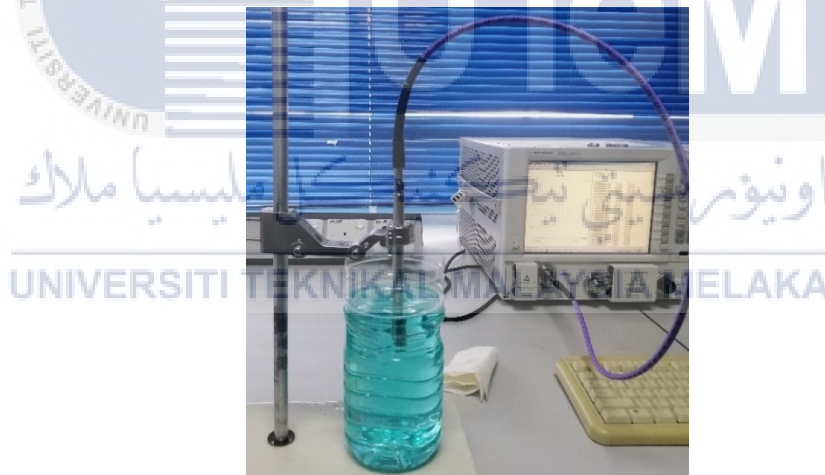


Figure 3. 23: Dielectric measurement process.

3.5.2 Single Input Single Output (1x1)

This SISO configuration is to test the path loss on every receiver. The testing only uses 2 antennas like the bistatic configuration, arranged as in the figure below.

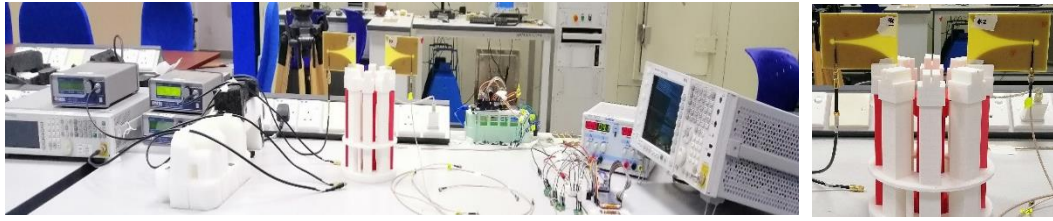


Figure 3.24: Measurement Setup in SISO configuration.

The result is then compared to the calibration process on subtopic 3.5.1 in order to observe the losses. This system specification is also using the same parameter as in Table 3.1.

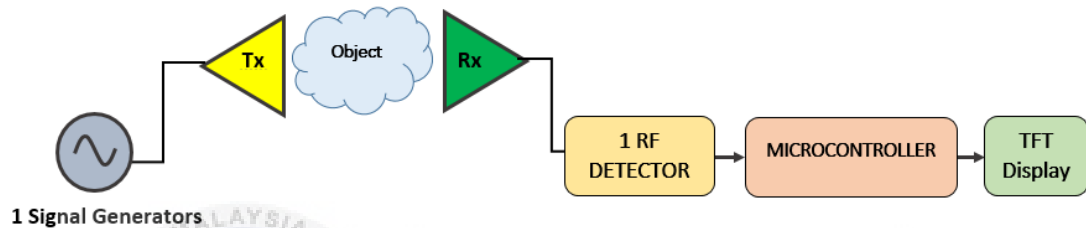


Figure 3.25: Block diagram of SISO measurement

As the output voltage of TFT screen keeps on fluctuating, an average of 10 values is taken from every reading to get the actual output voltage value. The value of the voltage is then converted to power by using this formula:

$$P_r = V_o \times \left(-\frac{1}{0.025} \right)$$

3.5.3 Single Input Multiple Output (1 x 2)

This configuration contain of two transmitters and two receivers. It is arranged as in Figure 3.24 to be tested on two conditions which are air and empty bottle. Table 3.1 shows the specification used for this whole system for all configurations. This configuration is also tested on the phase shifter. Table 3.9 is the arrangement of antennas with phase shifter as a transmitter in this configuration. The result can be found in Chapter 4.3.

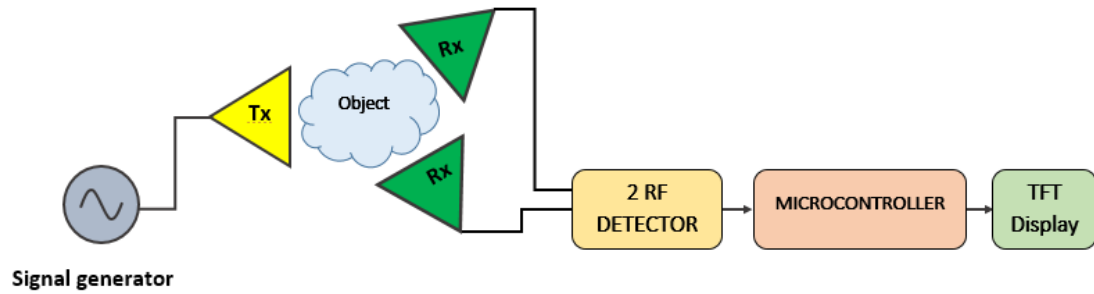


Figure 3. 26: Block diagram of MIMO of 2x2.

Table 3. 9: Arrangement of SIMO tested on free space.

Phase ($^{\circ}$) at Transmitter 1	Vout (V)	
0	Rx 1	Rx 2
45	Rx 1	Rx 2
90	Rx 1	Rx 2
135	Rx 1	Rx 2
180	Rx 1	Rx 2
270	Rx 1	Rx 2

3.5.4 Multiple Input Multiple Output.

3.5.4.1 Two Transmitter, Two Receiver (2x2)

This configuration is used for detection on free space and empty bottle. This test is done to analyze the behavioral pattern of output voltage and compare with the finding on MIMO of 4x4 when it detect free space and empty bottle. This test does not include phase shifter.

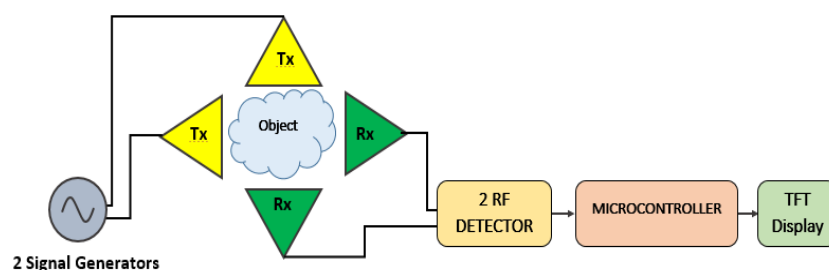


Figure 3. 27: Block diagram of MIMO (2x2)

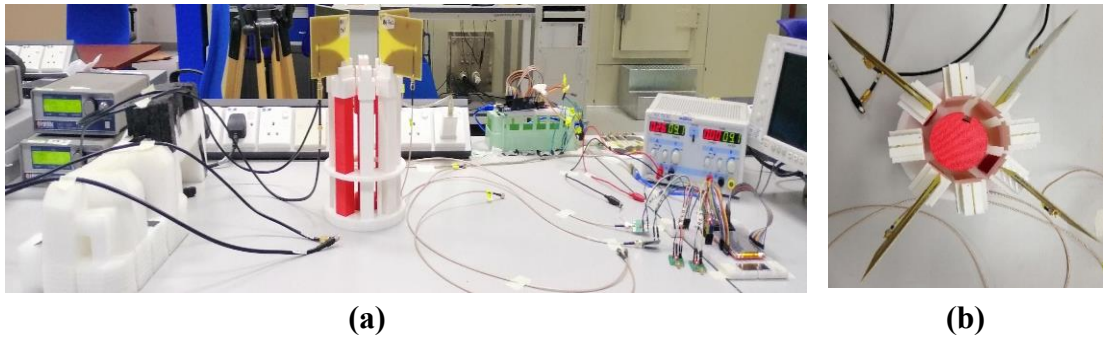


Figure 3. 28: (a) & (b) MIMO (2x2) configuration.

3.5.4.2 Four Transmitter, Four Receiver (4x4)

This MIMO (4x4) is the final setup for this system in order to test the material characterization and spatial object detection. This setup is also using the specification in Table 3.10. This setup consist of four transmitter (Tx1 – Tx4) and four receivers (Rx 1 – Rx 4) and all the signal transmitted simultaneously to each four receivers. This setup is tested on air (free space) for 0° , 45° & 90° phase shifter, empty bottle for 0° , 45° & 90° phase shifter, Detection of Material 1 for 0° , 45° & 90° phase shifter and detection of Material 2 + Material 1 for 0° , 45° & 90° phase shifter.

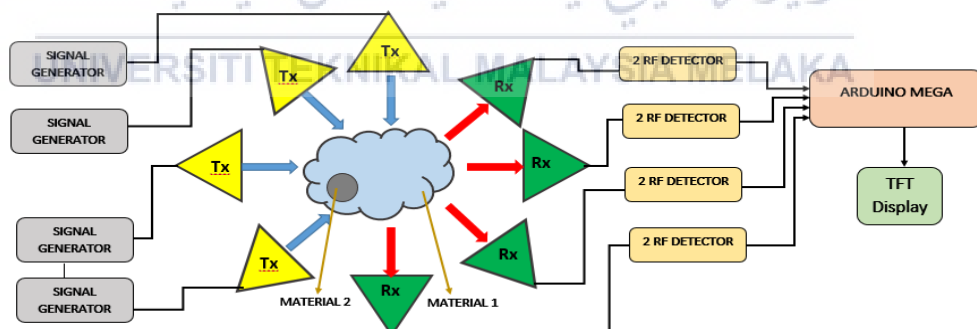


Figure 3. 29: Block Diagram of MIMO (4x4) configuration.

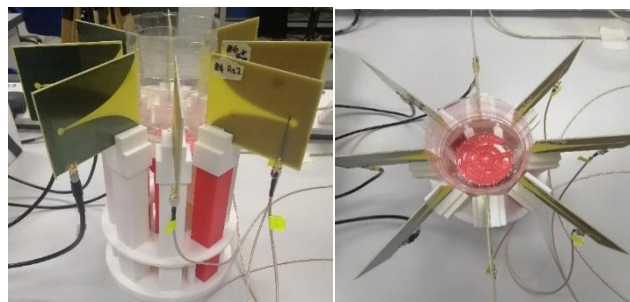


Figure 3. 30: Eight antennas in MIMO (4x4) configuration.

Table 3. 10: Variation of testing on MIMO (4x4)

Variation	Condition	Phase shifter		
		0 ⁰	45 ⁰	90 ⁰
1	Air (free space)	/	/	/
2	Empty bottle	/	/	/
3	Material 1	/	/	/
4	Material 1 + Material 2	/	/	/

3.5.5 Material Characterization

The system specification for material characterization testing is the same as Table 3.1. This test is done on all Material 1, which are water, soap, sand, soil, sugar, flour and plasticine such in figure 3.30. This testing is to measure the output voltage of Material 1 only in order to characterize them without the presence of any unknown material. Hence, when material 2 is inserted, we may observe the difference of its output voltage and this difference is discussed on the spatial detection subtopic.

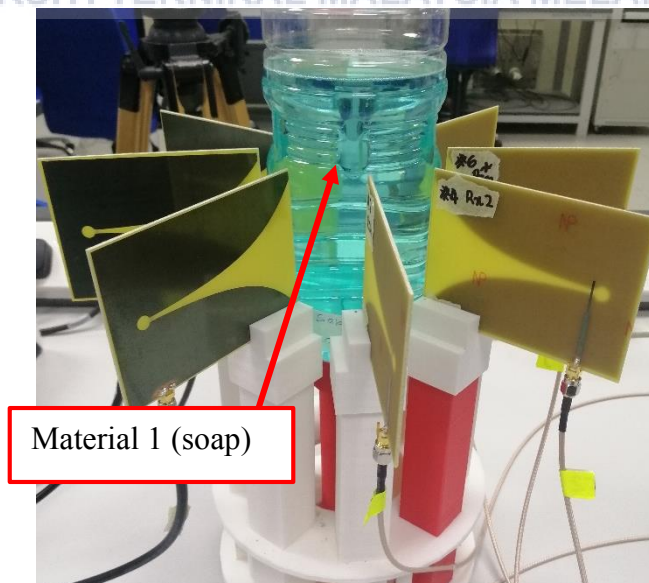
**Figure 3. 31: Material characterization testing on soap.**



Figure 3.32: List of Material 1, from left Soil, Sugar, Flour, Soap, Water, Soil and Plasticine.

3.5.6 Spatial Detection Test

The material used in this test are as in Table 3.11, where the material used is known as Material 1 and Material 2. Table 3.12 shows the variation Material 1+Material 2 for spatial detection testing. This testing is the most important test in order to detect the efficiency of this system on locating the object spatially.

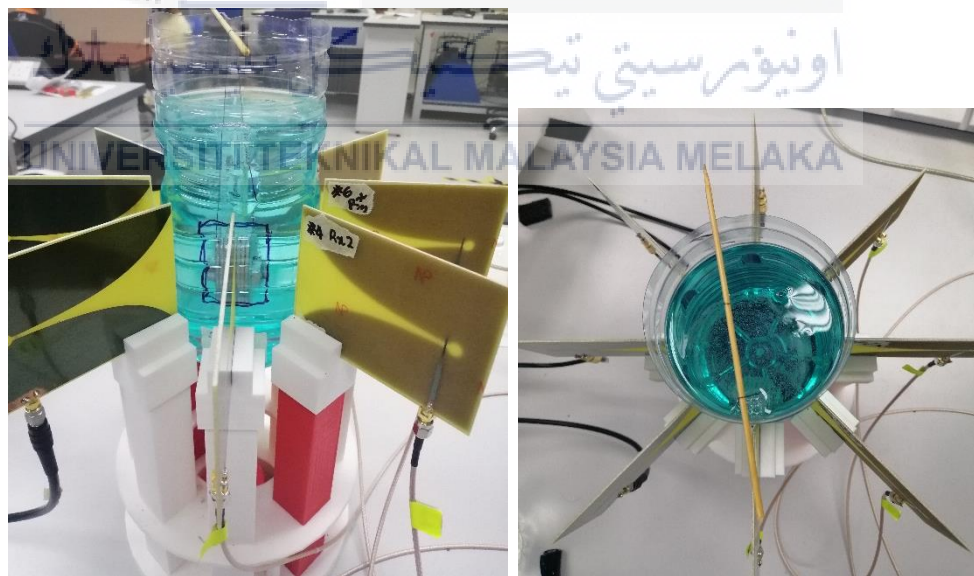


Figure 3.33: Spatial detection setup for Soap + Metal. Soap as Material 1 and Metal as Material 2.

Table 3. 11: Classification of Material 1 and Material 2.

	Material 1		Material 2
1	Liquid	Water	Metal
2		Soap	Plastic
3	Powdery	Sugar	Rubber
4		Sand	Lime
5		Flour	
6		Soil	
7	Solid	Plasticine	

**Figure 3. 34: List of Material 2, from left, Metal, Plastic, Lime and Rubber.****Table 3. 12: List of combination Material 1+Material 2.**

Material 1	Material 2
Water	Metal
	Rubber
Soap	Metal
	Lime
	Plastic
Flour	Plastic
	Lime
Sugar	Lime

	Metal
Sand	Rubber
	Plastic
Soil	Metal
	Plastic
Plasticine	Metal
	Lime

Figure 3.31 below shows the sensors arrangement of 0° , 45° , and 90° phase shifter antenna position and the location of Material 1 and Material 2 for the testing. Material 2 will be located inside the Material 1 and it will move towards every section of the antenna which represented as S1 to S8. S1 is at transmitter 1 (Tx1) in straight line with Receiver 1 (Rx1) which is S5, S2 at transmitter 2 (Tx2) in straight line with receiver 2 (Rx2) which is the S6 and so on. As a result, ideally if the location of Material 2 at S1 or S5, the changes of voltage value should occur at Rx1 which can be seen on Voltage 1 on TFT screen display.

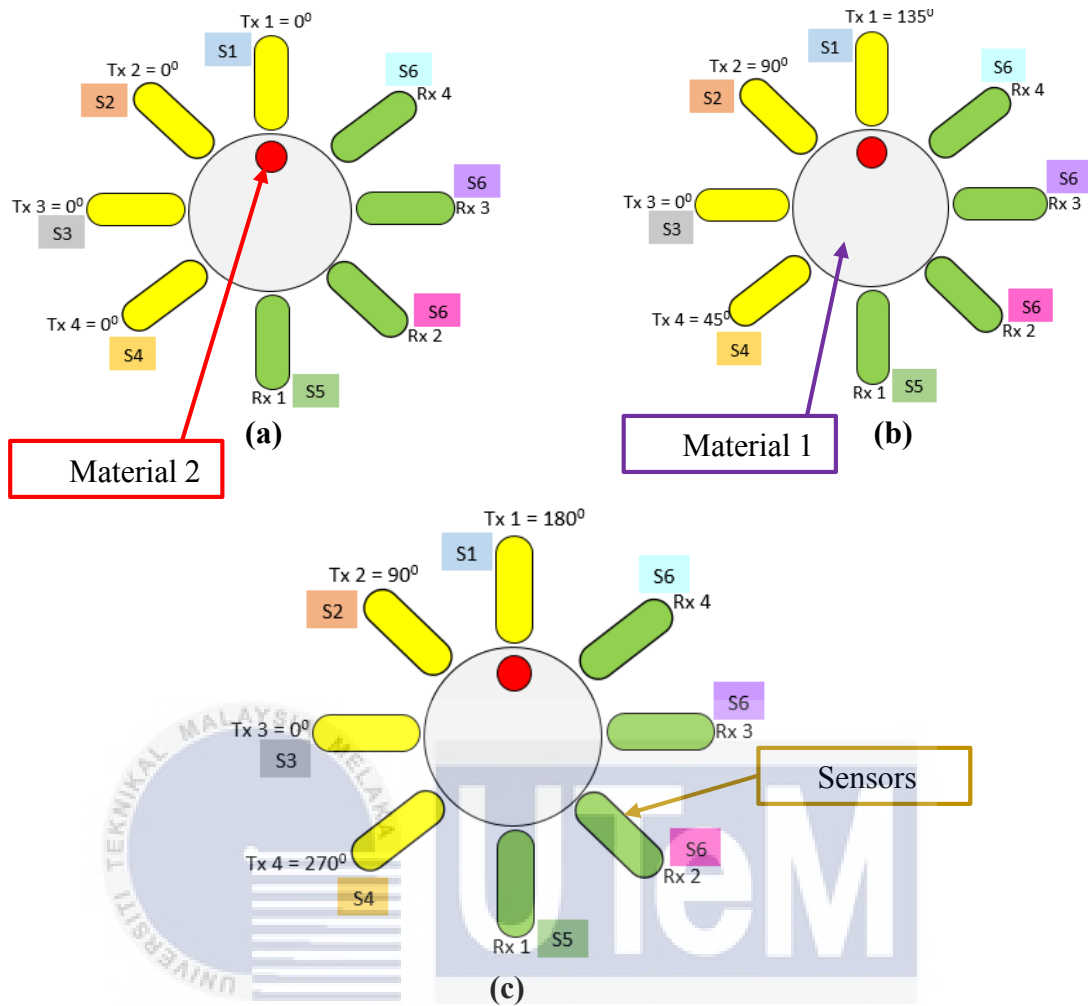


Figure 3. 35: Arrangement of sensors for spatial detection for (a) 0° phase shifter, (b) 45° phase shifter, and (c) 90° phase shifter.

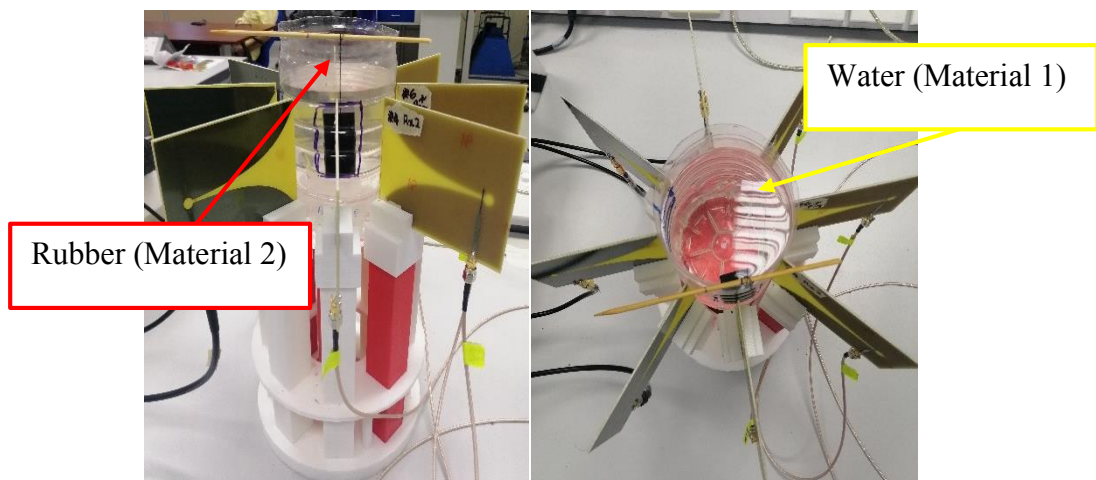


Figure 3. 36: Spatial Detection test.

3.6 Summary

The development for each component in this system; sensors, RF detector, and display processing unit are made in this chapter. The buildout on SIMO (1X2), MIMO (2X2) and MIMO (4X4) configurations system is also explained and analyzed. The configuration for MIMO (4x4) is used for material characterization and spatial object detection and all results will be stated on Chapter 4.



CHAPTER 4:

RESULT ANALYSIS AND DISCUSSION



In this chapter, the results for all components and testing are shown, especially on the simulation and measured result for sensors and converter. This chapter will also include the result of system testing for all configuration mentioned in Chapter 3.2.

4.1 Microwave Sensor Parameter

The original Vivaldi antenna (0^0) is built to operate at frequency range of 3 to 6GHz and the lowest return loss which is -43.497dB which falls at resonance frequency of 3.924GHz (refer figure 4.1). Hence, the 3.924GHz is used as operating frequency for all phase shifter and overall system. The directivity in figure 4.2 of the original antenna at 3.924GHz is 8.3351dB meanwhile gain at 3.924GHz in figure 4.3 is 6.421dB. More result on the radiation pattern, efficiency, gain, directivity and other for all phase shifters can be found in Appendix C.

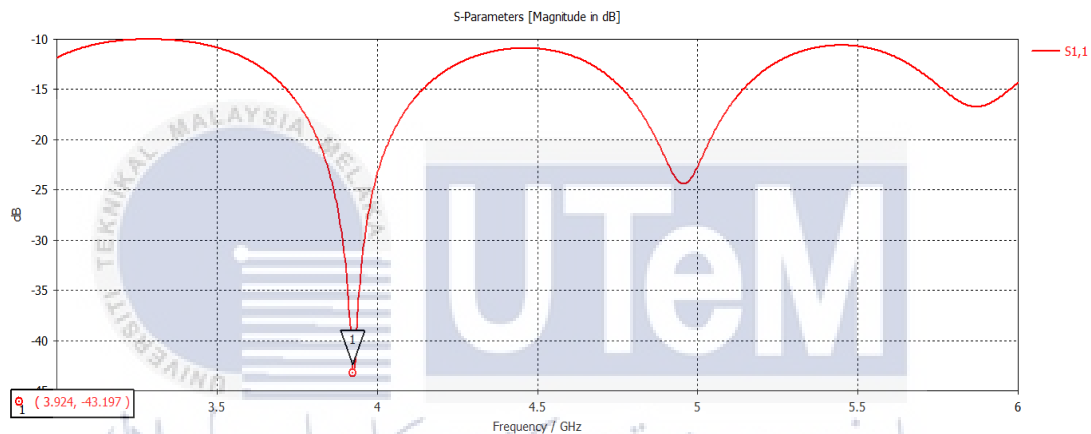


Figure 4. 1: Return Loss for original (0^0) antenna

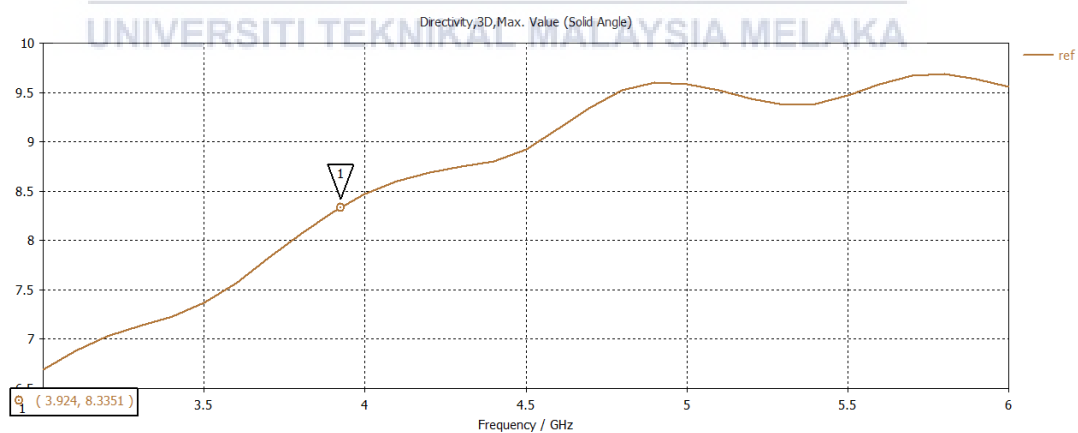


Figure 4. 2: Directivity for original (0^0) antenna at 3.924GHz.

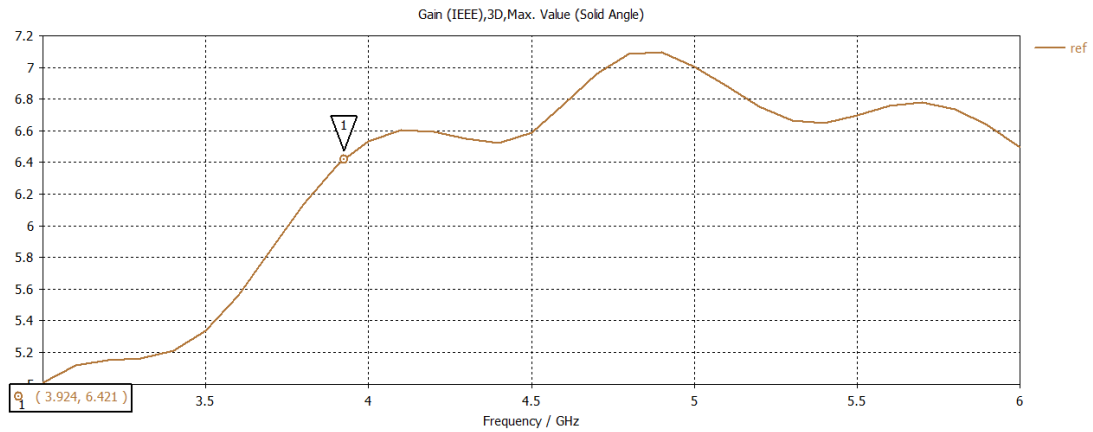


Figure 4. 3: Gain for original (0°) antenna at 3.924GHz.

Figure below shows the simulation comparison of return loss, S2,1, Gain, directivity and phase for original antenna and the 45° , 90° , 135° , 180° , and 270° phase shifter at the frequency of 3.924GHz.

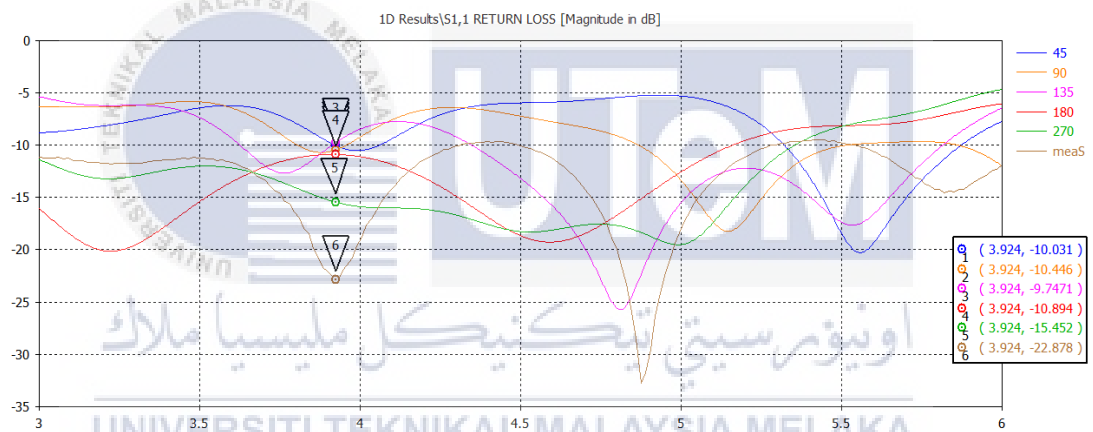


Figure 4. 4: Simulation comparison return loss for all phase shifters.

From figure 4.4, the lowest return loss at resonance frequency 3.924GHz for the phase shifters is -15.452dB for the 270° shifter. The 135° shifter only achieve -9.7471dB which almost meet the minimum reflection coefficient of -10dB. Meanwhile for 45° , 90° and 180° achieve right at the -10dB reflection coefficient. According to this result, 135° should show lowest efficiency towards the system.

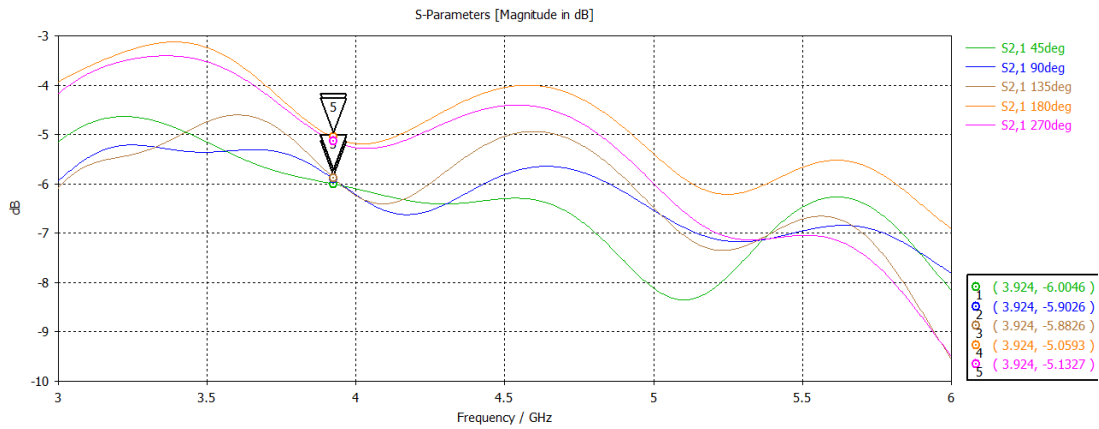


Figure 4. 5: Simulation comparison of S2,1 for all phase shifters.

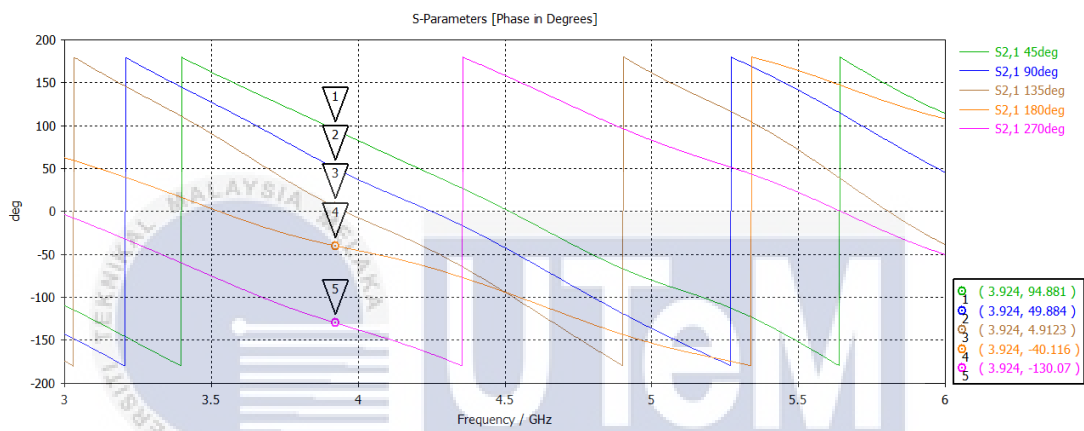


Figure 4. 6: Simulation comparison of phase for all phase shifters.

According to figure 4.6, the phase difference can be seen at the resonance frequency. The green, blue, brown and orange lines shows 45-degree phase difference between each other which make them the 45⁰ phase shifter. Meanwhile the pink, orange and blue lines, each has a phase difference of 90-degrees which make them the 90⁰ phase shifter sensor.

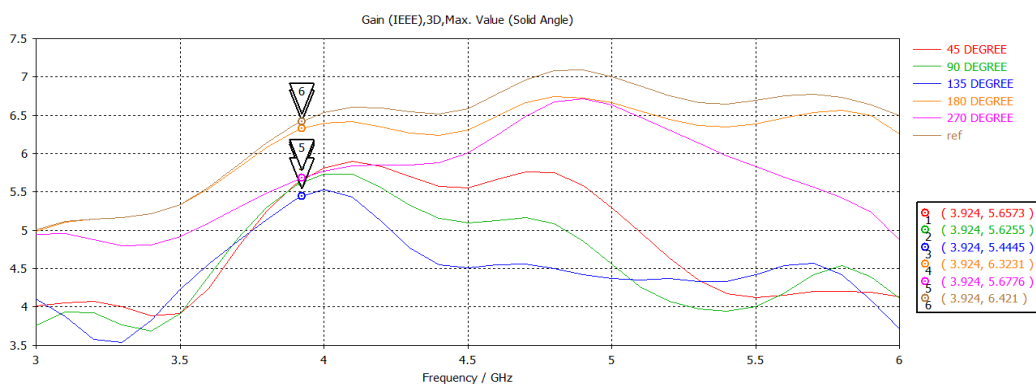


Figure 4. 7: Simulation comparison of gain at 3.924GHz for all phase shifters.

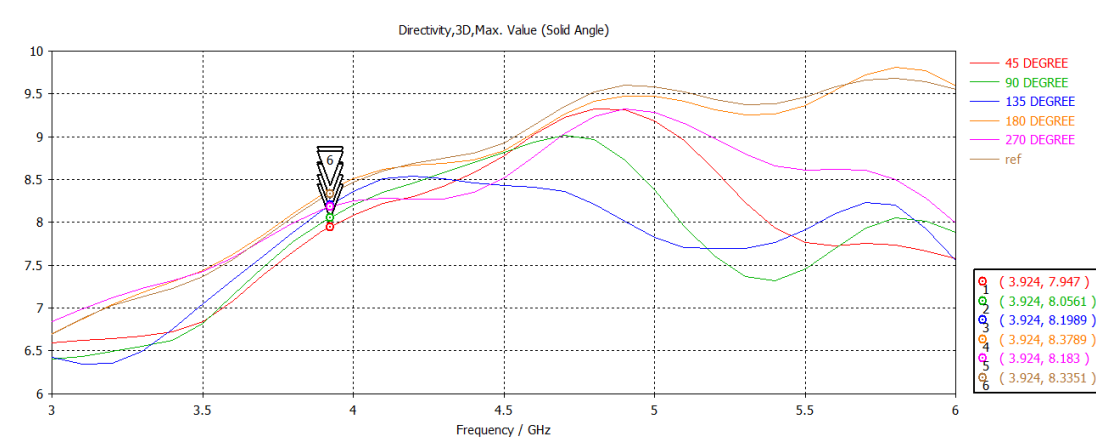


Figure 4. 8: Simulation comparison of directivity at 3.924GHz for all phase shifters.

From figure 4.7, the 45^0 , 90^0 , 135^0 and 270^0 have almost the same gain of 5dB, but for the 180^0 and 0^0 shows 1dB higher at the resonance frequency. Higher gain antennas achieve extra power by focusing on a reduced area, thus, the greater the gain, the smaller the area covered. Meanwhile on the directivity result at figure 4.8, all phase shifters have almost the same directivity, where all powers are radiated equally at 3.924GHz.

4.2 RF to DC Converter

It is necessary to first comprehend the module's behavior before proceeding with the analysis. Hence, the datasheet must first be carefully examined. From the datasheet, take a note that the output voltage produced by the AD8318 is inversely proportional to its input power. The input power decreases as the output voltage increases. The experimental result is compared to the datasheet to ensure that the AD8318 module used in this project is operating properly.

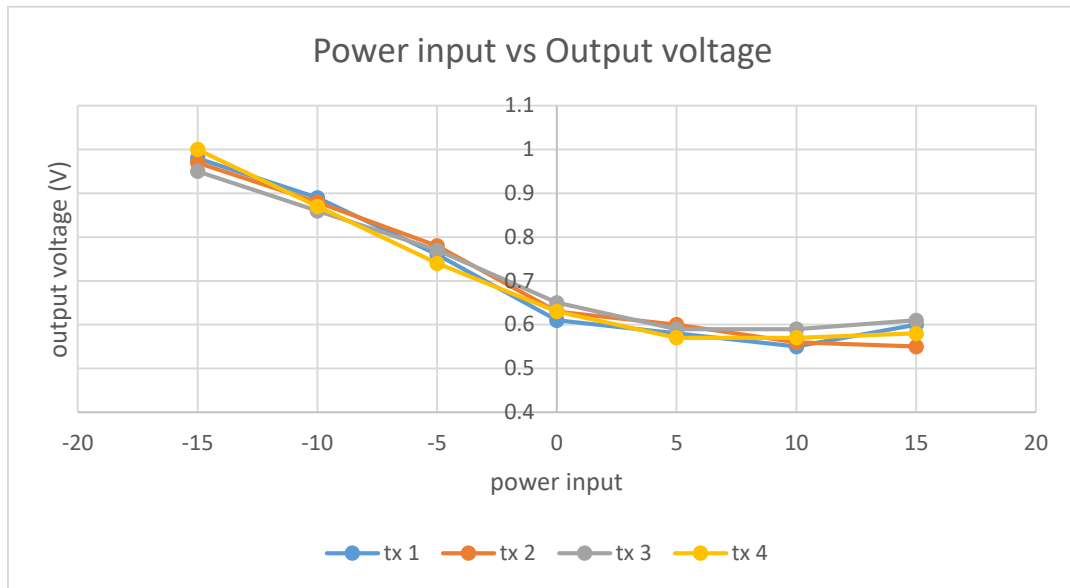


Figure 4. 9: Graph input power versus output voltage at 3.924GHz for all receiver

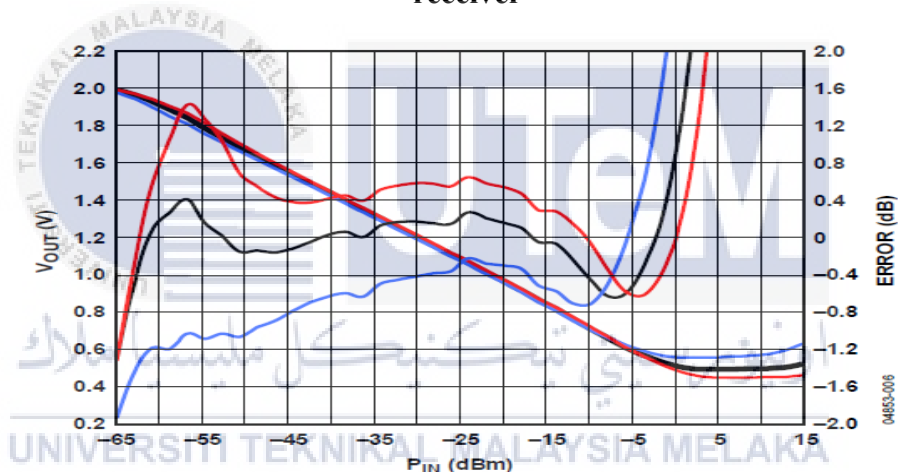


Figure 4. 10: Graph input power versus output voltage at 3.6GHz from datasheet

Figure 4.9 above shows the result of AD8318 module tested at frequency of 3.924GHz using 9V supply voltage with input power between -15dBm to 15dBm at all receiver output. From the figure above, we have decided to use the 15dBm as the input power for the whole system. Even though the datasheet result is at the 3.6GHz, the value is more or less the same to the measured value. Thus, this module is working properly.

4.3 Single Input Single Output, SISO (1x1)

The results show the output voltage value versus input power on SISO configuration at 3.924GHz with distance of 10cm and supply voltage of 9V.

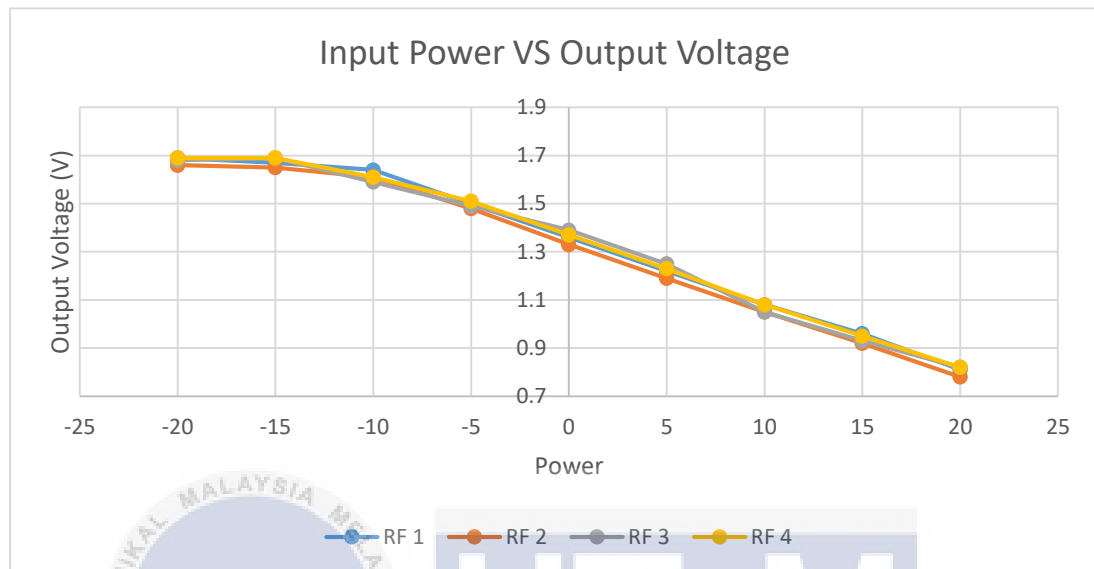


Figure 4. 11: SISO configuration at 3.924GHz with 10cm diameter.

From this test, the value of output voltage fluctuates for all receivers at all power input are the same. This means that SISO configurations testing towards empty space with diameter of 10cm on the RF detector is working properly at 3.924GHz. The test was also done with power input between -20dBm to 20dBm. The path loss is compared with figure 4.9. The average loss in voltage for all receiver is 0.628V.

4.4 Single Input Multiple Output, SIMO (1 x 2)

The result in figure 4.11 shows the output voltage from Receiver 1 and Receiver 2 when each phase shifter transmit the signal at 3.924GHz for distance of 10cm by using input power of 15dBm and supply voltage of 9V. Theoretically, the result for both receivers should be the same as it receive the signal from a single transmitter only. However, a huge difference of output voltage can be seen on the 45⁰ shifter at Rx2. This may be due to the poor return loss for this phase shifter. The higher the voltage difference, the harder for the system to detect the presence of material 2 because the

power received will be low. Meanwhile reading for 0° and 270° are the same for both receivers which make it better at detecting material. As for 95° , 135° and 180° only has a slight difference so the detection of material for these three phase shifter are still acceptable. Table 4.2 below shows the average output voltage for all phase shifter in this SIMO configuration.

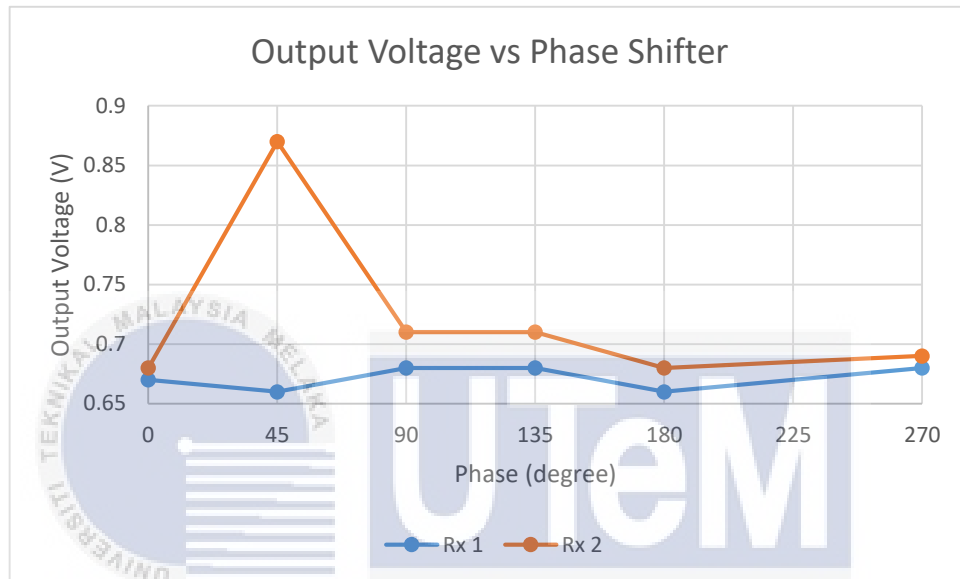


Figure 4. 12: Output voltage for all phase shifter, 0° , 45° , 90° , 135° , 180° and 270° at Receiver 1 and Receiver 2.

Table 4. 1: Average Voltage Output for SIMO configuration

Phase ($^{\circ}$) Tx1	Vout (V)		Average Vout (V)
	Rx 1	Rx 2	
0	0.67	0.68	0.68
45	0.66	0.87	0.77
90	0.68	0.71	0.69
135	0.68	0.71	0.69
180	0.66	0.68	0.67
270	0.68	0.69	0.69

From the result above, we can conclude that all phase shifter is working properly on free space (air).

4.5 Multiple Input Multiple Output, MIMO

4.5.1 Multiple Input Multiple Output (2 x 2)

This configuration was only tested on all the 0^0 phase antenna as to ensure that the signal can be transmitted and received properly. It is also done to test the difference of output voltage on air (free space) and empty bottle on the 0^0 phase shifter. First test Transmitter 1 and Transmitter 2 is used with the pairing of Receiver 1 and Receiver 2. Second test using Transmitter 3 and Transmitter 4 with Receiver 3 and Receiver 4.

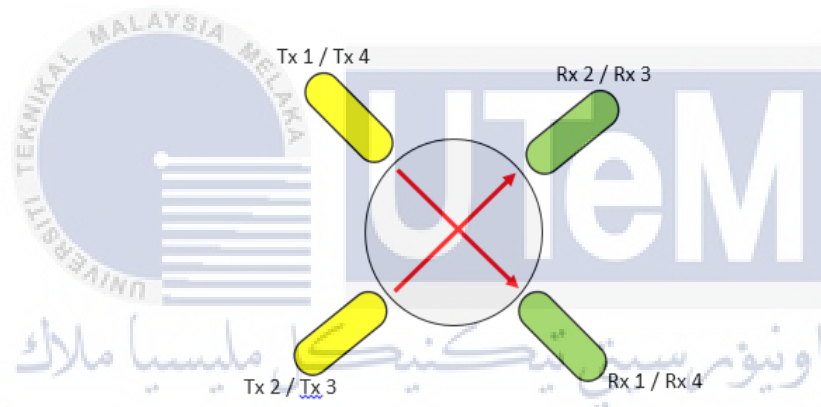


Figure 4. 13: Arrangement of antennas for MIMO (2x2)

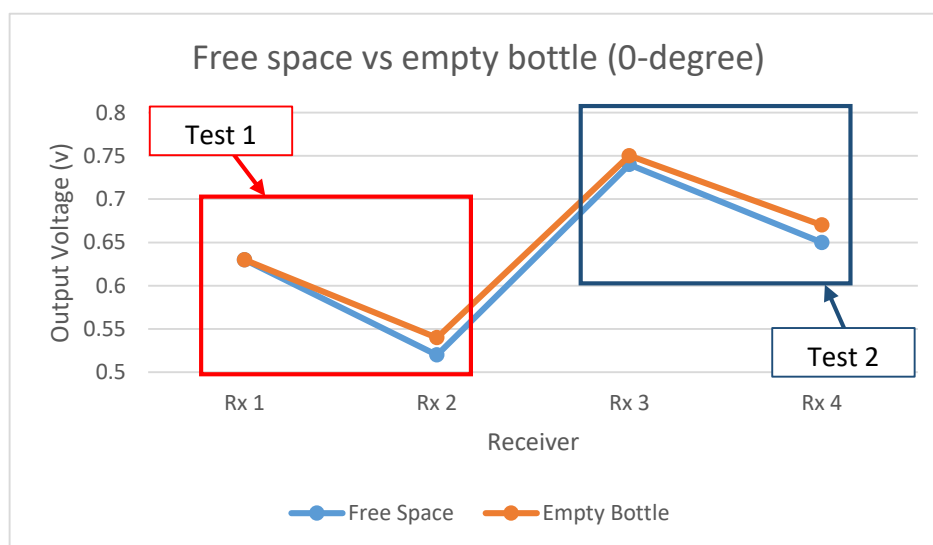


Figure 4. 14: Output Voltage for MIMO (2x2) on Air (Free space) and Empty Bottle.

Figure 4.14 above shows the combination for both test. We can see that there is not much difference when the sensors detecting the free space and empty bottle since inside the empty bottle is also containing air. The slight difference at Rx2, Rx3 and Rx4 proven that the system can still detect the presence of an empty bottle.

4.5.2 Multiple Input Multiple Output (4 x 4)

In this configuration, the phase shifter is used to test its detection on free space (air) and the empty bottle. Figure below shows the arrangement of antennas and its detection result for 45° and 90° phase shifter.

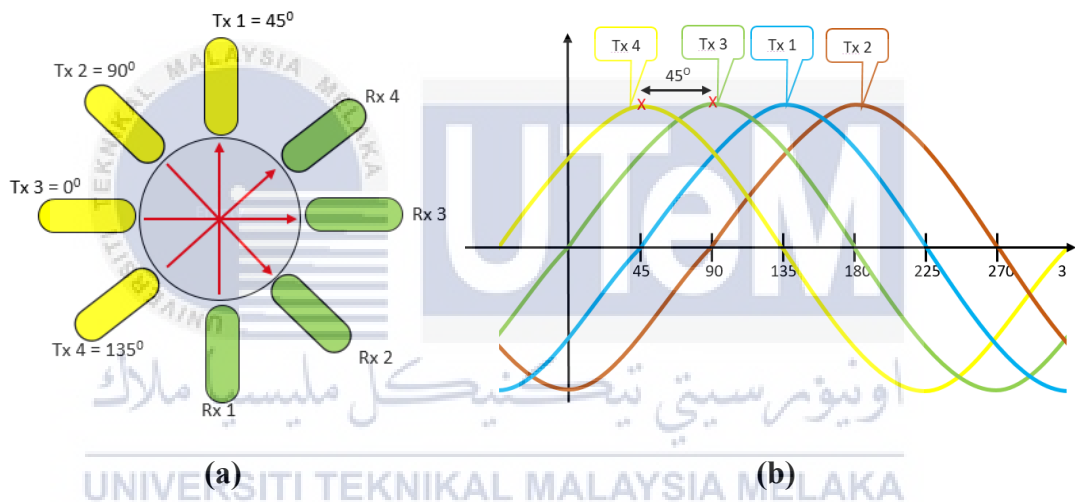


Figure 4. 15: (a) Arrangement of 45° phase shifter for free space and empty bottle detection on MIMO (4x4) configuration. (b) Signal transmitted from 45° phase shifter simultaneously.

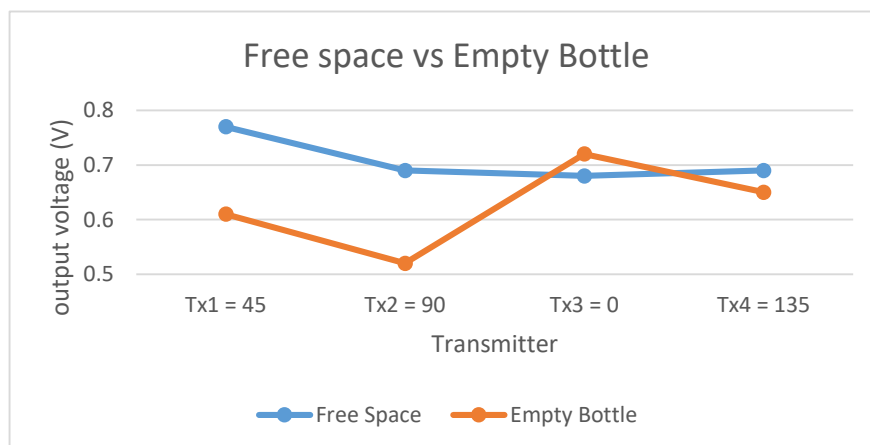


Figure 4. 16: Output Voltage for MIMO (4x4) on Air (Free space) and Empty Bottle for 45° phase shifter.

The arrangement of 45° phase shifter is set as in figure 4.15 to distant the time for each signal when they were transmitted simultaneously. Result on figure 4.16 shows a high difference of output voltage between free space detection and empty bottle detection. The difference are very obvious on Tx1 and Tx2. Meanwhile for Tx3 and Tx4, there are only slight different. From this difference, I can conclude that as the voltage difference is higher between both conditions, it would be easier to detect a material as the power received is low.

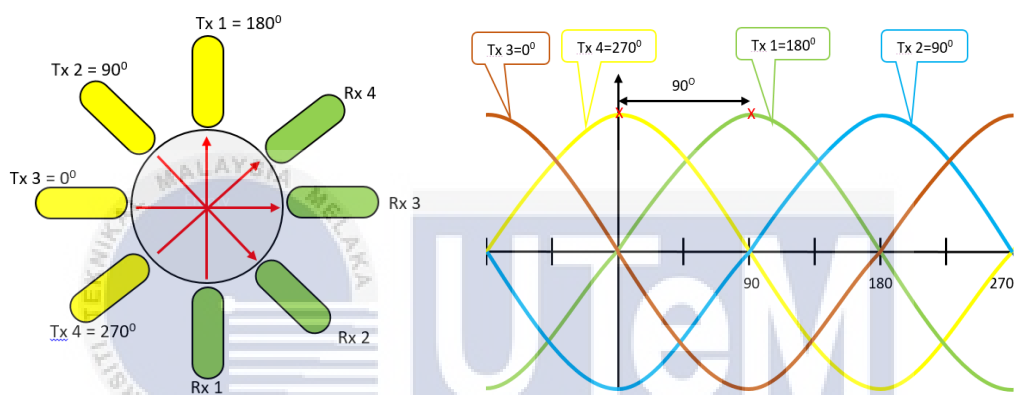


Figure 4. 17: (a) Arrangement of 90° phase shifter for free space and empty bottle detection on MIMO (4x4) configuration. (b) Signal transmitted from 90° phase shifter simultaneously.

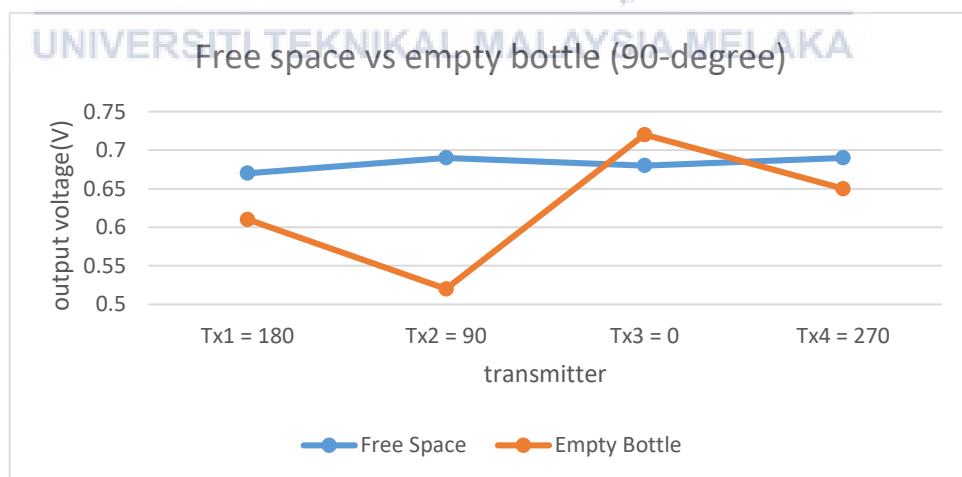


Figure 4. 18: Output Voltage for MIMO (4x4) on Air (Free space) and Empty Bottle for 90° phase shifter.

From figure 4.17, the phase shifter is arranged in such order to see whether or not the signal is collapsing. The paired signal of 270° versus 90° and 0° versus 180° can be

seen in the figure. Theoretically, when 270° and 90° signal collided, there should be no output. But, when an object is placed, for example, on the 0° path, the magnitude will change, and the remaining signal will still be transmitted to the receiver. So, from the result on figure 4.18 above, the receiver still manage to get all the output voltage for both conditions (free space and empty bottle), which means there is no signal cancellation for 90° phase shifter. A huge difference can be shown at 90° shifter when it detects the empty bottle. Result for 90° and 0° have almost the same output as figure 4.16 which means both transmitter are working properly at both configuration. Meanwhile the 180° and 270° shifter also shows a slight voltage difference, therefore both are also well-functioned.

4.6 Material Characterization

The result (refer appendix B) show that this system is able to characterize material whether solid, liquid or powder with all different phase shifter. Table below shows the average value dielectric constant for all Material 1 and Material 2.

Table 4. 2: Average value of dielectric constant for all material.

Material 1	ϵ_r	Material 2	ϵ_r
Water	69.33	Plastic	2.35
Soap	54.76	Rubber	5.14
Flour	2.66	Lime	27.26
Sand	1.98	Metal	∞
Sugar	2.05		
Soil	9.25		
Plasticine	4.93		

Based on table 4.3, the highest dielectric constant for Material 1 is water and the lowest is sand. Meanwhile for Material 2, Lime has the highest dielectric constant and the lowest is plastic. Material characterization is done for all Material 1 in all three types of phase shifter. Below are the output voltage result for all Material 1 only.

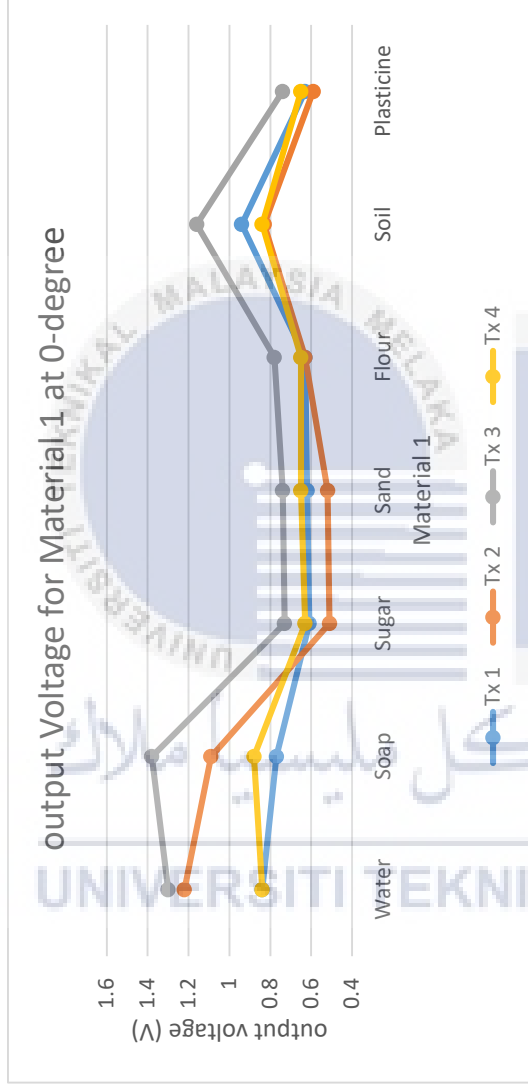


Figure 4. 19: Material 1 Characterization test on 0° phase shifter.

Table 4. 3: Output Voltage for Material 1 characterization on 0° phase shifter

Input Phase (°)	Water	Soap	Sugar	Sand	Flour	Soil	Plasticine
Tx 1= 0	0.84	0.77	0.61	0.62	0.63	0.94	0.63
Tx 2= 0	1.22	1.09	0.51	0.52	0.63	0.83	0.59
Tx 3= 0	1.3	1.38	0.73	0.74	0.78	1.16	0.74
Tx 4= 0	0.84	0.88	0.63	0.65	0.65	0.84	0.65

From result on the 0° shifter, output voltage for water and soap at Tx2 and Tx3 give large difference from at Tx1 and Tx4. Meanwhile, as the powder-type material such as sugar, sand and flour and the solid-type material, plasticine does not have much difference between all receivers. Hence, power received for all four materials mentioned are better.

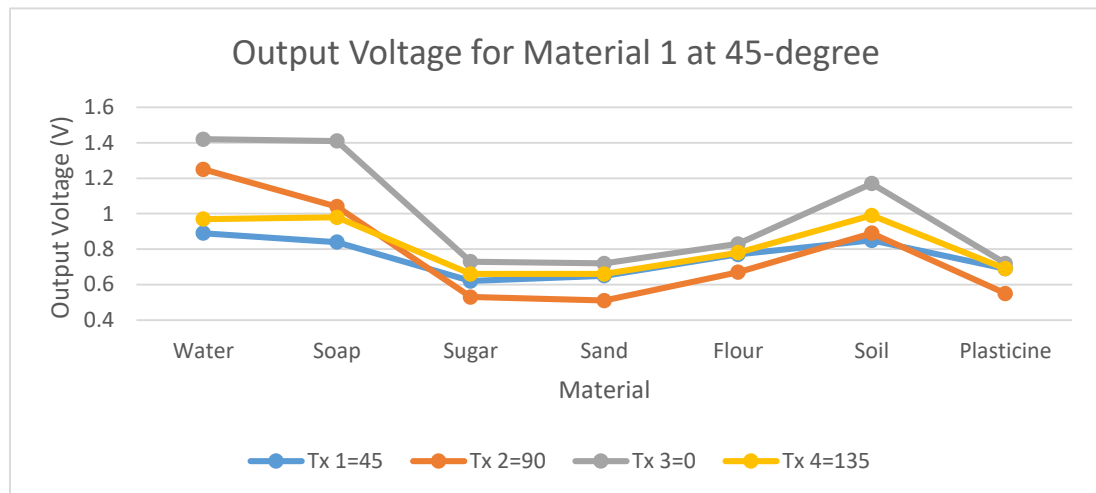


Figure 4. 20: Material 1 characterization on 45⁰ phase shifter.

Table 4. 4: Output Voltage for Material 1 characterization on 45⁰ phase shifter.

Input Phase (°)	Water	Soap	Sugar	Sand	Flour	Soil	Plasticine
Tx 1=45	0.89	0.84	0.62	0.65	0.77	0.85	0.69
Tx 2=90	1.25	1.04	0.53	0.51	0.67	0.89	0.55
Tx 3=0	1.42	1.41	0.73	0.72	0.83	1.17	0.72
Tx 4=135	0.97	0.98	0.66	0.66	0.78	0.99	0.69

Figure 4.19 shows the material characterization for 45⁰ phase shifter. From the graph, we can see that the pattern is almost the same as the 0⁰ shifter. Only the flour shows higher output voltage than in 0⁰ shifter.

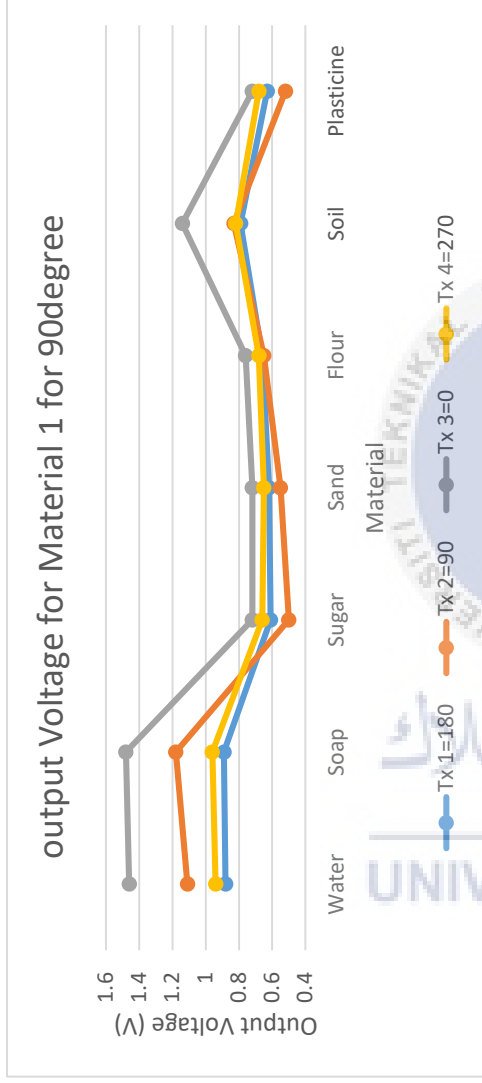


Figure 4. 21: Material 1 characterization on 90° phase shifter.

Table 4. 5: Output Voltage for Material 1 characterization on 90° phase shifter.

Phase (°)	Water	Soap	Sugar	Sand	Flour	Soil	Plasticine
Tx 1=180	0.88	0.89	0.61	0.62	0.66	0.79	0.63
Tx 2=90	1.11	1.18	0.5	0.55	0.65	0.83	0.52
Tx 3=0	1.46	1.48	0.72	0.72	0.76	1.14	0.72
Tx 4=270	0.94	0.96	0.66	0.65	0.68	0.82	0.68

The difference value of output voltage at every receivers help us determine what material is being tested. The higher the difference of output voltage in all receiver makes the material harder to detect as its power received is low. This can be seen on water and soap that shows high output voltage and the value is unstable for all phase shifter. From these three results, the 90° shifter on figure 4.21 tested on sugar, sand, flour, soil and plasticine shows better detection for material characterization as all receivers give almost the same output voltage at the same condition. Compared to water and soap, they both have high difference of output voltage value where the power received is low makes them poor a characterizing material. Hence, 90° shifter shows better result among all three phase shifter.

4.7 Spatial Detection Measurement

To acquire the greatest possible result, the outcomes of all materials and variations are examined. Out of all the variations from Appendix B, the combination of Soil (Material 1) + Plastic (Material 2) on the 0^0 shifter has the highest efficiency spatial detection. Thus, in this subtopic the result for Soil+Plastic will be shown for all three types of phase shifter. A detection of material 2 is analyzed when the right receiver shows the difference of voltage value on every sections of the sensors.

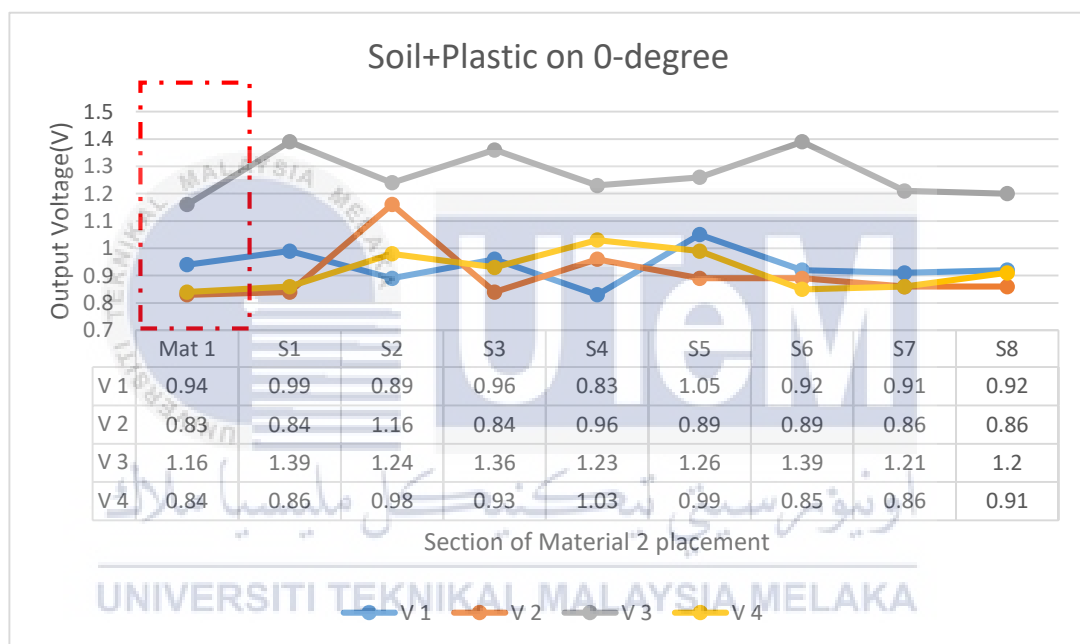


Figure 4. 22: Result for Soil+Plastic for 0^0 phase shifter

Figure 4.22 shows the graph reading of output voltage for Soil (Material 1) + Plastic (Material 2) in spatial detection test. The y-axis represent the value of output voltage and the x-axis represent the section (position) of Plastic. The initial value inside the red box is the output voltage of soil only without Material 2. Observe the change in the value and compare it with the output value of soil with plastic and soil without plastic for all positions (S1 to S8).

Table 4. 6: Difference of Vout when Material 2 is inserted for 0⁰ phase shifter.

	Vout (V)								Mat 1
	S1	S2	S3	S4	S5	S6	S7	S8	
Rx 1	0.05	-0.05	0.02	-0.11	0.11	-0.02	-0.03	-0.02	0.94
Rx 2	0.01	0.33↑	0.01	0.13	0.06	0.06	0.03	0.03	0.83
Rx 3	0.23↑	0.08	0.2↑	0.07	0.1	0.23↑	0.05↑	0.04	1.16
Rx 4	0.02	0.14	0.09	0.19↑	0.15↑	0.01	0.02	0.07↑	0.84

From table 4.7, the yellow box indicates the right receiver to detect highest difference of output voltage when it detect Material 2 at its section. Thus, the highest difference value should be seen in all yellow boxes in order to get 100% efficiency for spatial detection. Theoretically, when material 2 at S1, Rx1 should have higher voltage difference than other receiver. When material 2 is at S2, Rx2 should have higher difference than other receiver and so on.

However, in this test for the 0⁰ shifter, only S2, S3, S4, S7 and S8 can detect the location of material 2 correctly at the right receiver. At S1, Rx3 gets highest voltage difference of 0.23 instead of Rx1. At S5, the highest difference is at Rx4 with 0.15V higher instead of Rx1. As the system get five out of eight detections correct, so, this system only makes about 62.5% efficiency in detecting the location of plastic inside soil.

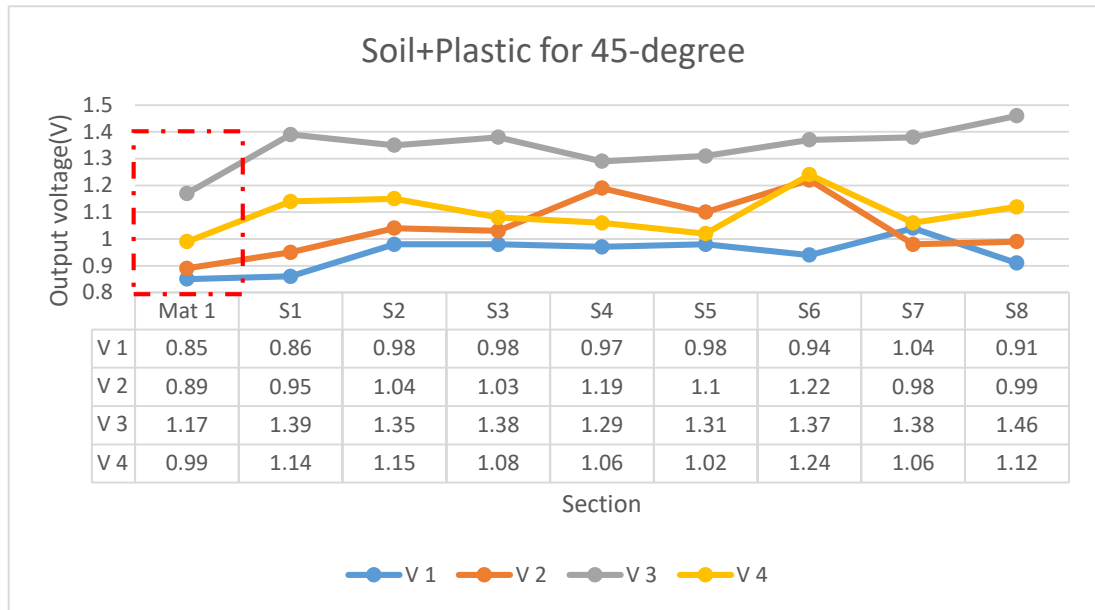


Figure 4. 23: Spatial Detection Result for Soil+Plastic for 45⁰ phase shifter

Table 4. 7: Difference of Vout when Material 2 is inserted for 45⁰ phase shifter

	Vout (V)								Mat 1
	S1	S2	S3	S4	S5	S6	S7	S8	
Rx 1	0.01	0.13	0.13	0.12	0.13	0.09	0.19	0.06	0.85
Rx 2	0.06	0.15	0.14	0.3 ↑	0.21 ↑	0.33 ↑	0.09	0.1	0.89
Rx 3	0.22 ↑	0.18 ↑	0.21 ↑	0.12	0.14	0.2	0.21 ↑	0.29 ↑	1.17
Rx 4	0.15	0.16	0.09	0.07	0.03	0.25	0.07	0.13	0.99

The same combination of Soil+Plastic was also done to the 45⁰ phase shifter to observe its efficiency. (Other combination can refer appendix B). Red box in figure 4.23 is the output voltage of material 1 (soil) only. When material 2 passes through S1, the reading at Rx3 is 1.39V which make it 0.22V higher than the output voltage of soil only at Rx3 of S1. Thus, the detection at S1 is incorrect, the same goes to S2, S4, S5 and S8. The only detection with correct highest output voltage is Rx3, Rx6 and Rx7. Which make this system is 37.5% efficient in locating the plastic inside soil.

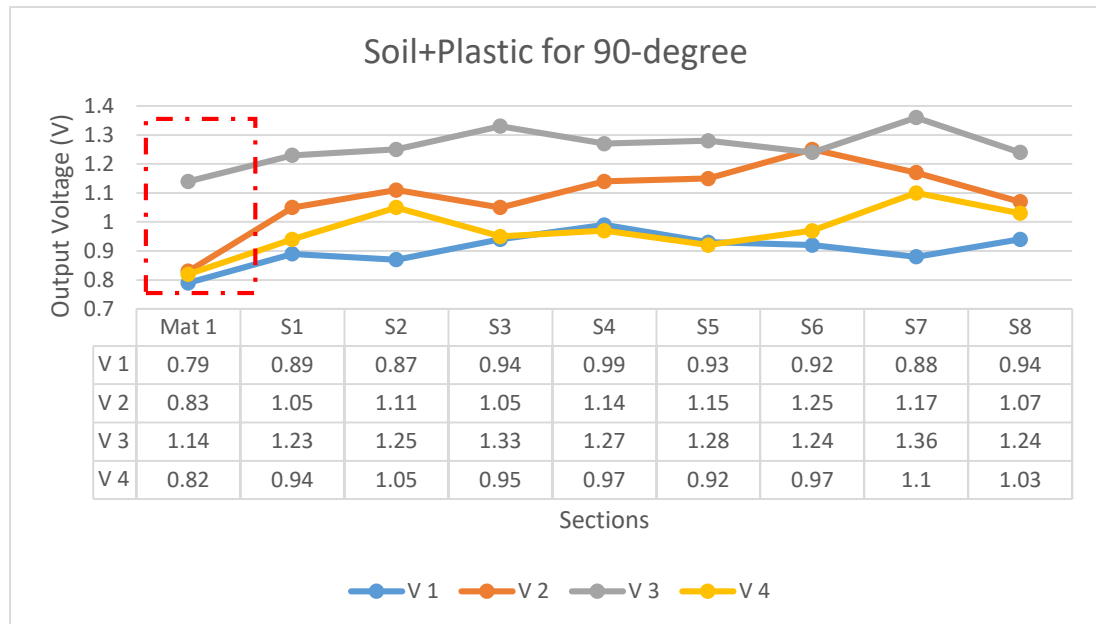


Figure 4. 24: Spatial Detection Result for Soil+Plastic for 90⁰ phase shifter

Table 4. 8: Difference of Vout when Material 2 is inserted for 90⁰ phase shifter

	Vout (V)								Mat 1
	S1	S2	S3	S4	S5	S6	S7	S8	
Rx 1	0.1	0.08	0.15	0.2	0.14	0.13	0.09	0.15	0.79
Rx 2	0.22 ↑	0.28 ↑	0.22 ↑	0.31 ↑	0.32 ↑	0.42 ↑	0.34 ↑	0.24 ↑	0.83
Rx 3	0.09	0.11	0.19	0.13	0.14	0.1	0.22	0.1	1.14
Rx 4	0.12	0.23	0.13	0.15	0.1	0.15	0.28	0.21	0.82

Last but not least, the same material variation is done to 90⁰ phase shifter. From the result, only Rx2 shows an obvious changes of voltage difference, and only 2 sections (S2 and S6) get the correct spatial detection which makes this system's efficiency is 25% only. The reading for soil only at S2 for Rx2 is 0.83V and when it detect plastic, it become 1.0V which is 0.28V higher than the initial value. Same with S6 which get 0.42V higher when it detect the plastic. Hence, I can conclude that either Tx2 or Rx2

sensor has a very high efficiency that it can easily detect the voltage difference even though the signal come from other direction.

Even so, table 4.10 below shows the average most efficient phase shifter after all combination has been tested on all three types of phase shifters.

Table 4. 9: Overall efficiency for all combinations on all phase shifter.

	Material 1	Material 2	Efficiency (%)		
			0°	45°	90°
Liquid	Water	Metal	25	25	37.5
		Rubber	37.5	25	50
	Soap	Metal	37.5	0	37.5
		Lime	25	25	12.5
		Plastic	25	25	25
Powdery	Flour	Plastic	25	12.5	37.5
		Lime	37.5	12.5	25
	Sugar	Metal	37.5	25	50
		Lime	12.5	37.5	12.5
	Sand	Plastic	25	25	37.5
		Rubber	25	0	25
	Soil	Metal	0	25	25
		Plastic	62.5	37.5	25
Solid	Plasticine	Metal	37.5	12.5	25
		Lime	25	37.5	25
Average Efficiency (%)			29.17	21.67	30

Based on table 4.10, there are some combination of material that is not efficient towards the system such as the Soil+Metal in 0° phase, Soap+Metal and Sand+Rubber in 45° phase shifter. Hence, the 45° is the most inefficient phase shifter for spatial detection. The 0° phase, on the other hand, has the average medium efficiency. Lastly, the 90° phase shifter has the highest average efficiency of 30%. The combination of Water+Rubber and Sugar+Metal in generates highest efficiency at the 90° shifter. There are only three variations that achieve more than 50% efficiency.

Despite the phase shifter, the dielectric constant of a material also affecting the system's efficiency. The highest average efficiency for Material 1 is Water, the liquid-type material which is 33.33%. Water has the highest dielectric constant ($\epsilon=69.33$) among the other Material 1. Meanwhile the lowest average efficiency is Sand ($\epsilon=1.98$) the powdery-type material with only 22.9% efficient. As for Material 2, Plastic with the lowest dielectric constant ($\epsilon=2.35$) has the highest average efficiency of 30.21% for spatial detection for the whole test. On the other hand, Lime has the lowest efficiency spatial detection of 23.96%.

4.8 Summary

The result shows that all phase shifters system is able to work properly as it can detect the changes in voltage for various material with different dielectric constant. Other than that, all phase shifter can also detect the location of material 2 inside material 1 in spatial detection test with highest efficiency of 62.5%.

CHAPTER 5:

CONCLUSION AND FUTURE WORKS



This chapter contains final clarification on all three types of phase shifter in the microwave imaging system for multistatic configuration for the spatial object detection. A research summary is offered, primarily to demonstrate the contribution that this research has made, followed by future suggestions.

5.1 Conclusion

The Microwave Imaging system using multistatic configuration with phase shifter was successfully developed. From all the tests being done, on SIMO (1x2), MIMO (2x2) and MIMO (4x), the system is able to detect material characterization by observing the changes of output voltage on every receiver. However, the best configuration for spatial object detection is the MIMO (4x4) where the signal cover on the whole object. Next, the 0° , 45° and 90° phase shifters were also designed based on the Vivaldi antenna structure as a sensors in this system. The difference of phase can be produced by adjusting the length of its feeding line. From the antenna result, some return loss of the phase shifter does not achieve -10dB which it effects the sensors performance on the spatial detection. The sensors with high efficiency gives better result in spatial object detection.

As mentioned in the previous chapter, the developed system has proven that not only it can characterize materials, but also spatially detect Material 2 inside Material 1 with the highest efficiency of 62.5%. The system most notable achievement is its ability to identify the plastic (as Material 2) inside the soil (as Material 1) according to its position. It can correctly locate the plastic with five out of eight correct detection at the proper location on the 0° phase shifter. It is proven when the output voltage shows some increment value when the object passes through the right section.

The dielectric constant for every material also affecting the detection in this system. The lower the dielectric constant for material 1, give the lower efficiency towards the system. But, the lower dielectric permittivity for material 2, gives the highest efficiency to the system. Even though the system is able to detect the location

of material 2. But, it still need an improvement as there are on three variations that achieve 50% efficiency.

However, the phase shifters also plays an important role in this system. Even though 90° phase shifter might have a signal cancellation (refer figure 4.16 (b)), but it is proven that when the signal passes through an object (an obstacle) its magnitude will change, causing the dispersed remaining signals are still being transmitted to the receiver. As for the 45° phase shifter, although the signal can be transmitted and received properly, but the combination of material 1 and material 2 somehow affecting the system's efficiency. Last but not least, the 0° degree phase shifter is also working properly with average efficiency of 29.17% that almost hit the efficiency of 90° phase.

5.2 Future Work and Recommendation

Based on the study a future recommendations can be made to achieve better efficiency for this system to develop a better spatial object detection system using phase shifter on the multistatic configuration. First and foremost, improve the antenna's return loss and efficiency. Some of the antennas in this system, especially the antenna with phase shifter only achieve between -9dB to -11dB at the resonance frequency of 3.924GHz. In order to achieve better efficiency, the return loss need to be lower than that. Therefore, not only it can improve the antenna's efficiency, but also improve its sensitivity to detect the changes of dielectric constant of a material. Next, improve the method of reading the output voltage on the TFT Display. The display value keeps on changing and it is very time consuming to calculate the average value for every readings. Lastly, adjust the combination of Material 1 and Material 2. Some of the system cannot detect the changes of output voltage because both of the combined material either has low dielectric constant or almost the same dielectric

constant. So, the combination should be high ϵ_r versus low ϵ_r , or the difference of ϵ_r for both materials are significantly different, so that the system can achieve a better efficiency in detecting the object spatially.



REFERENCES

- [1] Kang-Chun Peng, Chiu-Chin Lin and Cyuan-Fong Li, "A Compact X-Band Vector Analyzer for Microwave Imaging Sensing", *IEEE Sensors Journal*, Vol. 19, No. 9, May 1, 2019.
- [2] Martina T. Bevacqua and Rosa Scapatucci, "A Compressive Sensing Approach for 3D Breast Cancer Microwave Imaging With Magnetic Nanoparticles as Contrast Agent", *IEEE Transactions on Medical Imaging*, Vol. 35, No. 2, February 2016.
- [3] Emily Porter, Hadi Bahrami, Adam Santoreli and Benoit Gosselin, "A Wearable Microwave Antenna Array for Time-Domain Breast Tumor Screening", *IEEE Transactions on Medical Imaging*, Vol. 35, No. 6, June 2016.
- [4] Scott, S, "Three-Dimensional Microwave Imaging for Indoor Environments", UC Berkeley, Retrieved from <https://escholarship.org/uc/item/0cw3c1d4>, 2017.
- [5] Matteo Pastorino, "Applications of Microwave Imaging", *Microwave imaging*, April 2010.
- [6] Omasa, K., Hosoi, F., & Konishi, A., "3D LIDAR Imaging For Detecting And

Understanding Plant Responses And Canopy Structure" *Journal of Experimental Botany*, 58(4), 881–898 (2006).

- [7] Xie Xingyu and Mohamed A. Abou-Khousa, "Miniaturized 3D Directional Coupler for Compact Monostatic Microwave Imaging System", *A Petroleum Institute*, 2016.
- [8] Mike Cherniakov, Marina Gashinova, Marco Martorella and Chris Baker, "Bistatic and Multistatic Radar", *The 13th European Radar Conference*, 2016.
- [9] Mounia Boutkhil, Abdellah Driouach and Abdellah Khamlichi, "Detecting And Localizing Moving Targets Using Multistatic Radar System", *11th International Conference Interdisciplinarity in Engineering, INTER-ENG 2017*.
- [10] Lulu Wang, "Microwave Sensors for Breast Cancer Detection", *department Of Biomedical Engineering, School Of Instrument Science And Opto-Electronics Engineering*, 23 February 2018.
- [11] Ibrahim Akduman, Mehmet Cayoren and Hulya Sahinturk, "A New Multistatic System for Microwave Breast Cancer Imaging: Preliminary Design", *IEEE 2018*.
- [12] Jianxiong Zhou, Rongqiang Zhu, Ge Jiang, Lei Zhao and Binbin Cheng, "A Precise Wavenumber Domain Algorithm For Near Range Microwave Imaging By Cross MIMO Array", *transaction on microwave theory and techniques*, vol. 67, no. 4, april 2019.
- [13] M. Dvorsky, J. Gallion, and M.T. Ghasr, "Multistatic Microwave Synthetic Aperture (SAR) Imaging Using Orthogonal Binary Coding", *IEEE 2019*.

- [14] A.M. Abbosh, A. Zamani, and A.T. Mobashsher, "Real-Time Frequency-Based Multistatic Microwave Imaging for Medical Application", *school of ITEE, 2015*.
- [15] Nurul S. Hasim, Kismet A. H. Ping, Mohammad T. Islam, Md. Z. Mahmud, and Shafrida Sahrani, "A Slotted UWB Antipodal Vivaldi Antenna For Microwave Imaging Applications", in *Progress In Electromagnetics Research M, Vol. 80, 35-43, 2019*.
- [16] Aaron Zachary Hood, Tutku Karacolak and Erdem Topsakal, "A Small Antipodal Vivaldi Antenna for Ultrawide-Band Applications", *Antennas and Wireless Propagation Letter, Vol. 7, 2008*.
- [17] Stephan Kolb and Reinhard Stolle, "Improved Image Quality In Multistatic Microwave Gauging", *University of Applied Science Augsburg, 2011*.
- [18] Samira Al'Habsi, Thiraiya Al'Ruzaiqi and Khalid Al'Hadharami, "Development of Antenna for Microwave Imaging System Cancer Detection", *Department of Electronics and Communication, Middle East College, Sultanate of Oman. J Mol Imag Dynamic, 2016*.
- [19] S. El Marini, J. Zbitou, R. Mandry and A. Errkik, "Design of 45 Degree Microstrip Phase Shifter for Beam Forming Network Application Using Parallel Coupled Lines", *IEEE 2017*.
- [20] Chairunnisa, Diana Desiyanti and Achmad Munir, 'Capacitor-based Phase Shifter for 8 Element Antenna Feeding Network', *The 5th International Conference on Electrical Engineering and Informatics 2015 August 10-11, 2015, Bali, Indonesia*.

- [21] Chao-Hsiung and Tah-Hsiung Chu, "An Effective Usage of Vector Network Analyzer for Microwave Imaging", *Transaction on Microwave Theory and Techniques*, vol. 53, No. 9, September 2005.
- [22] Saba Rashid, Yizhi Wu and Xiobing Wang, "Design of a Cprrugated Tapered Slot Antenna for Microwave Imaging", *College of Information Science and Technology, Donghua University, Shanghai 2016*.
- [23] Rawia Ouali, Lotfi Osman, Tchanguiz Razban and Yann Mahe, "Design of Electrically Tunable Phase Shifter for Antenna Arrays Operating in Ku-band", *15th Mediterranean Microwave Symposium (MMS), Nov 2015, Lecce, Italy*.
- [24] Wriddhi Bhowmik and Shweta Srivastava, "Optimum Design of a 4x4 Planar Butler Matrix Array for WLAN Application", *Journal of Telecommunications*, Volume 2, Issue 1, April 2010.

اونیورسیتی تکنیکل ملیسیا ملاک

UNIVERSITI TEKNIKAL MALAYSIA MELAKA

APPENDICES

The appendices section comprises of 4 components which are listed below:-

APPENDIX A: Arduino source code

APPENDIX B: Raw data from laboratory experiments

APPENDIX C: Antenna simulation results

APPENDIX D: Experiment and laboratory work images

APPENDIX E: Datasheet for AD8318 module.

APPENDIX A

1. ARDUINO PROGRAMMING CODE

```

1. #include <UTFTGLUE.h>
2. UTFTGLUE myGLCD(0x9488, A2, A1, A3, A4, A0);
3.
4. #include <Adafruit_GFX.h> // Core graphics library
5. #include <MCUFRIEND_kbv.h> // Hardware-specific library
6. MCUFRIEND_kbv tft;
7.
8. #include <Fonts/FreeSans9pt7b.h>
9. #include <Fonts/FreeSans12pt7b.h>
10. #include <Fonts/FreeSerif12pt7b.h>
11. #include <FreeDefaultFonts.h>
12.
13. //Colors by HEX
14. #define LTBLUE 0xB6DF
15. #define LTTEAL 0xBF5F
16. #define LTGREEN 0xBFF7
17. #define LTCYAN 0xC7FF
18. #define LTRED 0xFD34

```

19. #define LTMAGENTA 0xFD5F

20. #define LTYELLOW 0xFFF8

21. #define LTORANGE 0xFE73

22. #define LTPINK 0xFDDF

23. #define LTPURPLE 0xCCFF

24. #define LTGREY 0xE71C

25.

26. #define BLUE 0x001F

27. #define TEAL 0x0438

28. #define GREEN 0x07E0

29. #define CYAN 0x07FF

30. #define RED 0xF800

31. #define MAGENTA 0xF81F

32. #define YELLOW 0xFFE0

33. #define ORANGE 0xFD20

34. #define PINK 0xF81F

35. #define PURPLE 0x801F

36. #define GREY 0xC618

37. #define WHITE 0xFFFF

38. #define BLACK 0x0000

39.

40. #define DKBLUE 0x000D

41. #define DKTEAL 0x020C

42. #define DKGREEN 0x03E0

43. #define DKCYAN 0x03EF

```

44. #define DKRED    0x6000
45. #define DKMAGENTA 0x8008
46. #define DKYELLOW 0x8400
47. #define DKORANGE 0x8200
48. #define DKPINK   0x9009
49. #define DKPURPLE 0x4010
50. #define DKGREY   0x4A49
51.
52. //Color table for scale
53. byte rgbtable[11][3] {
54.   {0, 0, 255},    //blue
55.   {0, 255, 160}, //cyan
56.   {128, 255, 0}, //green
57.   {255, 255, 0}, //yellow
58.   {255, 64, 0},  //orange
59.   {255, 0, 0}    //red
60. };
61.
62.
63.
64. uint16_t Control1, eightcolour;//this *and the next 4 lines* are to make sure the
    TFT LCD functions
65. uint16_t ID;
66.
67. void setup(void)

```

```

68. {
69.  ID = myGLCD.readID();
70.  if (ID == 0xB509) Control1 = myGLCD.readReg(0x00B);
71.  else Control1 = myGLCD.readReg(0x007);
72.
73.  myGLCD.InitLCD();//start LCD
74.  myGLCD.setRotation(1);//set orientation of LCD 0=port, 1= landscape 90,
    2=port 180, 3=landscape 270
75.  myGLCD.fillScreen(BLACK);//set background color
76.
77.  Serial.begin(9600);
78.  uint16_t ID = tft.readID();
79.  if (ID == 0xD3) ID = 0x9481;
80.  tft.begin(ID);
81.  tft.setRotation(1);
82.
83.  // voltage text line
84.  tft.fillScreen(BLACK); //fill background black
85.  showmsgXY(40, 170, 1, &FreeSans12pt7b, "Voltage:"); //voltage 1
86.  showmsgXY(40, 270, 1, &FreeSans12pt7b, "Voltage:"); //voltage 2
87. }
88. //-----
89. //drawColorBar(value 0-32, x coordinate of left of graph, y coordinate of top left
    corner of graph, size);
90.

```



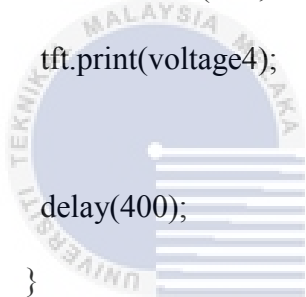
```

91. void drawColorBar(int value, int spotx, int spoty, int pix) {
92.   for (int i = 0; i < 10; i++) {
93.     if (i <= value) {
94.       myGLCD.setColor(rgbtable[i][0], rgbtable[i][1], rgbtable[i][2]);
95.     } else {
96.       myGLCD.setColor(0x0000);
97.     }
98.     myGLCD.fillRect(spotx + (i * 30), spoty, spotx + (i * 30) + 20 / 1, spoty + 28);
99.     //last digit was 18, now 38, controls length of boxes
100.  }
101.  void showmsgXY(int x, int y, int sz, const GFXfont *f, const char *msg)
102.  {
103.    int16_t x1, y1;
104.    uint16_t wid, ht;
105.    UNIVERSITI TEKNIKAL MALAYSIA MELAKA
106.    tft.setFont(f);
107.    tft.setCursor(x, y);
108.    tft.setTextColor(WHITE);
109.    tft.setTextSize(sz);
110.    tft.print(msg);
111.  }
112.  void loop() {
113.
114.    float voltage1 = analogRead(A7) * (5.0 / 1024.0);

```

```
115. float voltage2 = analogRead(A8) * (5.0 / 1024.0);
116. float voltage3 = analogRead(A9) * (5.0 / 1024.0);
117. float voltage4 = analogRead(A10) * (5.0 / 1024.0);
118.
119. if ((voltage1 < 0.1) && (voltage2 < 0.1) && (voltage3 < 0.1) && (voltage4
    < 0.1))
120. {
121.     voltage1 = 0.0;
122.     voltage2 = 0.0;
123.     voltage3 = 0.0;
124.     voltage4 = 0.0;
125. }
126.
127. tft.fillScreen(BLACK);
128. tft.setTextColor(WHITE);
129. tft.setTextSize(1);
130.
131. tft.setCursor(40, 75);
132. tft.print("Voltage 1:      V");
133. tft.setCursor(160, 75);
134. tft.print(voltage1);
135.
136. tft.setCursor(270, 75);
137. tft.print("Voltage 2:      V");
138. tft.setCursor(390, 75);
```

```
139. tft.print(voltage2);
140.
141. tft.setCursor(40, 225);
142. tft.print("Voltage 3:      V");
143. tft.setCursor(150, 225);
144. tft.print(voltage3);
145.
146. tft.setCursor(270, 225);
147. tft.print("Voltage 4:      V");
148. tft.setCursor(390, 225);
149. tft.print(voltage4);
150.
151. delay(400);
152. }
153.
154.
155.
156.
157.
158.
159.
160.
161.
162.
```



اونيورسيتي تيكنيكل مليسيا ملاك

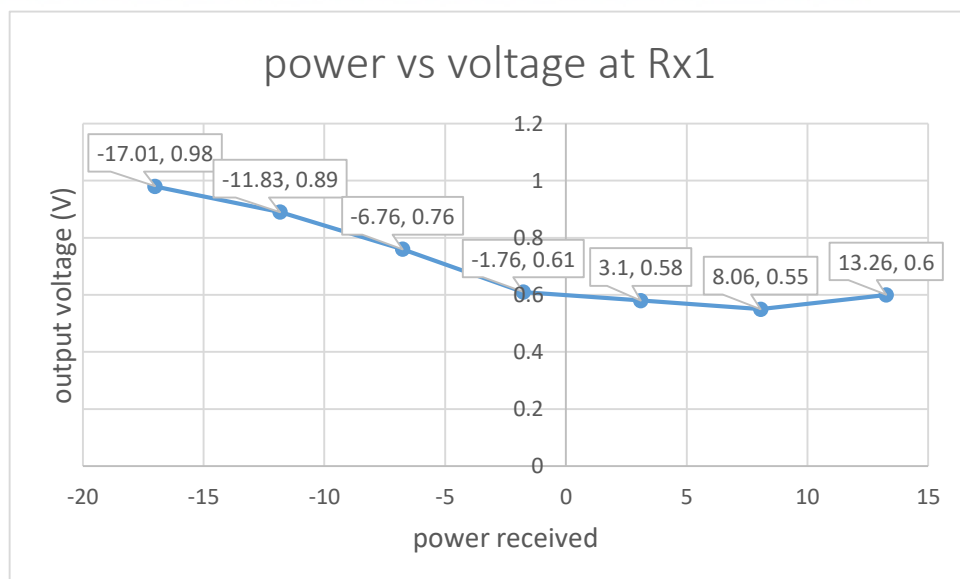
UNIVERSITI TEKNIKAL MALAYSIA MELAKA

APPENDIX B

1. CALIBRATION DATA FOR AD8318 MODULE WITH CABLE.

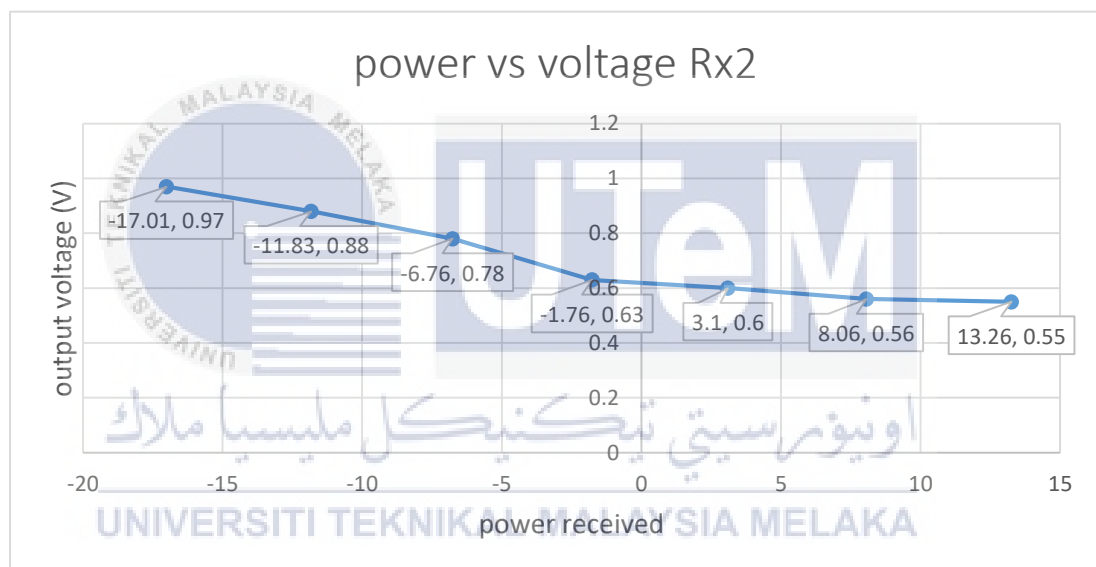
Power input versus output voltage on Rx 1 (First AD8318 module).

Rx 1	
Vout	Pin
0.98	-17.01
0.89	-11.83
0.76	-6.76
0.61	-1.76
0.58	3.1
0.55	8.06
0.6	13.26



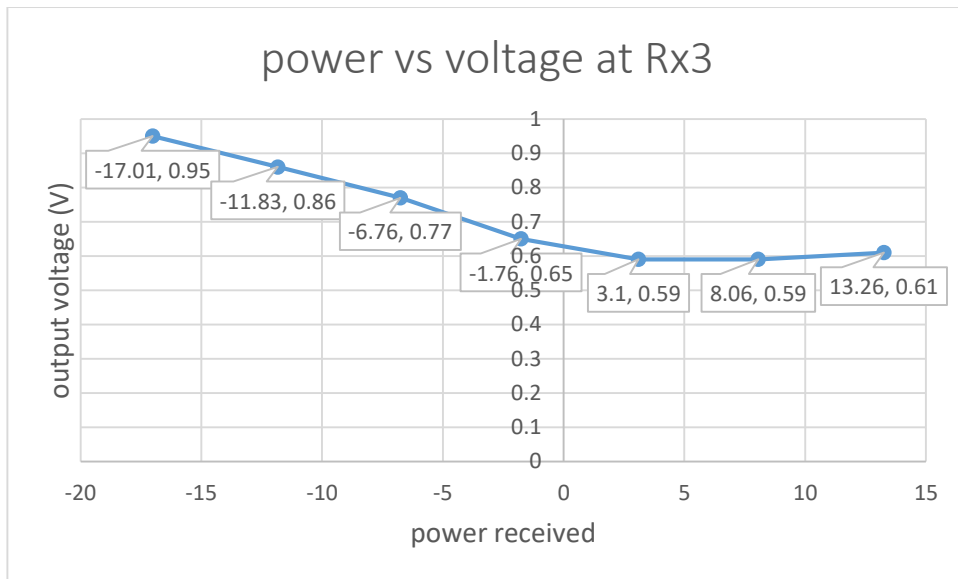
Power input versus output voltage on Rx 2 (Second AD8318 module).

Rx 2	
Vout	Pin
0.97	-17.01
0.88	-11.83
0.78	-6.76
0.63	-1.76
0.6	3.1
0.56	8.06
0.55	13.26



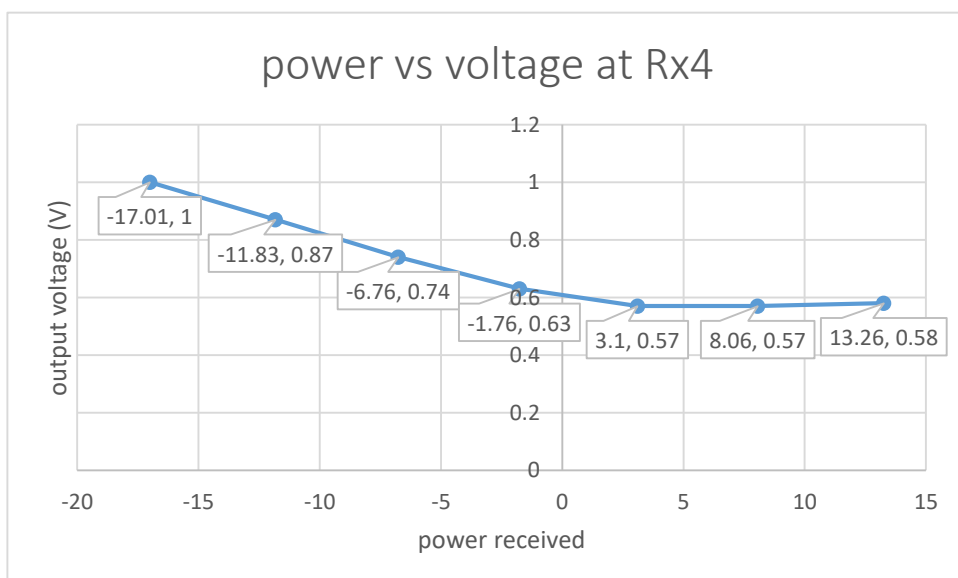
Power input versus output voltage on Rx 3 (third AD8318 module).

Rx 3	
Vout	Pin
0.95	-17.01
0.86	-11.83
0.77	-6.76
0.65	-1.76
0.59	3.1
0.59	8.06
0.61	13.26



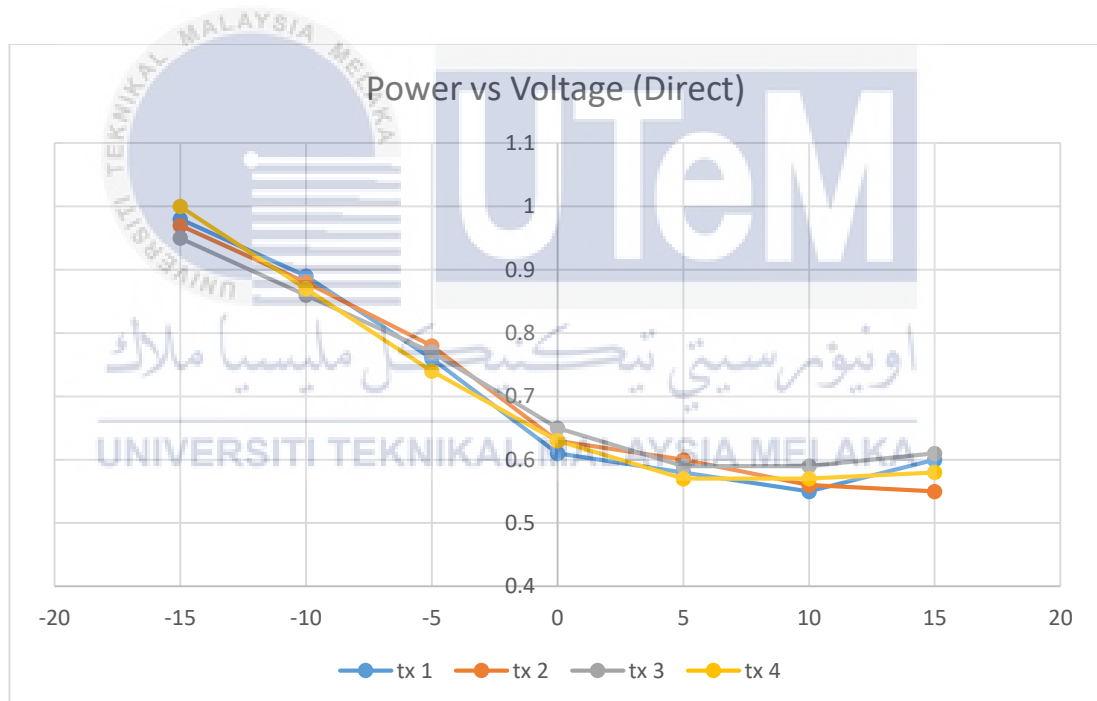
Power input versus output voltage on Rx 4 (Fourth AD8318 module).

Rx 4	
Vout	Pin
1	-17.01
0.87	-11.83
0.74	-6.76
0.63	-1.76
0.57	3.1
0.57	8.06
0.58	13.26



Power input versus output voltage on all receiver.

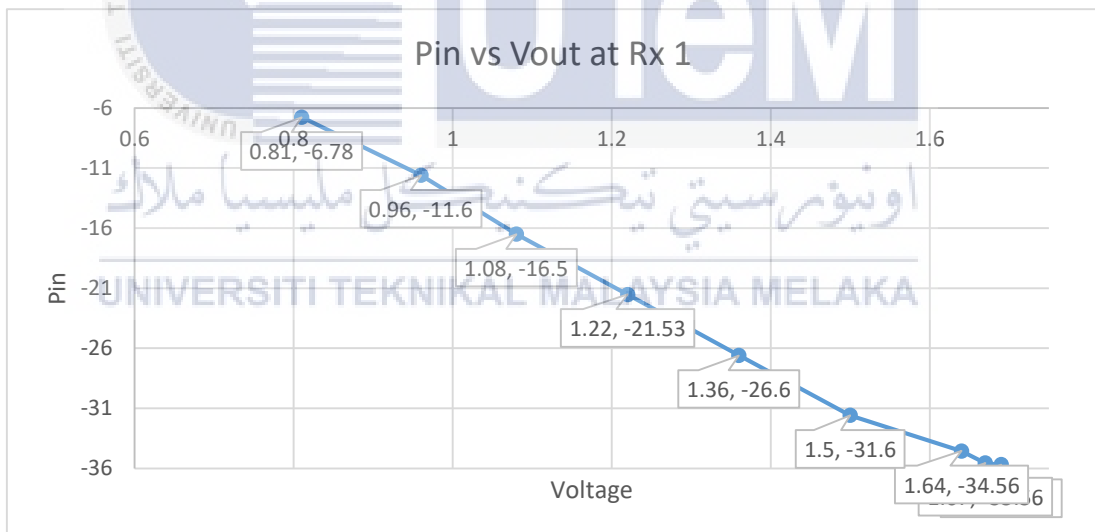
Pin	Vout			
	Rx 1	Rx 2	Rx 3	Rx 4
-17.01	0.98	0.97	0.95	1
-11.83	0.89	0.88	0.86	0.87
-6.76	0.76	0.78	0.77	0.74
-1.76	0.61	0.63	0.65	0.63
3.1	0.58	0.6	0.59	0.57
8.06	0.55	0.56	0.59	0.57
13.26	0.6	0.55	0.61	0.58



2. CALIBRATION DATA FOR AD8318 MODULE WIRELESS (SISO)

Power input versus output voltage on Rx 1 (First AD8318 module)

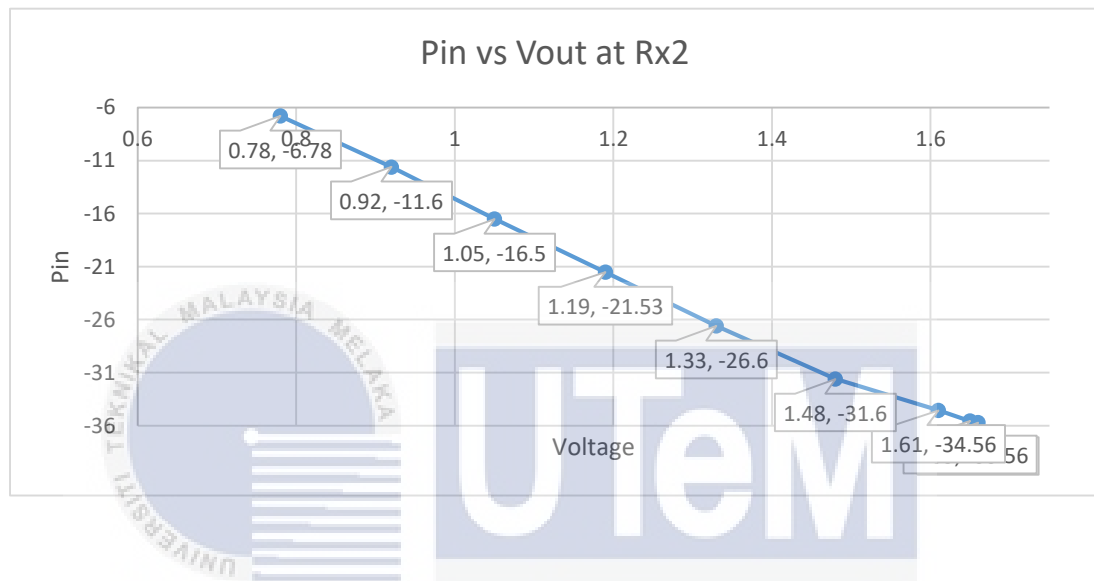
Rx 1		
Pin	Voltage	Pout
-20	1.69	-35.7
-15	1.67	-35.56
-10	1.64	-34.56
-5	1.5	-31.6
0	1.36	-26.6
5	1.22	-21.53
10	1.08	-16.5
15	0.96	-11.6
20	0.81	-6.78



Power input versus output voltage on Rx2 (Second AD8318 module)

Rx 2		
Pin	Voltage	Pout
-20	1.66	-35.7
-15	1.65	-35.56

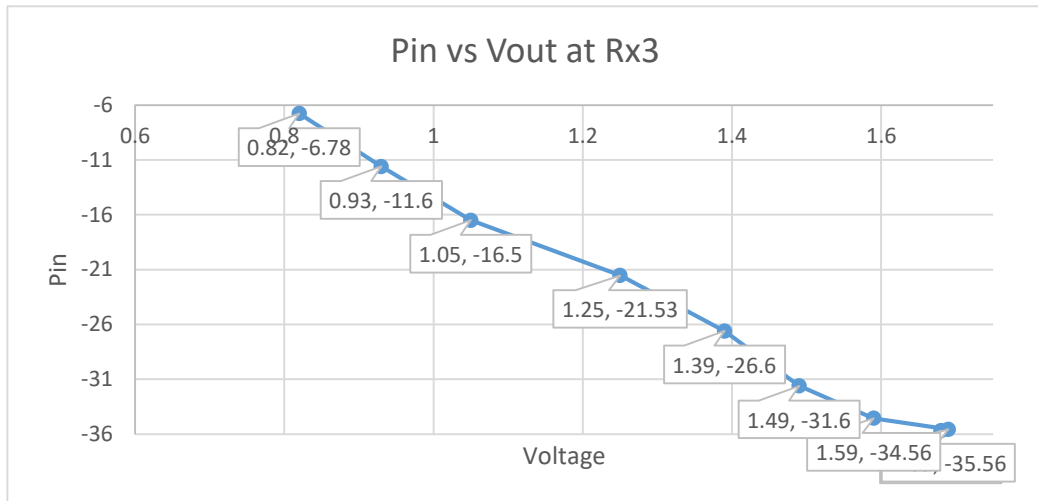
-10	1.61	-34.56
-5	1.48	-31.6
0	1.33	-26.6
5	1.19	-21.53
10	1.05	-16.5
15	0.92	-11.6
20	0.78	-6.78



Power input versus output voltage on Rx3 (Third AD8318 module)

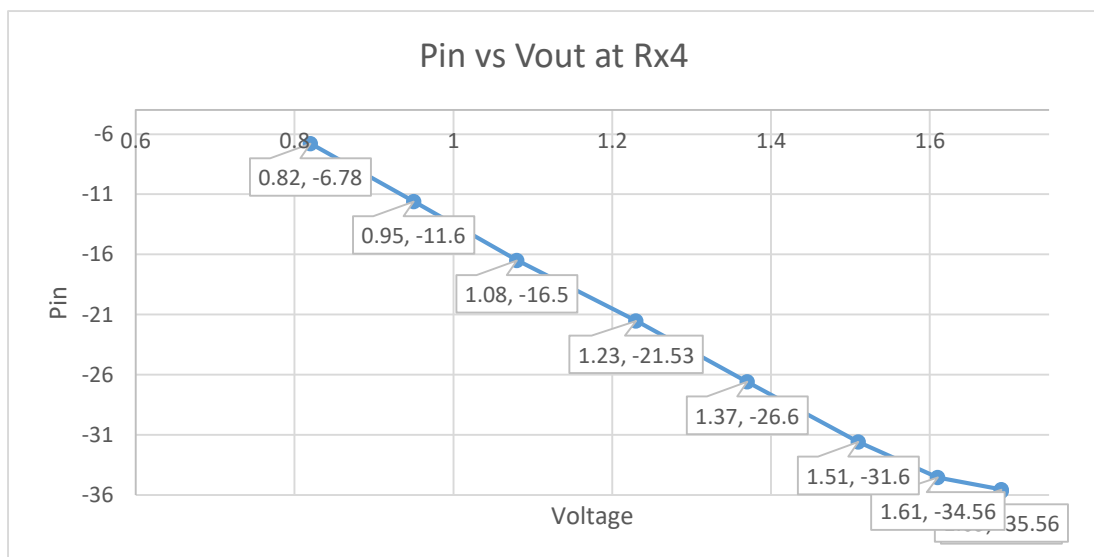
UNIVERSITI TEKNIKAL MALAYSIA MELAKA

Rx 3		
Pin	Voltage	Pout
-20	1.68	-35.7
-15	1.69	-35.56
-10	1.59	-34.56
-5	1.49	-31.6
0	1.39	-26.6
5	1.25	-21.53
10	1.05	-16.5
15	0.93	-11.6
20	0.82	-6.78



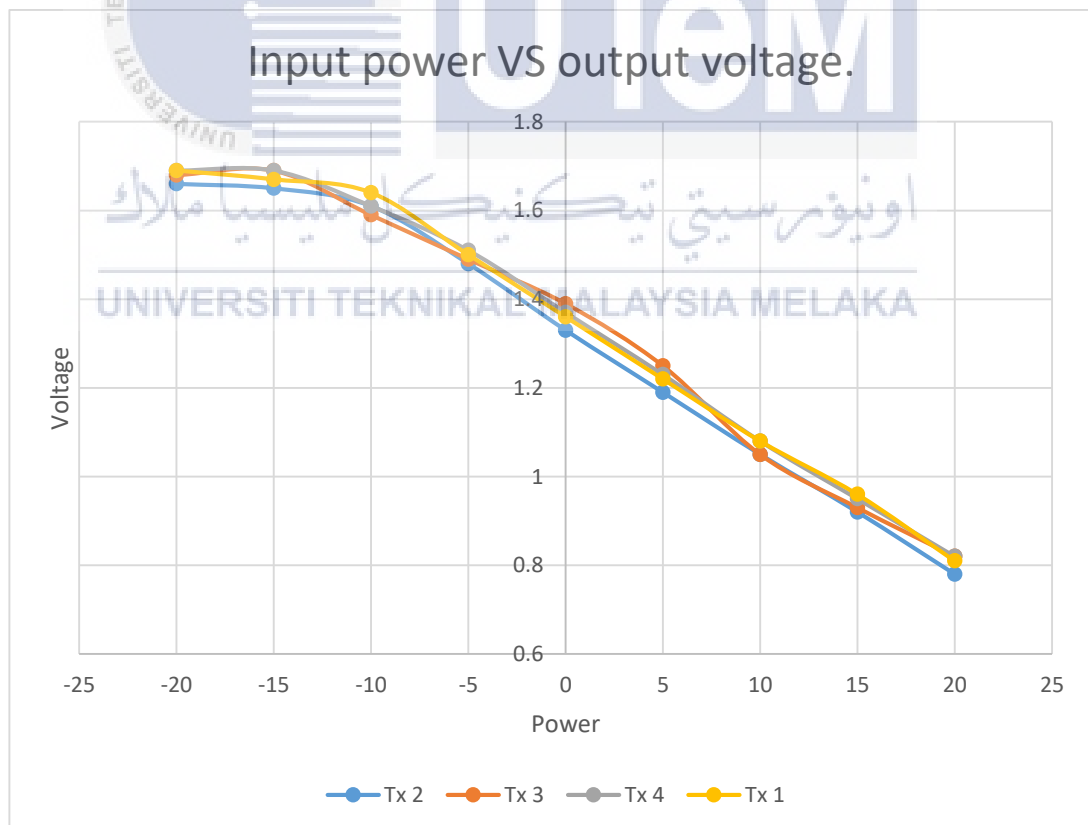
Power input versus output voltage on Rx4 (Fourth AD8318 module)

Rx 4		
Pin	Voltage	Pout
-20	1.69	-35.7
-15	1.69	-35.56
-10	1.61	-34.56
-5	1.51	-31.6
0	1.37	-26.6
5	1.23	-21.53
10	1.08	-16.5
15	0.95	-11.6
20	0.82	-6.78



Power input versus output voltage on all receiver.

Pin	Pout	Voltage			
		Rx 2	Rx 3	Rx 4	Rx 1
-20	-35.7	1.66	1.68	1.69	1.69
-15	-35.56	1.65	1.69	1.69	1.67
-10	-34.56	1.61	1.59	1.61	1.64
-5	-31.6	1.48	1.49	1.51	1.5
0	-26.6	1.33	1.39	1.37	1.36
5	-21.53	1.19	1.25	1.23	1.22
10	-16.5	1.05	1.05	1.08	1.08
15	-11.6	0.92	0.93	0.95	0.96
20	-6.78	0.78	0.82	0.82	0.81

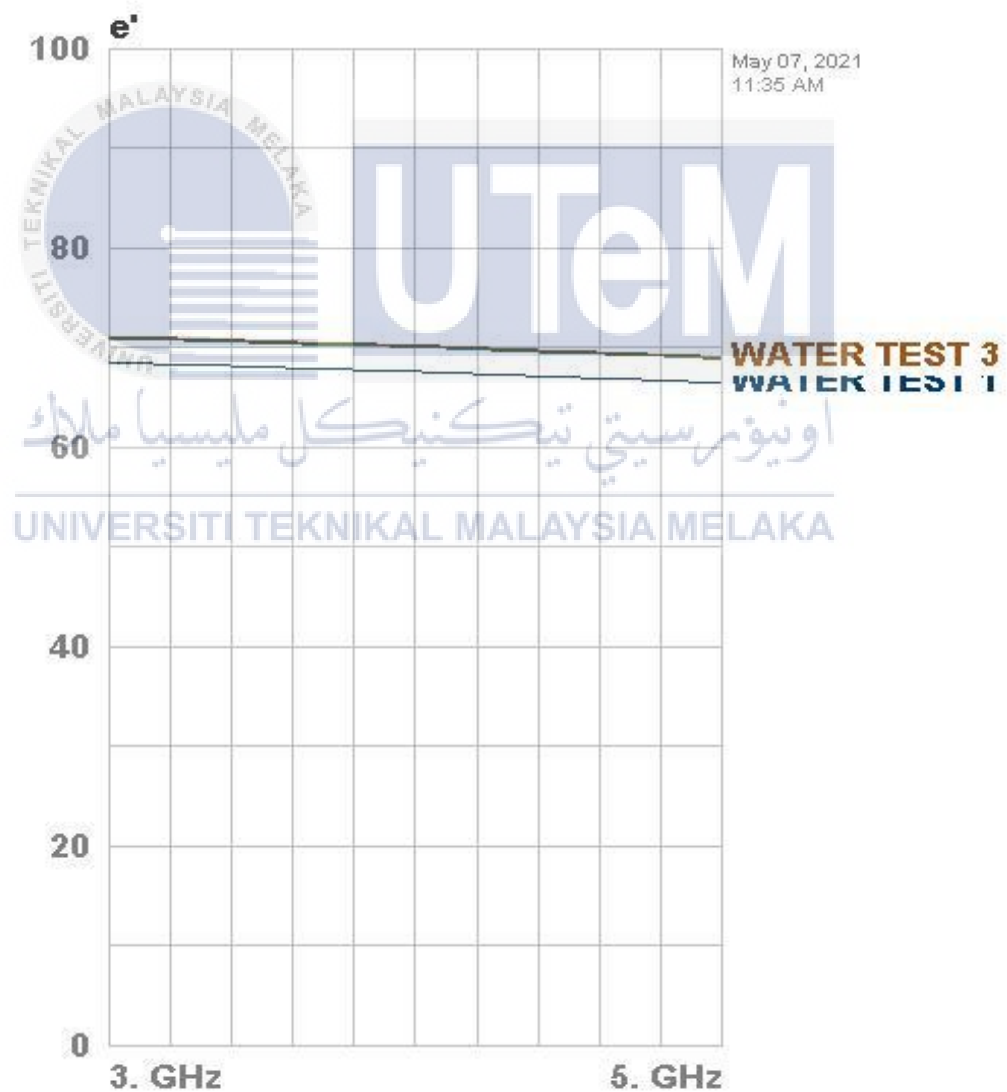


3. DIELECTRIC MEASUREMENT VALUE.

a. Water

	Memory 1	Imaginary	Memory 2	Imaginary	Memory 3	Imaginary
3.924 GHz	67.629	12.0594	70.09	12.31	70.25	12.27

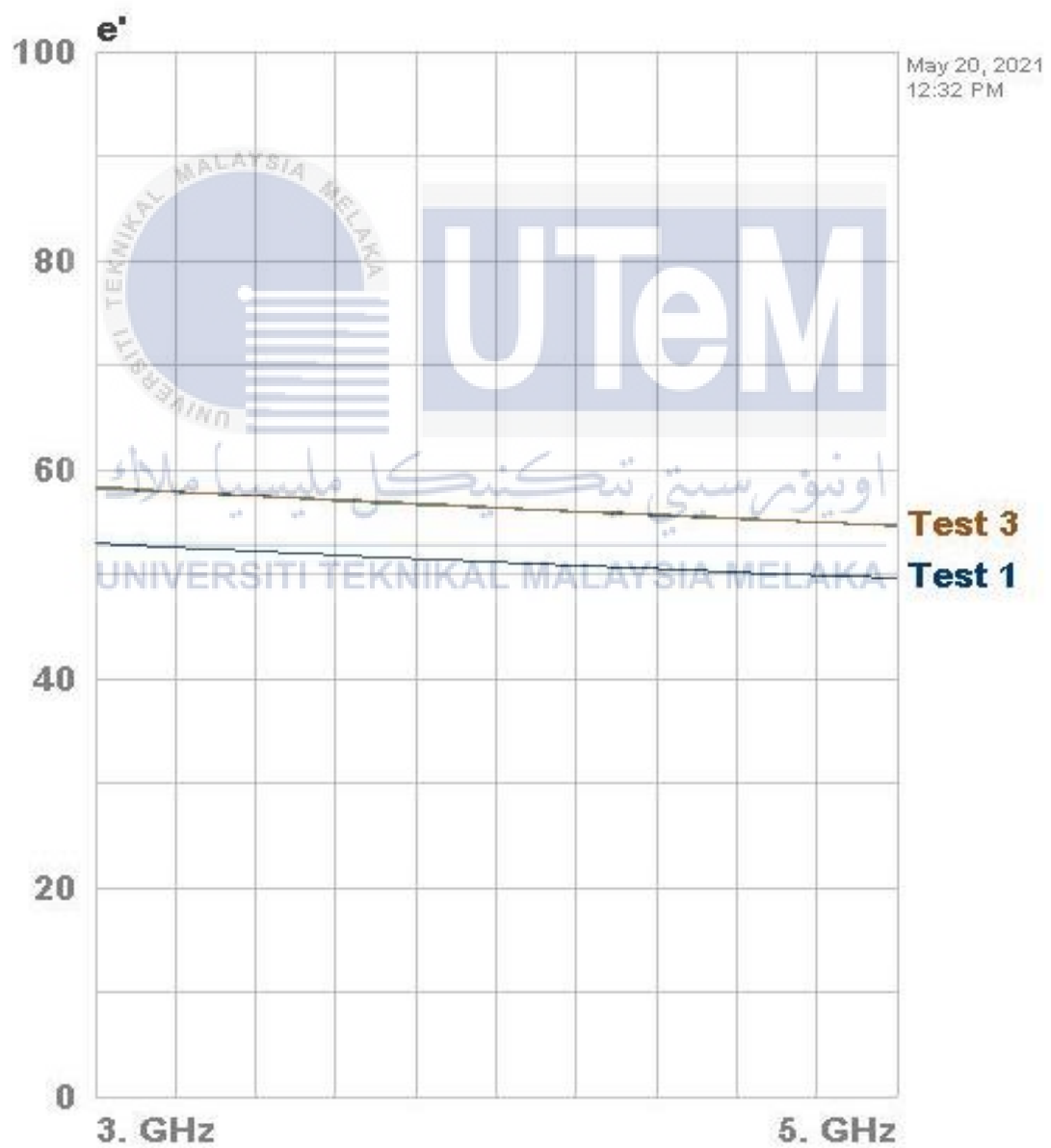
WATER



b. Soap

	Memory 1	Imaginary	Memory 2	Imaginary	Memory 3	Imaginary
3.924 GHz	51.29	24.27	56.45	26.78	56.54	26.70

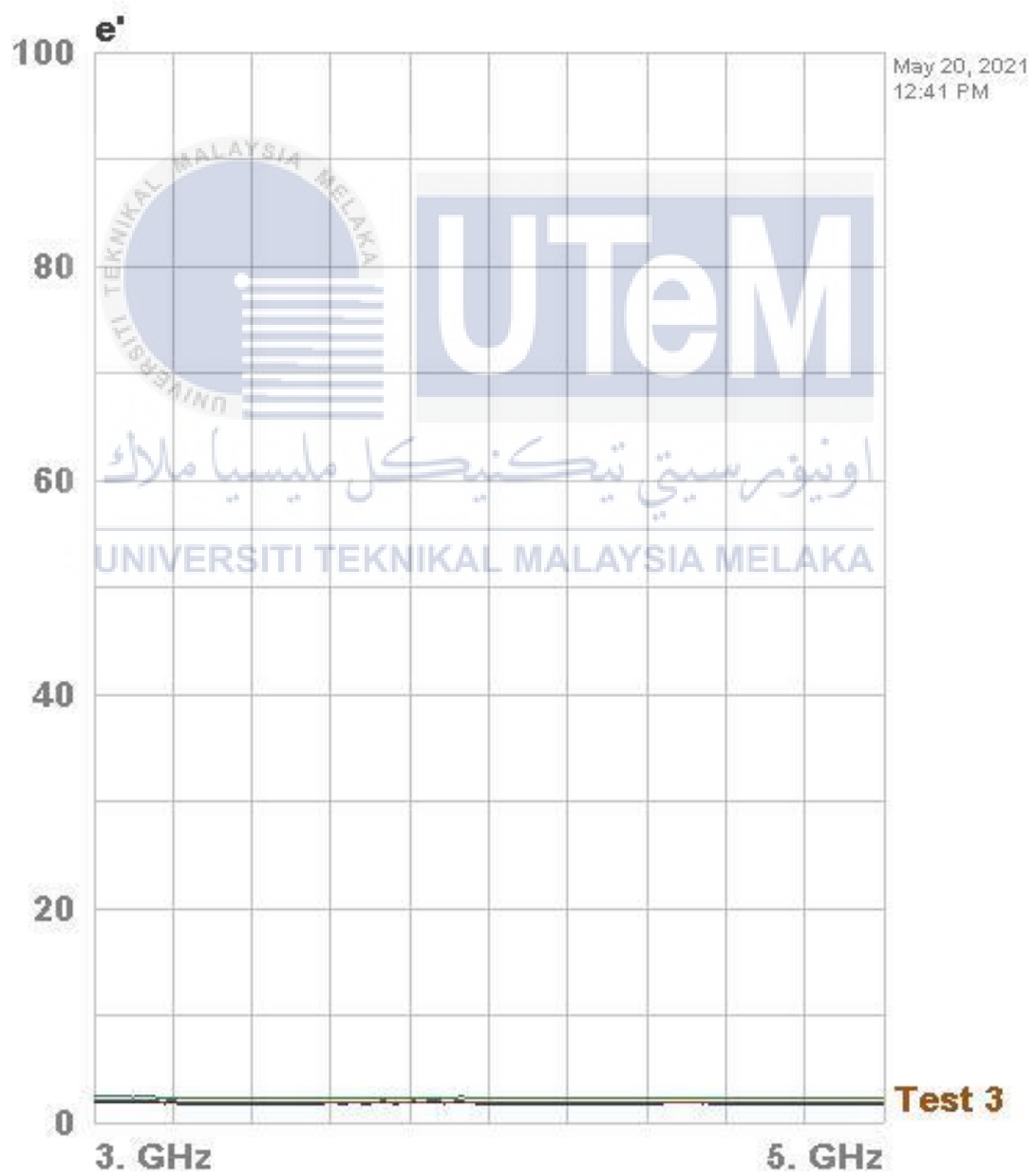
Sabun



c. Sugar

	Memory 1	Imaginary	Memory 2	Imaginary	Memory 3	Imaginary
3.924 GHz	1.79	-0.024	2.38	-0.045	1.98	-0.028

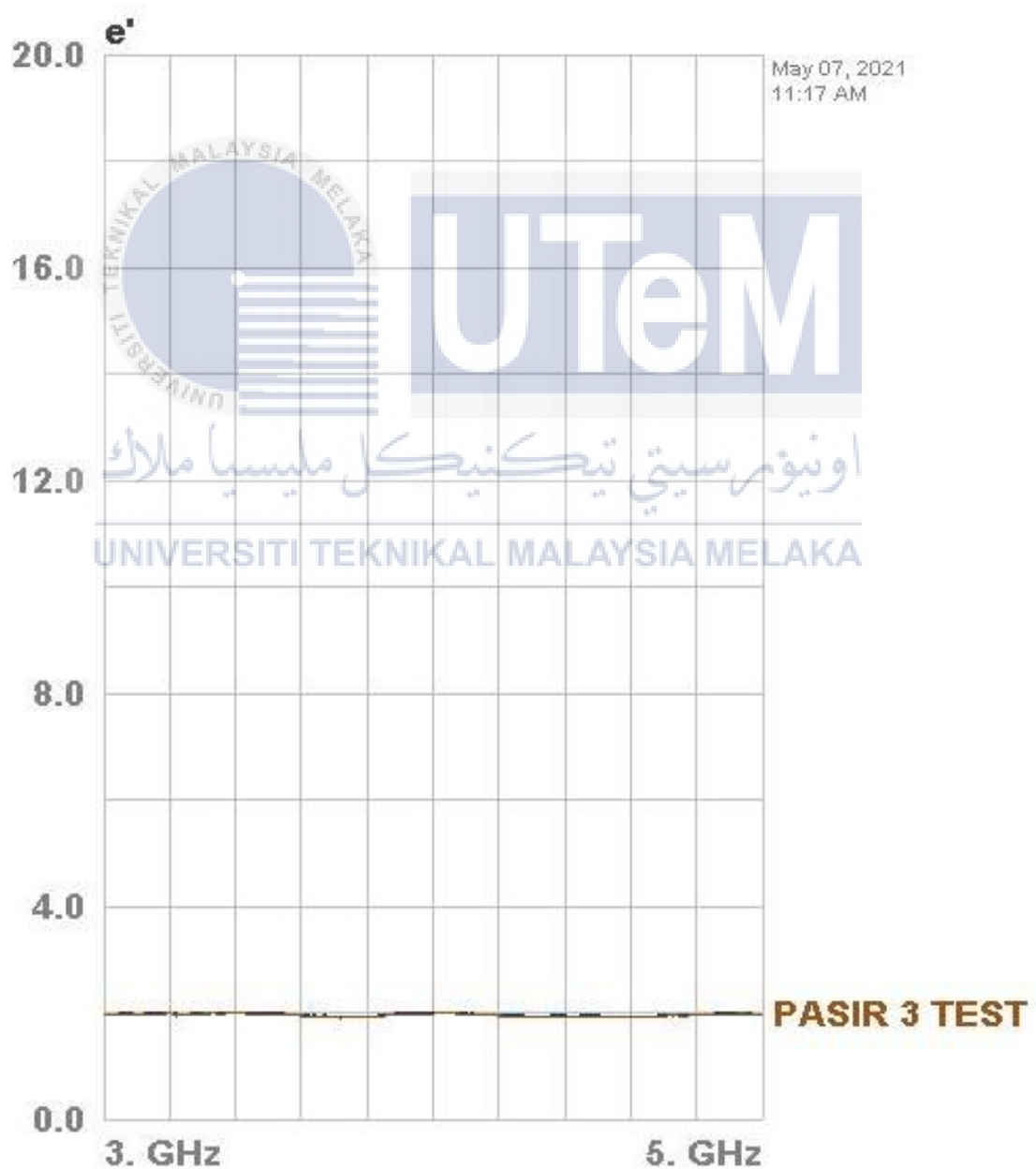
Sugar



d. Sand

	Memory 1	Imaginary	Memory 2	Imaginary	Memory 3	Imaginary
3.924 GHz	1.99	0.076	1.973	-0.0093	1.9753	-0.0033

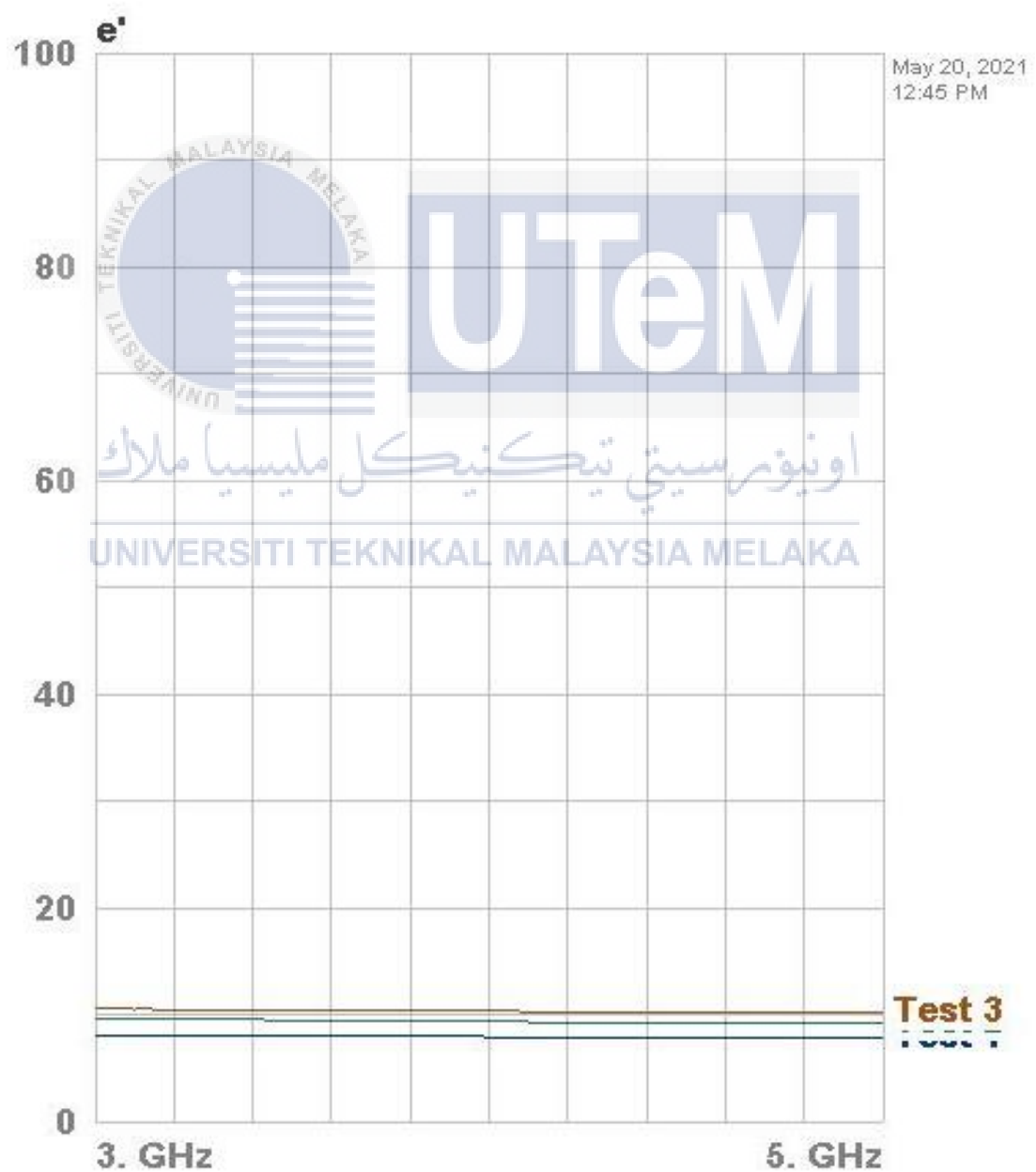
PASIR



e. Soil

	Memory 1	Imaginary	Memory 2	Imaginary	Memory 3	Imaginary
3.924 GHz	7.95	0.63	9.43	1.27	10.36	1.08

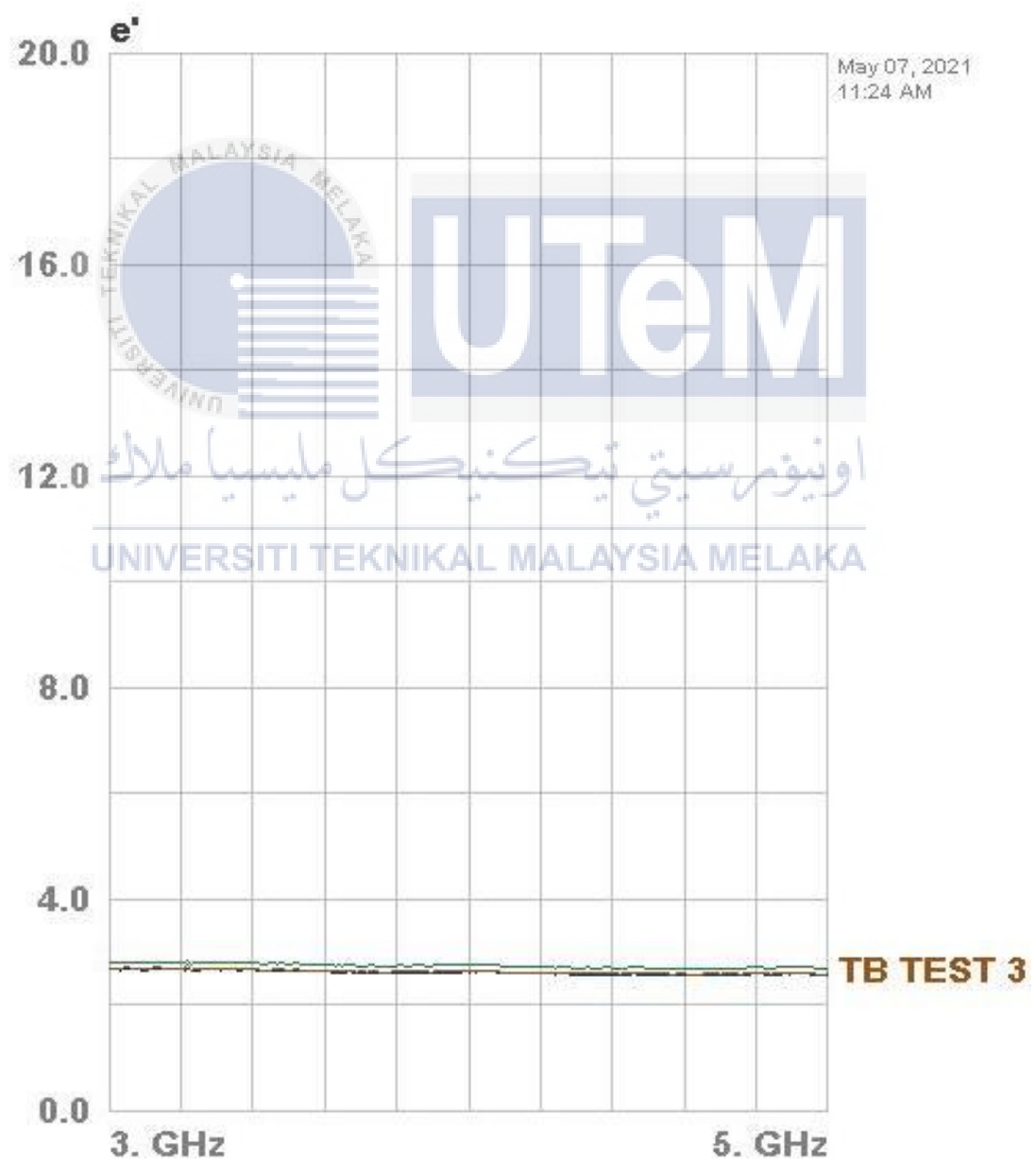
Soil



f. Flour

	Memory 1	Imaginary	Memory 2	Imaginary	Memory 3	Imaginary
3.924 GHz	2.61	0.18	2.74	0.2	2.63	0.18

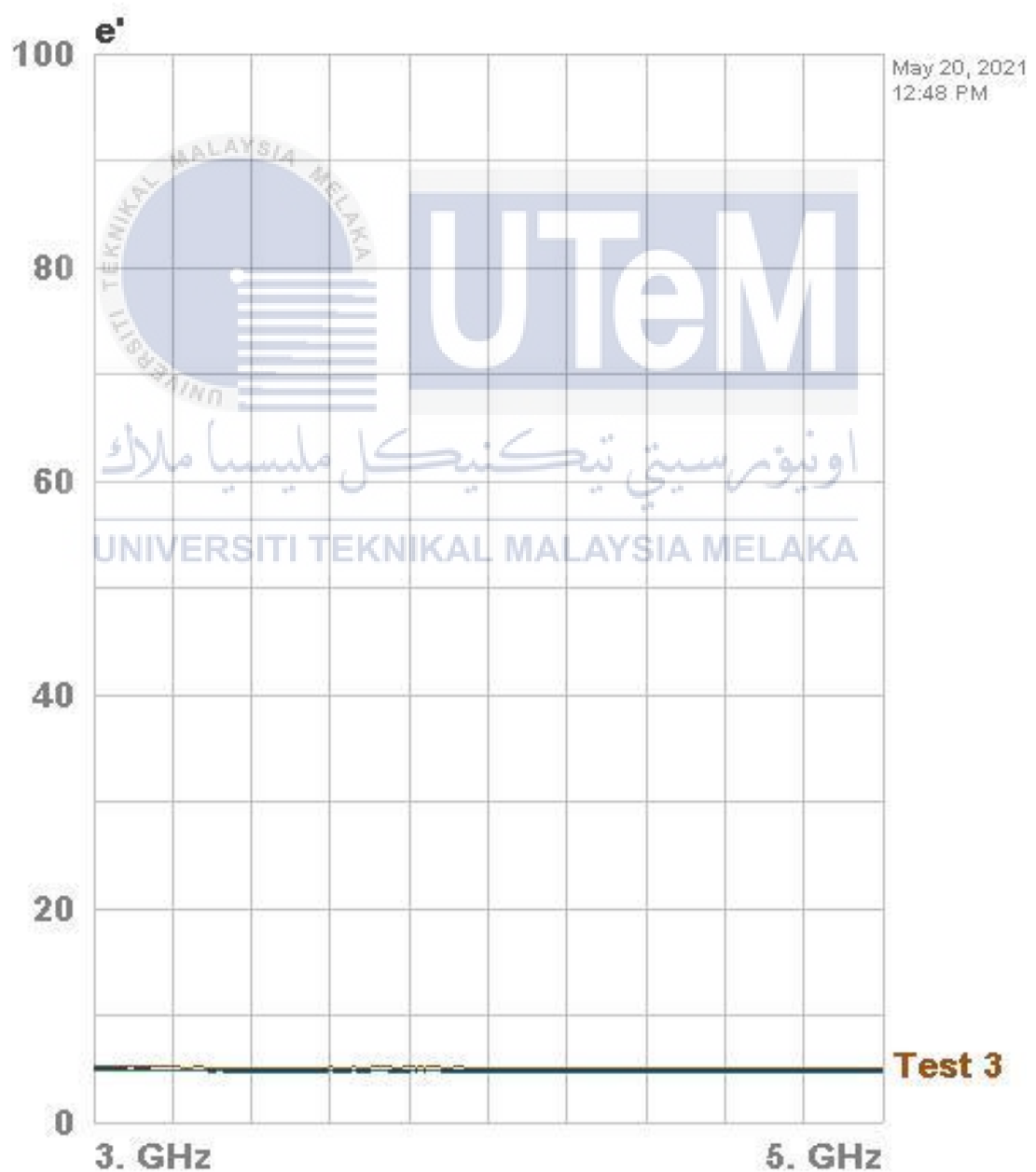
TEPUNG BERAS



g. Plasticine

	Memory 1	Imaginary	Memory 2	Imaginary	Memory 3	Imaginary
3.924 GHz	4.91	-0.106	4.74	-0.09	5.15	-0.1132

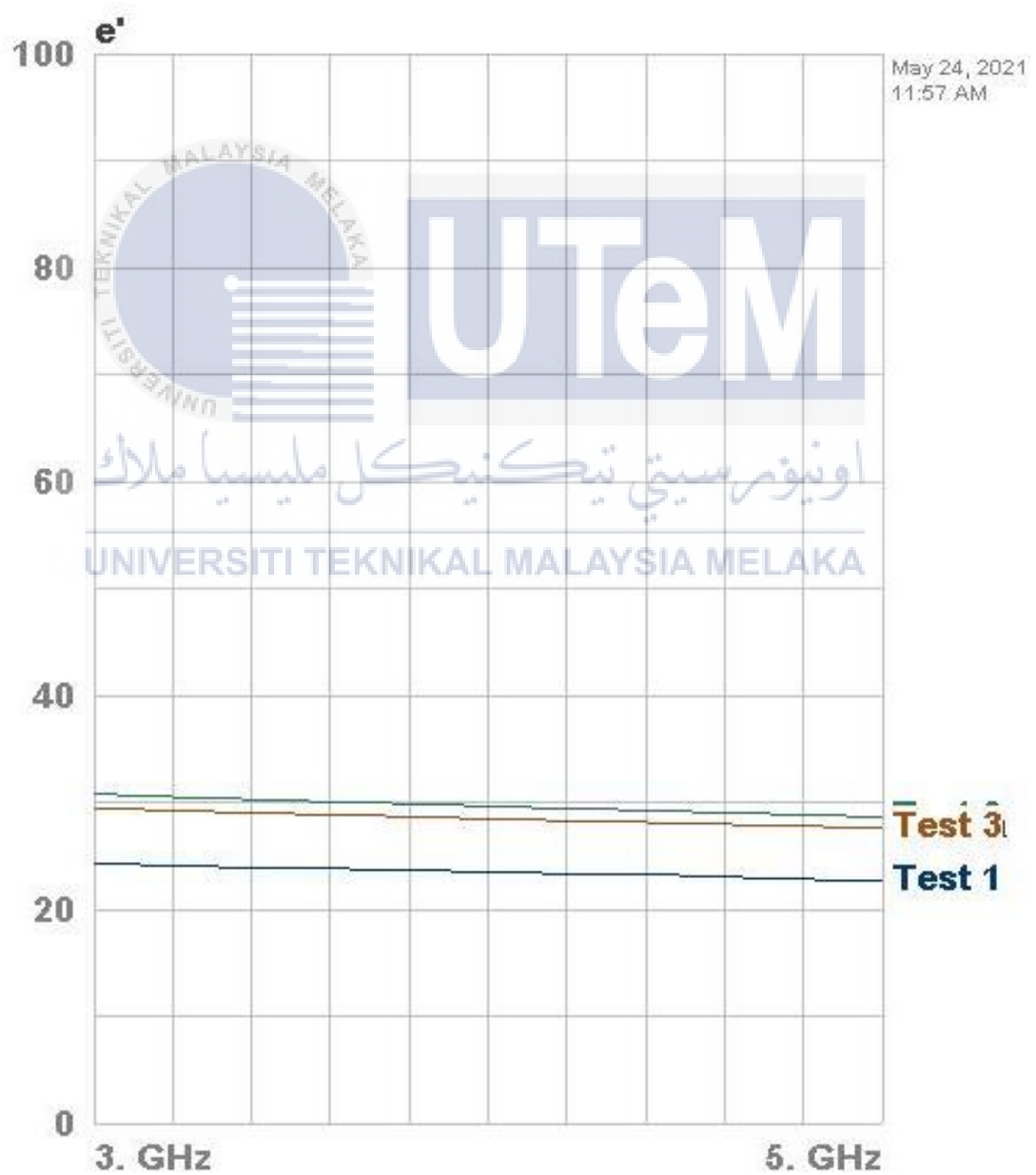
Plasticine



h. Lime

	Memory 1	Imaginary	Memory 2	Imaginary	Memory 3	Imaginary
3.924 GHz	23.55	5.84	29.72	7.98	28.52	7.53

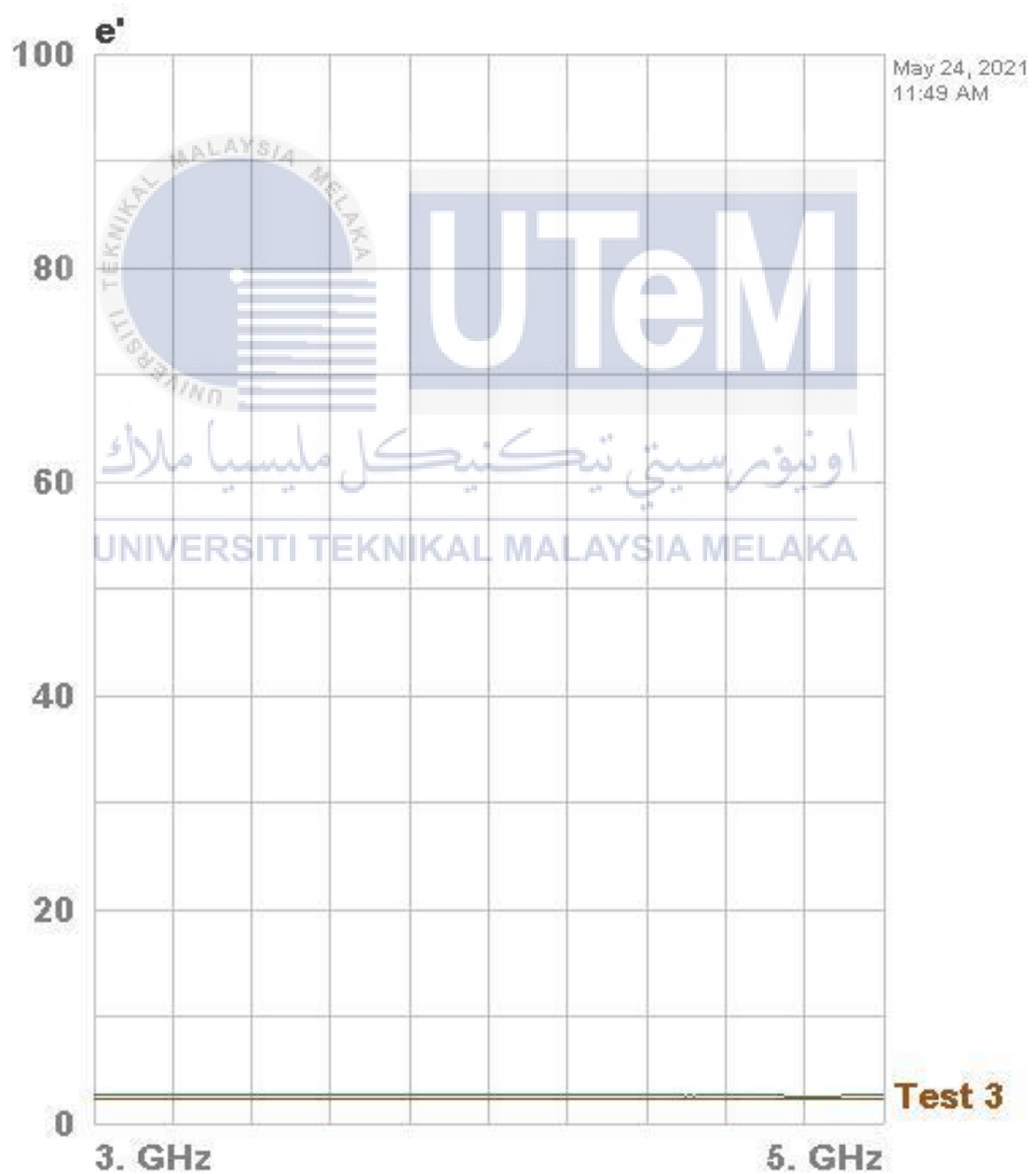
Lime



i. Plastic

	Memory 1	Imaginary	Memory 2	Imaginary	Memory 3	Imaginary
3.924 GHz	2.22	-0.0122	2.6	-0.0145	2.24	-0.0148

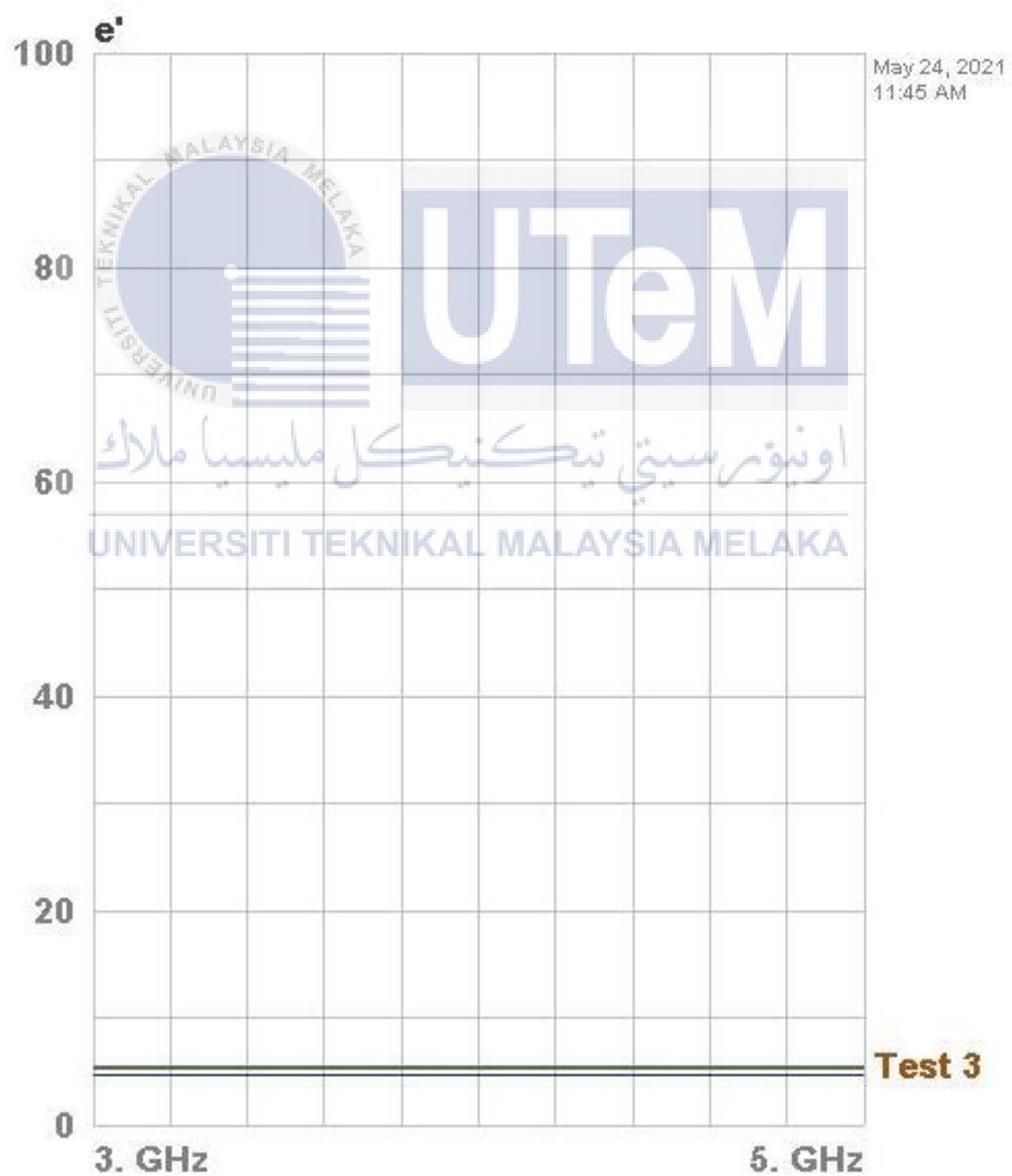
Plastic



j. Rubber

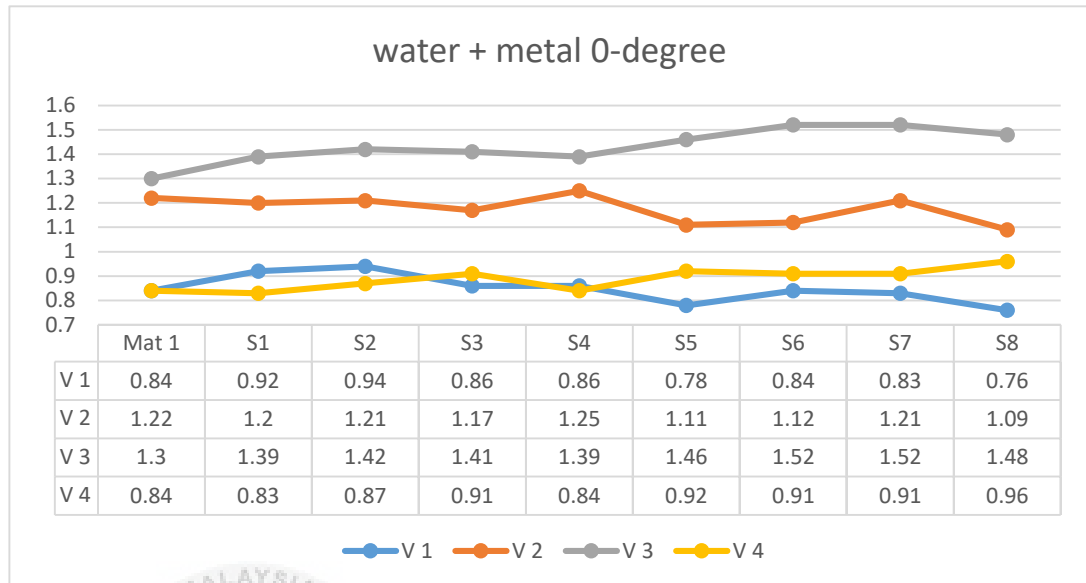
	Memory 1	Imaginary	Memory 2	Imaginary	Memory 3	Imaginary
3.924 GHz	4.666	-0.0498	5.48	-0.0546	5.2685	-0.0637

Rubber



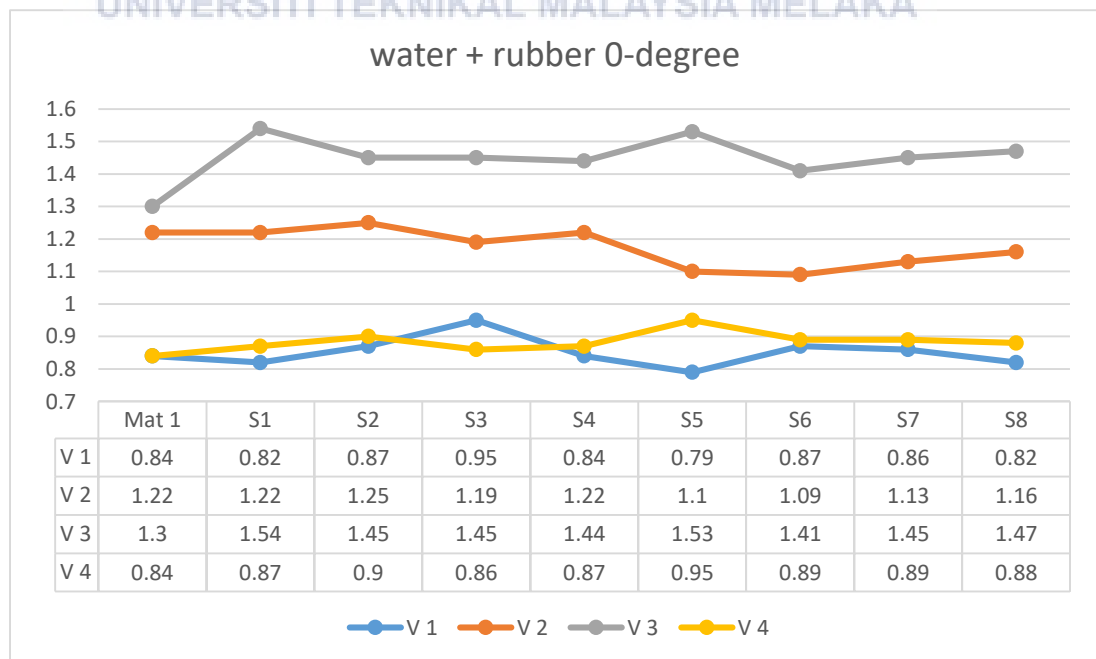
4. SPATIAL DETECTION RESULT FOR 0° PHASE SHIFTER

a. Water + Metal



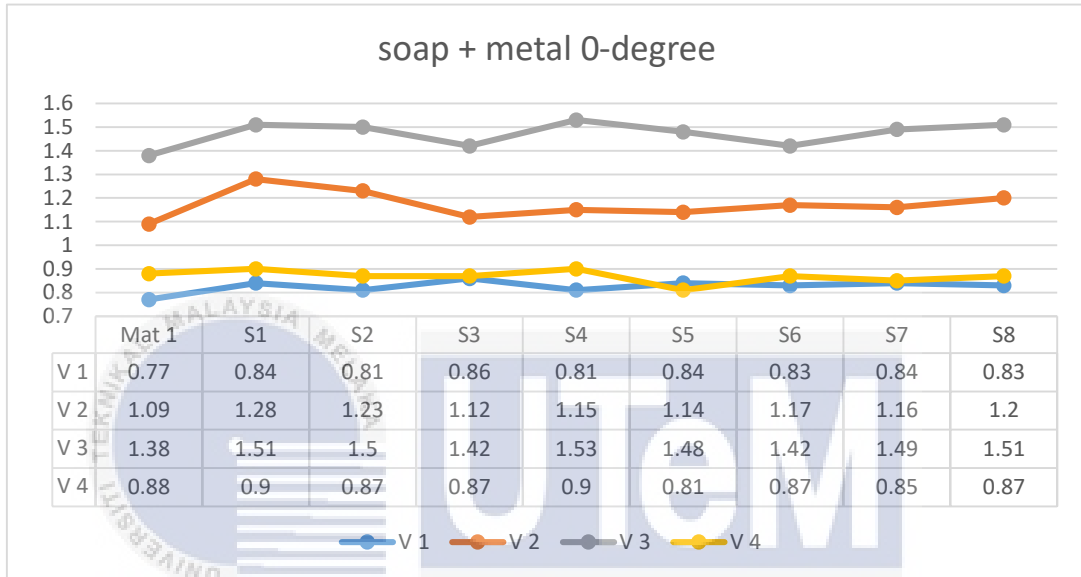
WATER + METAL	Vout (V)								Mat 1
	S1	S2	S3	S4	S5	S6	S7	S8	
V 1	0.08	0.1	0.02	0.02	-0.06	0	-0.01	-0.08	0.84
V 2	-0.02	-0.01	-0.05	0.03	-0.11	-0.1	-0.01	-0.13	1.22
V 3	0.09↑	0.12↑	0.11↑	0.09↑	0.16↑	0.22↑	0.22↑	0.18↑	1.3
V 4	-0.01	0.03	0.07	0	0.08	0.07	0.07	0.12	0.84

b. Water + Rubber



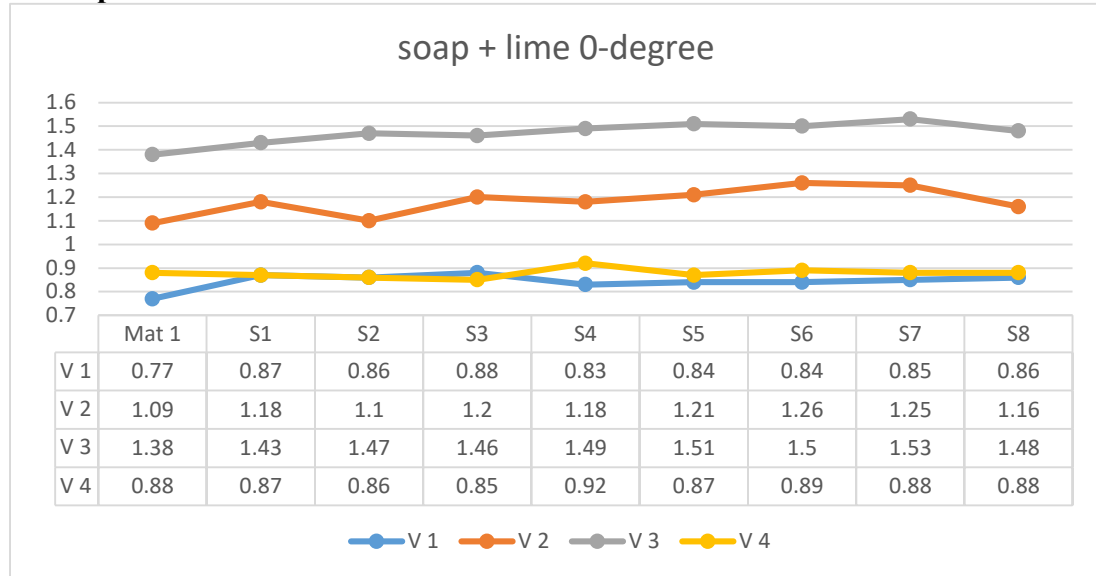
WATER + RUBBER	Vout (V)								Mat 1
	S1	S2	S3	S4	S5	S6	S7	S8	
V 1	-0.02	0.03	0.11	0	-0.05	0.03	0.02	-0.02	0.84
V 2	0	0.03	-0.03	0	-0.43	-0.13	-0.09	-0.06	1.22
V 3	0.24↑	0.15↑	0.15↑	0.14↑	-0.51↑	0.11	0.15↑	0.17↑	1.3
V 4	0.03	0.06	0.02	0.03	-0.05	0.05	0.05	0.04	0.84

c. Soap + Metal



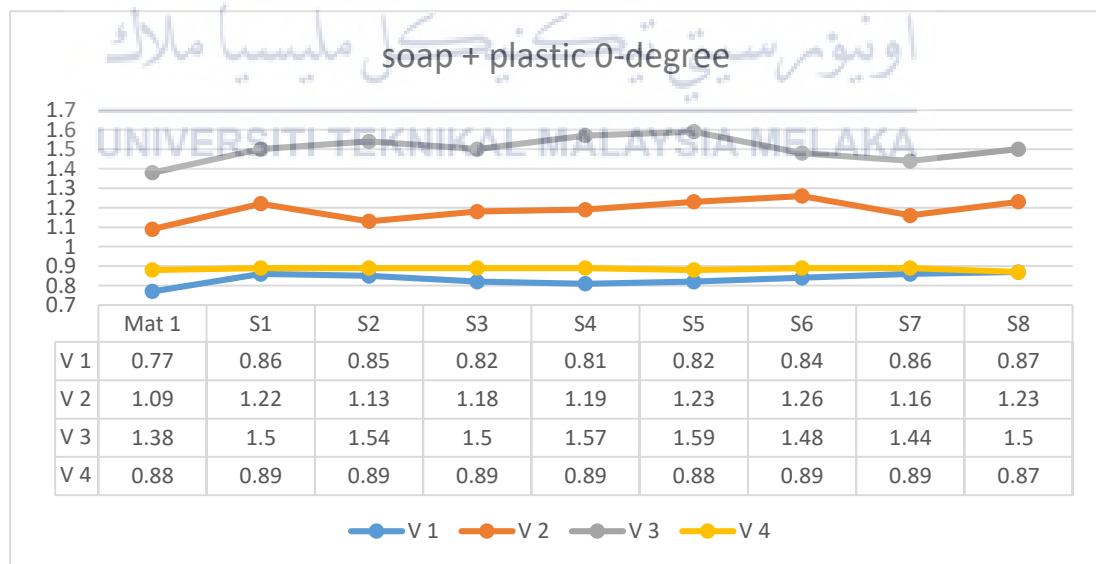
SOAP + METAL	Vout (V)								Mat 1
	S1	S2	S3	S4	S5	S6	S7	S8	
V 1	0.07	0.04	0.09↑	0.04	0.07	0.06	0.07	0.06	0.77
V 2	0.19↑	0.14↑	0.03	0.06	0.05	0.08↑	0.07	0.11	1.09
V 3	0.13	0.12	0.04	0.15↑	0.1↑	0.04	0.11↑	0.13↑	1.38
V 4	0.02	-0.01	-0.01	0.02	-0.07	-0.01	-0.03	-0.01	0.88

d. Soap + Lime



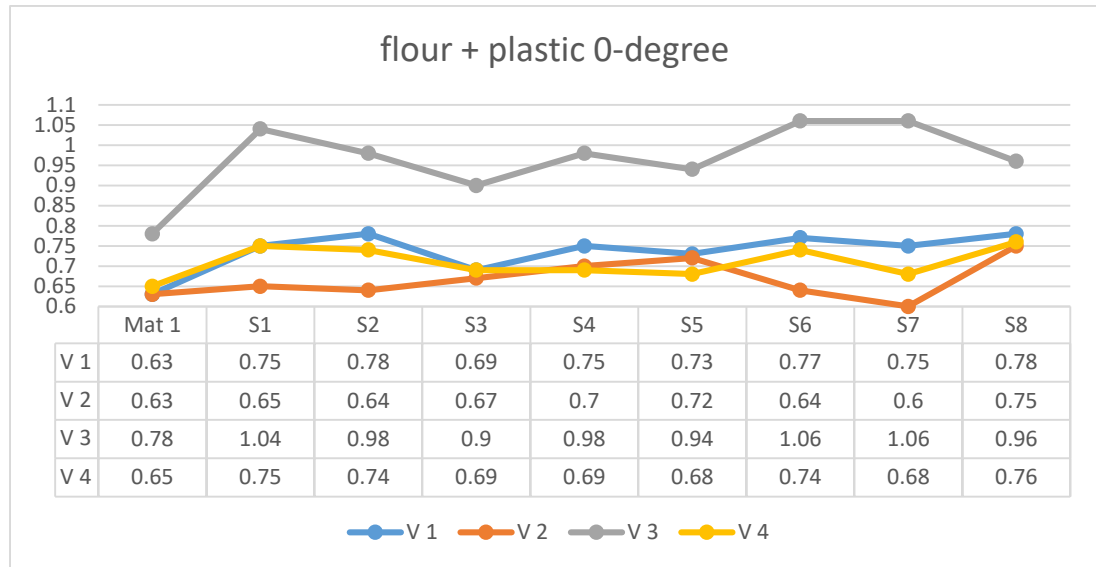
SOAP + LIME	Vout (V)								Mat 1
	S1	S2	S3	S4	S5	S6	S7	S8	
V 1	0.1 ↑	0.09 ↑	0.11 ↑	0.06	0.07	0.07	0.08	0.09	0.77
V 2	0.09	0.01	0.11 ↑	0.09	0.12	0.17 ↑	0.16 ↑	0.07	1.09
V 3	0.05	0.09 ↑	0.08	0.11 ↑	0.13 ↑	0.12	0.15	0.1 ↑	1.38
V 4	-0.01	-0.02	-0.03	0.04	-0.01	0.01	0	0	0.88

e. Soap + Plastic



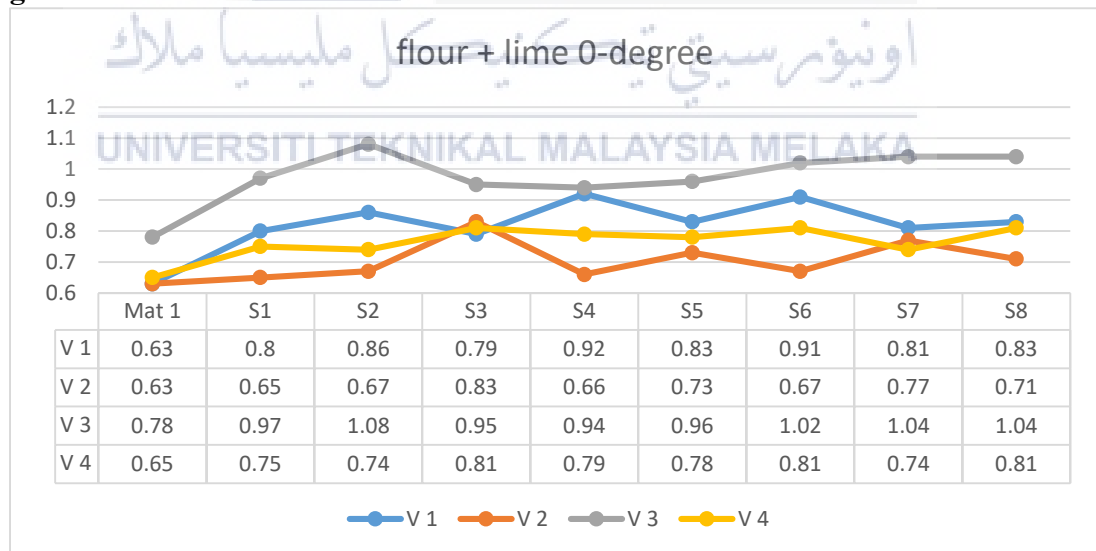
SOAP + PLASTIC	Vout (V)								Mat 1
	S1	S2	S3	S4	S5	S6	S7	S8	
V 1	0.09	0.08	0.05	0.04	0.05	0.07	0.09 ↑	0.1	0.77
V 2	0.13 ↑	0.04	0.09	0.1	0.14	0.17 ↑	0.07	0.14 ↑	1.09
V 3	0.12	0.16 ↑	0.12 ↑	0.19 ↑	0.21 ↑	0.1	0.06	0.12	1.38
V 4	0.01	0.01	0.01	0.01	0	0.01	0.01	-0.01	0.88

f. Flour + Plastic



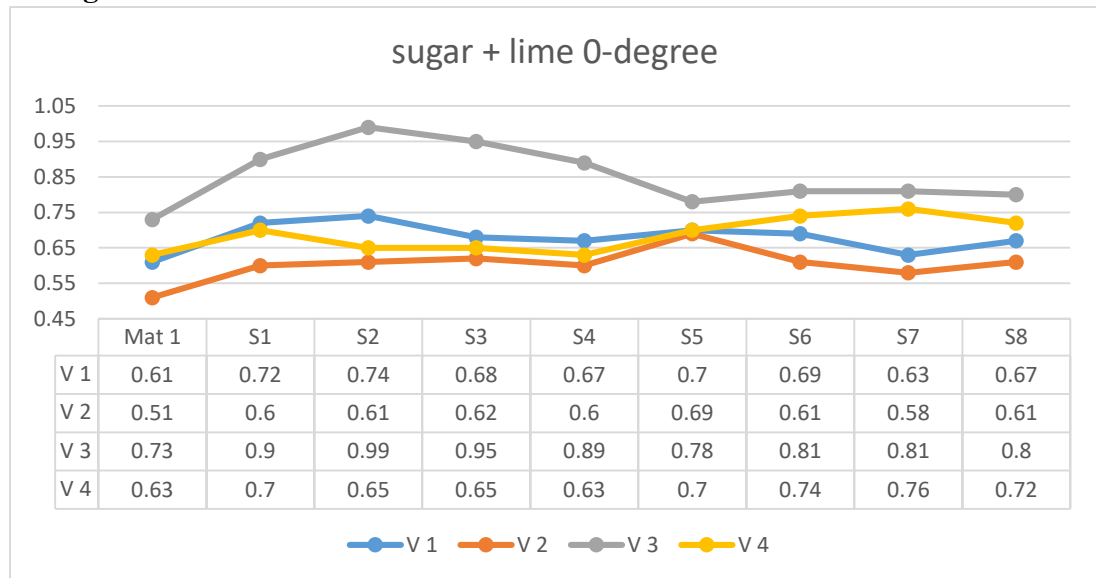
FLOUR + PLASTIC	Vout (V)								Mat 1
	S1	S2	S3	S4	S5	S6	S7	S8	
V 1	0.12	0.15	0.06	0.12 ↑	0.1	0.14	0.12	0.15	0.63
V 2	0.02	0.01	0.04	0.07	0.09	0.01	-0.03	0.12	0.63
V 3	0.26 ↑	0.2 ↑	0.12 ↑	0.2	0.16 ↑	0.28 ↑	0.28 ↑	0.18 ↑	0.78
V 4	0.1	0.09	0.04	0.04	0.03	0.09	0.03	0.11	0.65

g. Flour + Lime



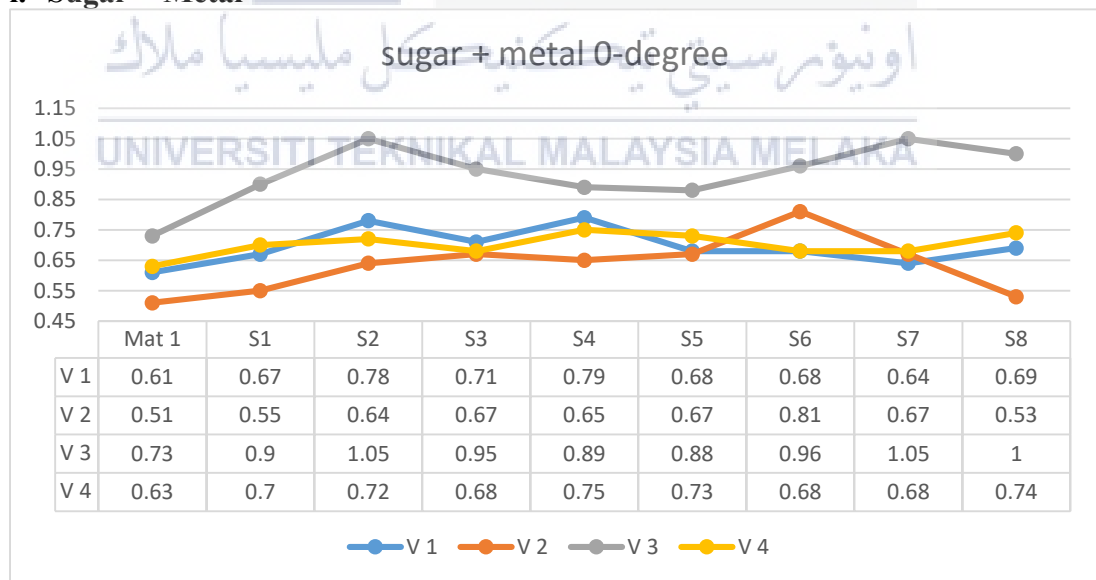
FLOUR + LIME	Vout (V)								Mat 1
	S1	S2	S3	S4	S5	S6	S7	S8	
V 1	0.17	0.23 ↑	0.16	0.29 ↑	0.2 ↑	0.28 ↑	0.18	0.2	0.63
V 2	0.02	0.04	0.2	0.03	0.1	0.04	0.14	0.08	0.63
V 3	0.19 ↑	0.3	0.17 ↑	0.16	0.18	0.24	0.26 ↑	0.26 ↑	0.78
V 4	0.1	0.09	0.16	0.14	0.13	0.16	0.09	0.16	0.65

h. Sugar + Lime



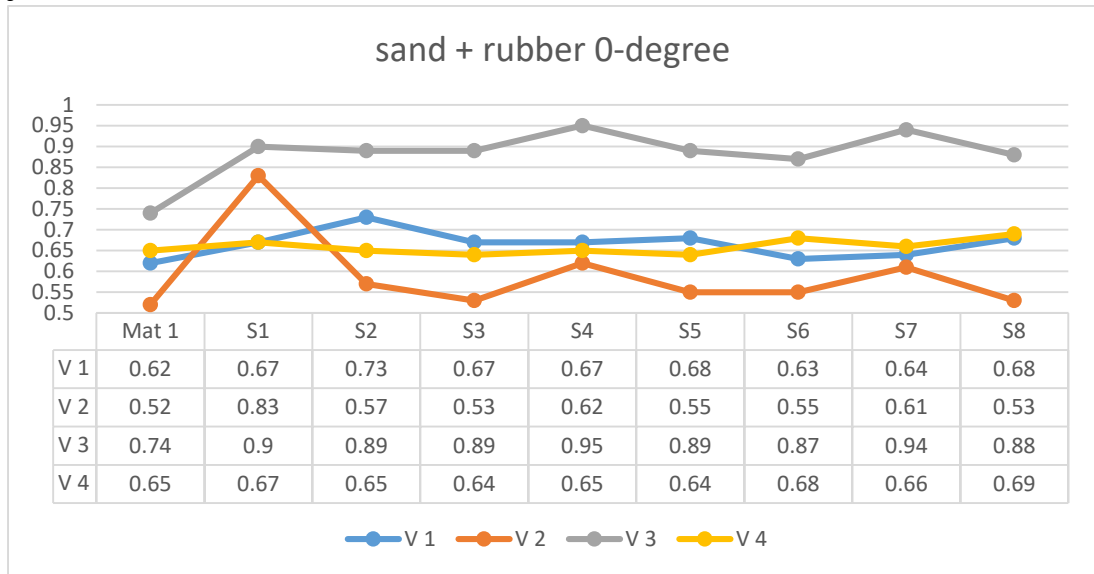
SUGAR +LIME	Vout (V)								Mat 1
	S1	S2	S3	S4	S5	S6	S7	S8	
V 1	0.11	0.13	0.07	0.06	0.09	0.08	0.02	0.06	0.61
V 2	0.09	0.1	0.11	0.09	0.18 ↑	0.1	0.07	0.1 ↑	0.51
V 3	0.17 ↑	0.26 ↑	0.22 ↑	0.16 ↑	0.05	0.08	0.08	0.07	0.73
V 4	0.07	0.02	0.02	0	0.07	0.11 ↑	0.13 ↑	0.09	0.63

i. Sugar + Metal



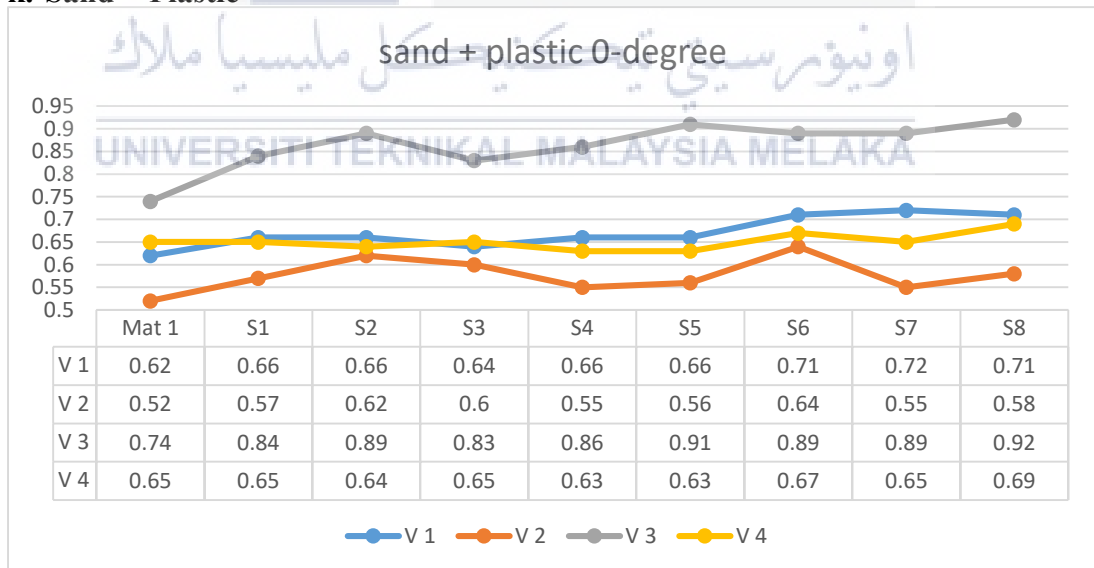
SUGAR + METAL	Vout (V)								Mat 1
	S1	S2	S3	S4	S5	S6	S7	S8	
V 1	0.06	0.17	0.1	0.18 ↑	0.07	0.07	0.03	0.08	0.61
V 2	0.04	0.13	0.16	0.14	0.16 ↑	0.3 ↑	0.16	0.02	0.51
V 3	0.17 ↑	0.32 ↑	0.22 ↑	0.16	0.15	0.23	0.32 ↑	0.27 ↑	0.73
V 4	0.07	0.09	0.05	0.12	0.1	0.05	0.05	0.11	0.63

j. Sand + Rubber



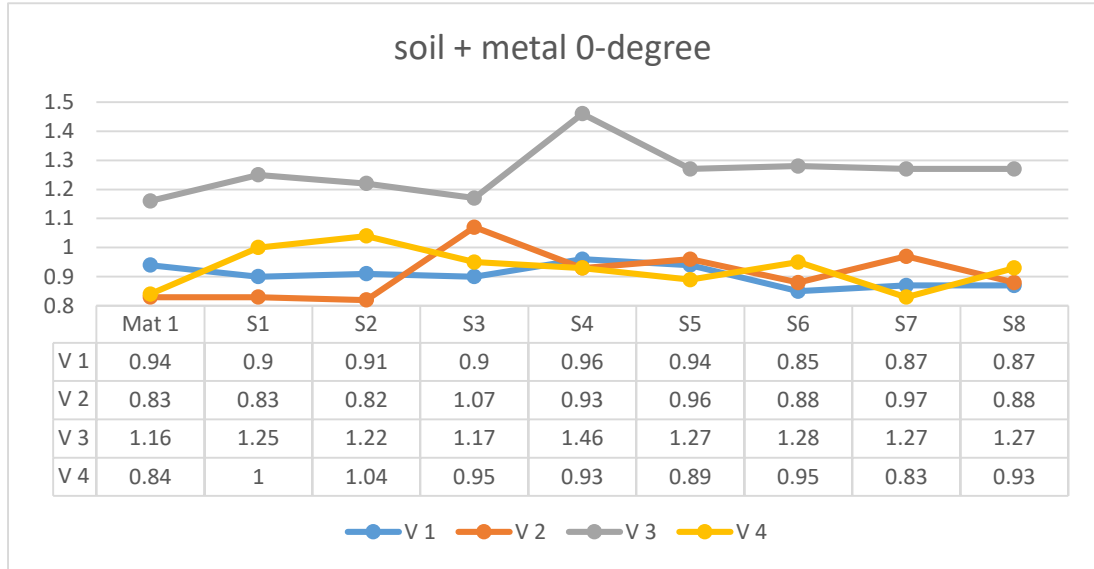
SAND + RUBBER	Vout (V)								Mat 1
	S1	S2	S3	S4	S5	S6	S7	S8	
V 1	0.05	0.11	0.05	0.05	0.06	0.01	0.02	0.06	0.62
V 2	0.31 ↑	0.05	0.01	0.1	0.03	0.03	0.09	0.01	0.52
V 3	0.16	0.15 ↑	0.15 ↑	0.21 ↑	0.15 ↑	0.13 ↑	0.2 ↑	0.14 ↑	0.74
V 4	0.02	0	-0.01	0	-0.01	0.03	0.01	0.04	0.65

k. Sand + Plastic



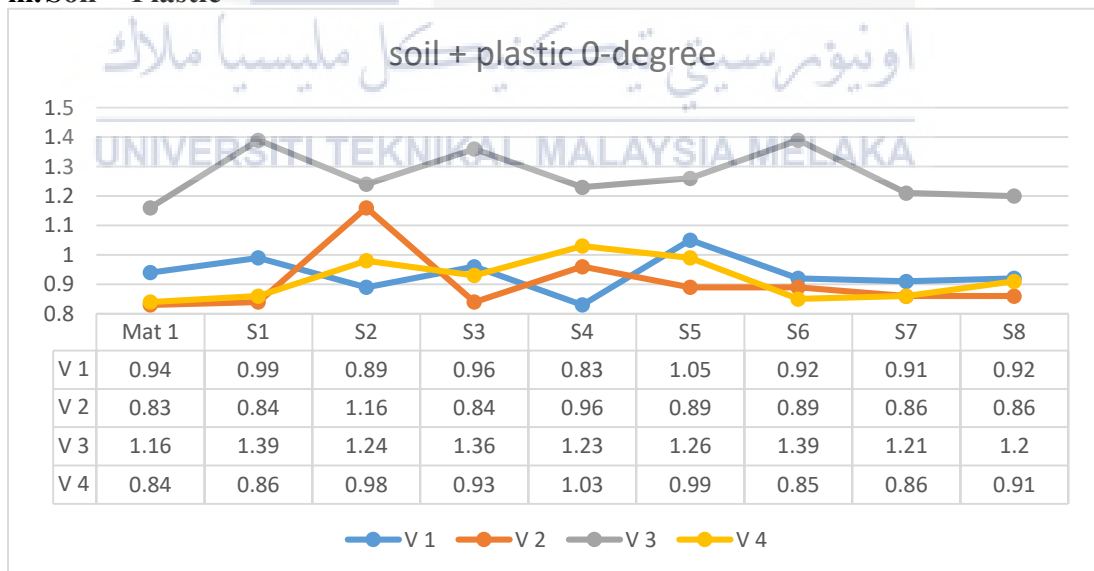
SAND + PLASTIC	Vout (V)								Mat 1
	S1	S2	S3	S4	S5	S6	S7	S8	
V 1	0.04	0.04	0.02	0.04	0.04	0.09	0.1	0.09	0.62
V 2	0.05	0.1	0.08	0.03	0.04	0.12	0.03	0.06	0.52
V 3	0.1 ↑	0.15 ↑	0.09 ↑	0.12 ↑	0.17 ↑	0.15 ↑	0.15 ↑	0.18 ↑	0.74
V 4	0	-0.01	0	-0.02	-0.02	0.02	0	0.04	0.65

l. Soil + Metal



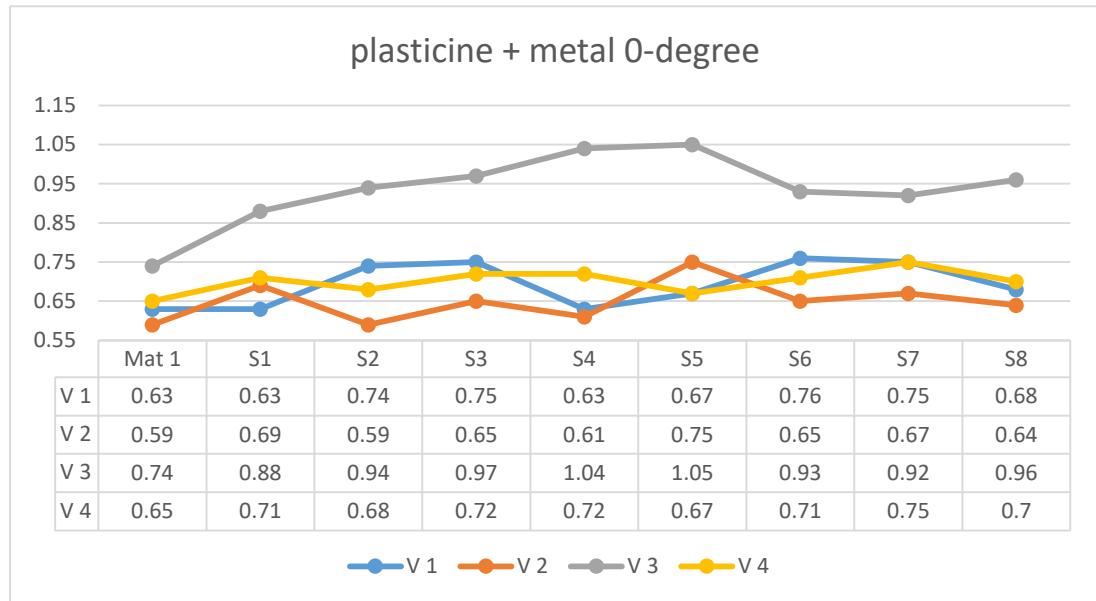
SOIL + METAL	Vout (V)								Mat 1
	S1	S2	S3	S4	S5	S6	S7	S8	
V 1	-0.04	-0.03	-0.04	0.02	0	-0.09	-0.07	-0.07	0.94
V 2	0	-0.01	0.24 ↑	0.1	0.13 ↑	0.05	0.14 ↑	0.05	0.83
V 3	0.09	0.06 ↑	0.01	0.3 ↑	0.11	0.12 ↑	0.11	0.11 ↑	1.16
V 4	0.16 ↑	0.2	0.11	0.09	0.05	0.11	-0.01	0.09	0.84

m. Soil + Plastic



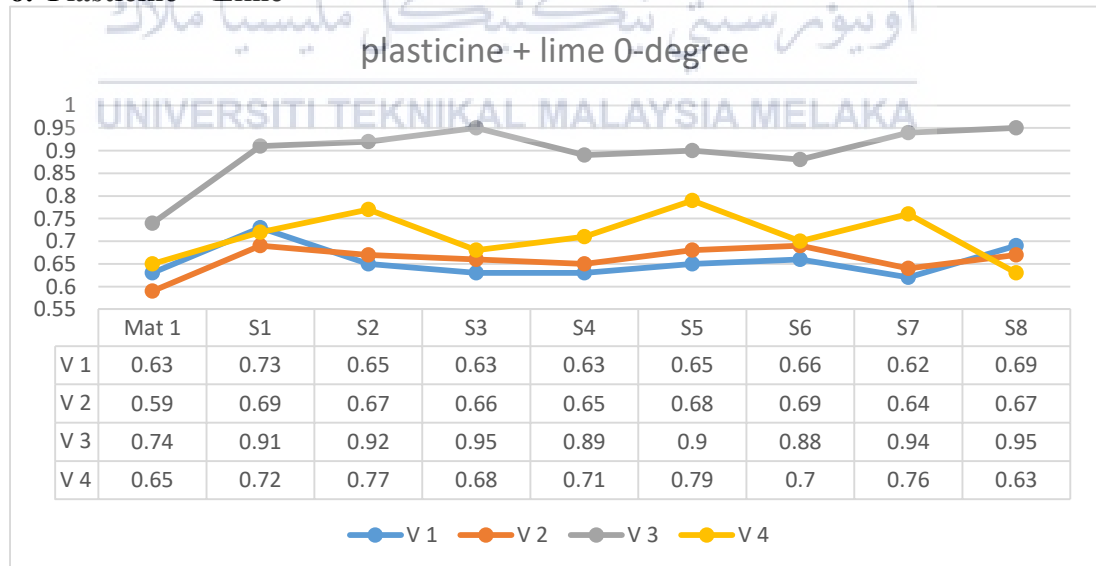
SOIL + PLASTIC	Vout (V)								Mat 1
	S1	S2	S3	S4	S5	S6	S7	S8	
V 1	0.05	-0.05	0.02	-0.11	0.11	-0.02	-0.03	-0.02	0.94
V 2	0.01	0.33 ↑	0.01	0.13	0.06	0.06	0.03	0.03	0.83
V 3	0.23 ↑	0.08	0.2 ↑	0.07	0.1	0.23 ↑	0.05 ↑	0.04	1.16
V 4	0.02	0.14	0.09	0.19 ↑	0.15 ↑	0.01	0.02	0.07 ↑	0.84

n. Plasticine + Metal



PLASTICI NE + METAL	Vout (V)								Mat 1
	S1	S2	S3	S4	S5	S6	S7	S8	
V 1	0	0.11 ↑	0.12	0	0.04	0.13	0.12	0.05	0.63
V 2	0.1	0	0.06	0.02	0.16	0.06	0.08	0.05	0.59
V 3	0.14 ↑	0.2	0.23 ↑	0.3	0.31 ↑	0.19 ↑	0.18 ↑	0.22 ↑	0.74
V 4	0.06	0.03	0.07	0.07 ↑	0.02	0.06	0.1	0.05	0.65

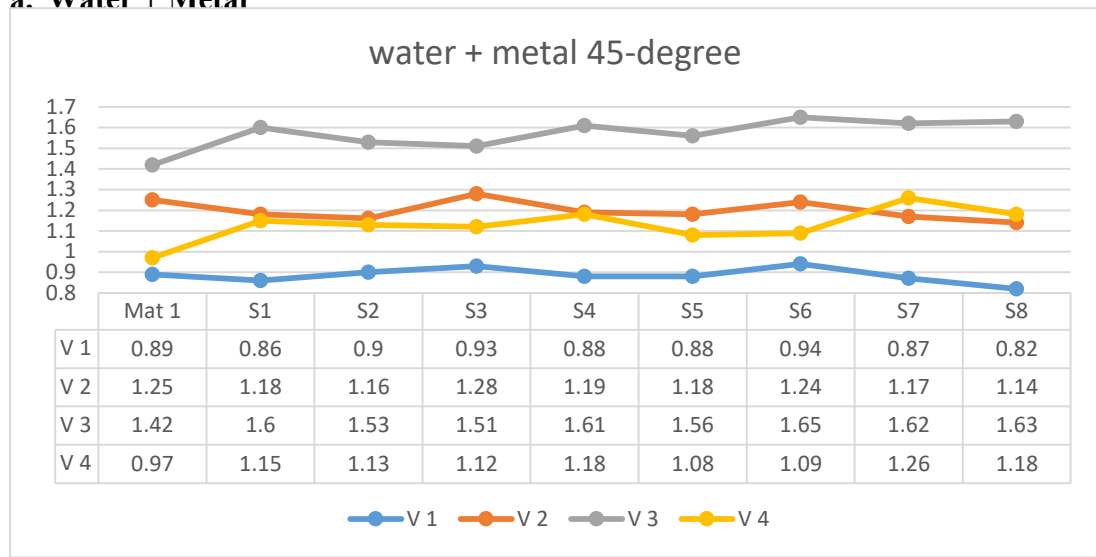
o. Plasticine + Lime



PLASTICI NE + LIME	Vout (V)								Mat 1
	S1	S2	S3	S4	S5	S6	S7	S8	
V 1	0.1	0.02	0	0	0.02	0.03	-0.01	0.06	0.63
V 2	0.1	0.08	0.07	0.06	0.09	0.07	0.05	0.08	0.59
V 3	0.17 ↑	0.18 ↑	0.21 ↑	0.15 ↑	0.16 ↑	-0.08 ↓	0.2 ↑	0.21 ↑	0.74
V 4	0.07	0.12	0.03	0.06	0.14	0.01	0.11	-0.02	0.65

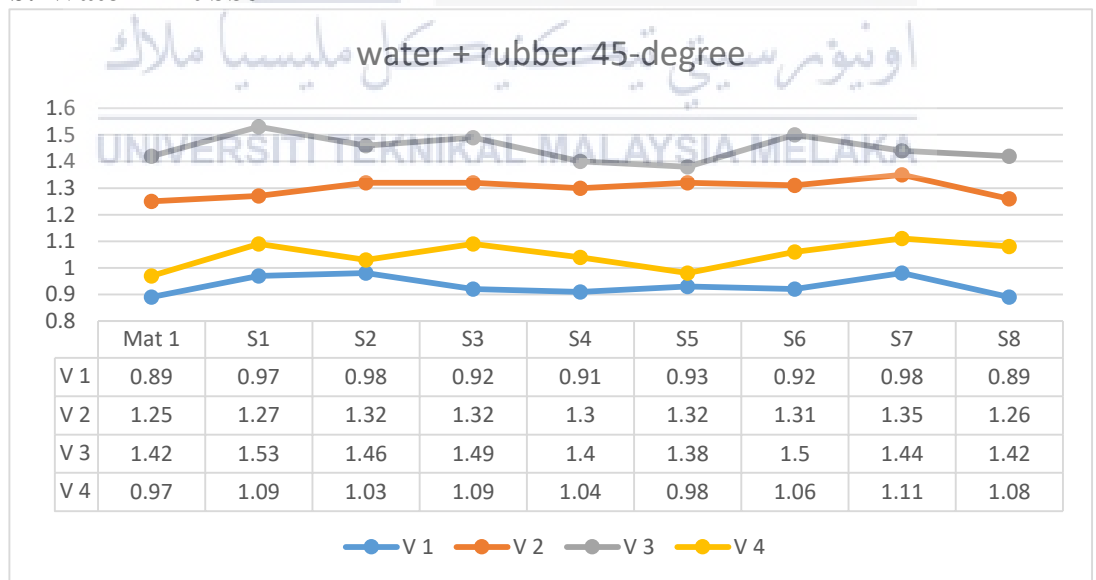
5. SPATIAL DETECTION RESULT FOR 45° PHASE SHIFTER

a. Water + Metal



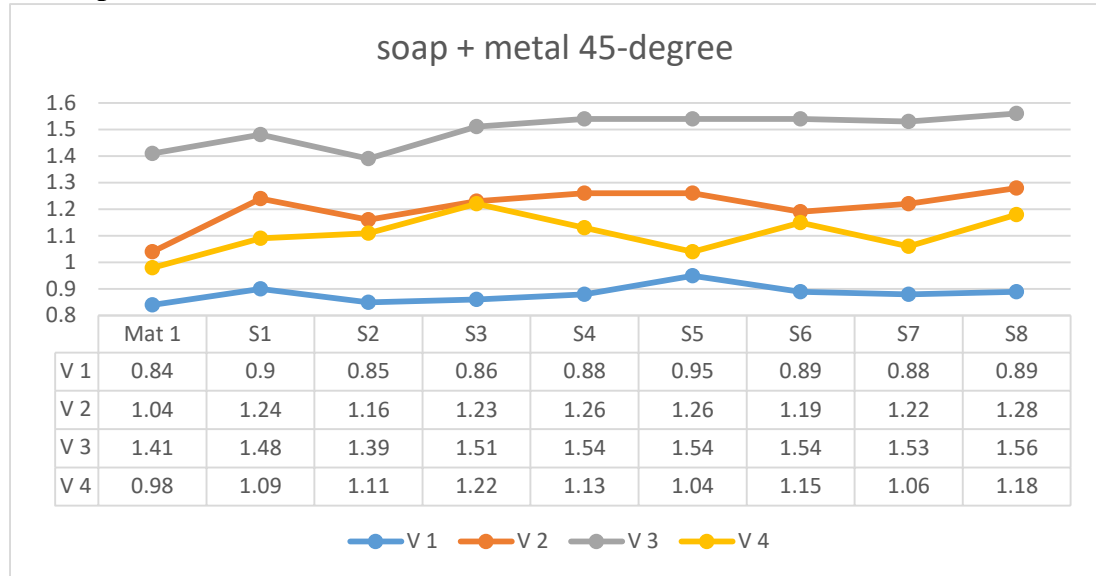
WATER + METAL	Vout (V)								
	S1	S2	S3	S4	S5	S6	S7	S8	Mat 1
V 1	-0.03	0.01	0.04	-0.01	-0.01	0.05	-0.02	-0.07	0.89
V 2	-0.07	-0.09	0.03	-0.06	-0.07	-0.01	-0.08	-0.11	1.25
V 3	0.18 ↑	0.11	0.09	0.19	0.14 ↑	0.23 ↑	0.2	0.21 ↑	1.42
V 4	0.18 ↑	0.16 ↑	0.15 ↑	0.21 ↑	0.11	0.12	0.29 ↑	0.21 ↑	0.97

b. Water + Rubber



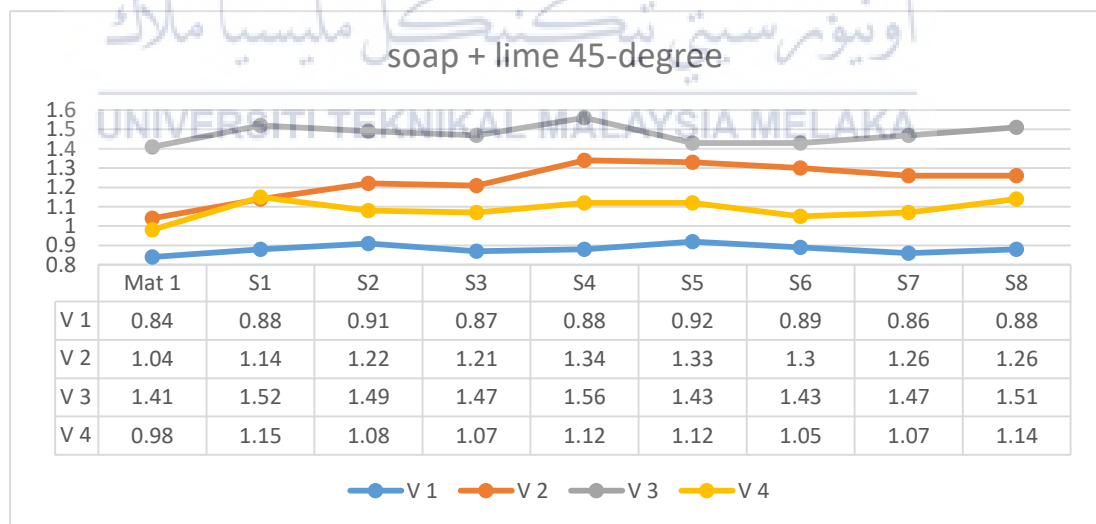
WATER + RUBBER	Vout (V)								
	S1	S2	S3	S4	S5	S6	S7	S8	Mat 1
V 1	0.08	0.09 ↑	0.03	0.02	0.04	0.03	0.09	0	0.89
V 2	0.02	0.07	0.07	0.05	0.07 ↑	0.06	0.1	0.01	1.25
V 3	0.11	0.04	0.07	-0.02	-0.04	0.08	0.02	0	1.42
V 4	0.12 ↑	0.06	0.12 ↑	0.07 ↑	0.01	0.09 ↑	0.14 ↑	0.11 ↑	0.97

c. Soap + Metal



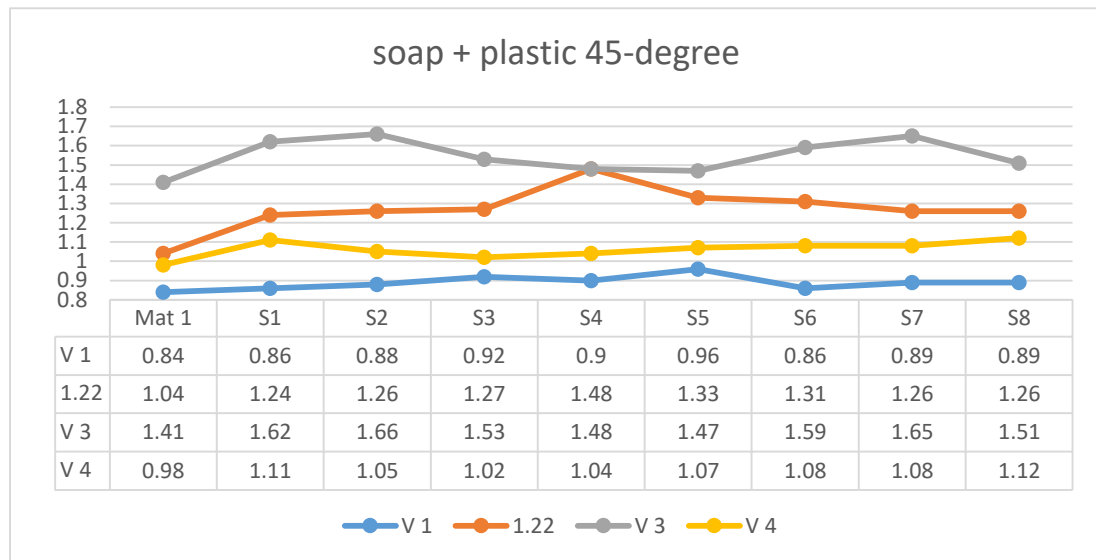
SOAP + METAL	Vout (V)								
	S1	S2	S3	S4	S5	S6	S7	S8	Mat 1
V 1	0.06	0.01	0.02	0.04	0.11	0.05	0.04	0.05	0.84
V 2	0.2	0.12	0.19	0.22 ↑	0.22 ↑	0.15	0.18 ↑	0.24 ↑	1.04
V 3	0.07	-0.02	0.1	0.13	0.13	0.13	0.12	0.15	1.41
V 4	0.11 ↑	0.13 ↑	0.24 ↑	0.15	0.06	0.17 ↑	0.08	0.2	0.98

d. Soap + Lime



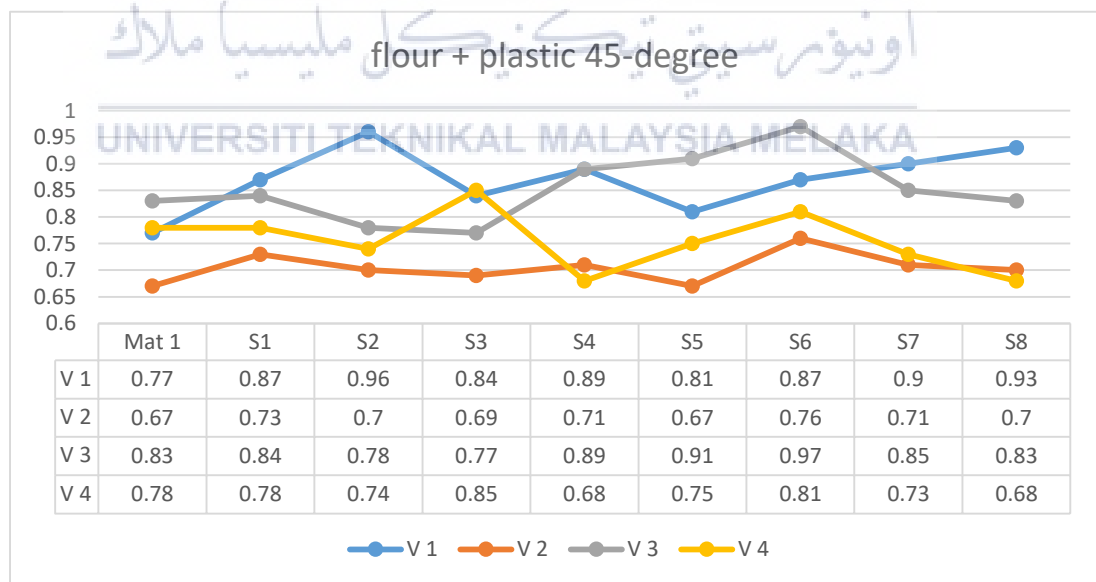
SOAP + LIME	Vout (V)								
	S1	S2	S3	S4	S5	S6	S7	S8	Mat 1
V 1	0.04	0.07	0.03	0.04	0.08	0.05	0.02	0.04	0.84
V 2	0.1	0.18 ↑	0.17 ↑	0.3	0.29 ↑	0.26 ↑	0.22 ↑	0.22 ↑	1.04
V 3	0.11	0.08	0.06	0.15 ↑	0.02	0.02	0.06	0.1	1.41
V 4	0.17 ↑	0.1	0.09	0.14	0.14	0.07	0.09	0.16	0.98

e. Soap + Plastic



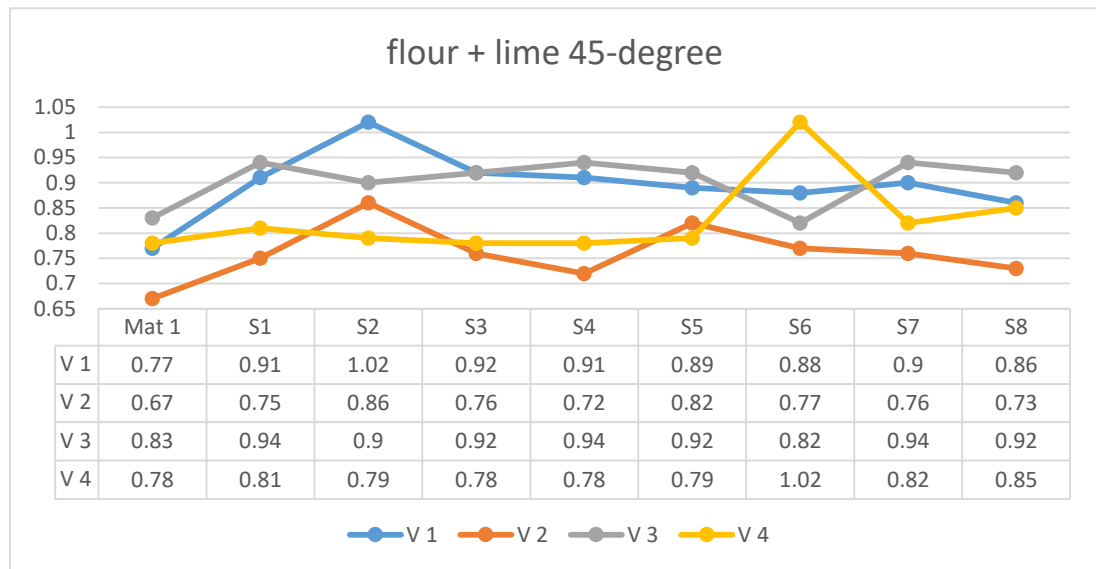
SOAP + PLASTIC	Vout (V)								Mat 1
	S1	S2	S3	S4	S5	S6	S7	S8	
V 1	0.02	0.04	0.08	0.06	0.12	0.02	0.05	0.05	0.84
V 2	0.2	0.22	0.23 ↑	0.44 ↑	0.29 ↑	0.27 ↑	0.22	0.22 ↑	1.04
V 3	0.21 ↑	0.25 ↑	0.12	0.07	0.06	0.18	0.24 ↑	0.1	1.41
V 4	0.13	0.07	0.04	0.06	0.09	0.1	0.1	0.14	0.98

f. Flour + Plastic



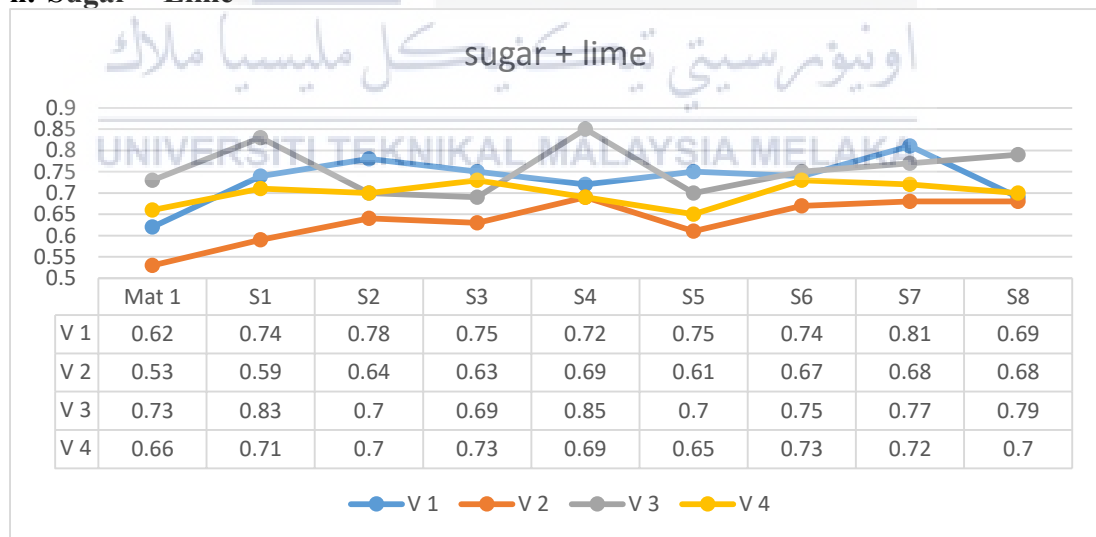
FLOUR + PLASTIC	Vout (V)								Mat 1
	S1	S2	S3	S4	S5	S6	S7	S8	
V 1	0.1 ↑	0.19 ↑	0.07 ↑	0.12 ↑	0.04	0.1	0.13 ↑	0.16 ↑	0.77
V 2	0.06	0.03	0.02	0.04	0	0.09	0.04	0.03	0.67
V 3	0.01	-0.05	-0.06	0.06	0.08 ↑	0.14 ↑	0.02	0	0.83
V 4	0	-0.04	0.07 ↑	-0.1	-0.03	0.03	-0.05	-0.1	0.78

g. Flour + Lime



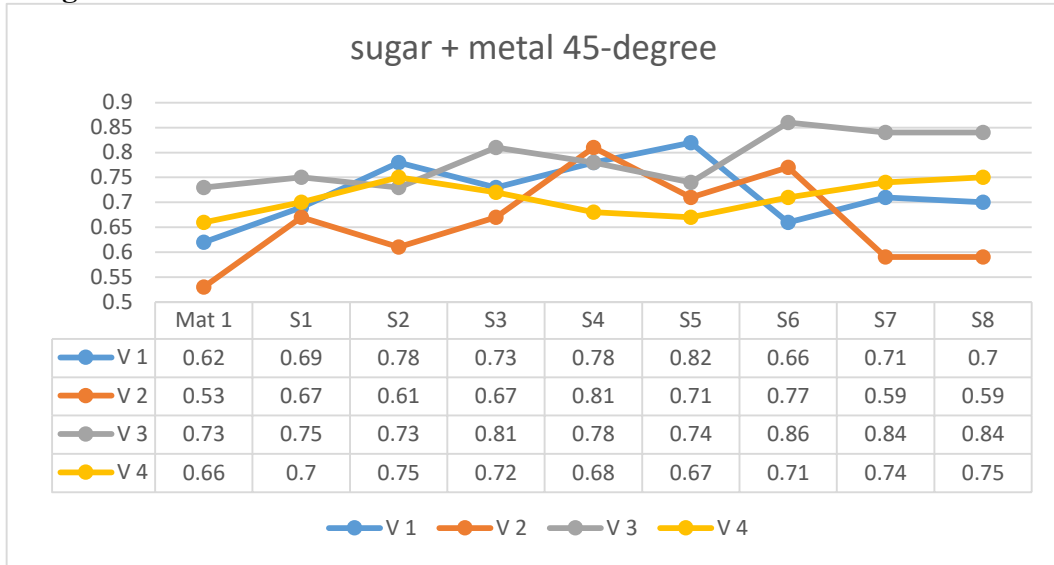
FLOUR + LIME	Vout (V)									Mat 1
	S1	S2	S3	S4	S5	S6	S7	S8		
V 1	0.14 ↑	0.25 ↑	0.15 ↑	0.14 ↑	0.12	0.11	0.13 ↑	0.09 ↑	0.77	
V 2	0.08	0.19	0.09	0.05	0.15 ↑	0.1	0.09	0.06	0.67	
V 3	0.11	0.07	0.09	0.11	0.09	-0.01	0.11	0.09 ↑	0.83	
V 4	0.03	0.01	0	0	0.01	0.24 ↑	0.04	0.07	0.78	

h. Sugar + Lime



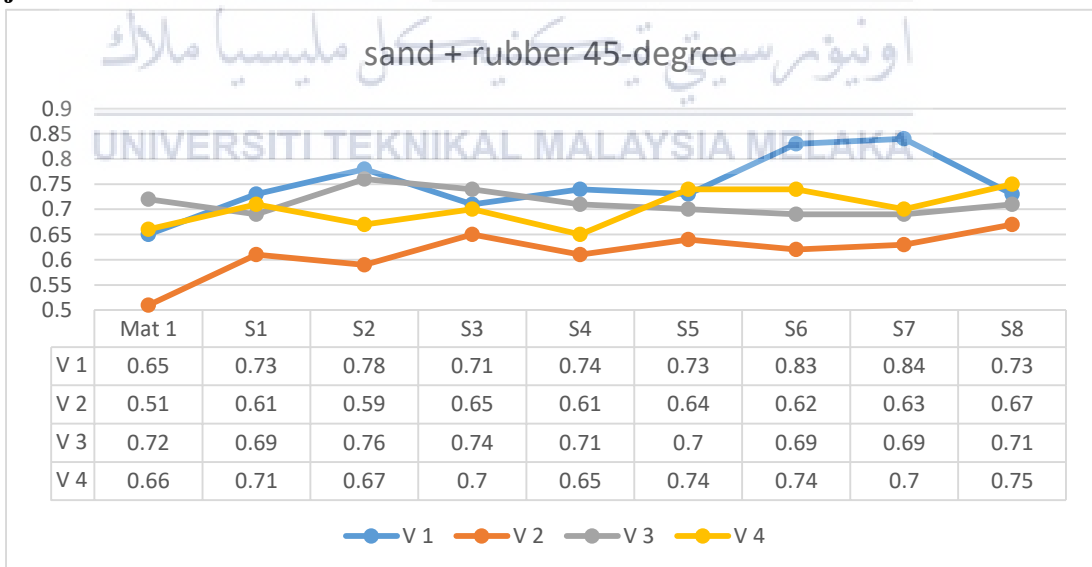
SUGAR + LIME	Vout (V)									Mat 1
	S1	S2	S3	S4	S5	S6	S7	S8		
V 1	0.12 ↑	0.16 ↑	0.13 ↑	0.1	0.13 ↑	0.12	0.19 ↑	0.07	0.62	
V 2	0.06	0.11	0.1	0.16 ↑	0.08	0.14 ↑	0.15	0.15 ↑	0.53	
V 3	0.1	-0.03	-0.04	0.12	-0.03	0.02	0.04	0.06	0.73	
V 4	0.05	0.04	0.07	0.03	-0.01	0.07	0.06	0.04	0.66	

i. Sugar + Metal



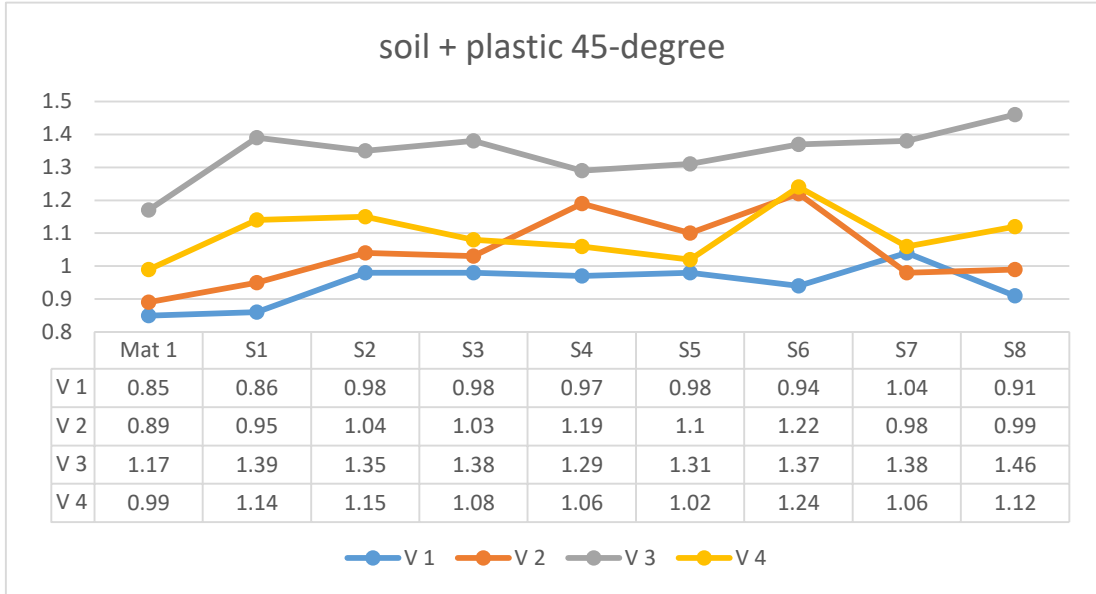
SUGAR + METAL	Vout (V)								
	S1	S2	S3	S4	S5	S6	S7	S8	Mat 1
V 1	0.07	0.16 ↑	0.11	0.16	0.2	0.04	0.09	0.08	0.62
V 2	0.14 ↑	0.08	0.14 ↑	0.28 ↑	0.18 ↑	0.24 ↑	0.06	0.06	0.53
V 3	0.02	0	0.08	0.05	0.01	0.13	0.11 ↑	0.11 ↑	0.73
V 4	0.04	0.09	0.06	0.02	0.01	0.05	0.08	0.09	0.66

j. Sand + Rubber



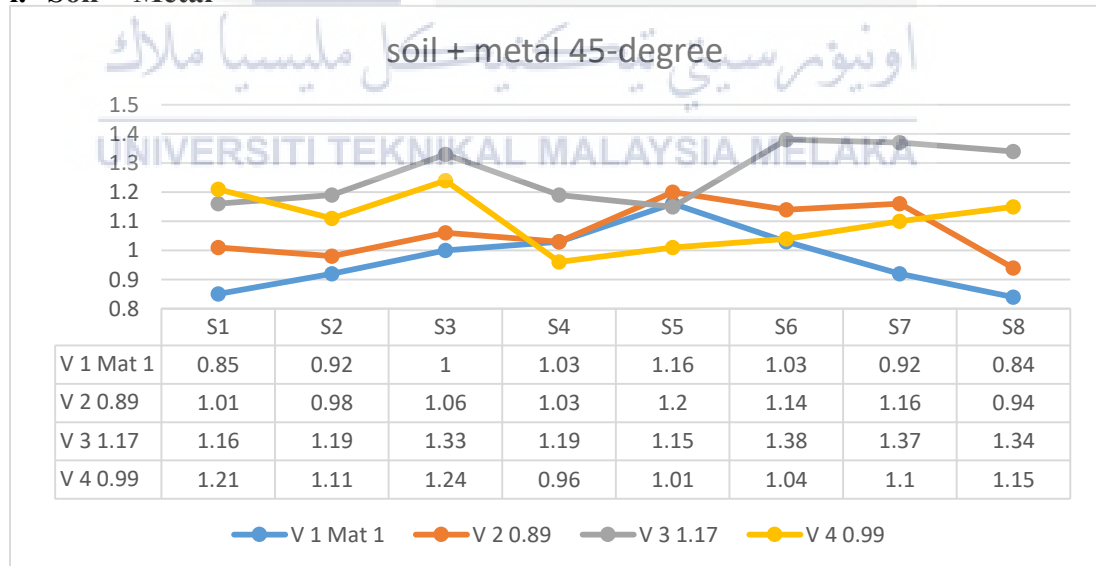
SAND + RUBBER	Vout (V)								
	S1	S2	S3	S4	S5	S6	S7	S8	Mat 1
V 1	0.08	0.13 ↑	0.06	0.09	0.08	0.18 ↑	0.19 ↑	0.08	0.65
V 2	0.1 ↑	0.08	0.14 ↑	0.1 ↑	0.13 ↑	0.11	0.12	0.16 ↑	0.51
V 3	-0.03	0.04	0.02	-0.01	-0.02	-0.03	-0.03	-0.01	0.72
V 4	0.05	0.01	0.04	-0.01	0.08	0.08	0.04	0.09	0.66

k. Sand + Plastic



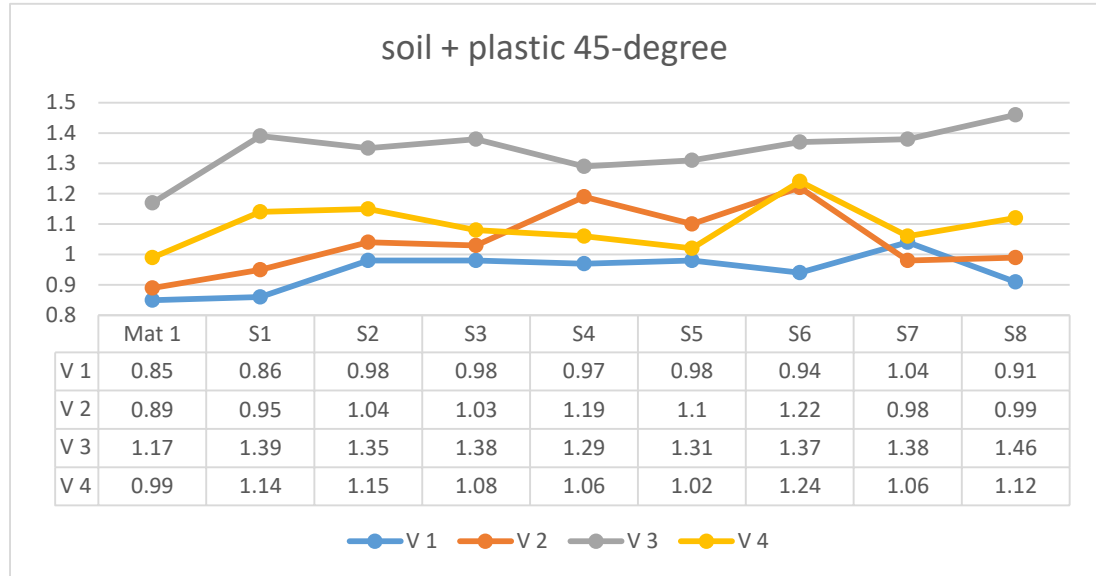
SAND + PLASTIC	Vout (V)								
	S1	S2	S3	S4	S5	S6	S7	S8	Mat 1
V 1	0.18 ↑	0.18 ↑	0.04	0.16 ↑	0.02	0.1	0.24 ↑	0.07	0.65
V 2	0.09	0.13	0.14 ↑	0.1	0.12 ↑	0.14 ↑	0.13	0.08 ↑	0.51
V 3	-0.01	0.07	0	-0.01	-0.03	0.01	0.02	-0.02	0.72
V 4	0	0.01	0	0.03	0.06	-0.01	-0.01	0	0.66

l. Soil + Metal



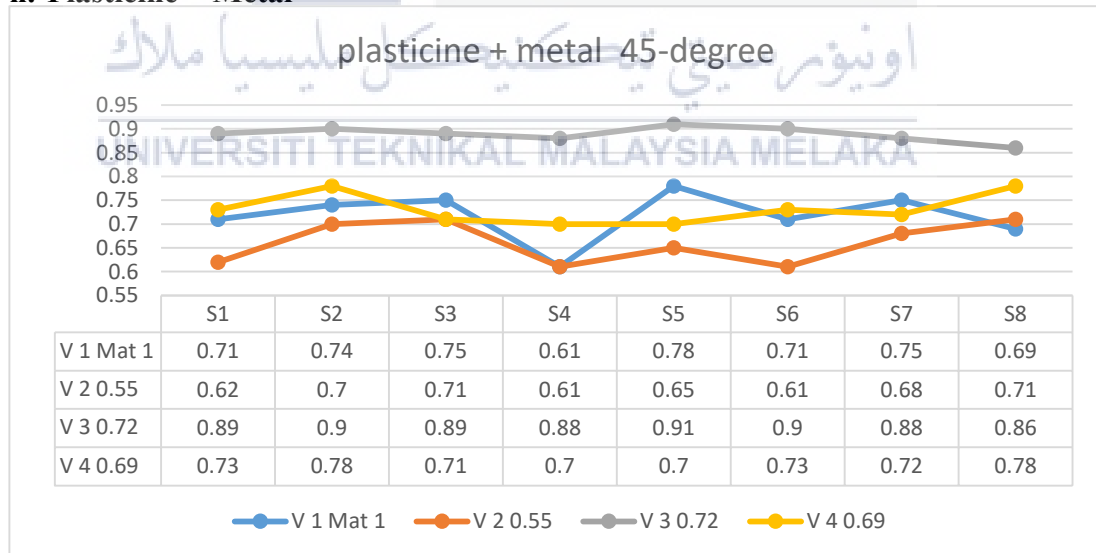
SOIL + METAL	Vout (V)								
	S1	S2	S3	S4	S5	S6	S7	S8	Mat 1
V 1	0	0.07	0.15	0.18 ↑	0.31 ↑	0.18	0.07	-0.01	0.85
V 2	0.12	0.09	0.17	0.14	0.31 ↑	0.25 ↑	0.27 ↑	0.05	0.89
V 3	-0.01	0.02	0.16	0.02	-0.02	0.21	0.2	0.17 ↑	1.17
V 4	0.22 ↑	0.12 ↑	0.25 ↑	-0.03	0.02	0.05	0.11	0.16	0.99

m. Soil + Plastic



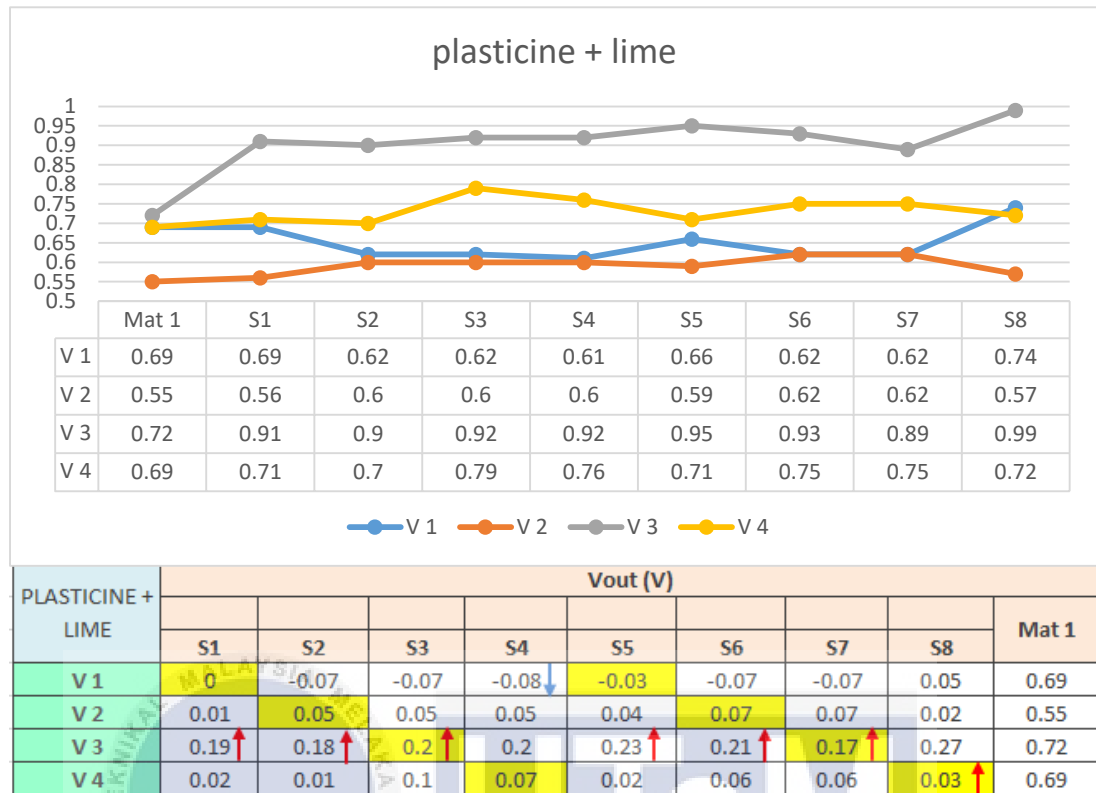
SOIL + PLASTIC	Vout (V)								
	S1	S2	S3	S4	S5	S6	S7	S8	Mat 1
V 1	0.01	0.13	0.13	0.12	0.13	0.09	0.19	0.06	0.85
V 2	0.06	0.15	0.14	0.3 ↑	0.21 ↑	0.33 ↑	0.09	0.1	0.89
V 3	0.22 ↑	0.18 ↑	0.21 ↑	0.12	0.14	0.2	0.21 ↑	0.29 ↑	1.17
V 4	0.15	0.16	0.09	0.07	0.03	0.25	0.07	0.13	0.99

n. Plasticine + Metal



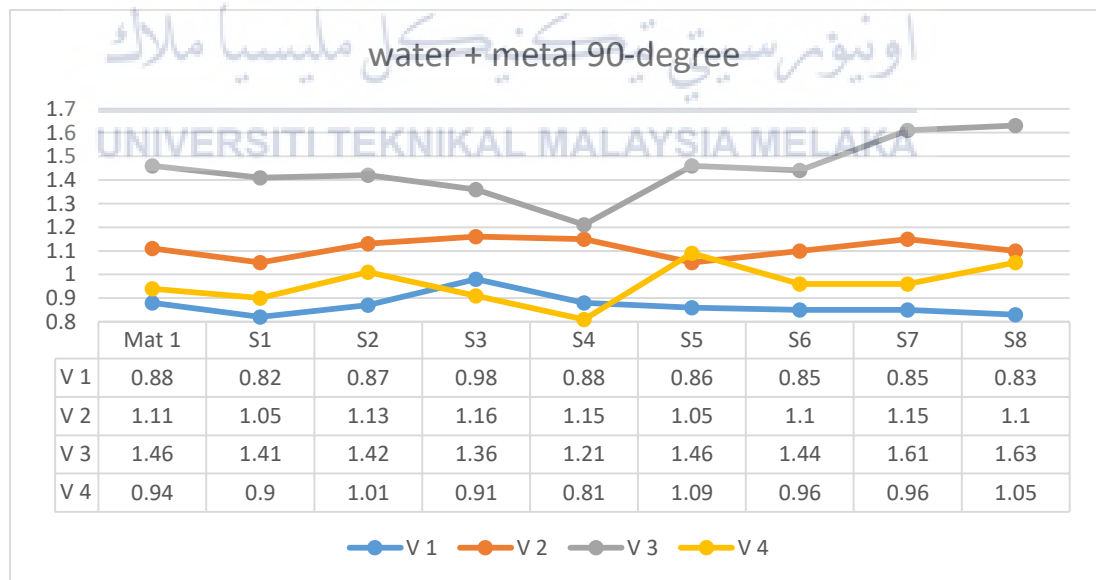
PLASTICINE + METAL	Vout (V)								
	S1	S2	S3	S4	S5	S6	S7	S8	Mat 1
V 1	0.02	0.05	0.06	-0.08	0.09	0.02	0.06	0	0.69
V 2	0.07	0.15	0.16	0.06	0.1	0.06	0.13	0.16 ↑	0.55
V 3	0.17 ↑	0.18 ↑	0.17 ↑	0.16 ↑	0.19 ↑	0.18 ↑	0.16 ↑	0.14	0.72
V 4	0.04	0.09	0.02	0.01	0.01	0.04	0.03	0.09	0.69

o. Plasticine + Lime



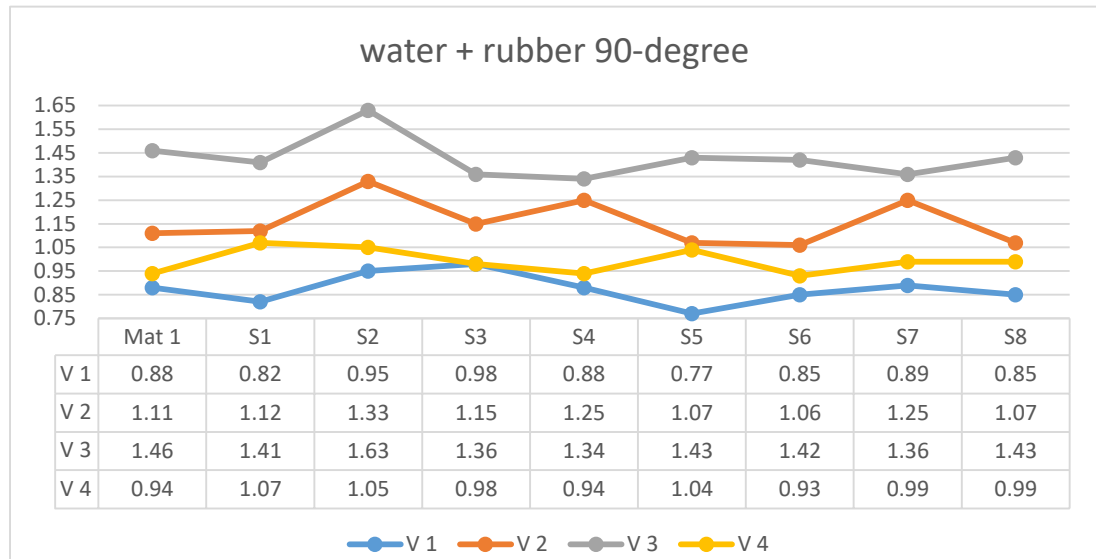
6. SPATIAL DETECTION RESULT FOR 90° PHASE SHIFTER

a. Water + Metal



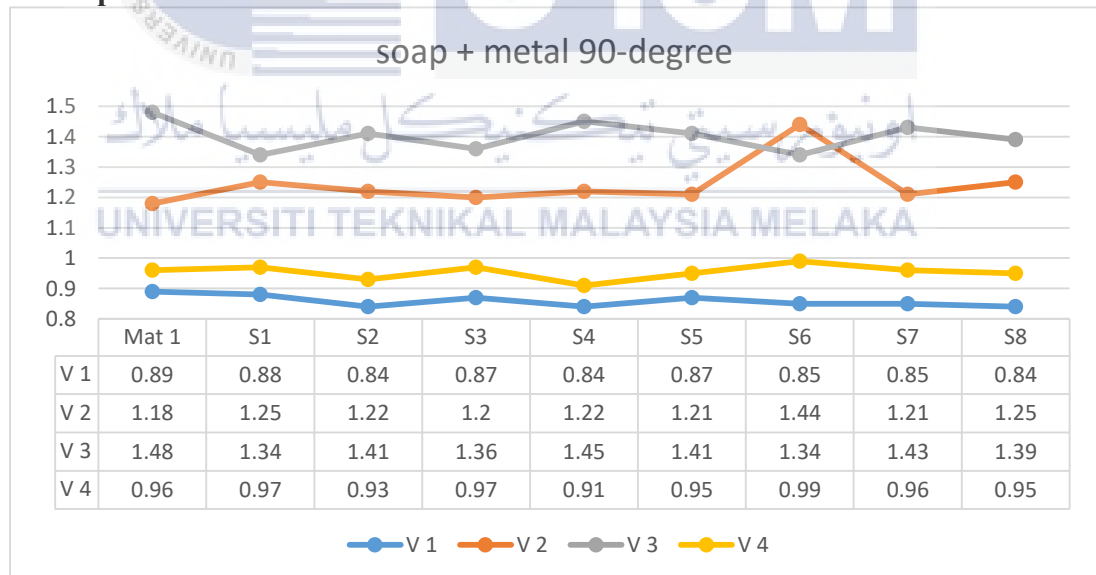
WATER + METAL	Vout (V)								
	S1	S2	S3	S4	S5	S6	S7	S8	Mat 1
V 1	-0.06↓	-0.01	0.1↑	0	-0.02	-0.03↓	-0.03	-0.05	0.88
V 2	-0.06↓	0.02	0.05	0.04	-0.06	-0.01	0.04	-0.01	1.11
V 3	-0.05	-0.04	-0.1↓	-0.25↓	0	-0.02	0.15↑	0.17↑	1.46
V 4	-0.04	0.07↑	-0.03	-0.13	0.15↑	0.02	0.02	0.11	0.94

b. Water + Rubber



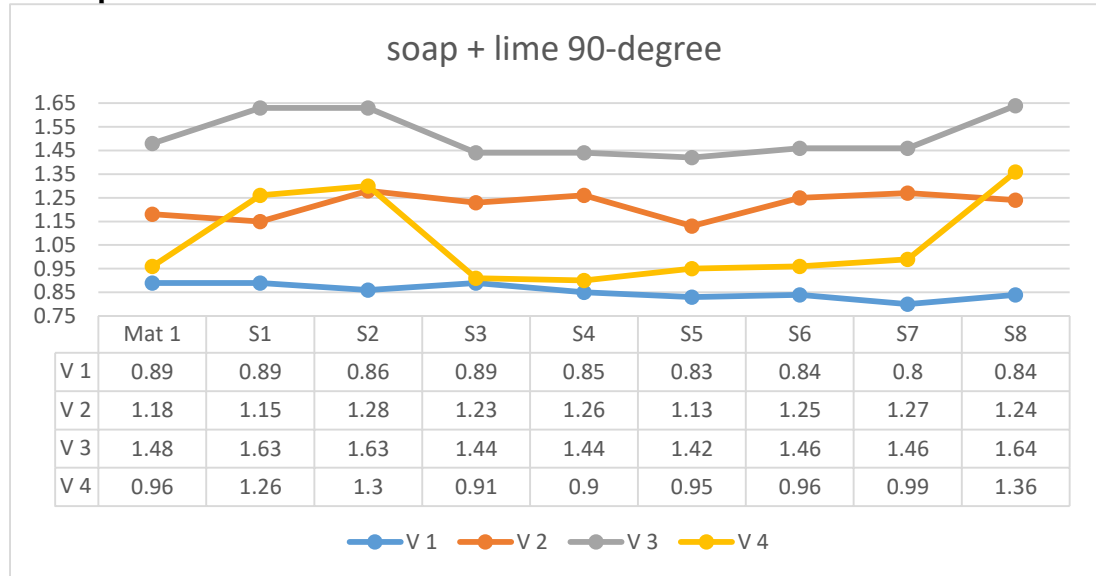
WATER + RUBBER	Vout (V)								
	S1	S2	S3	S4	S5	S6	S7	S8	Mat 1
V 1	-0.06	0.07	0.1 ↑	0	-0.88	-0.03	0.01	-0.03	0.88
V 2	0.01	0.22 ↑	0.04	0.14 ↑	-1.11	-0.05 ↓	0.14 ↑	-0.04	1.11
V 3	-0.05	0.17	-0.1 ↓	-0.12	-1.46 ↓	-0.04	-0.1	-0.03	1.46
V 4	0.13 ↑	0.11	0.04	0	-0.94	-0.01	0.05	0.05 ↑	0.94

c. Soap + Metal



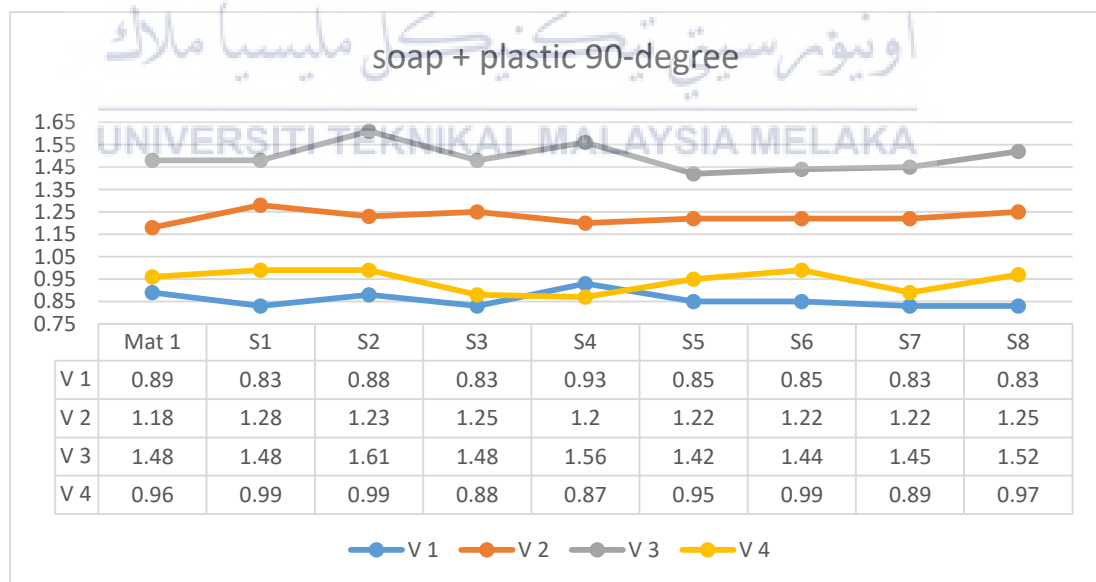
SOAP + METAL	Vout (V)								
	S1	S2	S3	S4	S5	S6	S7	S8	Mat 1
V 1	-0.01	-0.05	-0.02	-0.89	-0.02	-0.04	-0.04	-0.05	0.89
V 2	0.07	0.04	0.02	-1.18	0.03	0.26 ↑	0.03	0.07	1.18
V 3	-0.14 ↓	-0.07 ↓	-0.12 ↓	-1.48 ↓	-0.07 ↓	-0.14	-0.05 ↓	-0.09 ↓	1.48
V 4	0.01	-0.03	0.01	-0.96	-0.01	0.03	0	-0.01	0.96

d. Soap + Lime



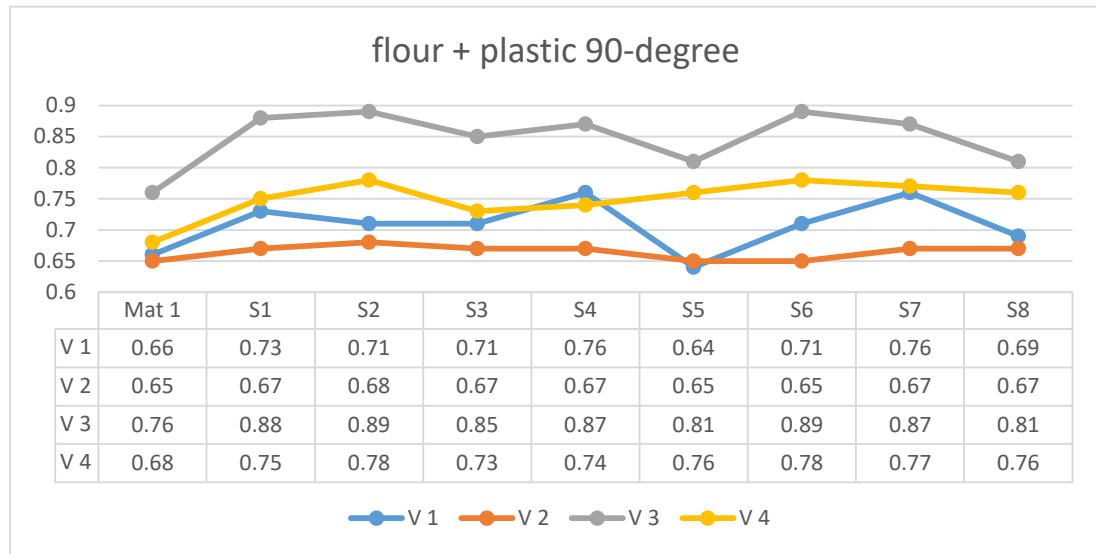
SOAP + LIME	Vout (V)								Mat 1
	S1	S2	S3	S4	S5	S6	S7	S8	
V 1	0	-0.03	0	-0.04	-0.06	-0.89	-0.09	-0.05	0.89
V 2	-0.03	0.1	-0.05	0.08	-0.05	-1.18	0.09	0.06	1.18
V 3	0.15	0.15	-0.04	-0.04	-0.06	-1.48	-0.02	0.16	1.48
V 4	0.3	0.34	-0.05	-0.06	-0.01	-0.96	0.03	0.4	0.96

e. Soap + Plastic



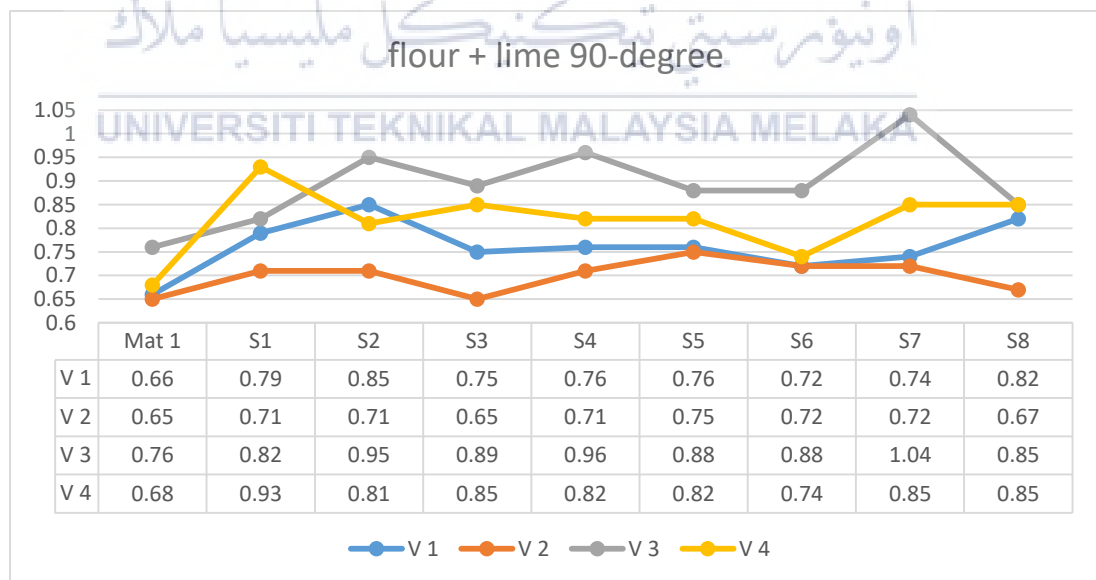
SOAP + PLASTIC	Vout (V)								Mat 1
	S1	S2	S3	S4	S5	S6	S7	S8	
V 1	-0.06	-0.01	-0.06	0.04	-0.04	-0.04	-0.06	-0.06	0.89
V 2	0.1	0.05	0.07	0.02	0.04	0.04	0.04	0.07	1.18
V 3	0	0.13	0	0.08	-0.06	-0.04	-0.03	0.04	1.48
V 4	0.03	0.03	-0.08	-0.09	-0.01	0.03	-0.07	0.01	0.96

f. Flour + Plastic



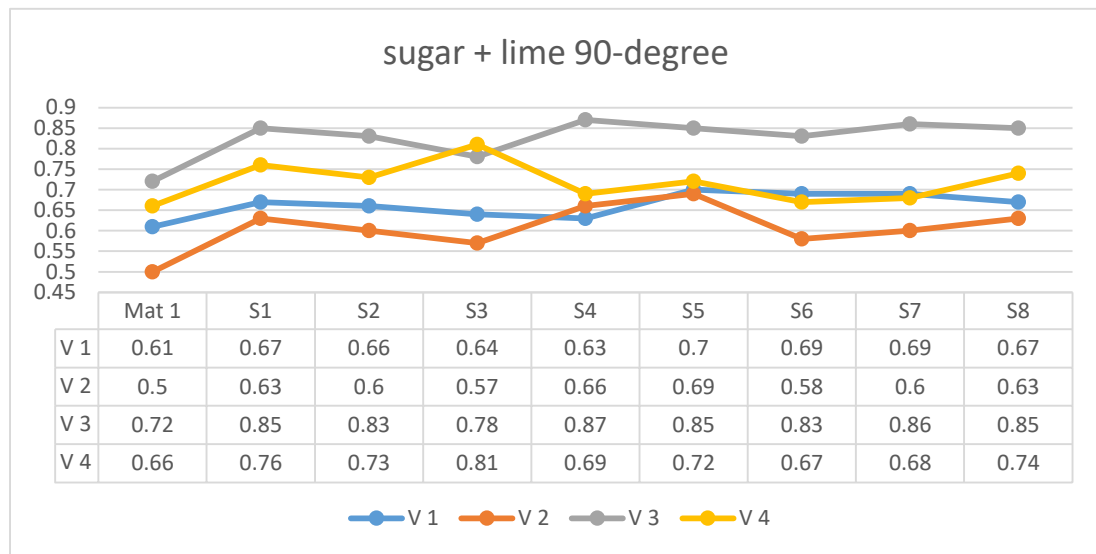
FLOUR + PLASTIC	Vout (V)								
	S1	S2	S3	S4	S5	S6	S7	S8	Mat 1
V 1	0.07	0.05	0.05	0.1	-0.02	0.05	0.1	0.03	0.66
V 2	0.02	0.03	0.02	0.02	0	0	0.02	0.02	0.65
V 3	0.12 ↑	0.13 ↑	0.09 ↑	0.11 ↑	0.05	0.13 ↑	0.11 ↑	0.05	0.76
V 4	0.07	0.1	0.05	0.06	0.08 ↑	0.1	0.09	0.08 ↑	0.68

g. Flour + Lime



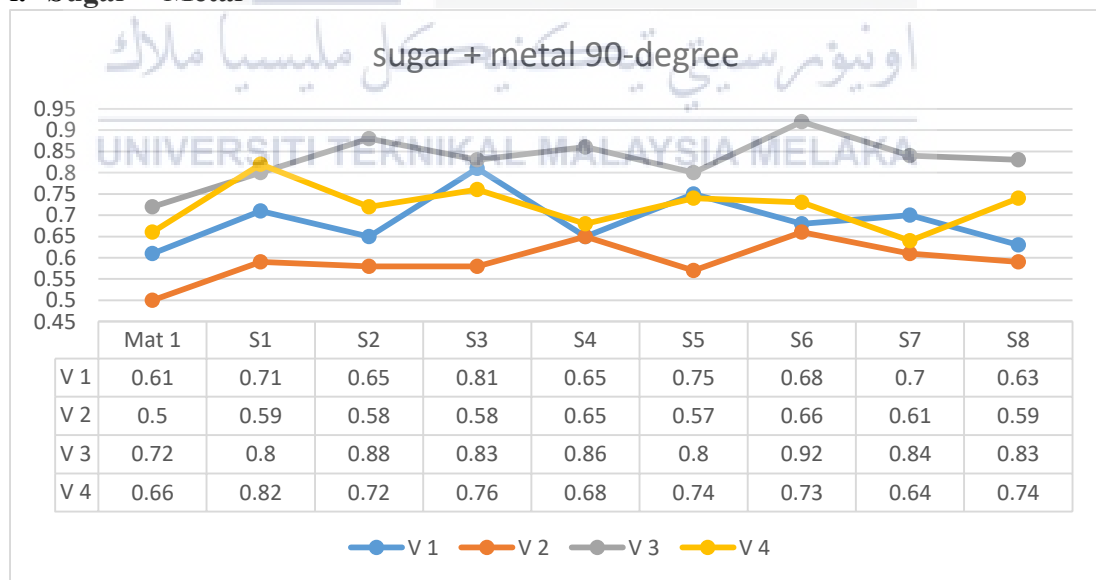
FLOUR + LIME	Vout (V)								
	S1	S2	S3	S4	S5	S6	S7	S8	Mat 1
V 1	0.13	0.19 ↑	0.09	0.1	0.1	0.06	0.08	0.16 ↑	0.66
V 2	0.06	0.06	0	0.06	0.1	0.07	0.07	0.02	0.65
V 3	0.06	0.19 ↑	0.13	0.2	0.12	0.12 ↑	0.28 ↑	0.09	0.76
V 4	0.25 ↑	0.13	0.17 ↑	0.14 ↑	0.14 ↑	0.06	0.17	0.17	0.68

h. Sugar + Lime



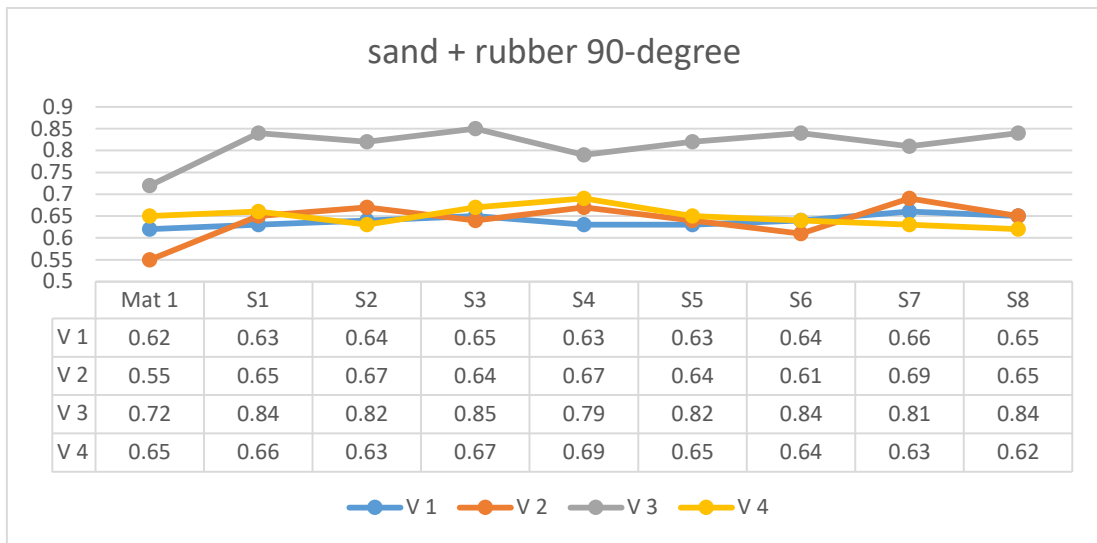
SUGAR + LIME	Vout (V)								Mat 1
	S1	S2	S3	S4	S5	S6	S7	S8	
V 1	0.06	0.05	0.03	0.02	0.09	0.08	0.08	0.06	0.61
V 2	0.13 ↑	0.1 ↑	0.07	0.16 ↑	0.19 ↑	0.08	0.1	0.13 ↑	0.5
V 3	0.13 ↑	0.11 ↑	0.06	0.15	0.13	0.11 ↑	0.14 ↑	0.13 ↑	0.72
V 4	0.1	0.07	0.15 ↑	0.03	0.06	0.01	0.02	0.08	0.66

i. Sugar + Metal



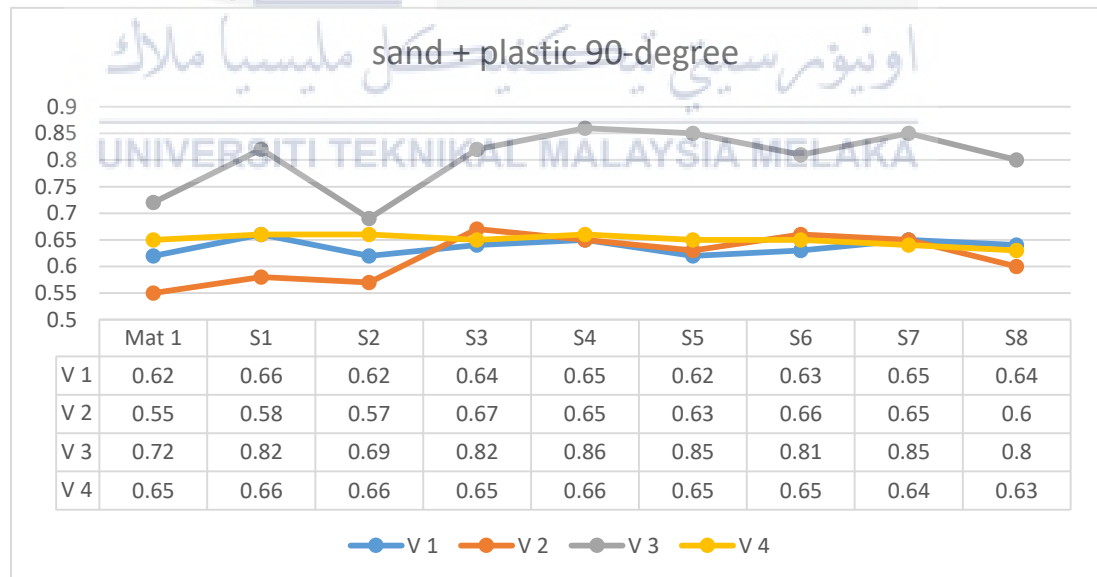
SUGAR + METAL	Vout (V)								Mat 1
	S1	S2	S3	S4	S5	S6	S7	S8	
V 1	0.1	0.04	0.2	0.04	0.14 ↑	0.07	0.09	0.02	0.61
V 2	0.09	0.08	0.08	0.15 ↑	0.07	0.16 ↑	0.11	0.09	0.5
V 3	0.08	0.16 ↑	0.11 ↑	0.14	0.08	0.2	0.12 ↑	0.11 ↑	0.72
V 4	0.16 ↑	0.06	0.1	0.02	0.08	0.07	-0.02	0.08	0.66

j. Sand + Rubber



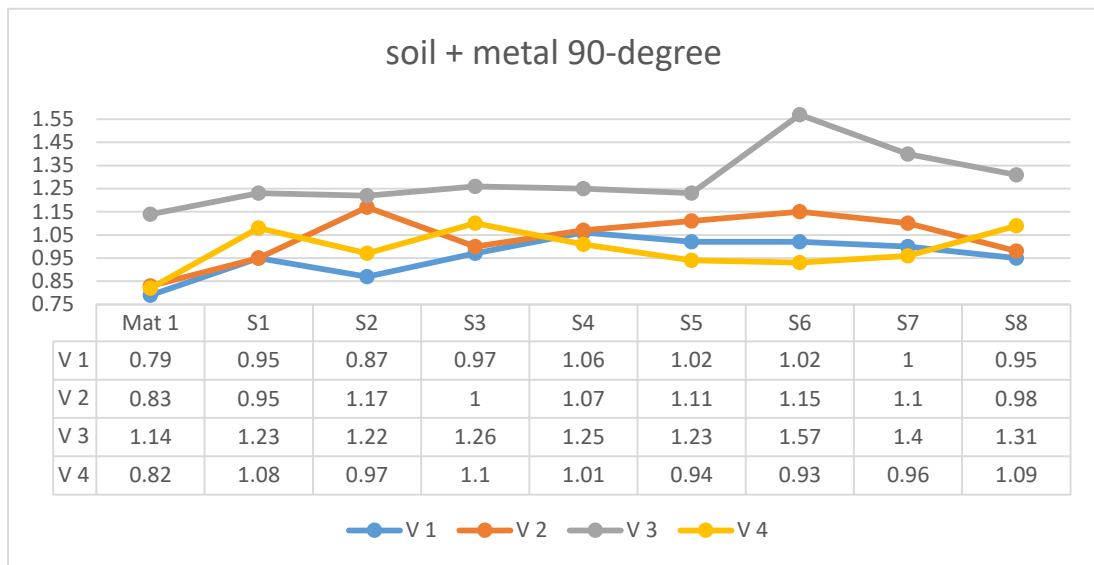
SAND + RUBBER	Vout (V)								
	S1	S2	S3	S4	S5	S6	S7	S8	Mat 1
V 1	0.01	0.02	0.03	0.01	0.01	0.02	0.04	0.03	0.62
V 2	0.1	0.12 ↑	0.09	0.12 ↑	0.09	0.06	0.14 ↑	0.1	0.55
V 3	0.12 ↑	0.1	0.13 ↑	0.07	0.1 ↑	0.12 ↑	0.09	0.12 ↑	0.72
V 4	0.01	-0.02	0.02	0.04	0	-0.01	-0.02	-0.03	0.65

k. Sand + Plastic



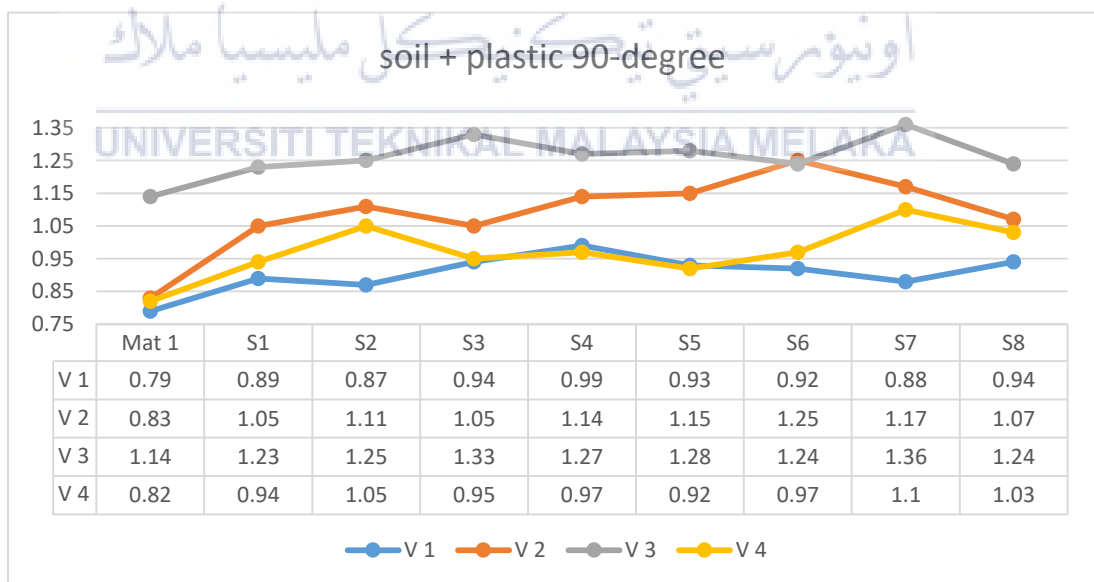
SAND + RUBBER	Vout (V)								
	S1	S2	S3	S4	S5	S6	S7	S8	Mat 1
V 1	0.01	0.02	0.03	0.01	0.01	0.02	0.04	0.03	0.62
V 2	0.1	0.12 ↑	0.09	0.12 ↑	0.09	0.06	0.14 ↑	0.1	0.55
V 3	0.12 ↑	0.1	0.13 ↑	0.07	0.1 ↑	0.12 ↑	0.09	0.12 ↑	0.72
V 4	0.01	-0.02	0.02	0.04	0	-0.01	-0.02	-0.03	0.65

l. Soil + Metal



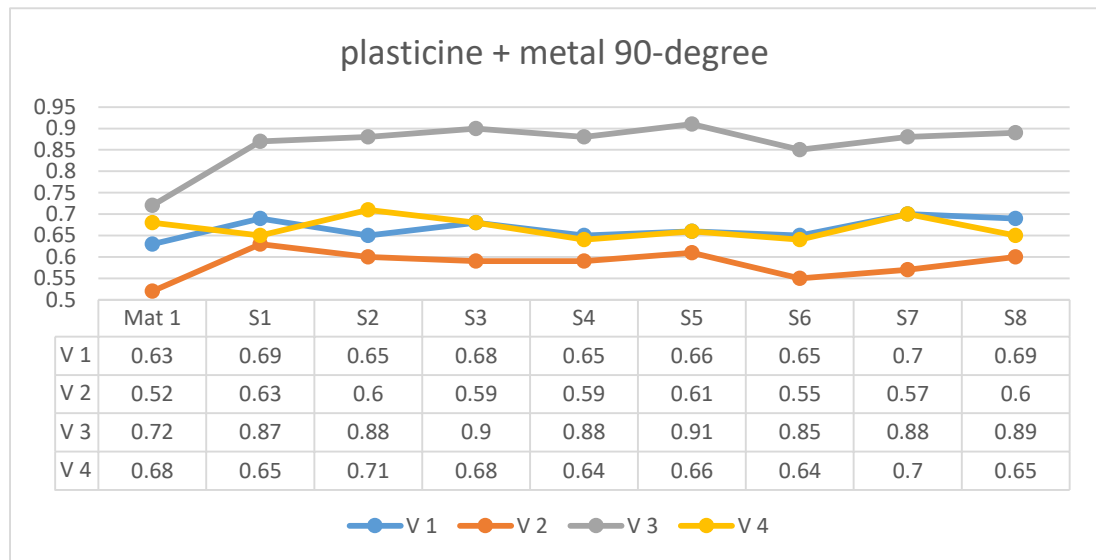
SOIL + METAL	Vout (V)								Mat 1
	S1	S2	S3	S4	S5	S6	S7	S8	
V 1	0.16	0.08	0.18	0.27 ↑	0.23	0.23	0.21	0.16	0.79
V 2	0.12	0.34 ↑	0.17	0.24	0.28 ↑	0.32	0.27 ↑	0.15	0.83
V 3	0.09	0.08	0.12	0.11	0.09	0.43 ↑	0.26	0.17	1.14
V 4	0.26 ↑	0.15	0.28 ↑	0.19	0.12	0.11	0.14	0.27 ↑	0.82

m. Soil + Plastic



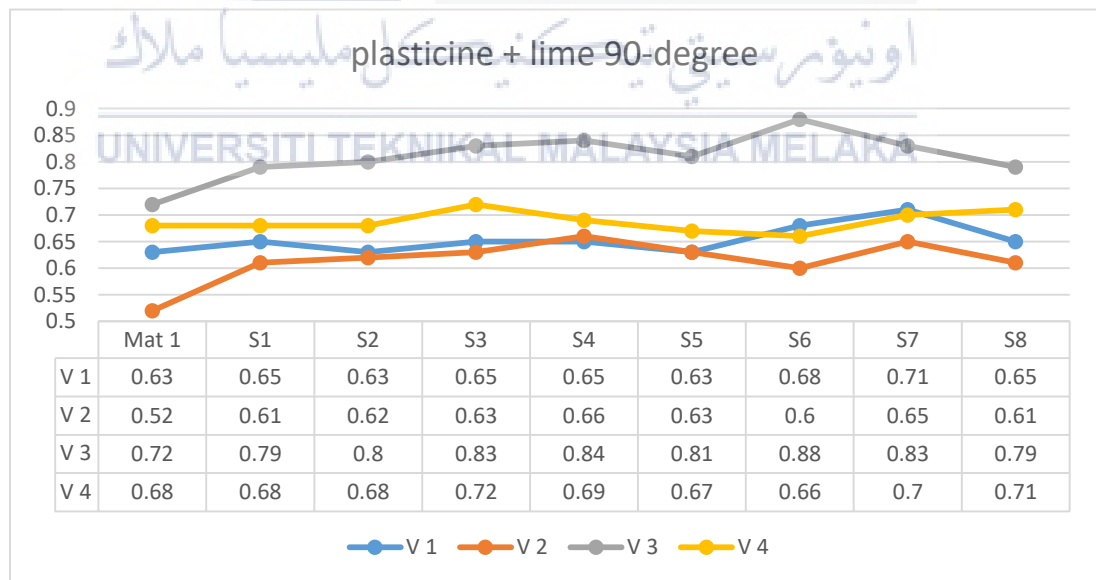
SOIL + PLASTIC	Vout (V)								Mat 1
	S1	S2	S3	S4	S5	S6	S7	S8	
V 1	0.1	0.08	0.15	0.2	0.14	0.13	0.09	0.15	0.79
V 2	0.22 ↑	0.28 ↑	0.22 ↑	0.31 ↑	0.32 ↑	0.42 ↑	0.34 ↑	0.24 ↑	0.83
V 3	0.09	0.11	0.19	0.13	0.14	0.1	0.22	0.1	1.14
V 4	0.12	0.23	0.13	0.15	0.1	0.15	0.28	0.21	0.82

n. Plasticine + Metal



PLASTICINE + METAL	Vout (V)								Mat 1
	S1	S2	S3	S4	S5	S6	S7	S8	
V 1	0.06	0.02	0.05	0.02	0.03	0.02	0.07	0.06	0.63
V 2	0.11	0.08	0.07	0.07	0.09	0.03	0.05	0.08	0.52
V 3	0.15 ↑	0.16 ↑	0.18 ↑	0.16 ↑	0.19 ↑	0.13 ↑	0.16 ↑	0.17 ↑	0.72
V 4	-0.03	0.03	0	-0.04	-0.02	-0.04	0.02	-0.03	0.68

o. Plasticine + Lime



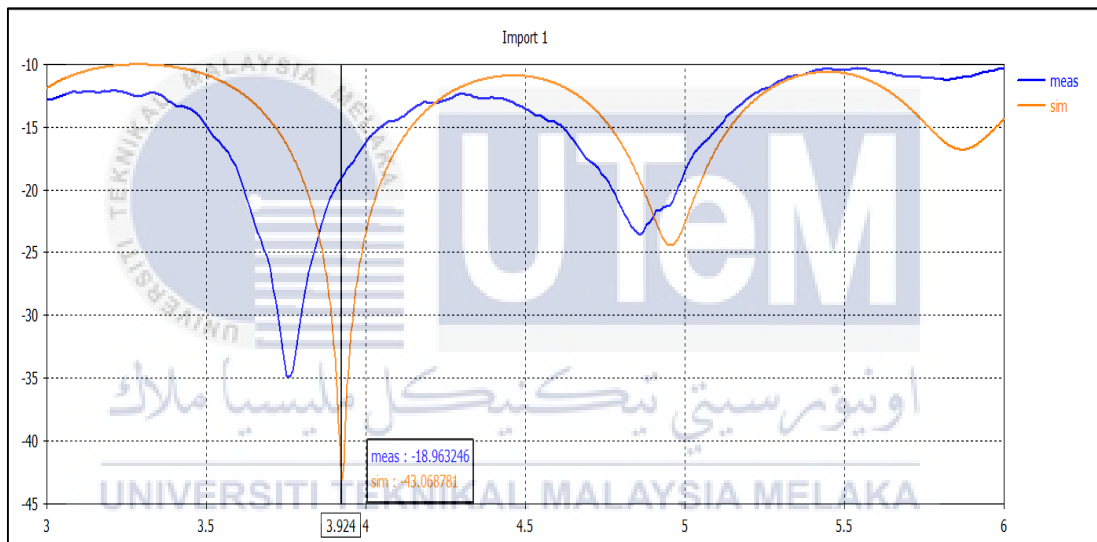
PLASTICINE + LIME	Vout (V)								Mat 1
	S1	S2	S3	S4	S5	S6	S7	S8	
V 1	0.02	0	0.02	0.02	0	0.05	0.08	0.02	0.63
V 2	0.09 ↑	0.1 ↑	0.11 ↑	0.14 ↑	0.11 ↑	0.08	0.13 ↑	0.09 ↑	0.52
V 3	0.07	0.08	0.11 ↑	0.12	0.09	0.16 ↑	0.11	0.07	0.72
V 4	0	0	0.04	0.01	-0.01	-0.02	0.02	0.03	0.68

APPENDIX C

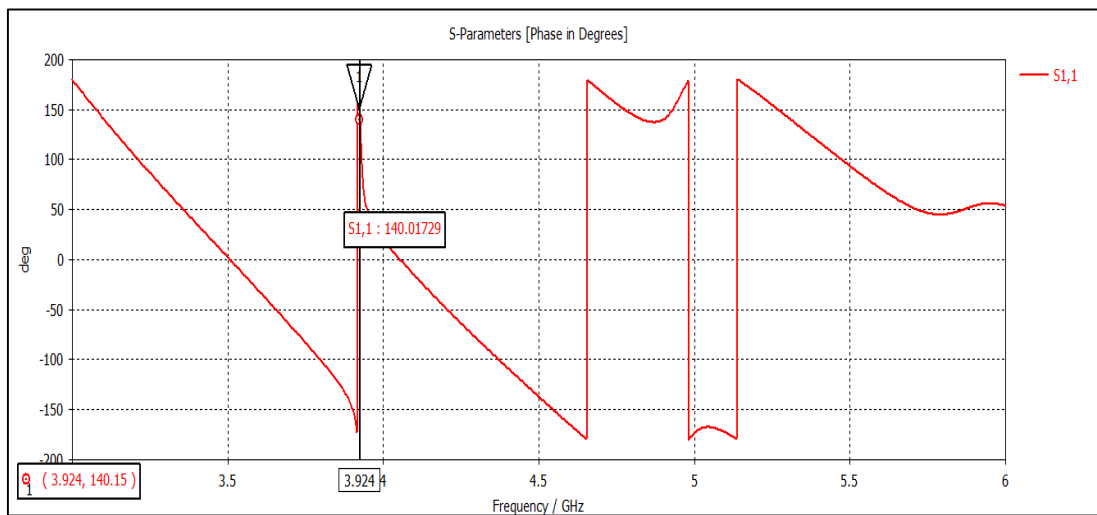
1. ANTENNA SIMULATION AND MEASUREMENT RESULT

a. 0° Phase Shifter

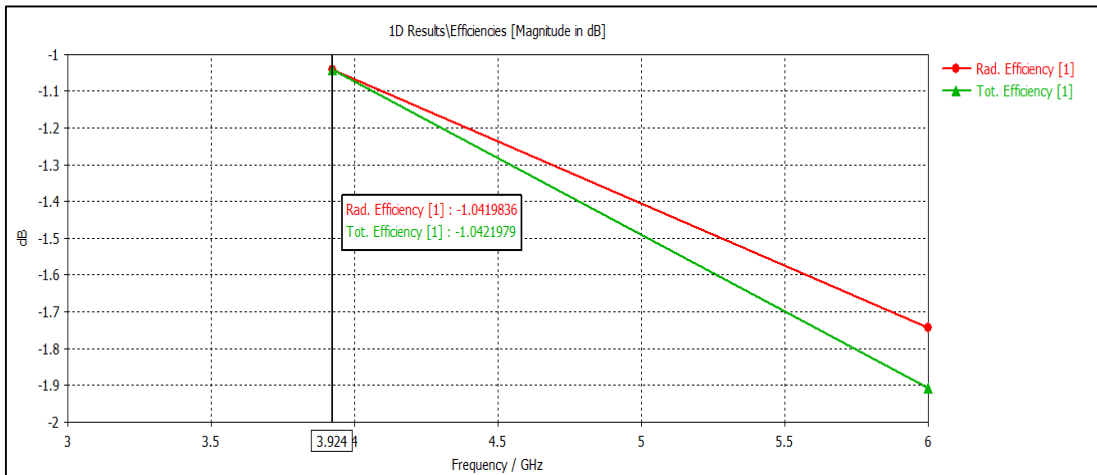
Return loss for simulation and measured.



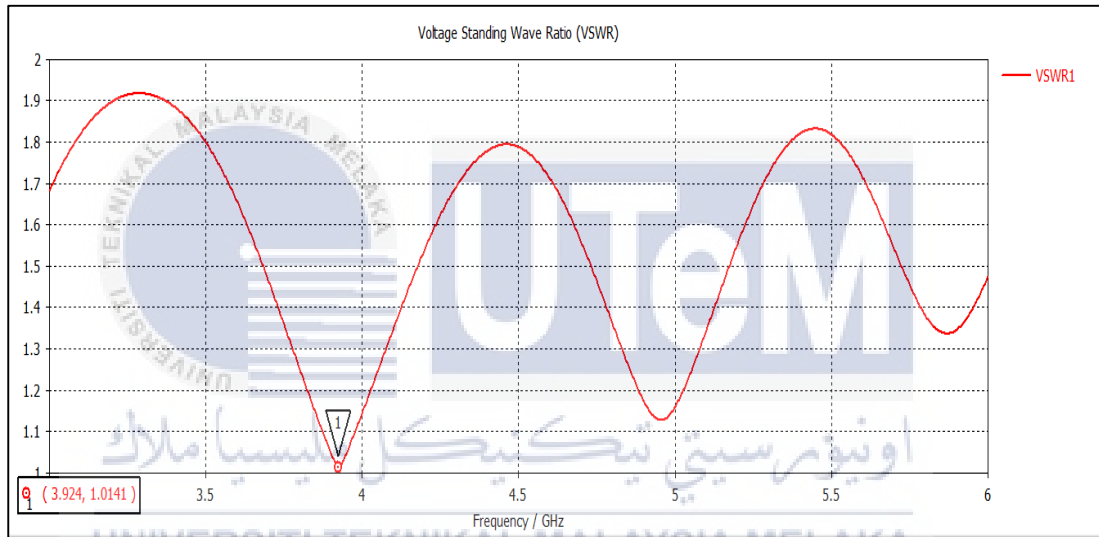
Phase



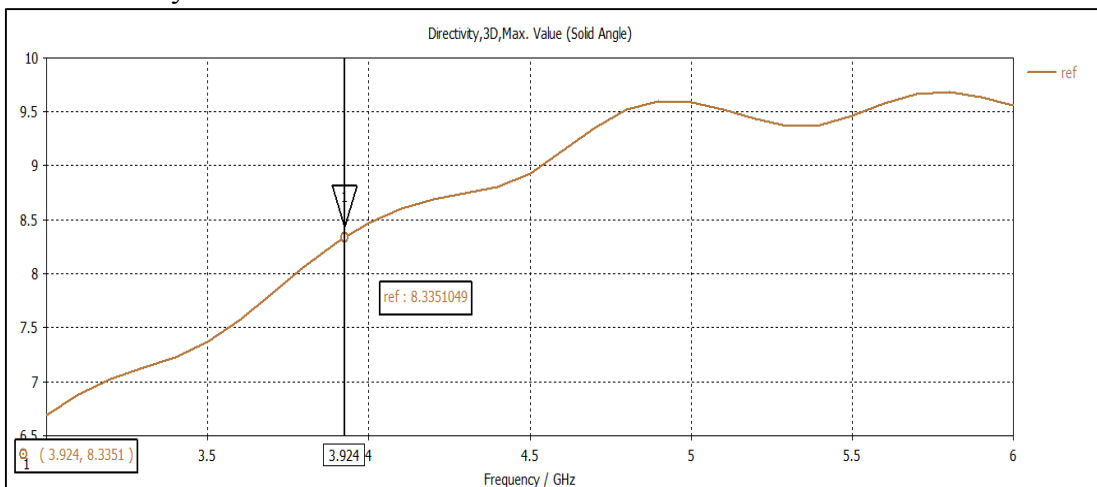
Efficiency



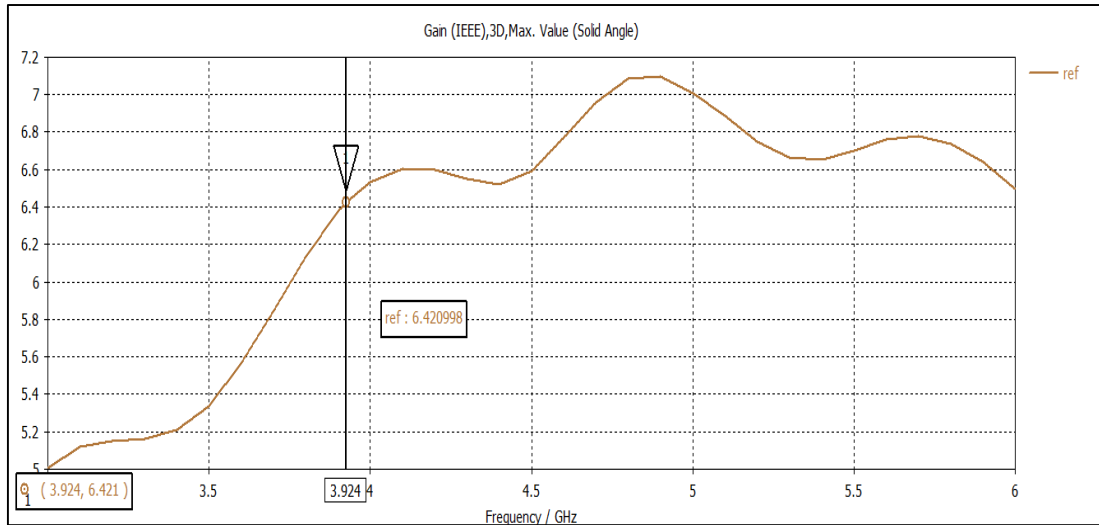
VSWR



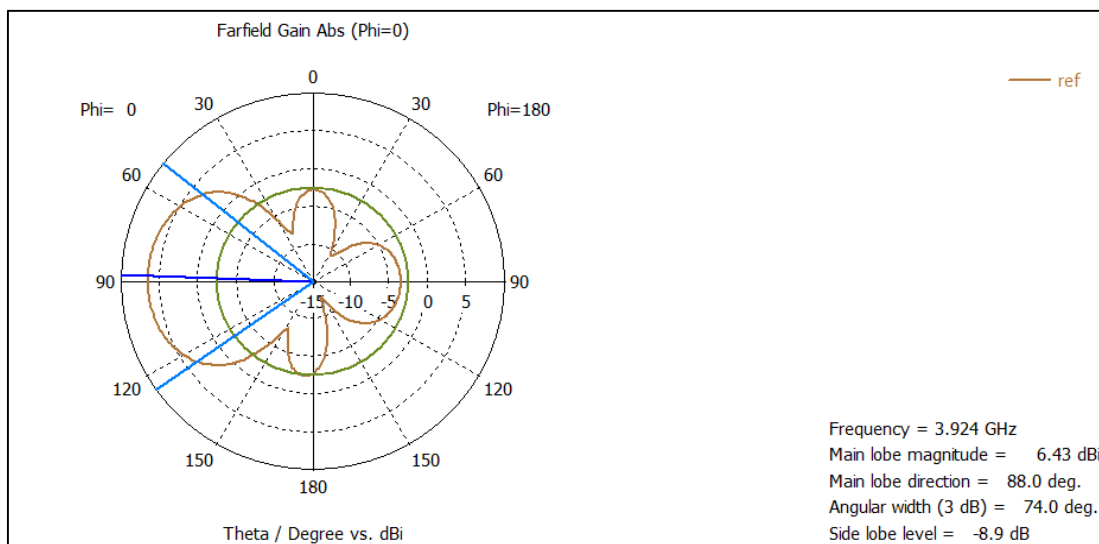
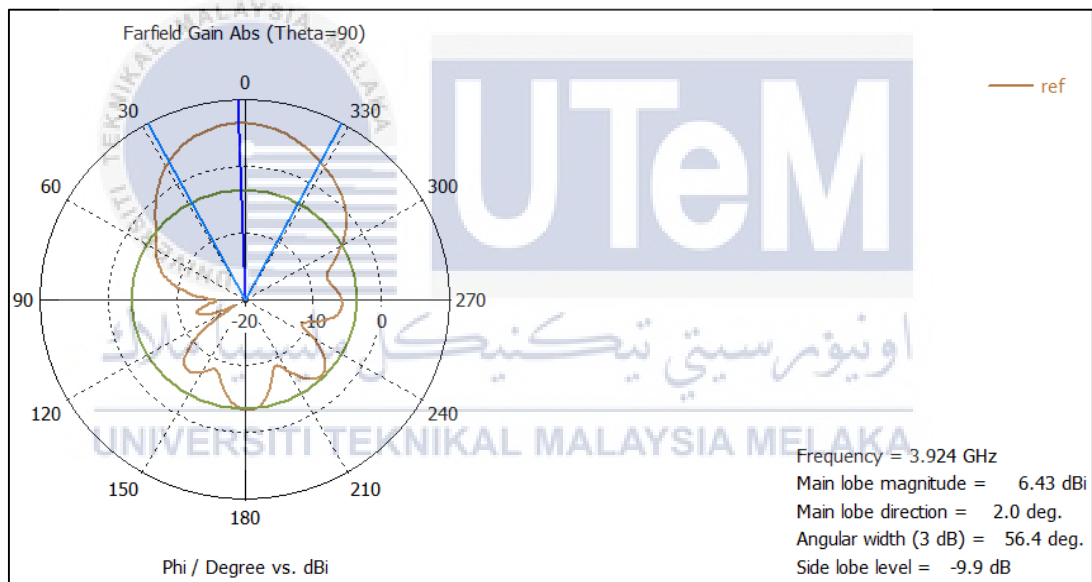
Directivity



Realized gain

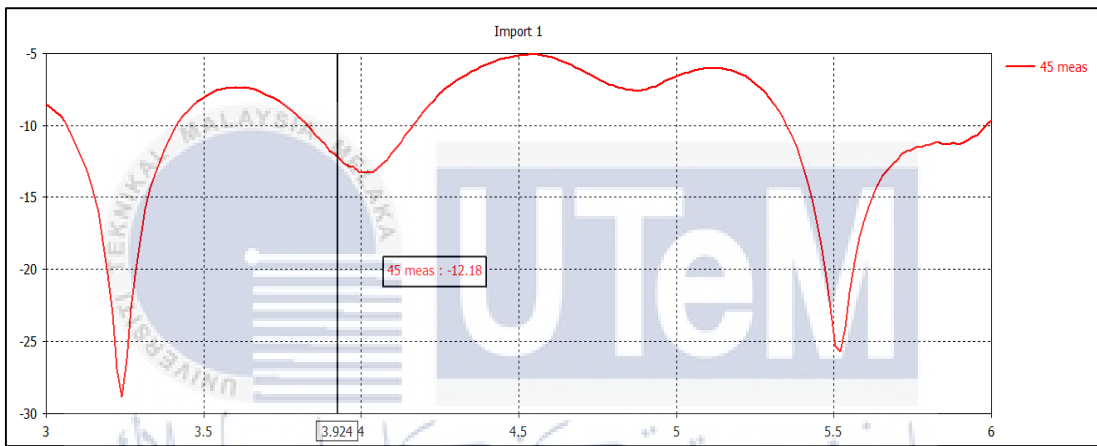
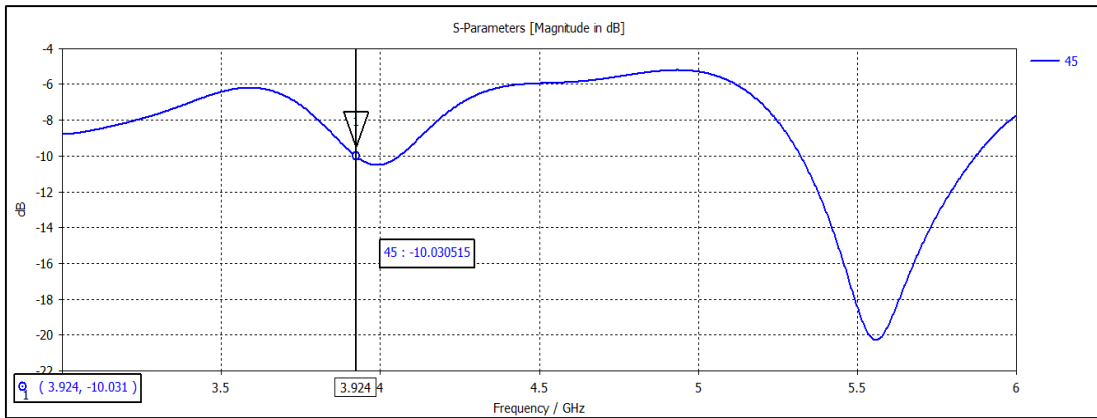


Farfield result at Theta = 90 & Phi = 0

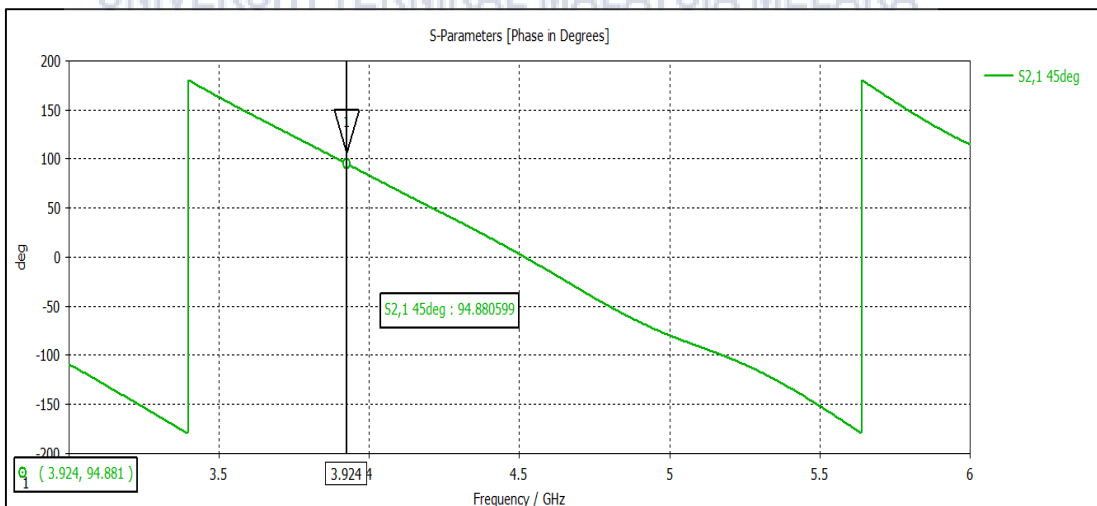


b. 45° Phase Shifter

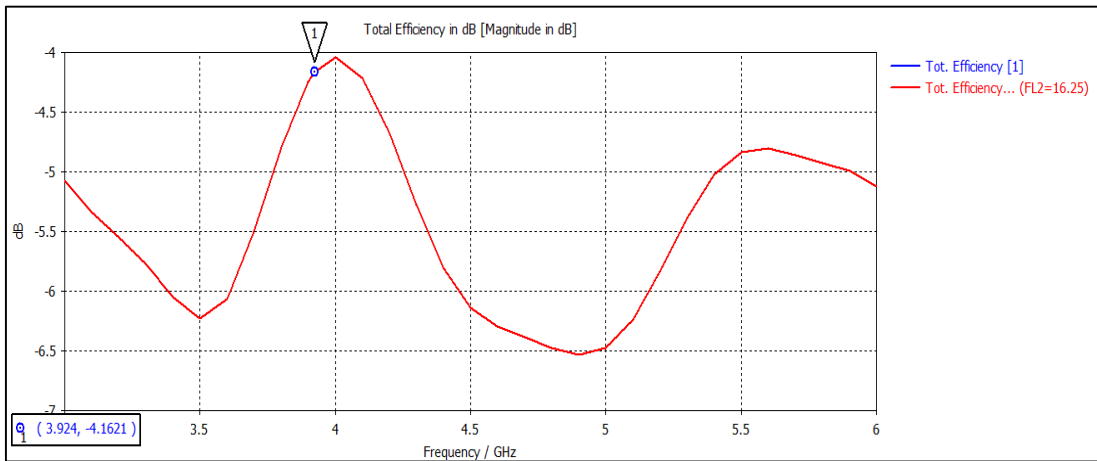
Return loss simulation & measured.



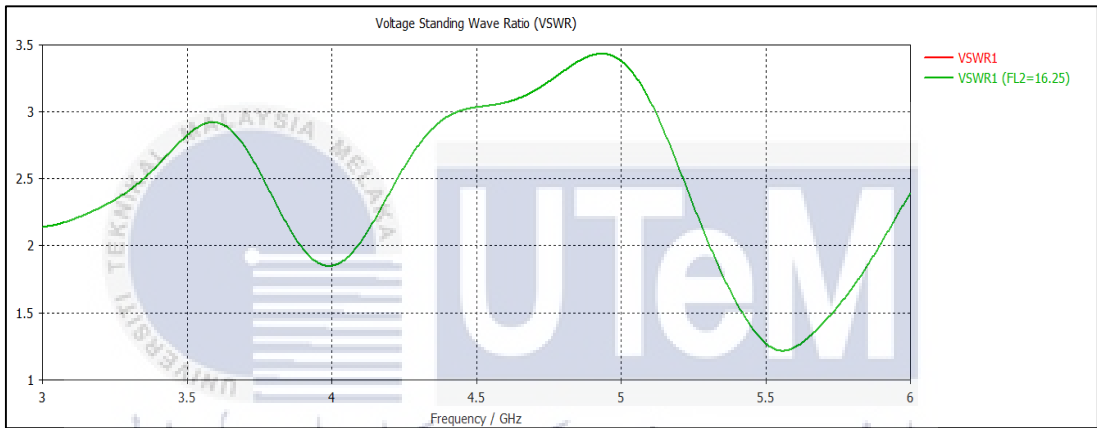
Phase



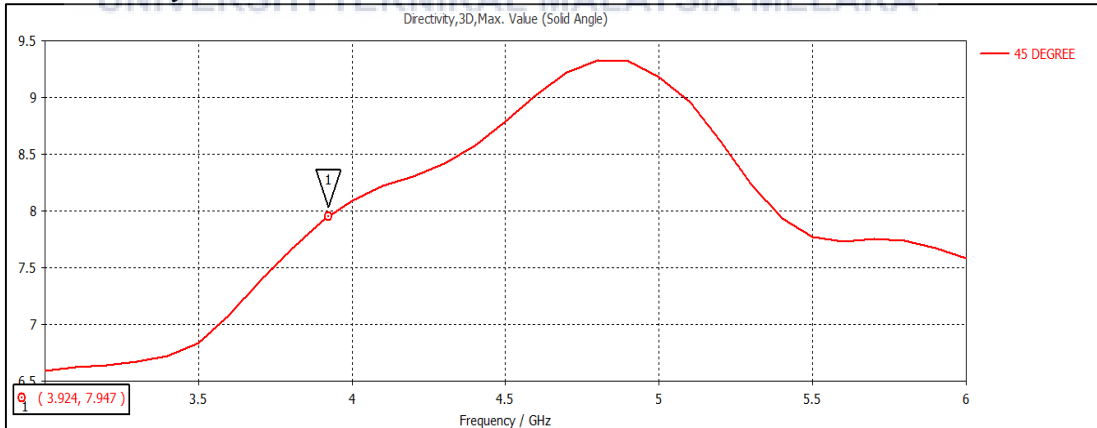
Efficiency



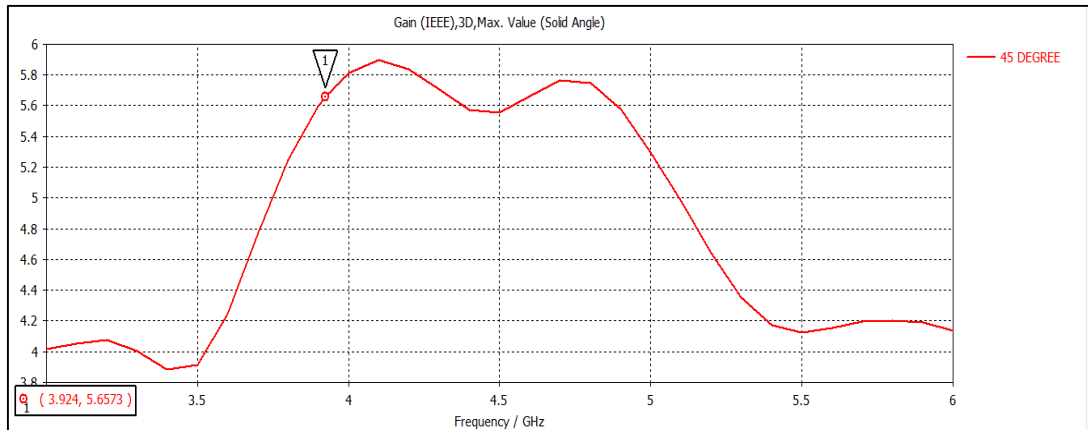
VSWR



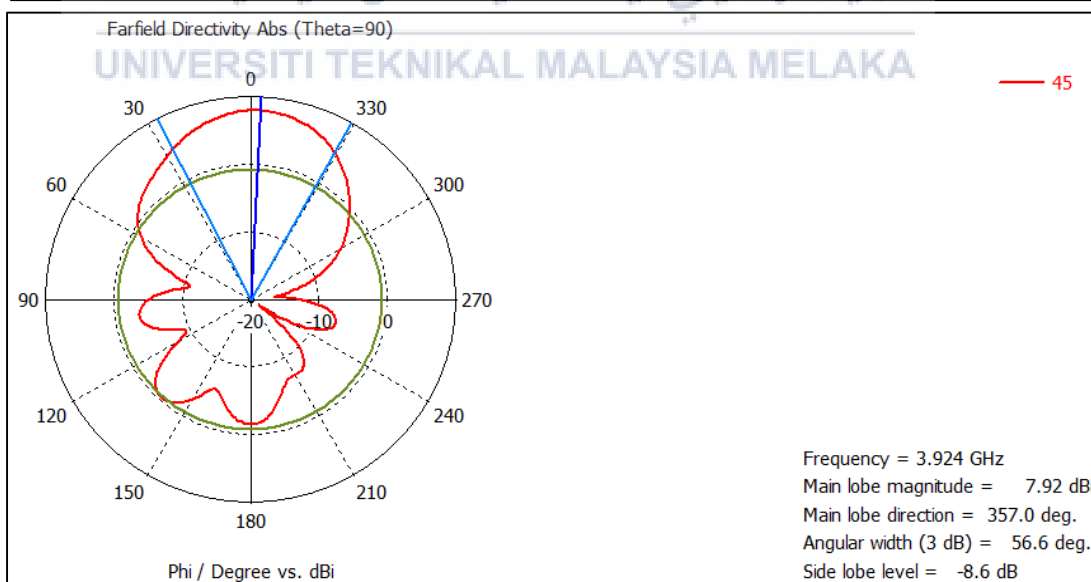
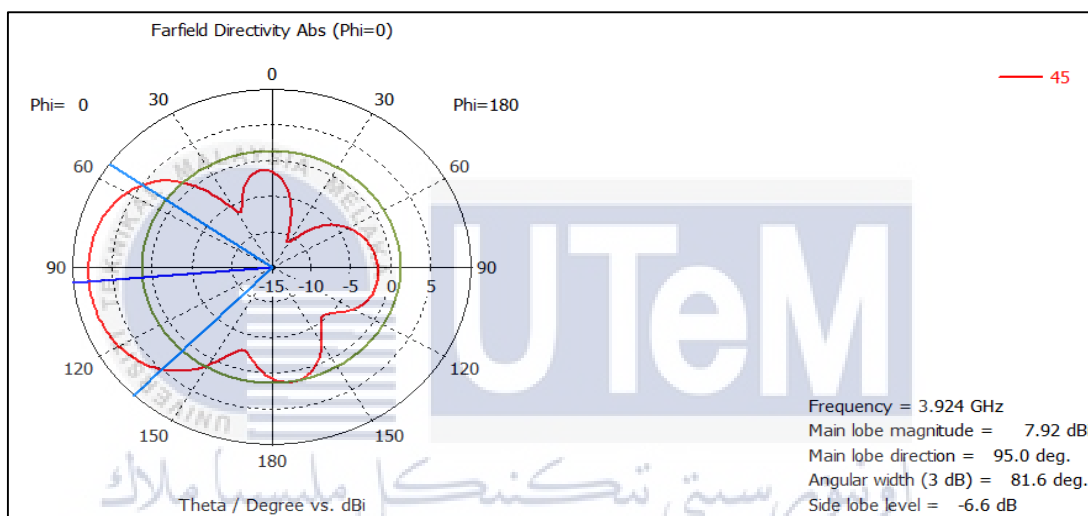
Directivity



Realized gain

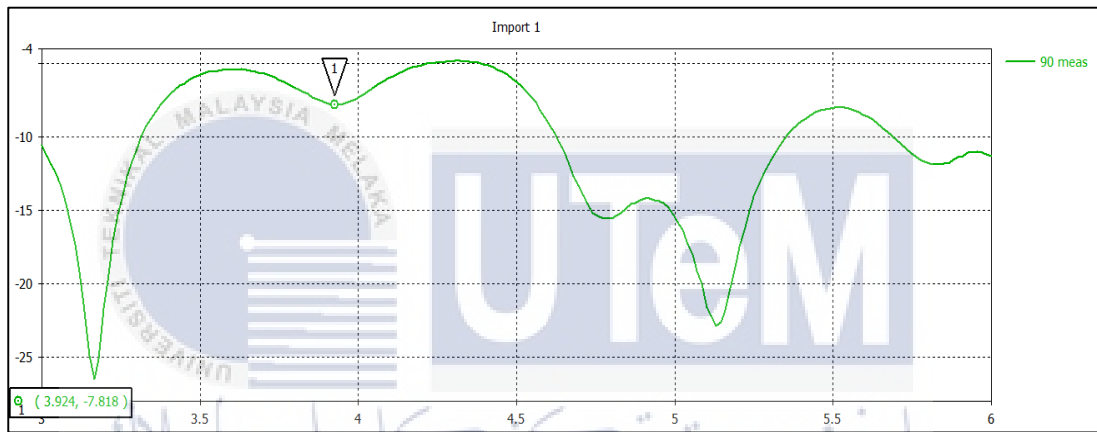
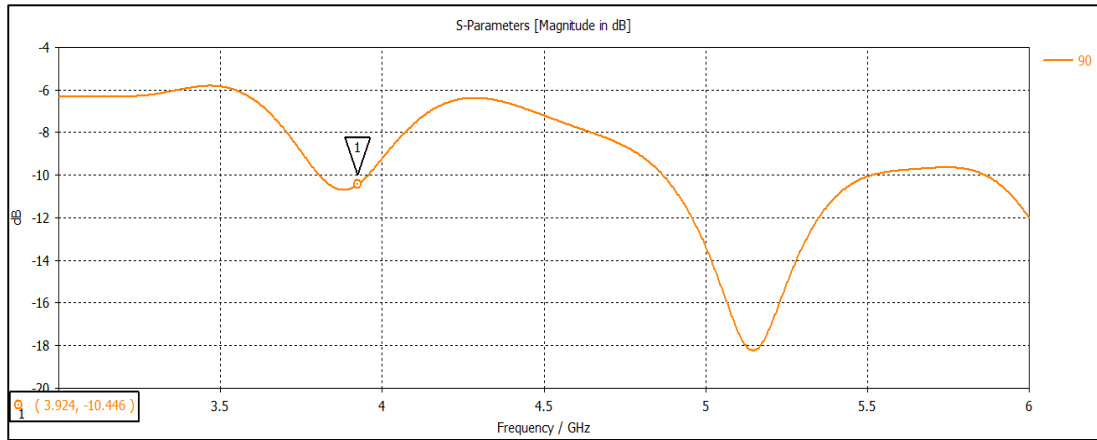


Farfield result at Theta = 90 & Phi = 0

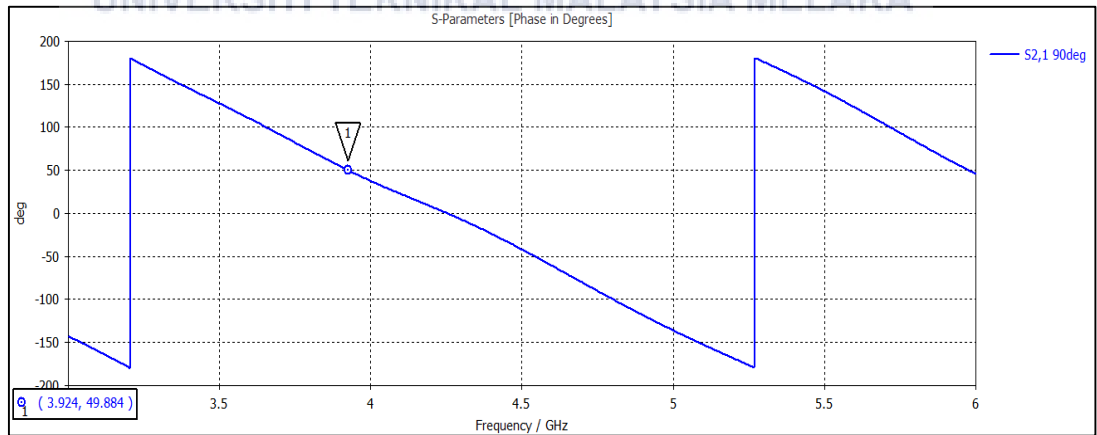


c. 90° phase Shifter

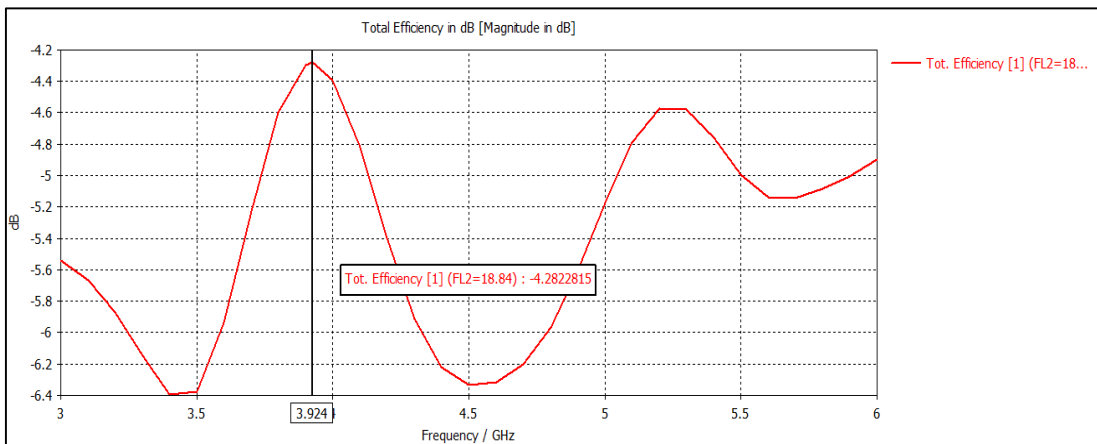
Return loss simulation & measured.



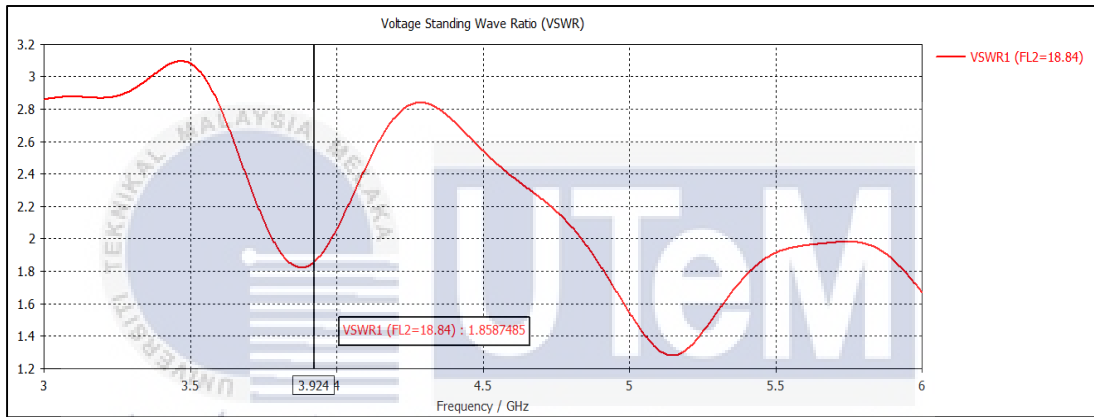
Phase



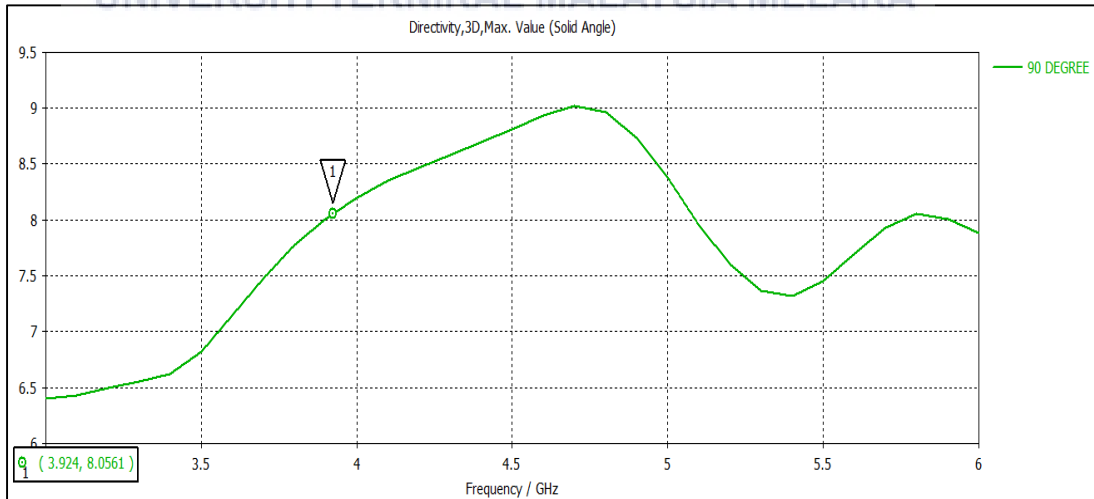
Efficiency



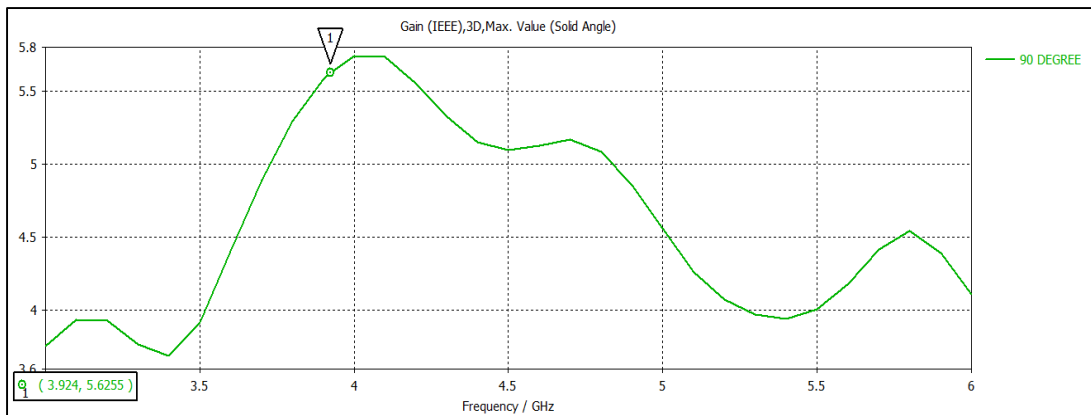
VSWR



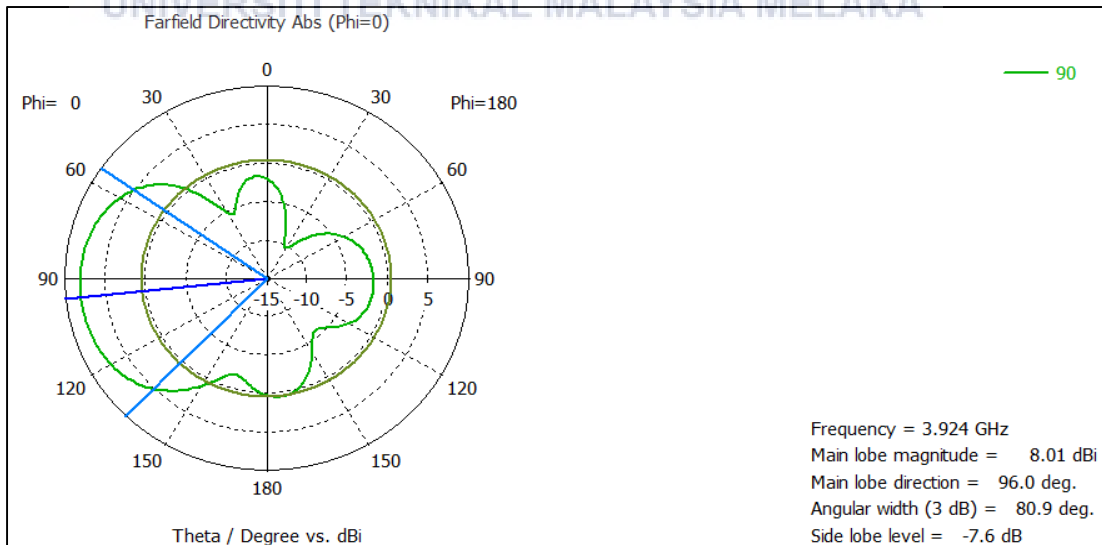
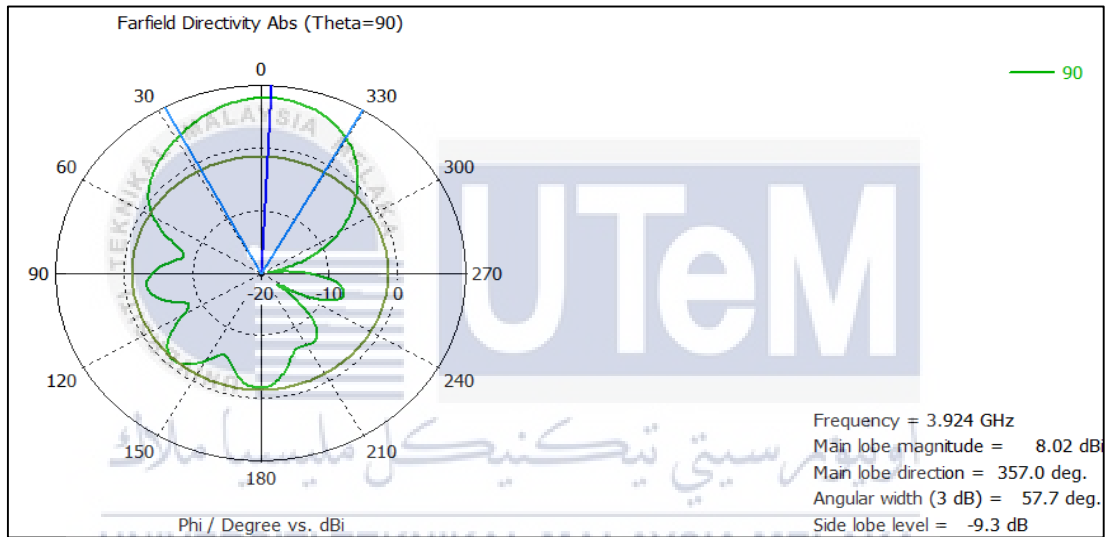
Directivity



Realized gain

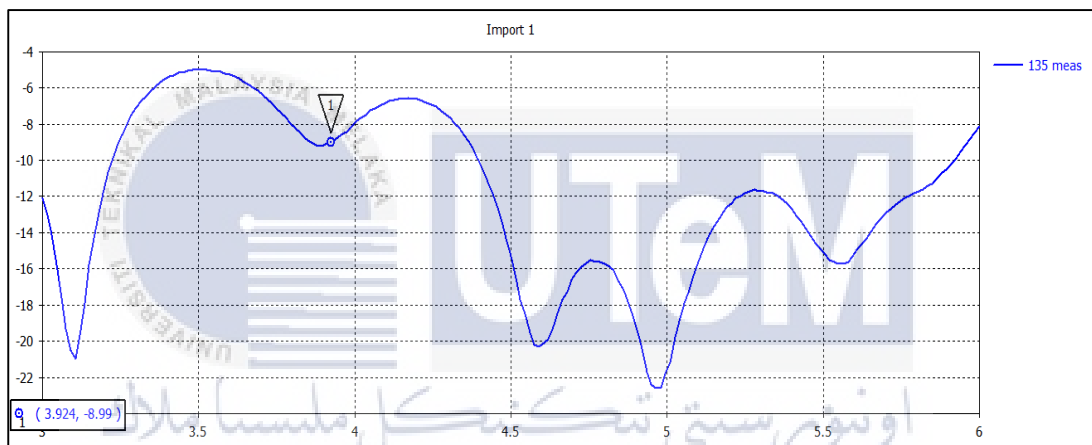
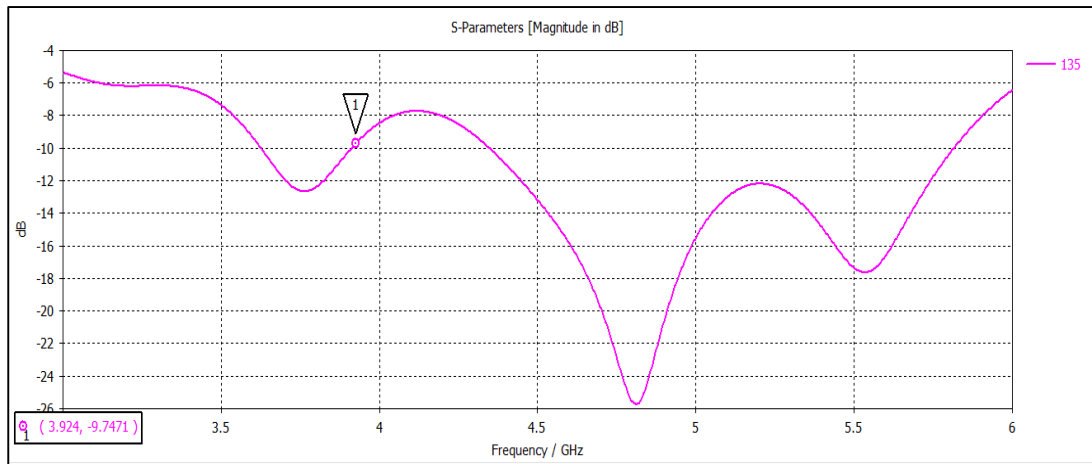


Farfield result at Theta = 90 & Phi = 0



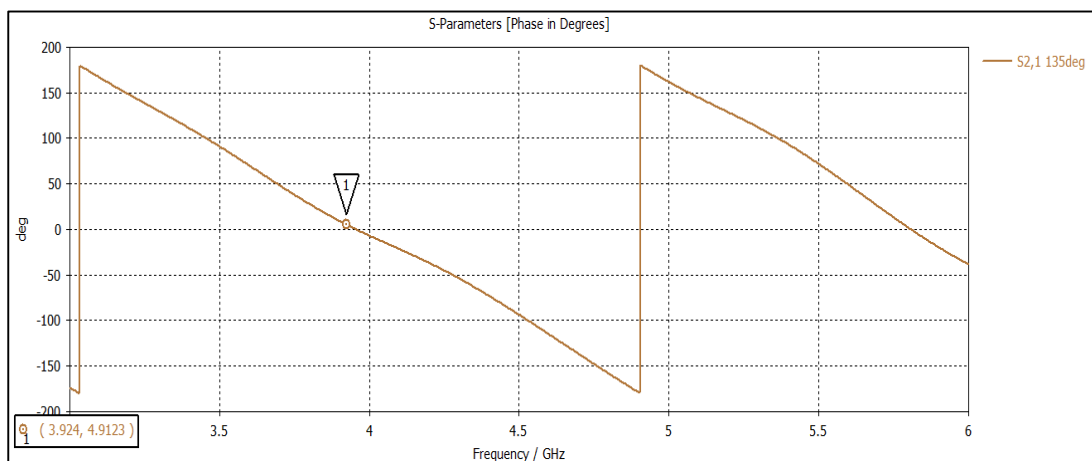
d. 135° Phase Shifter

Return loss simulation & measured.

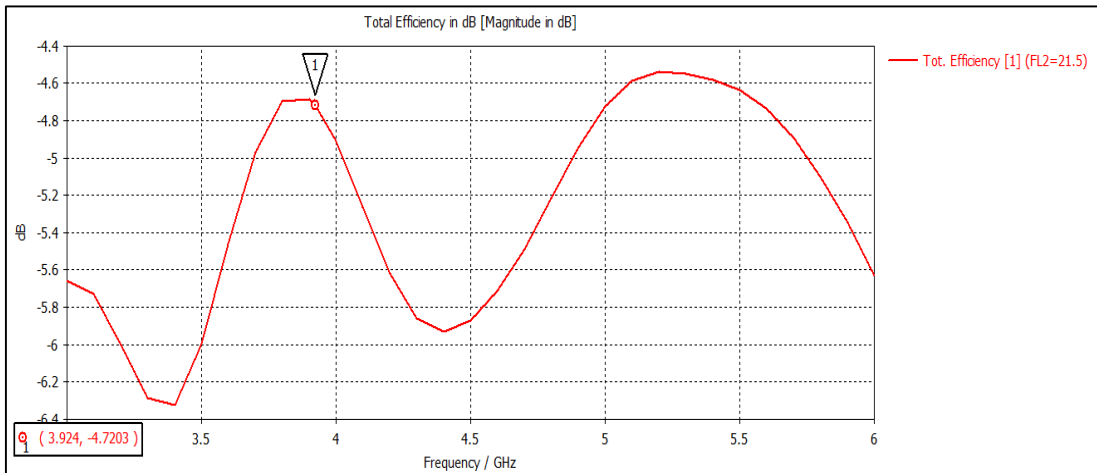


UNIVERSITI TEKNIKAL MALAYSIA MELAKA

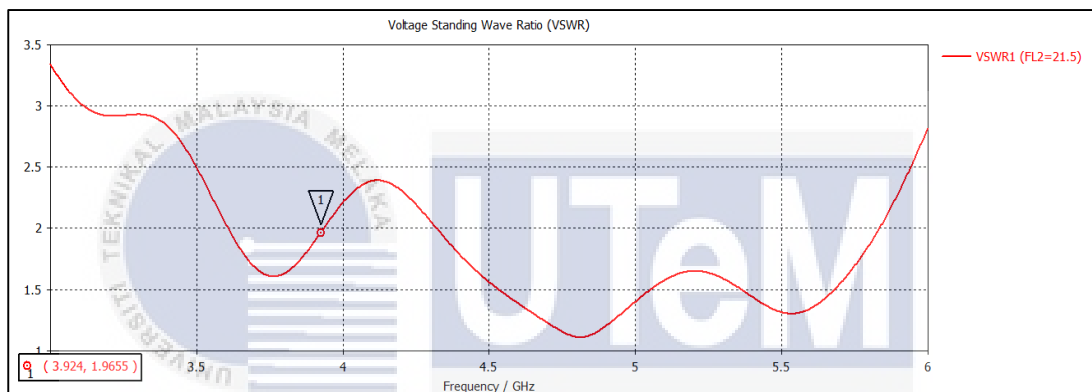
Phase



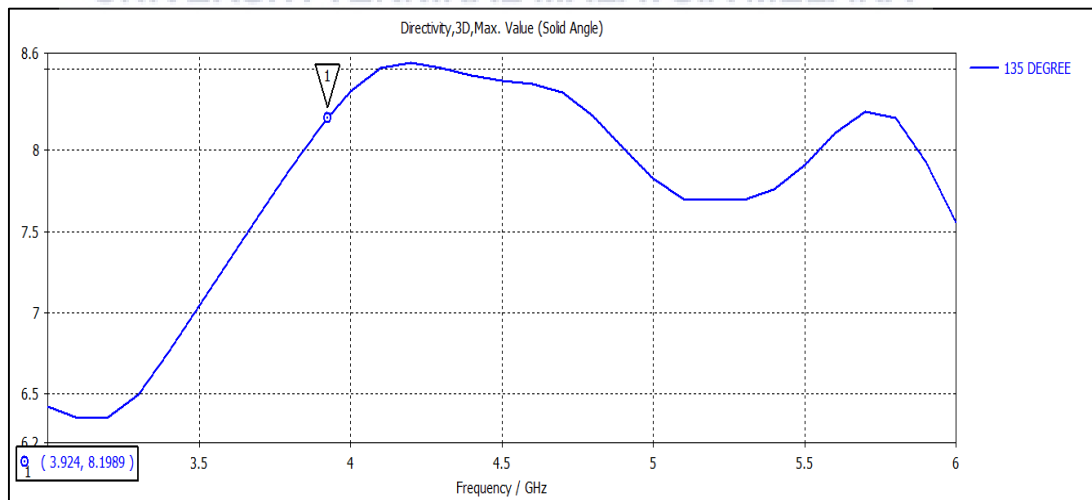
Efficiency



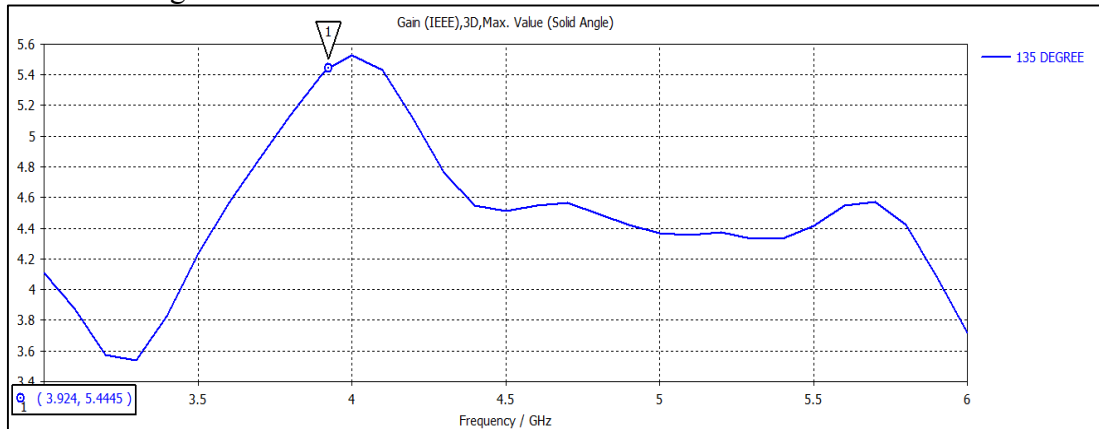
VSWR



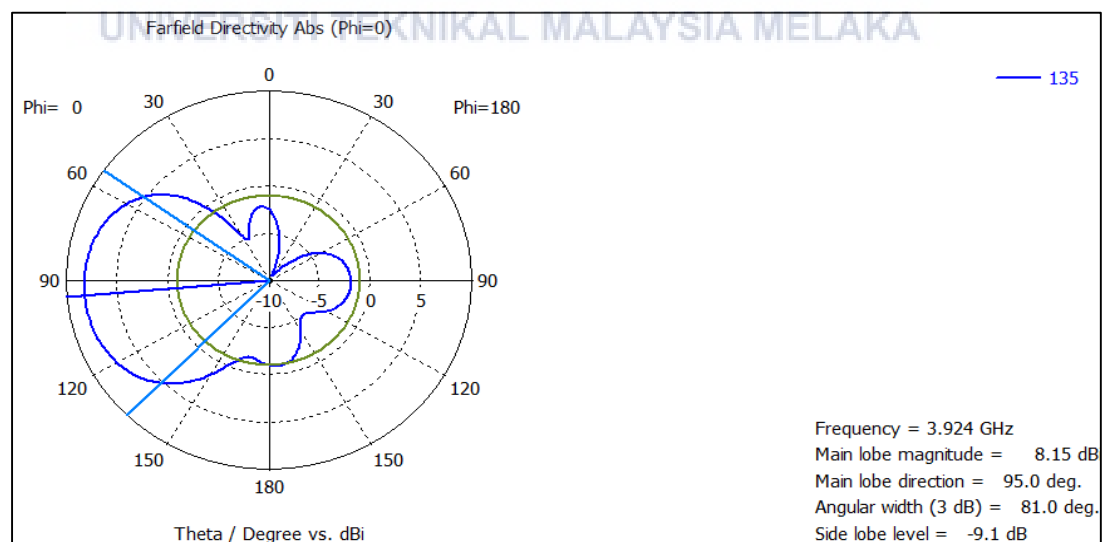
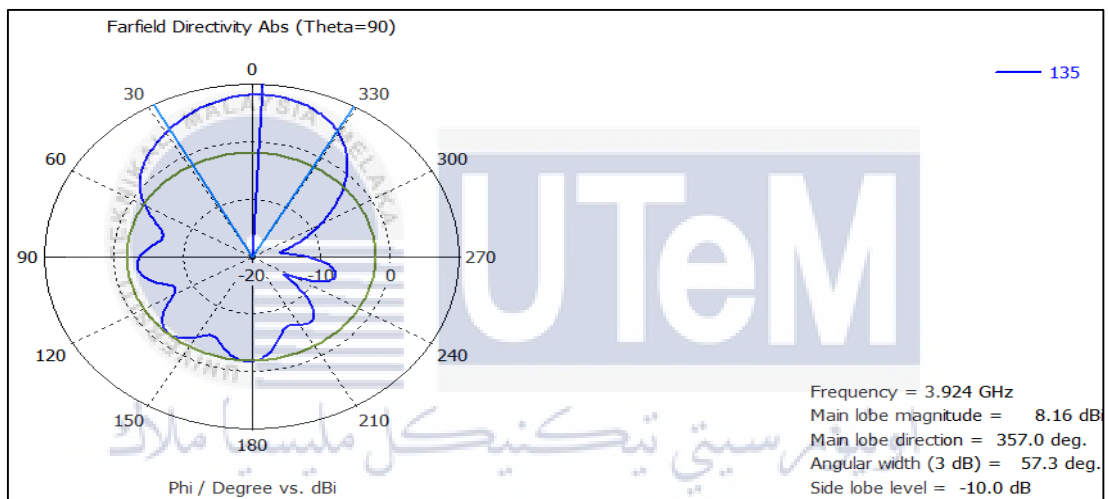
Directivity



Realized gain

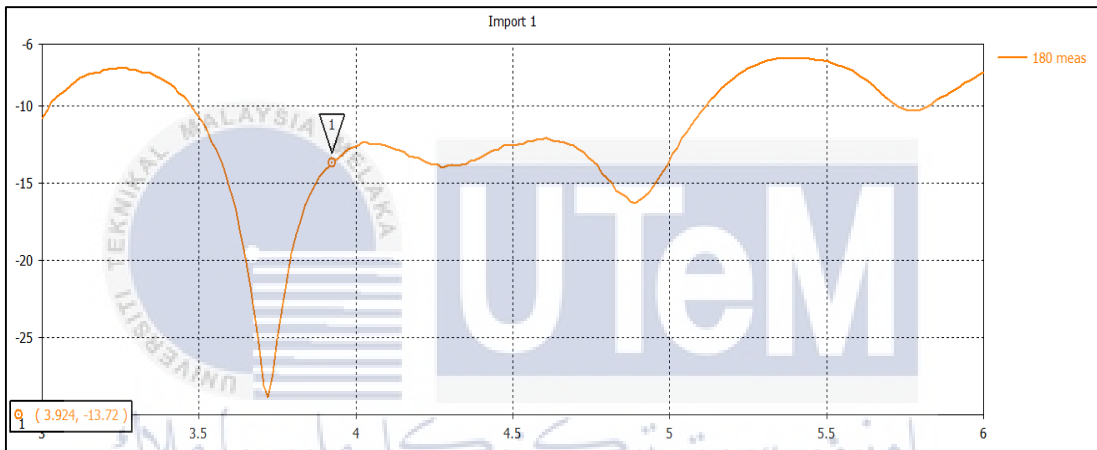
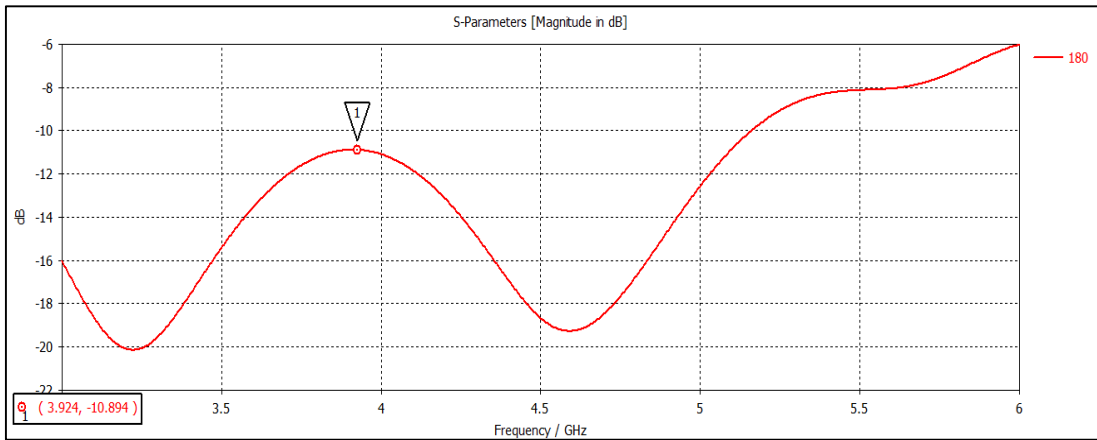


Farfield result at Theta = 90 & Phi = 0

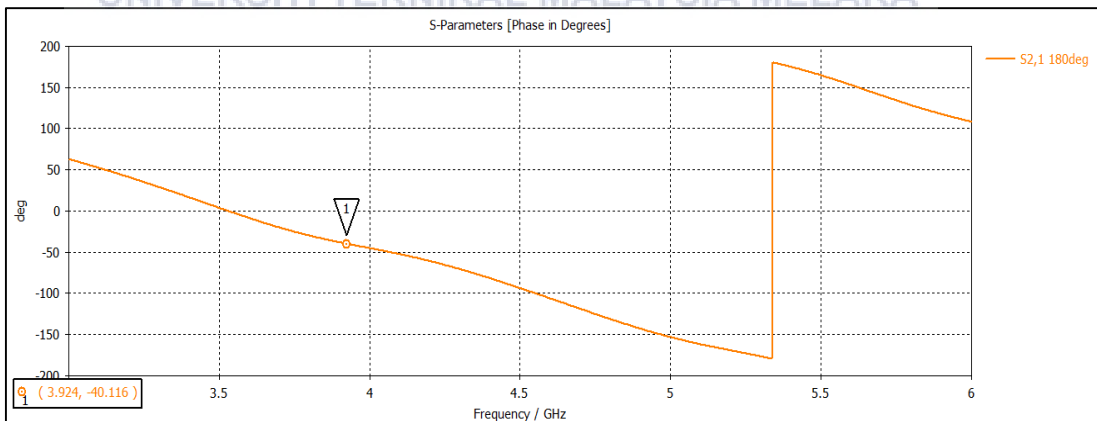


e. 180° Phase Shifter

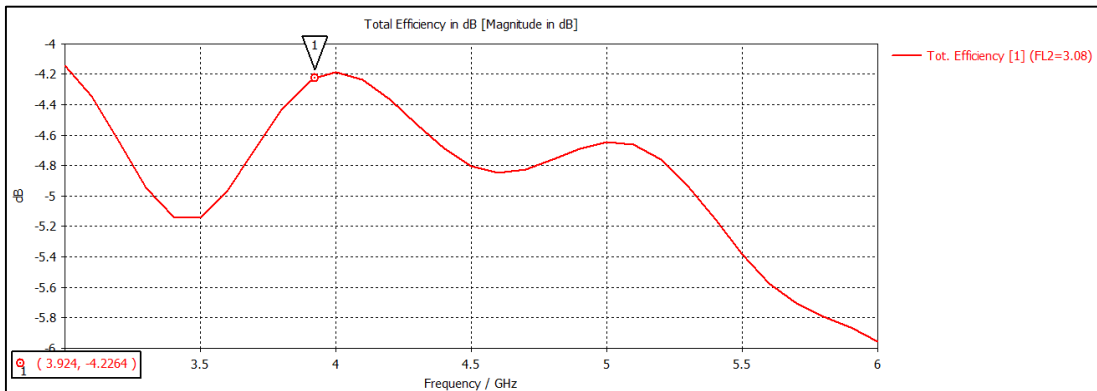
Return loss simulation & measured.



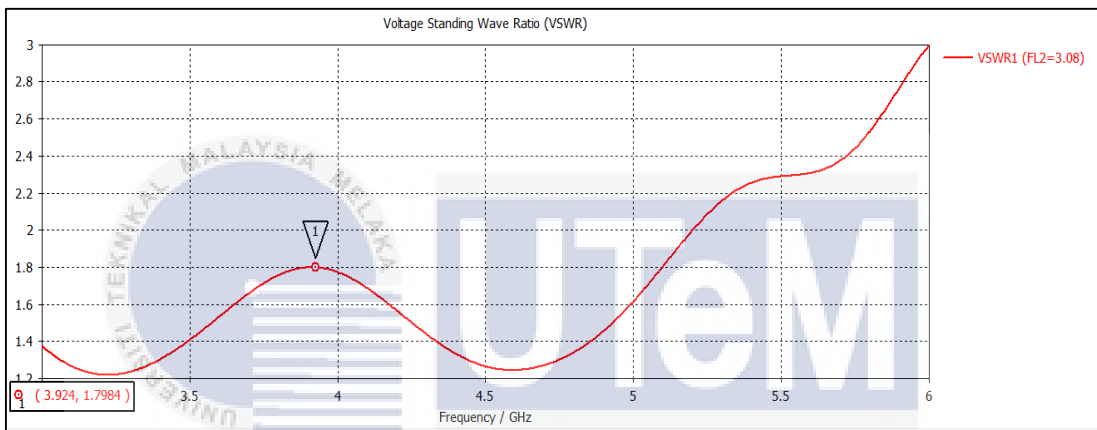
Phase



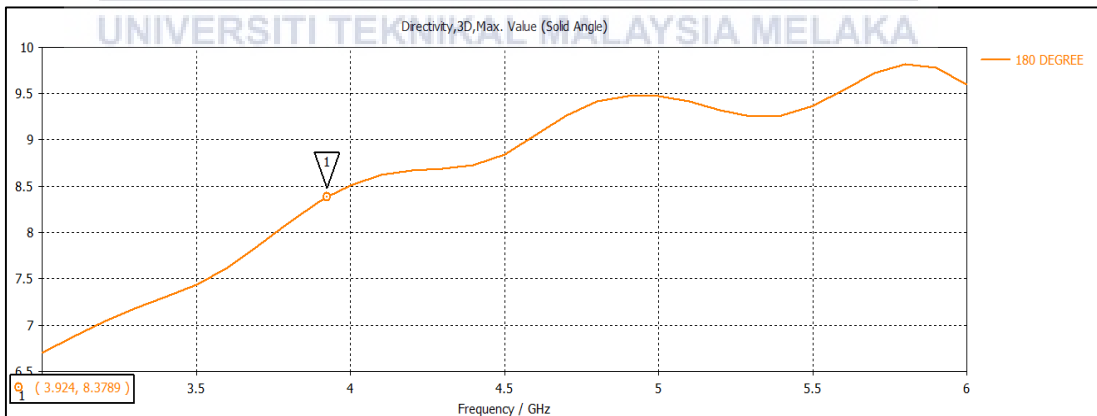
Efficiency



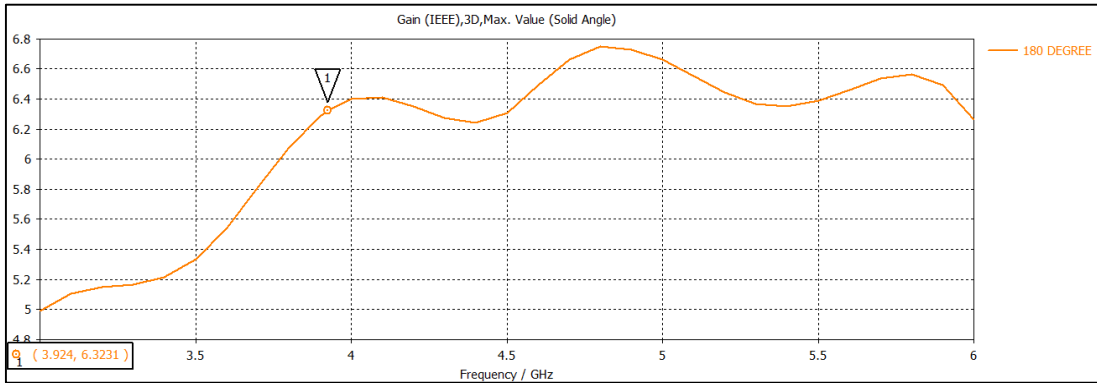
VSWR



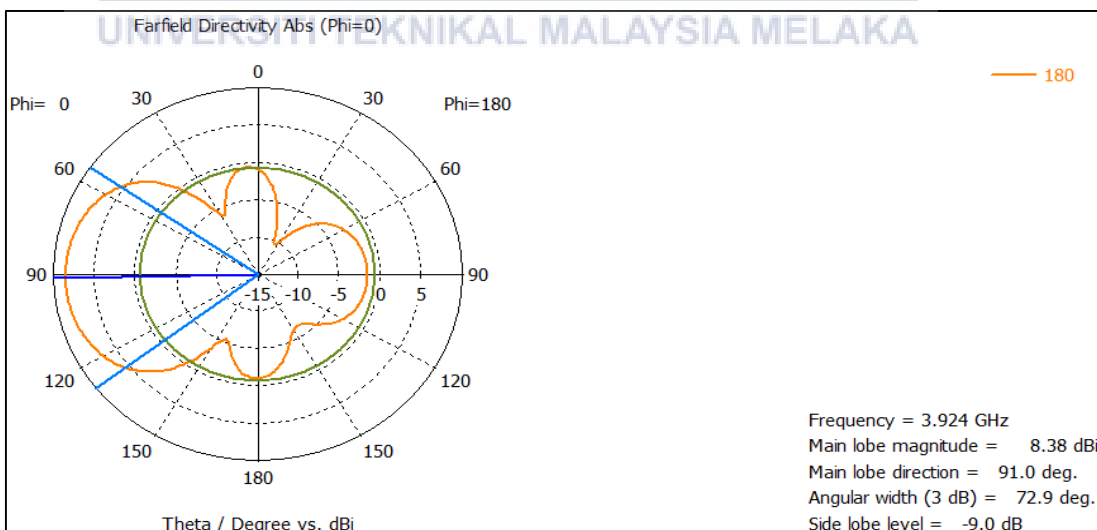
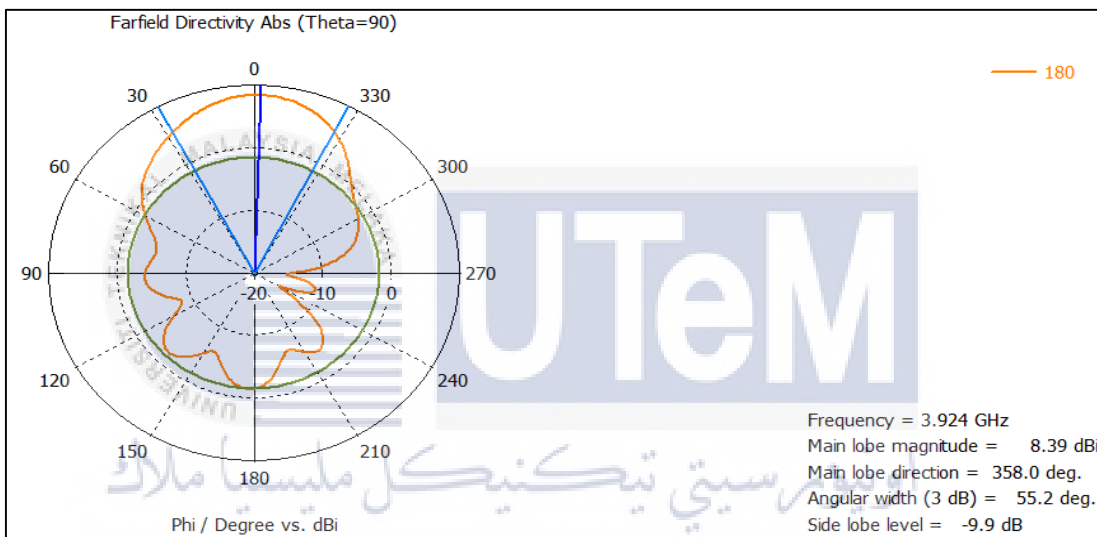
Directivity



Realized gain

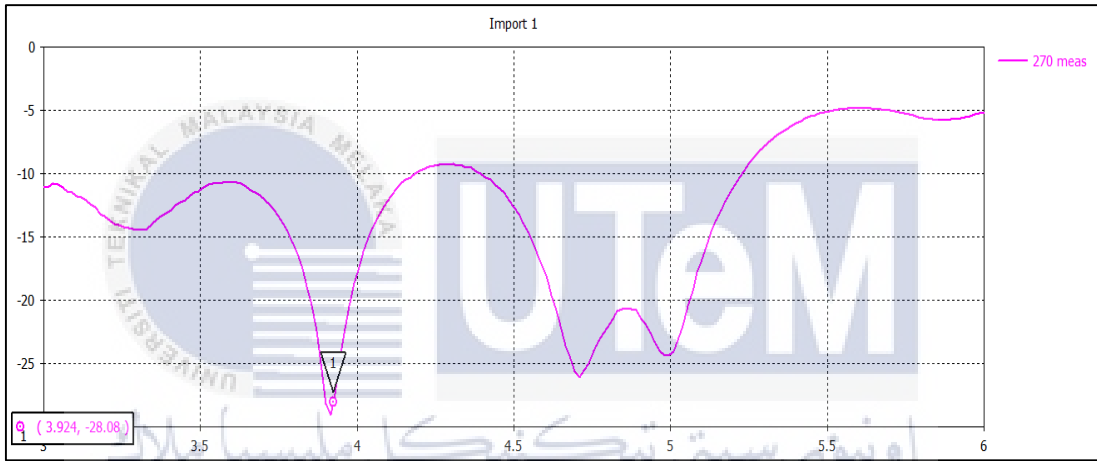
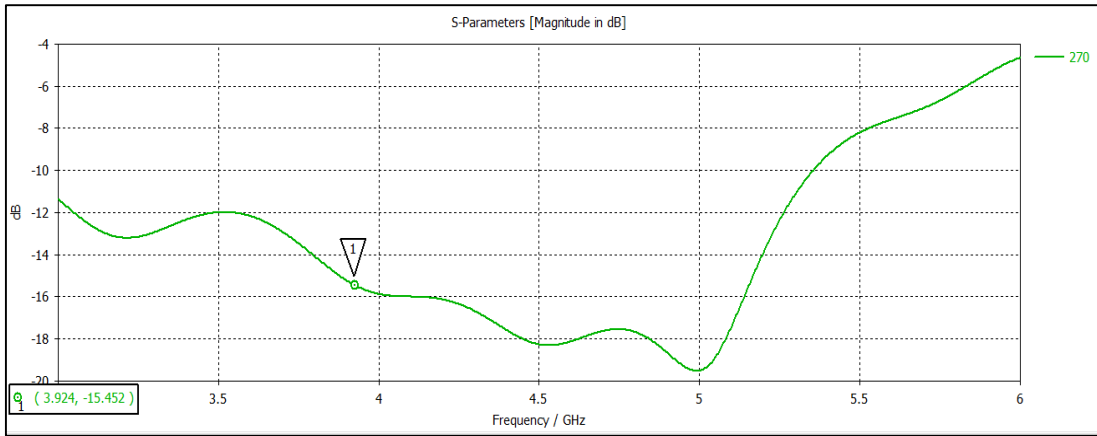


Farfield result at Theta = 90 & Phi = 0

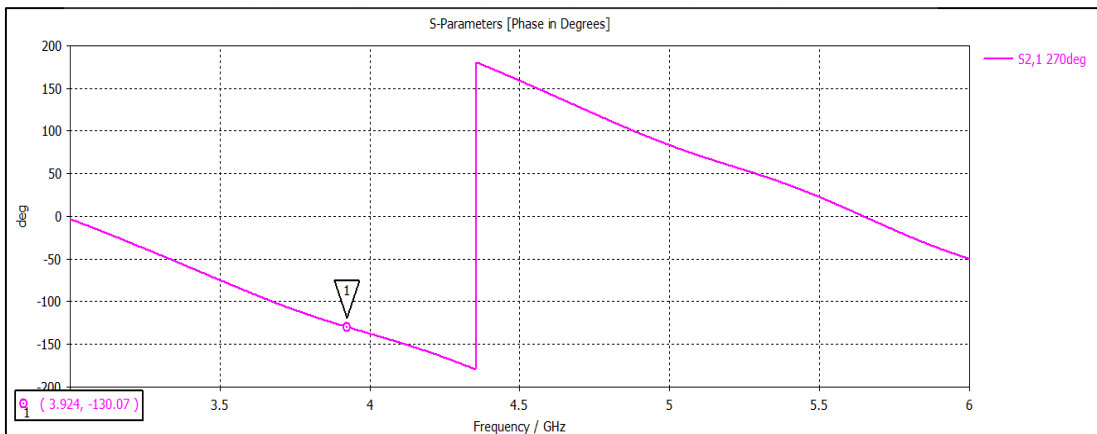


f. 270° Phase Shifter

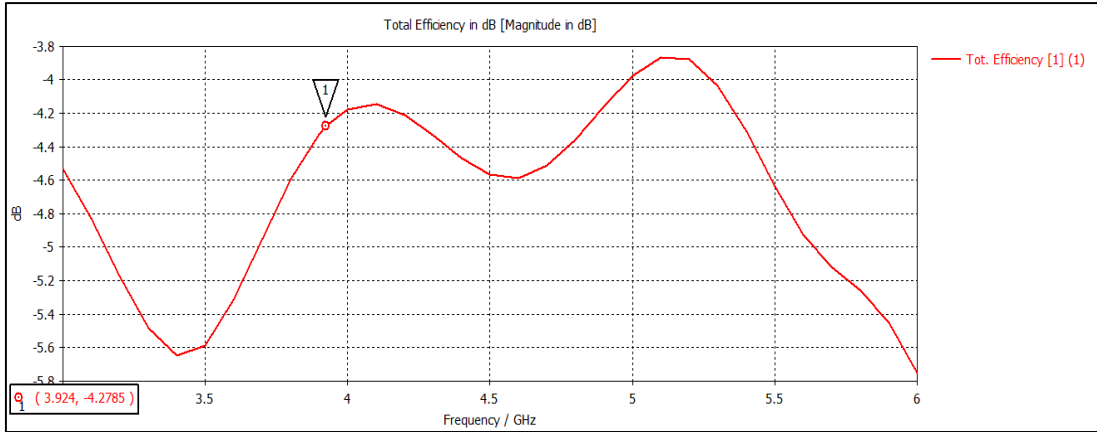
Return loss simulation & measured.



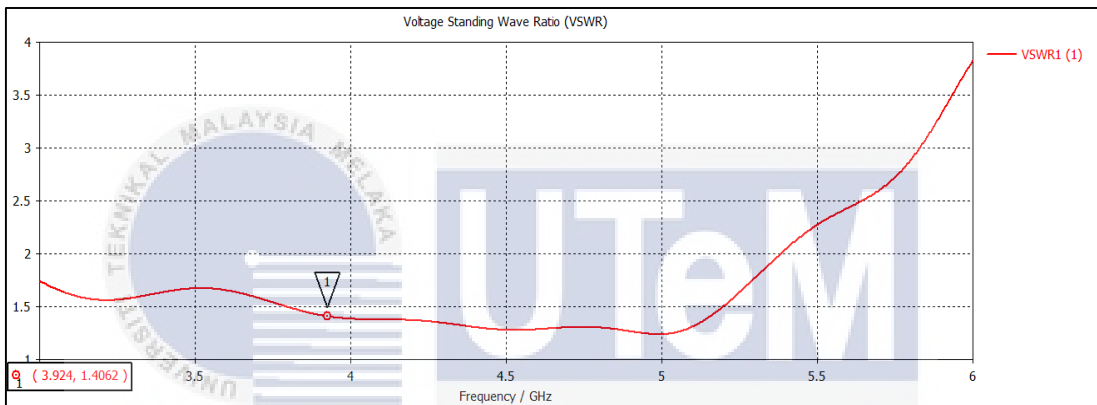
Phase



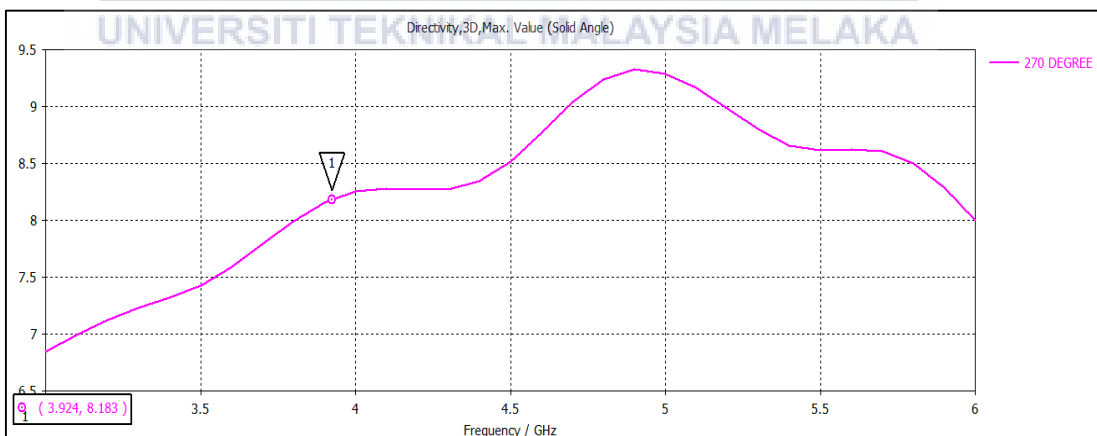
Efficiency



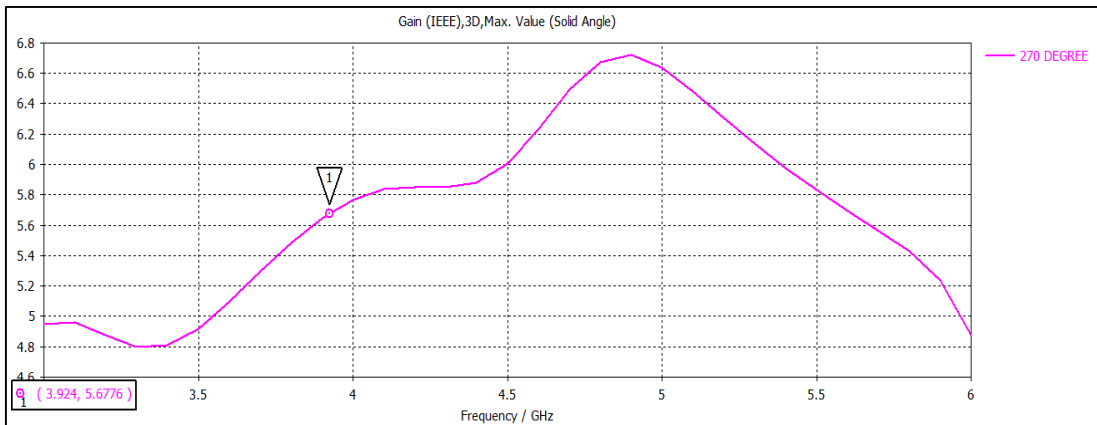
VSWR



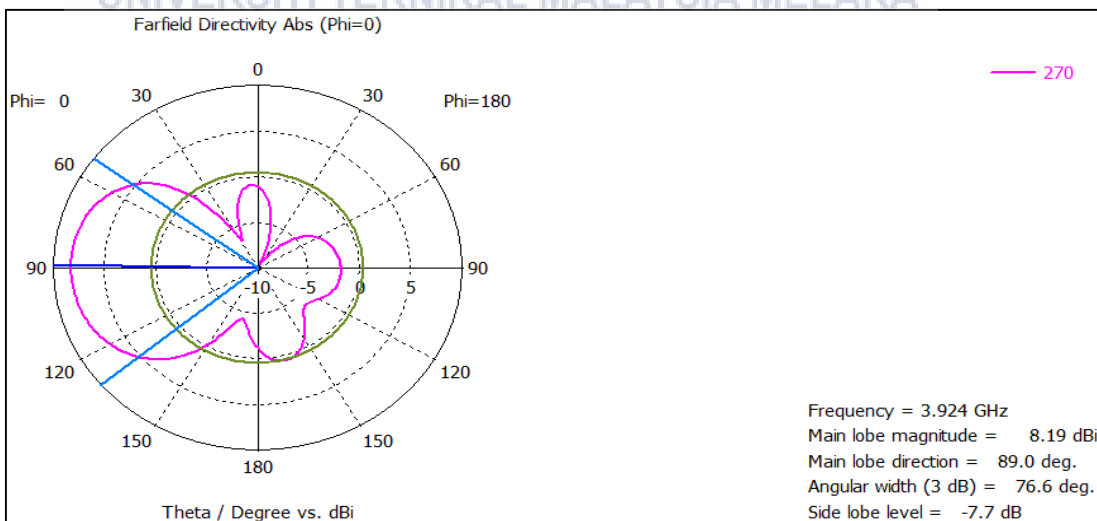
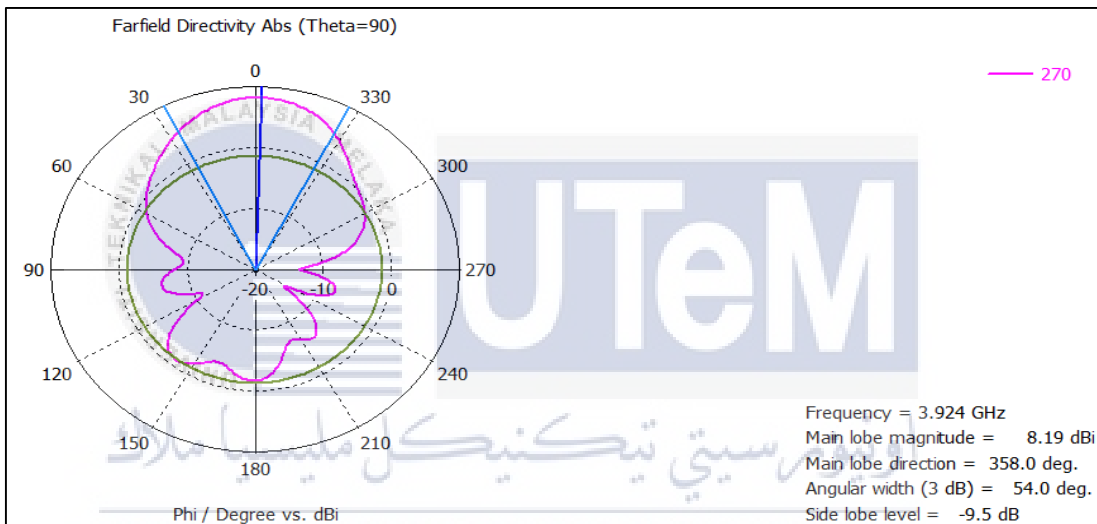
Directivity



Realized gain

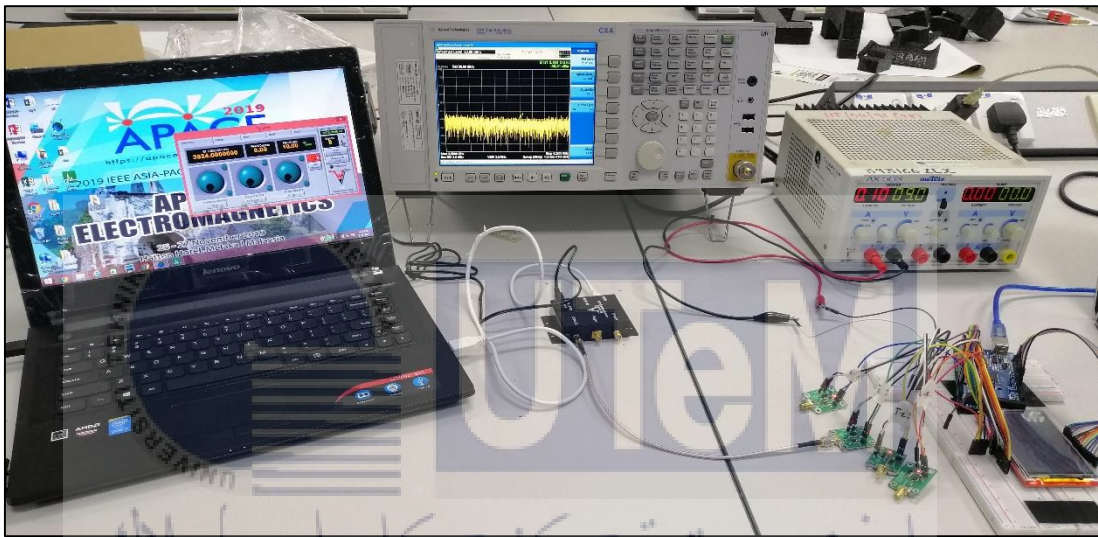


Farfield result at Theta = 90 & Phi = 0

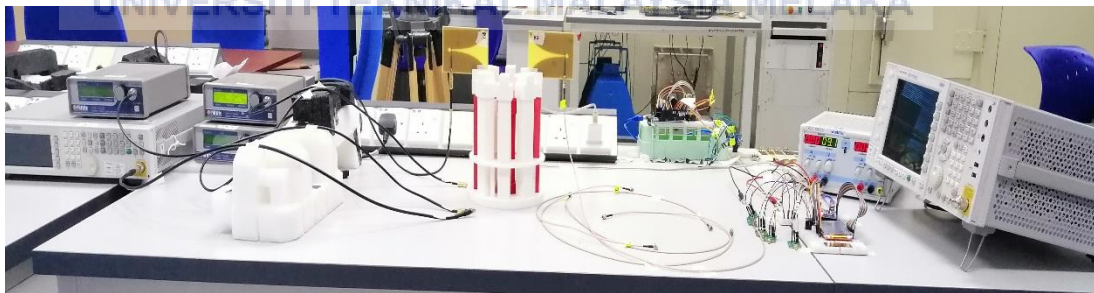


APPENDIX D

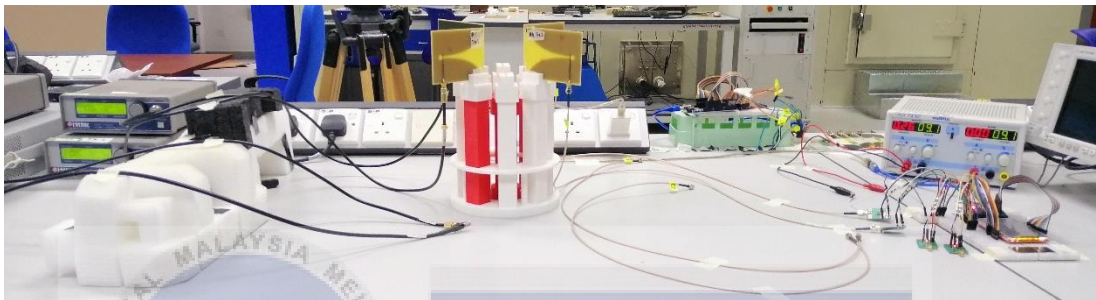
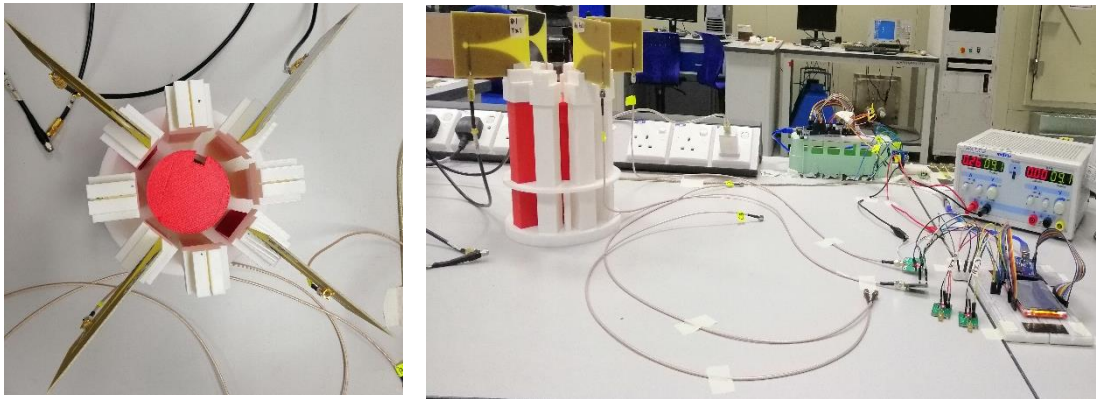
1. RF DETECTOR TESTING



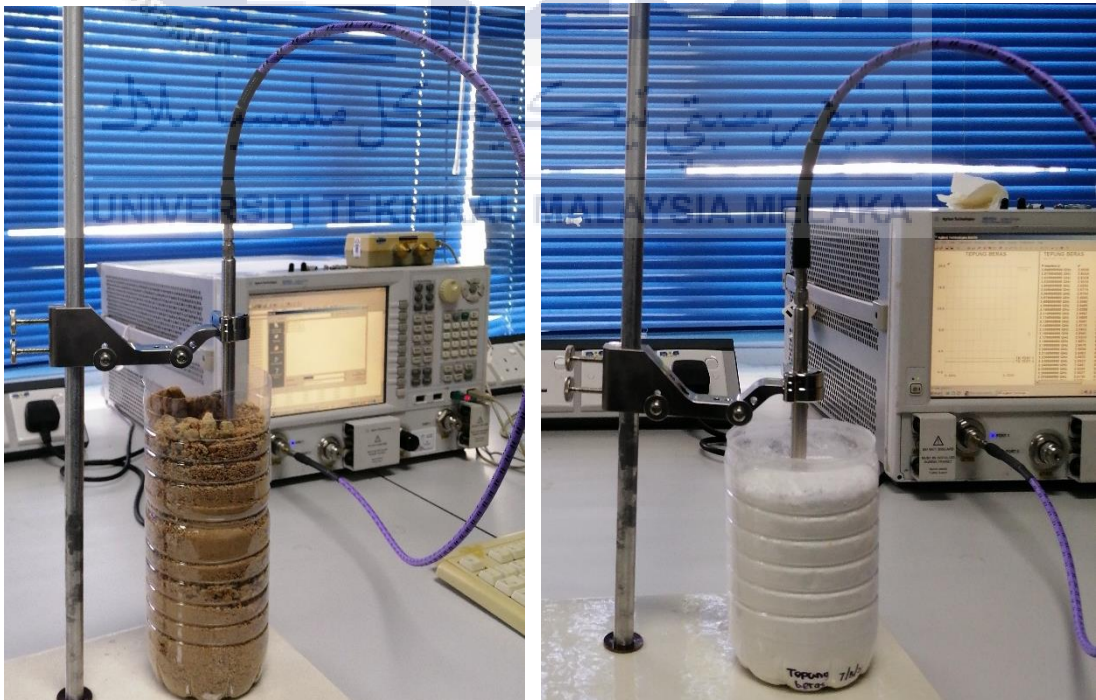
2. SIMO CONFIGURATION

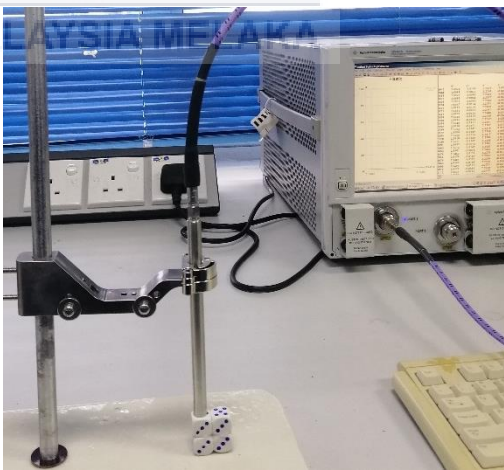
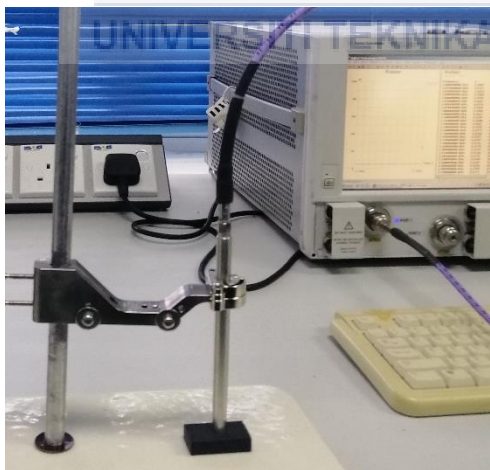
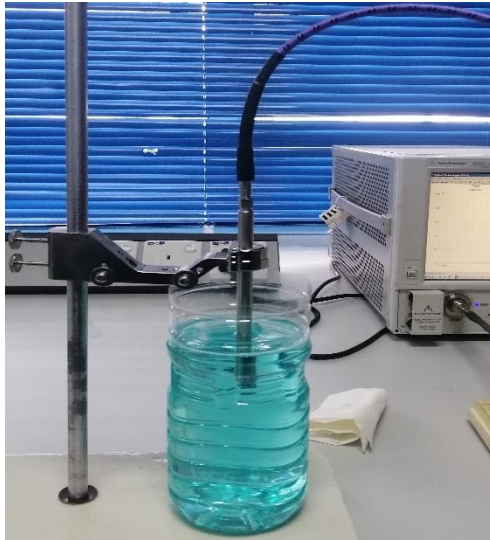


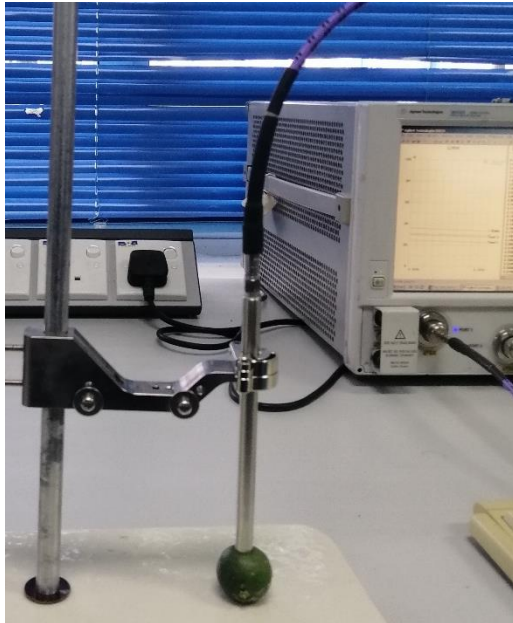
3. MIMO CONFIGURATION



4. MATERIAL TESTING FOR DIELECTRIC CONSTANT



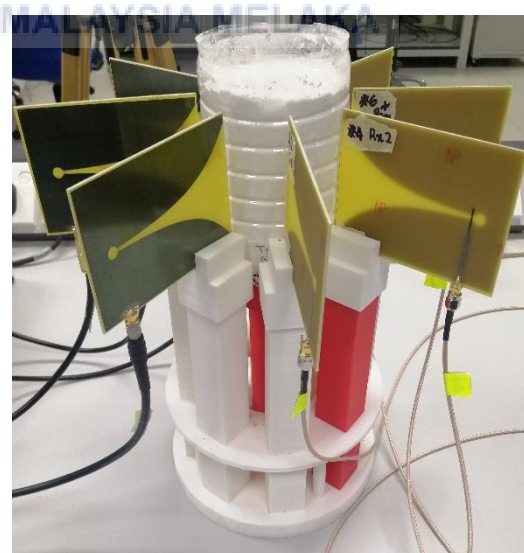
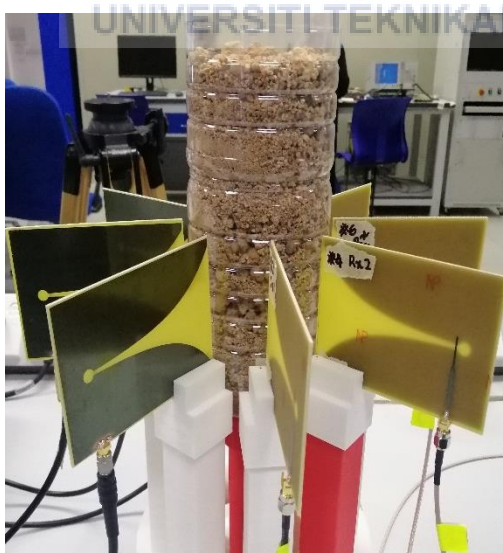
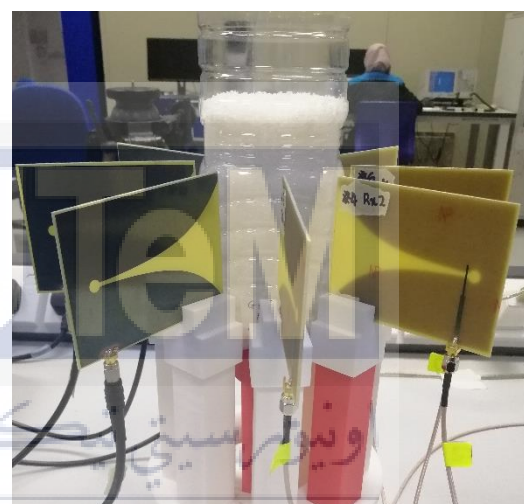
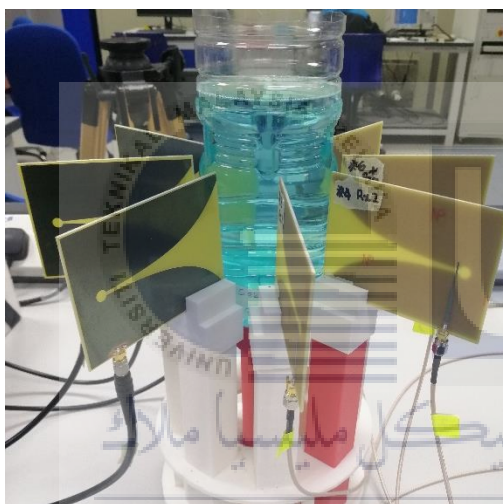
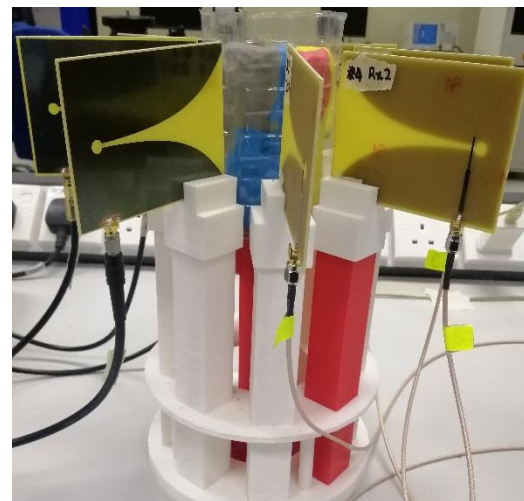
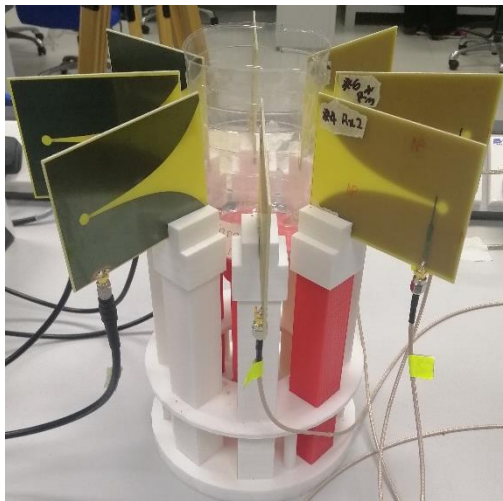


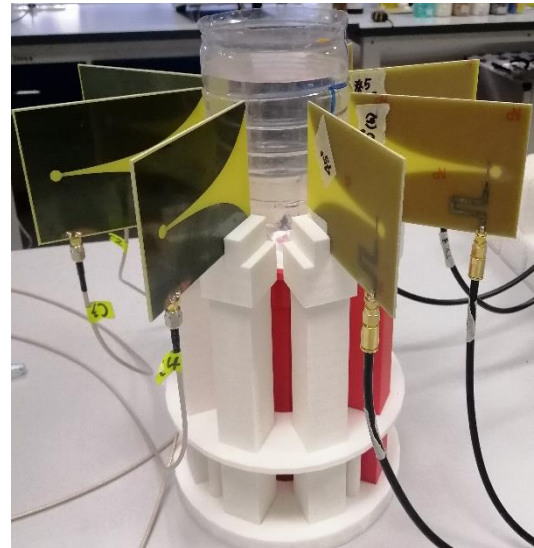
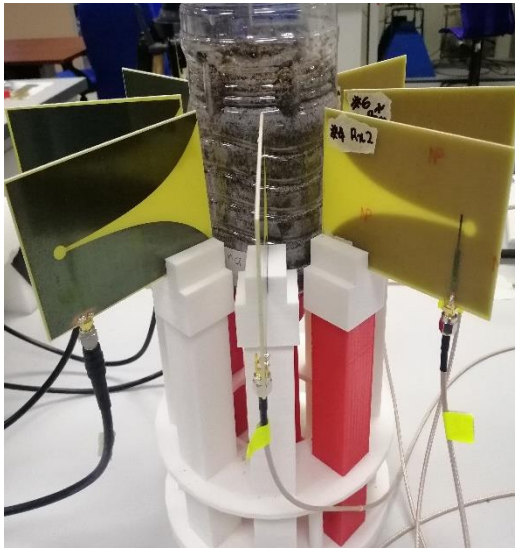


اونيورسيتي تيكنيكل مليسيا ملاك

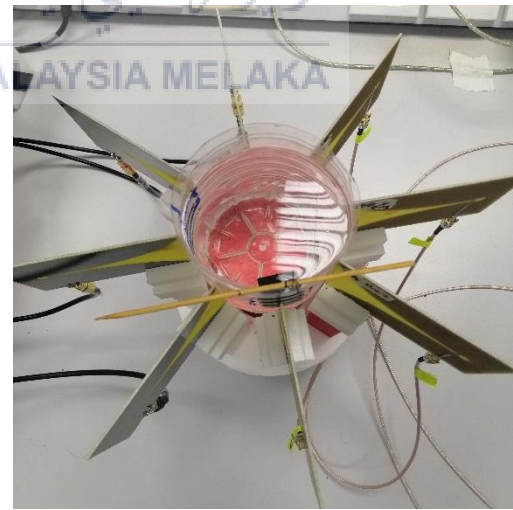
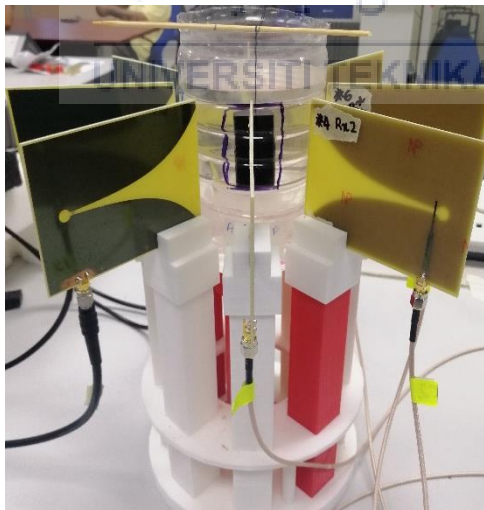
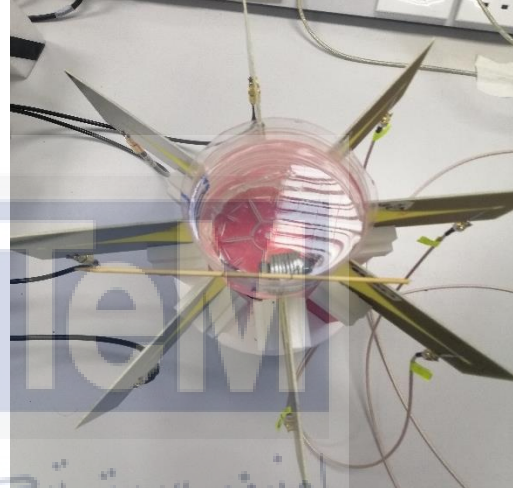
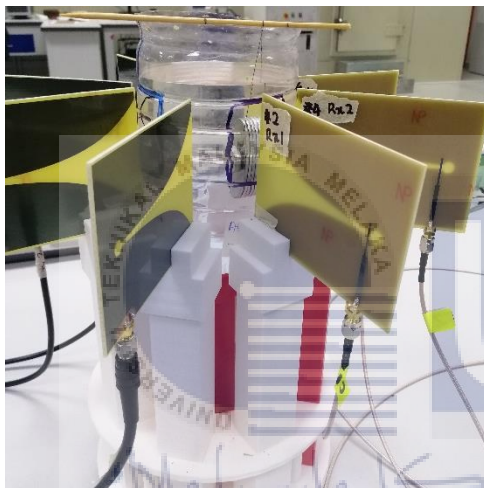
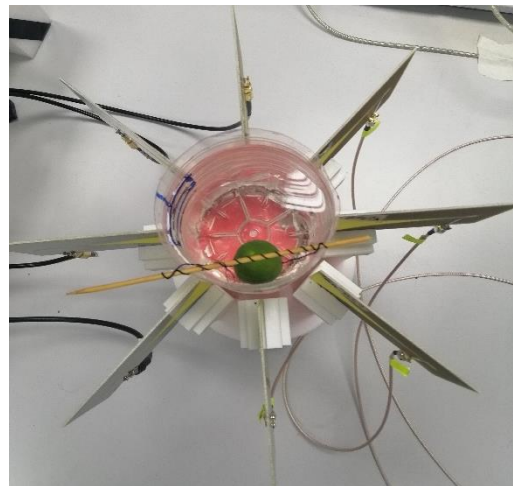
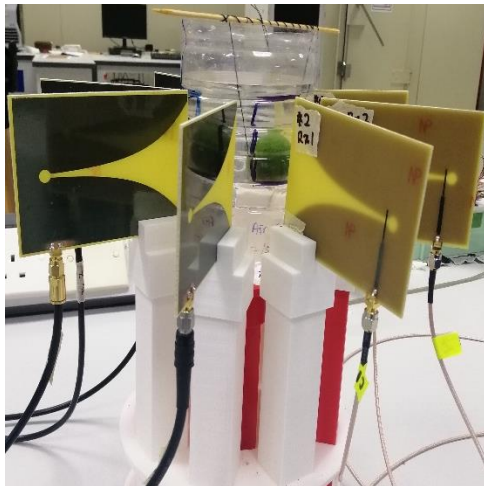
UNIVERSITI TEKNIKAL MALAYSIA MELAKA

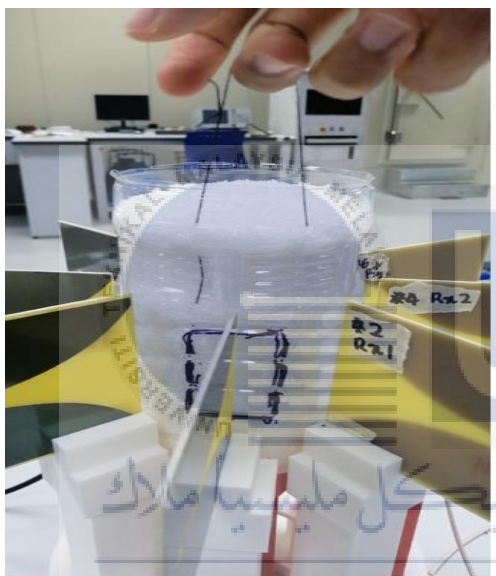
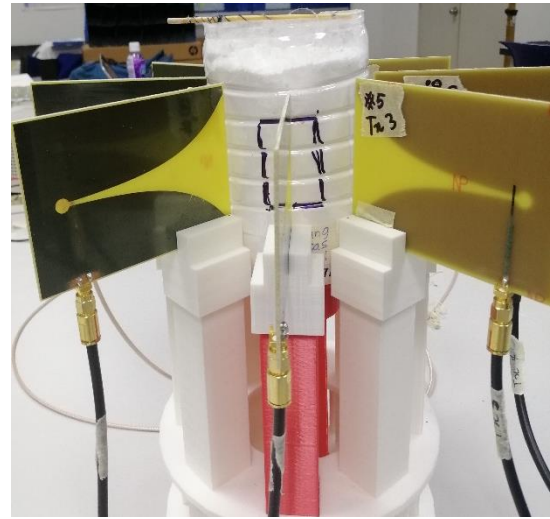
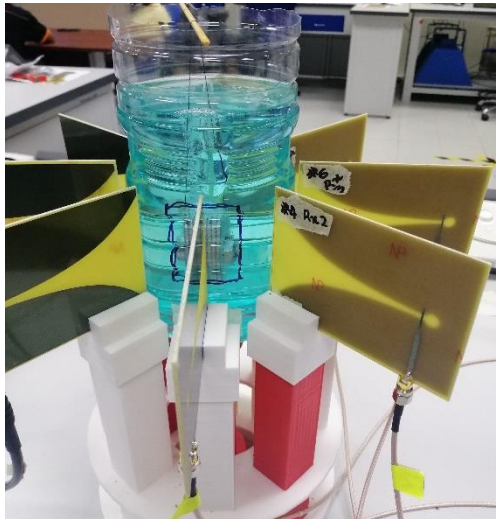
5. MATERIAL CHARACTERIZATION





6. SPATIAL DETECTION





APPENDIX E

1. AD8318 MODULE DATASHEET



1 MHz to 8 GHz, 70 dB Logarithmic Detector/Controller

Data Sheet

AD8318

FEATURES

Wide bandwidth: 1 MHz to 8 GHz
High accuracy: ± 1.0 dB over 55 dB range ($f < 5.8$ GHz)
Stability over temperature: ± 0.5 dB
Low noise measurement/controller output (VOUT)
Pulse response time: 10 ns/12 ns (fall/rise)
Integrated temperature sensor
Small footprint LFCSP
Power-down feature: < 1.5 mW at 5 V
Single-supply operation: 5 V at 68 mA
Fabricated using high speed SiGe process

APPLICATIONS

RF transmitter PA setpoint control and level monitoring
RSSI measurement in base stations, WLAN, WiMAX, and radars

GENERAL DESCRIPTION

The AD8318 is a demodulating logarithmic amplifier, capable of accurately converting an RF input signal to a corresponding decibel-scaled output voltage. It employs the progressive compression technique over a cascaded amplifier chain, each stage of which is equipped with a detector cell. The device is used in measurement or controller mode. The AD8318 maintains accurate log conformance for signals of 1 MHz to 6 GHz and provides useful operation to 8 GHz. The input range is typically 60 dB (referenced to 50 Ω) with error less than ± 1 dB. The AD8318 has a 10 ns response time that enables RF burst detection to beyond 45 MHz. The device provides unprecedented logarithmic intercept stability vs. ambient temperature conditions. A 2 mV/ $^{\circ}$ C slope temperature sensor output is also provided for additional system monitoring. A single supply of 5 V is required. Current consumption is typically 68 mA. Power consumption decreases to < 1.5 mW when the device is disabled.

The AD8318 can be configured to provide a control voltage to a VGA, such as a power amplifier or a measurement output, from Pin VOUT. Because the output can be used for controller applications, wideband noise is minimal.

In this mode, the setpoint control voltage is applied to VSET. The feedback loop through an RF amplifier is closed via VOUT, the output of which regulates the amplifier output to a magnitude corresponding to VSET. The AD8318 provides 0 V to 4.9 V output capability at the VOUT pin, suitable for controller applications. As a measurement device, Pin VOUT is externally connected to VSET to produce an output voltage, V_{OUT} , which is

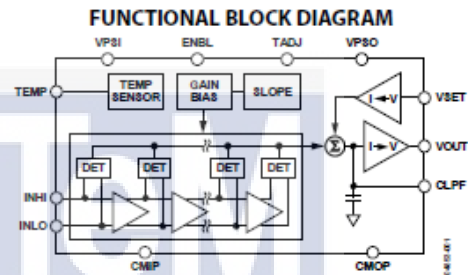


Figure 1.

a decreasing linear-in-dB function of the RF input signal amplitude.

The logarithmic slope is nominally -25 mV/dB but can be adjusted by scaling the feedback voltage from VOUT to the VSET interface. The intercept is 20 dBm (referenced to 50 Ω , CW input) using the INHI input. These parameters are very stable against supply and temperature variations.

The AD8318 is fabricated on a SiGe bipolar IC process and is available in a 4 mm \times 4 mm, 16-lead LFCSP for the operating temperature range of -40° C to $+85^{\circ}$ C.

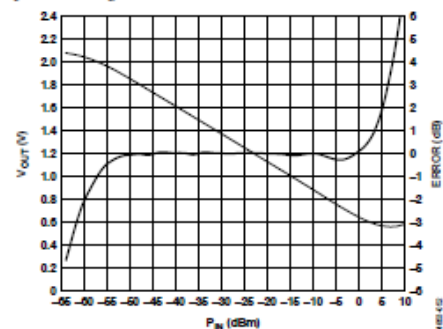


Figure 2. Typical Logarithmic Response and Error vs. Input Amplitude at 5.8 GHz